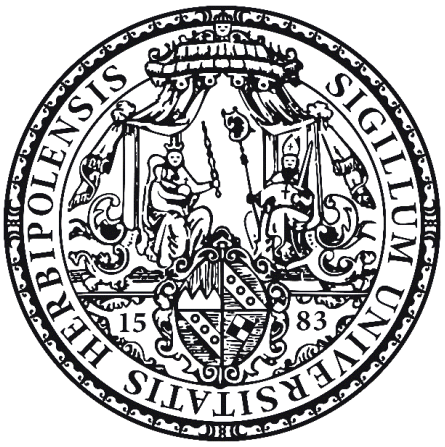

Diffusion kinetics of organic compounds and water in plant cuticular model wax under the influence of diffusing barrier-modifying adjuvants

Diffusionskinetiken organischer Verbindungen und Wasser in pflanzlichem kutikulärem Modellwachs unter dem Einfluss von diffundierenden, barriere-modifizierenden Adjuvantien

Doctoral thesis for a doctoral degree
at the Graduate School of Life Sciences,
Julius-Maximilians-Universität Würzburg,
Section Integrative Biology

submitted by

Marcel Kunz

from

Berlin

Würzburg 2022

Submitted on: ……..……..

Office stamp

Members of the Thesis Committee

Chairperson: Prof. Dr. Christian Janzen

Primary Supervisor: Prof. Dr. Markus Riederer

Supervisor (Second): Prof. Dr. Dirk Becker

Supervisor (Third): Dr. Christian Popp

Supervisor (Fourth): Dr. Markus Burghardt

Date of Public Defence: ……..……

Date of Receipt of Certificates: ……..

Table of contents

Summary

To reach their target site, systemic pesticides must enter the plant from a spray droplet applied in the field. The uptake of an active ingredient (AI) takes place via the barrier-forming cuticular membrane, which is the outermost layer of the plant, separating it from the surrounding environment. Formulations are usually used which, in addition to the AI, also contain stabilizers and adjuvants. Adjuvants can either have surface-active properties or they act directly as barrier-modifying agents. The latter are grouped in the class of accelerating adjuvants, whereby individual variants may also have surface-active properties. The uptake of a pesticide from a spray droplet depends essentially on its permeability through the cuticular barrier. Permeability defines a combined parameter, which is the product of AI mobility and AI solubility within the cuticle. In recent decades, several tools have been developed that allowed the determination of individual parameters of organic compound penetration across the cuticular membrane. Nevertheless, earlier studies showed that mainly cuticular waxes are the barrier-determining component of the cuticular membrane and additionally, it was shown that mainly the very-long-chain aliphatic compounds (VLCAs) are responsible for establishing an effective barrier. However, the barrier-determining role of the individual VLCAs, being classified according to their respective functional groups, is still unknown.

Therefore, the following objectives were pursued and achieved in this work: (1) A new ATR-FTIR-based approach was developed to measure the temperature-dependent real-time diffusion kinetics of organic models for active ingredients (AIs) in paraffin wax, exclusively consisting of very-long chain alkanes. (2) The developed ATR-FTIR approach was applied to determine the diffusion kinetics of self-accelerating adjuvants in cuticular model waxes of different VLCA composition. At the same time, wax-specific changes were recorded in the respective IR spectra, which provided information about the respective wax modification. (3) The ATR-FTIR method was used to characterize the diffusion kinetics, as well as to determine the wax-specific sorption capacities for an AI-modeling organic compound and water in cuticular model waxes after adjuvant treatment. Regarding the individual chemical compositions and structures, conclusions were drawn about the adjuvant-specific modes of action (MoA).

Summary

In the first chapter, the ATR-FTIR based approach to determine organic compound diffusion kinetics in paraffin wax was successfully established. The diffusion kinetics of the AI modelling organic compounds heptyl parabene (HPB) and 4-cyanophenol (CNP) were recorded, comprising different lipophilicities and molecular volumes typical for AIs used in pesticide formulations. Derived diffusion coefficients ranged within 10^{-15} m^2 s^{-1}, thus being thoroughly higher than those obtained from previous experiments using an approach solely investigating desorption kinetics in reconstituted cuticular waxes. An ln-linear dependence between the diffusion coefficients and the applied diffusion temperature was demonstrated for the first time in cuticular model wax, from which activation energies were derived. The determined activation energies were 66.2 ± 7.4 kJ mol^{-1} and 56.4 ± 9.8 kJ mol^{-1}, being in the expected range of already well-founded activation energies required for organic compound diffusion across cuticular membranes, which again confirmed the significant contribution of waxes to the cuticular barrier. Deviations from the assumed Fickian diffusion were attributed to co-occurring water diffusion and apparatus-specific properties.

In the second and third chapter, mainly the diffusion kinetics of accelerating adjuvants in the cuticular model waxes candelilla wax and carnauba wax were investigated, and simultaneously recorded changes in the wax-specific portion of the IR spectrum were interpreted as indications of plasticization. For this purpose, the oil derivative methyl oleate, as well as the organophosphate ester TEHP and three non-ionic monodisperse alcohol ethoxylates (AEs) C12E2, C12E4 and C12E6 were selected. Strong dependence of diffusion on the respective principal components of the mainly aliphatic waxes was demonstrated. The diffusion kinetics of the investigated adjuvants were faster in the n-alkane dominated candelilla wax than in the alkyl ester dominated carnauba wax. Furthermore, the equilibrium absorptions, indicating equilibrium concentrations, were also higher in candelilla wax than in carnauba wax. It was concluded that alkyl ester dominated waxes feature higher resistance to diffusion of accelerating adjuvants than alkane dominated waxes with shorter average chain lengths due to their structural integrity. This was also found either concerning candelilla/policosanol (n-alcohol) or candelilla/rice bran wax (alkyl-esters) blends: with increasing alcohol concentration, the barrier function was decreased, whereas it was increased with increasing alkyl ester concentration. However, due to the high variability of the individual diffusion curves, only a trend could be assumed here, but significant differences

were not shown. The variability itself was described in terms of fluctuating crystalline arrangements and partial phase separation of the respective wax mixtures, which had inevitable effects on the adjuvant diffusion. However, diffusion kinetics also strongly depended on the studied adjuvants. Significantly slower methyl oleate diffusion accompanied by a less pronounced reduction in orthorhombic crystallinity was found in carnauba wax than in candelilla wax, whereas TEHP diffusion was significantly less dependent on the respective wax structure and therefore induced considerable plasticization in both waxes. Of particular interest was the AE diffusion into both waxes. Differences in diffusion kinetics were also found here between candelilla blends and carnauba wax. However, these depended equally on the degree of ethoxylation of the respective AEs. The lipophilic C12E2 showed approximately Fickian diffusion kinetics in both waxes, accompanied by a drastic reduction in orthorhombic crystallinity, especially in candelilla wax, whereas the more hydrophilic C12E6 showed significantly retarded diffusion kinetics associated with a smaller effect on orthorhombic crystallinity. The individual diffusion kinetics of the investigated adjuvants sometimes showed drastic deviations from the Fickian diffusion model, indicating a self-accelerating effect. Hence, adjuvant diffusion kinetics were accompanied by a distinct initial lag phase, indicating a critical concentration in the wax necessary for effective penetration, leading to sigmoidal rather than to exponential diffusion kinetics.

The last chapter dealt with the adjuvant-affected diffusion of the AI modelling CNP in candelilla and carnauba wax. Using ATR-FTIR, diffusion kinetics were recorded after adjuvant treatment, all of which were fully explicable based on the Fickian model, with high diffusion coefficients ranging from 10^{-14} to 10^{-13} m^2 s^{-1}. It is obvious that the diffusion coefficients presented in this work consistently demonstrated plasticization induced accelerated CNP mobilities. Furthermore, CNP equilibrium concentrations were derived, from which partition- and permeability coefficients could be determined. Significant differences between diffusion coefficients (mobility) and partition coefficients (solubility) were found on the one hand depending on the respective waxes, and on the other hand depending on treatment with respective adjuvants. Mobility was higher in candelilla wax than in carnauba wax only after methyl oleate treatment. Treatment with TEHP and AEs resulted in higher CNP mobility in the more polar alkyl ester dominated carnauba wax. The partition coefficients, on the other hand, were significantly lower after methyl oleate treatment in both candelilla and carnauba wax as

followed by TEHP or AE treatment. Models were designed for the CNP penetration mode considering the respective adjuvants in both investigated waxes. Co-penetrating water, which is the main ingredient of spray formulations applied in the field, was likely the reason for the drastic differences in adjuvant efficacy. Especially the investigated AEs favored an enormous water uptake in both waxes with increasing ethoxylation level. Surprisingly, this effect was also found for the lipophilic TEHP in both waxes. This led to the assumption that the AI permeability is not exclusively determined by adjuvant induced plasticization, but also depends on a "secondary plasticization", induced by adjuvant-attracted co-penetrating water, consequently leading to swelling and drastic destabilization of the crystalline wax structure.

The successful establishment of the presented ATR-FTIR method represents a milestone for the study of adjuvant and AI diffusion kinetics in cuticular waxes. In particular, the simultaneously detectable wax modification and, moreover, the determinable water uptake form a perfect basis to establish the ATR-FTIR system as a universal screening tool for wax-adjuvants-AI-water interaction in crop protection science.

Zusammenfassung

Um ihren Zielort zu erreichen, müssen systemische Pestizide aus einem auf dem Feld ausgebrachten Sprühtropfen in die Pflanze gelangen. Die Aufnahme eines Wirkstoffs (AI) erfolgt über die barrierebildende Kutikularmembran, die äußerste Schicht der Pflanze, die sie von der Umgebung trennt. In der Regel werden Formulierungen verwendet, die neben dem AI auch Stabilisatoren und Adjuvantien enthalten. Adjuvantien können entweder oberflächenaktive Eigenschaften haben oder sie wirken direkt als barrieremodifizierende Substanzen. Letztere werden in der Klasse der beschleunigenden Adjuvantien zusammengefasst, wobei einzelne Varianten auch oberflächenaktive Eigenschaften haben können. Die Aufnahme eines Pestizids aus einem Sprühtropfen hängt im Wesentlichen von seiner Durchlässigkeit durch die kutikuläre Barriere ab. Die Permeabilität ist ein kombinierter Parameter, der sich aus der Mobilität und der Löslichkeit des Wirkstoffs in der Kutikula ergibt. In den letzten Jahrzehnten wurden mehrere Methoden entwickelt, die die Bestimmung einzelner Parameter der Permeation organischer Verbindungen durch die Kutikularmembran ermöglichen. Frühere Studien zeigten jedoch, dass hauptsächlich kutikuläre Wachse die barrierebestimmende Komponente der Kutikula darstellen, und darüber hinaus wurde gezeigt, dass hauptsächlich die sehr langkettigen aliphatischen Verbindungen (VLCAs) für die Errichtung einer wirksamen Barriere verantwortlich sind. Die Rolle der einzelnen VLCAs, die nach ihren jeweiligen funktionellen Gruppen klassifiziert werden, ist jedoch in Bezug auf die Bestimmung der Barriereeigenschaften noch unbekannt.

Daher wurde in dieser Arbeit folgende Ziele verfolgt und erreicht: (1) Ein neuer ATR-FTIR-basierter Ansatz wurde entwickelt, um die temperaturabhängige Echtzeit-Diffusionskinetik von organischen Modellen für Wirkstoffe (AI) in ausschließlich aus Alkanen bestehendem Paraffinwachs zu messen. (2) Der entwickelte ATR-FTIR-Ansatz wurde zur Bestimmung der Diffusionskinetik von selbstbeschleunigenden Adjuvantien in kutikulären Modellwachsen unterschiedlicher VLCA-Zusammensetzung angewendet. Gleichzeitig wurden wachsspezifische Veränderungen in den jeweiligen IR-Spektren aufgezeichnet, welche Informationen über die jeweilige Wachsmodifikation lieferten. (3) Die ATR-FTIR-Methode wurde zur Charakterisierung der Diffusionskinetik, sowie zur Bestimmung der wachsspezifischen Sorptionskapazitäten für eine AI-modellierende organische Verbindung

und von Wasser in kutikulären Modellwachsen nach Adjuvans-Behandlung verwendet. Im Hinblick auf die einzelnen chemischen Zusammensetzungen und Strukturen wurden Rückschlüsse auf die adjuvansspezifischen Wirkweisen (MoA) gezogen.

Im ersten Kapitel wurde der ATR-FTIR-basierte Ansatz zur Bestimmung der Diffusionskinetik organischer Verbindungen in Paraffinwachs erfolgreich etabliert. Es wurde die Diffusionskinetik der organischen AI-Modellverbindungen Heptylparaben (HPB) und 4-Cyanophenol (CNP) aufgezeichnet, die unterschiedliche Lipophilitäten und Molekülvolumina aufweisen, wie sie für AIs in Pestizidformulierungen typisch sind. Die abgeleiteten Diffusionskoeffizienten lagen im Bereich von 10^{-15} m^2 s^{-1} und waren damit höher als die zuvor in rekonstituierten kutikulären Wachsen beobachteten Diffusionskoeffizienten. Zum ersten Mal wurde eine ln-lineare Abhängigkeit zwischen den Diffusionskoeffizienten und der angewandten Diffusionstemperatur in kutikulärem Modellwachs nachgewiesen, aus der schließlich Aktivierungsenergien abgeleitet wurden. Die ermittelten Aktivierungsenergien betrugen 66.2 ± 7.4 kJ mol^{-1} und 56.4 ± 9,8 kJ mol^{-1} und lagen damit im erwarteten Bereich der bereits gut begründeten Aktivierungsenergien, die für die Diffusion organischer Verbindungen durch kutikuläre Membranen erforderlich sind. Dies bestätigte abermals den signifikanten Beitrag der Wachse zur kutikulären Barriere. Abweichungen von der angenommenen Fick'schen Diffusion wurden auf die gleichzeitig stattfindende Wasserdiffusion und gerätespezifische Artefakte zurückgeführt.

Im zweiten und dritten Kapitel wurde vor allem die Diffusionskinetik von beschleunigenden Adjuvantien in den kutikulären Modellwachsen Candelillawachs und Carnaubawachs untersucht und gleichzeitig aufgezeichnete Veränderungen im wachspezifischen Teil des IR-Spektrums als Hinweise auf eine Plastifizierung interpretiert. Zu diesem Zweck wurden das Ölderivat Methyloleat, sowie der Organophosphatester TEHP und drei nichtionische monodisperse Alkoholethoxylate (AEs) C12E2, C12E4 und C12E6 ausgewählt. Es wurde eine starke Abhängigkeit der Adjuvansdiffusion von den jeweiligen Hauptkomponenten der hauptsächlich aliphatisch strukturierten Wachse nachgewiesen. So war die Diffusionskinetik der untersuchten Adjuvantien in dem hauptsächlich aus n-Alkanen bestehenden Candelillawachs schneller als in dem von Alkylestern dominierten Carnaubawachs. Darüber hinaus waren die Gleichgewichtsabsorptionen, die auf Gleichgewichtskonzentrationen hinweisen, in Candelillawachs ebenfalls höher als in Carnaubawachs. Daraus wurde gefolgert,

dass Wachse mit hohen Alkylesteranteilen aufgrund ihrer strukturellen Integrität einen höheren Widerstand gegen die Diffusion von beschleunigenden Adjuvantien aufweisen als Wachse mit kürzeren durchschnittlichen Kettenlängen. Dies wurde auch bei Candelilla/Policosanol- (n-Alkohol) oder Candelilla/Reiskleiewachs-Mischungen (Alkylester) festgestellt: Mit steigender Alkoholkonzentration nahm die Barrierefunktion ab, während sie mit steigender Alkylesterkonzentration zunahm. Aufgrund der hohen Variabilität der einzelnen Diffusionskurven konnte hier jedoch nur ein Trend vermutet werden, signifikante Unterschiede zeigten sich jedoch nicht. Die Variabilität selbst wurde mit schwankenden kristallinen Anordnungen und teilweiser Phasentrennung der jeweiligen Wachsmischungen erklärt, die sich zwangsläufig auf die Diffusion der Adjuvantien auswirkten. Die Diffusionskinetik hing jedoch auch stark von den untersuchten Adjuvantien ab. In Carnaubawachs wurde eine deutlich langsamere Methyloleat-Diffusion festgestellt, die mit einer weniger ausgeprägten Verringerung der orthorhombischen Kristallinität einherging als in Candelillawachs, während die TEHP-Diffusion deutlich weniger von der jeweiligen Wachsstruktur abhängig war und in beiden Wachsen eine erhebliche Plastifizierung bewirkte. Von besonderem Interesse war die AE-Diffusion in den untersuchten Wachsen. Auch hier wurden Unterschiede in der Diffusionskinetik zwischen Candelillamischungen und Carnaubawachs festgestellt. Diese hingen jedoch gleichermaßen vom Ethoxylierungsgrad der jeweiligen AEs ab. Das lipophile C12E2 zeigte in beiden Wachsen eine annähernd Fick‘sche Diffusionskinetik, die mit einer drastischen Verringerung der orthorhombischen Kristallinität einherging, insbesondere im Candelillawachs, während das hydrophilere C12E6 eine deutlich verzögerte Diffusionskinetik zeigte, die mit einer geringeren Auswirkung auf die orthorhombische Kristallinität einherging. Die individuellen Diffusionskinetiken der untersuchten Adjuvantien zeigten teilweise drastische Abweichungen vom Fick‘schen Diffusionsmodell, was auf einen selbstbeschleunigenden Effekt hindeutet. Die Diffusionskinetik der Adjuvantien wurde von einer ausgeprägten anfänglichen Verzögerungsphase begleitet, die auf das Erreichen einer kritischen Konzentration im Wachs hindeutet. Es wird angenommen, dass aufgrund der initialen Verzögerungsphase letztlich sigmoidale, statt Fick’sche Diffusionskinetiken vorlagen.

Das letzte Kapitel befasste sich mit der adjuvansbeeinflussten Diffusion der für Wirkstoffe modellhaften organischen Substanz CNP in Candelilla- und Carnaubawachs. Mittels ATR-FTIR

wurden Diffusionskinetiken nach Adjuvans-Behandlung aufgezeichnet, die alle auf der Grundlage des Fick'schen Modells vollständig erklärbar waren, einhergehend mit hohen Diffusionskoeffizienten von 10^{-14} bis 10^{-13} m^2 s^{-1}. Es ist offensichtlich, dass die in dieser Arbeit vorgestellten Diffusionskoeffizienten durchweg eine durch die Plastifizierung bedingte erhöhte CNP-Mobilität belegen. Darüber hinaus wurden CNP-Gleichgewichtskonzentrationen abgeleitet, aus denen Verteilungs- und Permeabilitätskoeffizienten bestimmt werden konnten. Signifikante Unterschiede zwischen Diffusionskoeffizienten (Mobilität) und Verteilungskoeffizienten (Löslichkeit) wurden zum einen in Abhängigkeit von den jeweiligen Wachsen und zum anderen in Abhängigkeit von den jeweiligen Adjuvantien festgestellt. Die CNP-Mobilität war in Candelillawachs nur nach Behandlung mit Methyloleat höher als in Carnaubawachs. Die Behandlung mit TEHP und AEs führte zu einer höheren CNP-Mobilität in dem polaren, von Alkylestern dominierten Carnaubawachs. Die Verteilungskoeffizienten hingegen waren nach der Behandlung mit Methyloleat sowohl in Candelilla- als auch in Carnaubawachs deutlich niedriger als nach der Behandlung mit TEHP oder AE. Es wurden Modelle für den CNP-Penetrationsmodus unter Berücksichtigung der jeweiligen Adjuvantien in den beiden untersuchten Wachsen entwickelt. Der Grund für die drastischen Unterschiede in der Wirksamkeit der Adjuvantien liegt wahrscheinlich im Ko-Penetrieren von Wasser, dem Hauptbestandteil der auf dem Feld angewandten Spritzformulierungen. Insbesondere die untersuchten AEs begünstigten eine enorme Wasseraufnahme in beiden Wachsen mit zunehmendem Ethoxylierungsgrad. Überraschenderweise wurde dieser Effekt auch für das lipophile TEHP in beiden Wachsen gefunden. Dies führte zu der Vermutung, dass die AI-Permeabilität nicht ausschließlich durch die adjuvansinduzierte Plastifizierung bestimmt wird, sondern auch von einer "sekundären Plastifizierung" abhängt, die durch die Ko-Penetration von Wasser induziert wird und so zur Quellung und drastischen Destabilisierung der kristallinen Wachsstruktur führt.

Die erfolgreiche Etablierung der vorgestellten ATR-FTIR-Methode stellt einen Meilenstein für die Untersuchung der Diffusionskinetik von Adjuvantien und AIs in kutikulären Wachsen dar. Insbesondere die gleichzeitig nachweisbare Wachsmodifikation und darüber hinaus die bestimmbare Wasseraufnahme bilden eine perfekte Grundlage, um das ATR-FTIR-System als universelles Screening-Tool für Wachs-Adjuvans-AI-Wasser-Interaktionen in der Pflanzenschutzwissenschaft zu etablieren.

Abbreviations

2.4 DB	4-(2,4-dichlorophenoxy) butyric acid
^{2}H-NMR	deuterium nuclear magnetic resonance spectroscopy
AE	alcohol ethoxylate
AFM	atomic force microscopy
AI	active ingredient
ATR	attenuated total reflection
BSTFA	n,o-bis-(trimethylsilyl) trifluoroacetamide
C12E2	diethylene glycol monododecyl ether
C12E4	tetraethylene glycol monododecyl ether
C12E6	hexaethylene glycol monododecyl ether
CM	cuticular membrane
cmc	critical micelle concentration
CNP	4-cyanophenol
D_2O	deuterium oxide
DSC	differential scanning calorimetry
EO	ethylene oxide monomer
ESR	electron spin resonance spectroscopy
FID	flame ionization detector
FTIR	Fourier-transform infrared spectroscopy
GC	gas chromatography
Ge	Germanium
HPB	heptyl parabene
HLB	hydrophilic-lipophilic balance
IR	infrared spectroscopy
LCL	lower confidence interval
LEI	lower secondary electron image
MeO	methyl oleate
MIR	mid-infrared spectroscopy
MoA	mode of action
MS	mass spectrometry

Abbreviations

MX	chloroform treated membrane/matrix
PAN	polyacrylonitrile
PE	polyethylene
PET	polyethylene terephthalate
PP	polypropylene
PVA	polyvinyl alcohol
PXD	pinoxaden
RH	relative humidity (%)
RI	refractive index
SEM	scanning electron microscopy
Si	Silicon
TBP	tri-n-butyl-phosphate
TEHP	tris(2-ethylhexyl) phosphate
UCL	upper confidence interval
UDOS	unilateral desorption from the outer surface
VLCA	very long-chain aliphatic compound
XRD	x-ray diffraction
ZnSe	Zinc selenide

1 Introduction

1.1 The plant cuticle

In the course of land invasion around 460 million years ago, plants had to get used to completely new environments and habitats. One of the most important steps for the acclimatization to land was developing the so called “plant cuticle” (Riederer and Müller, 2008). The plant cuticle is described as a thin morphological layer which covers all aerial organs of higher land-living plants (Martin and Juniper, 1970). It is the outermost layer that separates the interior of the plant from its mostly dry environment. The cuticle acts as multifunctional barrier and possesses several properties which makes it suitable as the outermost layer to the plants surrounding environment. One of the most important features might be the effective barrier to prevent the plant from desiccation and water loss (Riederer and Schreiber, 2001). Besides being the main barrier against desiccation, the cuticle protects the plant from the uptake of organic compounds, such as pesticides (Riederer and Schönherr, 1985). Other important properties of plant cuticles are the UV-radiation attenuation and the prevention of intense adhesion of dust particles and pollen (Krauss *et al.*, 1997; Holmes and Keiller, 2002; Kunst *et al.*, 2005). Stability maintenance of the plant structural integrity is also provided by the cuticle (Bargel *et al.*, 2006; Shepherd and Wynne Griffiths, 2006). On the one hand it is flexible enough to brave weather conditions like strong winds, precipitation and leaf-to-leaf contact, but on the other hand it is sturdy enough to keep the integrity of the plant structure intact. Additionally, the plant cuticle prevents organ fusion and constitutes a mechanical barrier in terms of host-pathogen interaction (Kolattukudy, 1985; Tanaka and Machida, 2008; Smirnova *et al.*, 2013; Serrano *et al.*, 2014).

Generally, the plant cuticular membrane (CM) can be divided in two different main layers. The first layer is the so called cutin matrix layer (MX), which is mainly composed of crosslinked C16 and C18 fatty acid esters traversed by polysaccharide strands (Heredia, 2003; López-Casado *et al.*, 2007; Fich *et al.*, 2016). The second layer is mainly composed by solvent-soluble lipids, called cuticular waxes. These waxes can either be embedded in the cutin matrix (intracuticular waxes) or be overlaid on the cutin matrix (epicuticular waxes) (Jeffree, 1996). Recent studies showed exclusively the intracuticular wax fraction building up the transpiration barrier (Jetter and Riederer, 2016; Zeisler and Schreiber, 2016; Zeisler-Diehl *et al.*, 2018). A more detailed model for the plant cuticle architecture is given by Bird (2008), which describes the CM as a

two-compartment system harboring the cuticular layer, and the cuticle proper (Figure 1) (Bird, 2008). In this model, the cuticle layer is mainly composed of cutin and is attached to adjacent epidermal cells of the plant cell wall, whereas the cuticle proper almost exclusively consists of cutin with embedded intracuticular waxes (Jeffree, 1996). Most plant cuticles of different species additionally possess epicuticular wax films, sometimes even with above situated epicuticular wax crystals terminating the plants outer surface (Jeffree, 1986; Barthlott *et al.*, 1998).

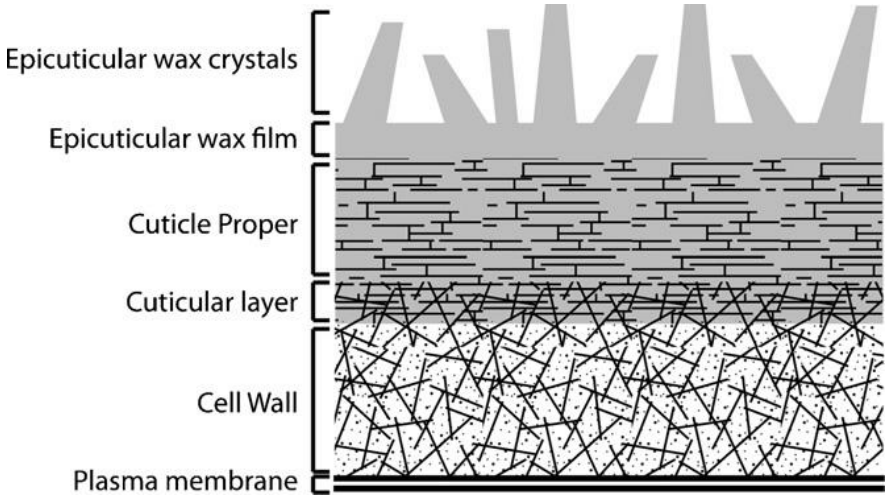

Figure 1. Schematic cross section of the plant cuticle and adjacent fractions (Bird, 2008).

The thickness of CMs differs greatly from species to species. Reported values range from 20 nm (*Arabidopsis thaliana*) for leaves up to 30 µm (*Malus domestica*) for fruits (Schreiber and Schönherr, 2009). Since diffusional pathways for water and organic solutes can be longer than the cuticle thickness, correlations of cuticle thickness with permeability and transpiration rates have failed up to now (Schreiber and Riederer, 1996b; Riederer and Schreiber, 2001; Schuster *et al.*, 2016; Bueno *et al.*, 2019).

Early studies have shown that the barrier properties of CMs are almost exclusively established by cuticular waxes and not by the cutin matrix (Schönherr, 1976; Riederer and Schönherr, 1985). The chemical composition of these waxes is strongly species dependent, respectively (Jetter *et al.*, 2008). One major group of wax constituents are cyclic components like pentacyclic triterpenoids, aromatics, tocopherols and sterols. However, recent studies have shown that the cyclic wax fraction, does not contribute to the waxy barrier of cuticular waxes against organic compound uptake (Vogg *et al.*, 2004; Jetter and Riederer, 2016; Staiger *et al.*, 2019). To elucidate the role of cyclic components in cuticular waxes several attempts have

been performed. Cuticular triterpenoids were postulated to act as nano-fillers to increase cuticular stability (Tsubaki *et al.*, 2013). Besides, it was hypothesized that cyclic compounds inhibit thermal expansion of cutin what consequently would lead to mechanical damage of the cuticular barrier (Schuster *et al.*, 2016). Furthermore, triterpenoids possess antimicrobial properties, which might play a role in pathogen resistance for plants (Wolska *et al.*, 2010). However, there is no proof for the exact function of cyclic components in cuticular wax composition yet. The second major compound class of cuticular waxes is summarized as so called very-long-chain-aliphatic components (VLCAs) (Yeats and Rose, 2013; Jetter and Riederer, 2016). This group of constituents includes primary n-alkanes, n-alcohols, fatty acids and derivative molecules with chain lengths between 20 to 40 carbon atoms. Besides these compounds, long chain alkyl esters with higher carbon chain lengths up to 64 carbon atoms also belong to the group of VLCAs (Yeats and Rose, 2013). Recent studies showed this fraction exclusively contributing the barrier properties against organic compound penetration (Staiger *et al.*, 2019). However, no evidence of the contribution of individual VLCA components in the wax has been found so far. It has been postulated that bridging of multiple crystallites occurs when two VLCA fractions exist in a wax that have a minimum difference in their average chain length of 10 carbon atoms. This is assumed for example, in the wax of *Phoenix dactylifera*, which has a fraction with an average chain length of 31.3 carbon atoms and a fraction with an average chain length of 51.3 carbon atoms, which is mainly dominated by long-chain alkyl esters (Bueno *et al.*, 2019).

To gain a deeper knowledge on how aliphatic constituents act as main barrier against cuticular penetration, relations of chemical and structural properties need to be analyzed in detail.

1.2 Molecular structure and barrier properties of cuticular waxes

On a molecular level, cuticular waxes consist of at least three distinct regions with different degrees of order and composition (Riederer and Schreiber, 1995). A schematic diagram of the molecular structure of plant cuticular waxes is given in (Figure 2).

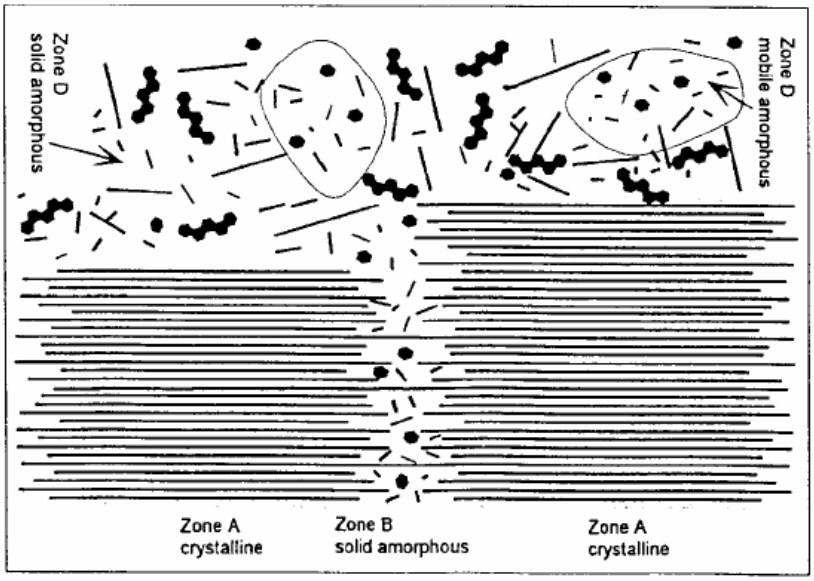

Figure 2. Schematic overview of the molecular structure of plant cuticular waxes (taken from Riederer & Schreiber, 1995).

Regarding transport properties for water and organic solutes, the crystalline fraction of cuticular waxes (zone A) ist the most important one (Fox, 1958). The middle portions of long aliphatic chains are regularly aligned here. X-ray diffraction (XRD) studies hypothesized that long hydrocarbon chains of VLCAs are assembled in an orthorhombic crystal lattice transforming into a hexagonal crystal state at elevated temperatures just below the respective melting point (Basson and Reynhardt, 1988; Reynhardt and Riederer, 1991). Inaccessible structures like platelets or flakes are formed within crystalline wax structures (Riederer and Schreiber, 1995). VLCAs in cuticular waxes typically show species-dependent chain-length distributions. Consequently, parts of aliphatic constituents cannot be fully integrated into crystalline regions. Thus, protruding chain-ends, which might be functional groups like hydroxyls, carboxylic acids, methyl chain ends, etc., fill the space between two adjacent flakes of zone A, thereby forming the amorphous zone B (Sitte and Rennier, 1963; Riederer and Schreiber, 1995). NMR studies could show that, in contrast to zone A, zone B has a much higher degree of motional freedom. Components might not be incorporated neither in zone A nor in zone B, because of steric reasons (e. g. cyclic compounds) or by their low melting point, thereby forming the amorphous zone D. This zone can partly be solid amorphous and also be liquid amorphous at elevated temperatures, filling the voids between chain ends located in amorphous zone B. Additionally zone D may form clusters outside of zone B, consequently harboring larger molecules like cyclic components (Riederer and Schreiber,

1995). To complete the various possible wax zones, Zone C must also be mentioned. This zone only occurs in synthetic Fischer-Tropsch waxes and represents amorphous areas as well as defects within crystalline zone A (Lourens and Reynhardt, 1979). To the authors knowledge, there are no hints for zone C existing in cuticular waxes so far (Riederer and Schreiber, 1995). Due to steric reasons or low solubilities of small molecules, the crystalline zone A is almost inaccessible for inorganic solutes, organic compounds as well as for adjuvants and active ingredients (Ais) of pesticide mixtures. Therefore, penetration of these compounds is almost exclusively known to take place in amorphous zones B and D (Riederer and Schreiber, 1995).

1.3 Transport mechanisms across the plant cuticle

Besides limiting diffusion of water, the plant cuticle also allows organic compounds like pesticide molecules to permeate into the plant (Riederer and Schreiber, 1995). Minerals, nutrients and other small molecules can either penetrate the cuticle as leachates or by transpiration (Tukey Jr, 1970; Burghardt and Riederer, 2008). Polar organic molecules and non-electrolytes like agrochemicals may enter the plant via different cuticular pathways (Riederer and Schreiber, 1995). These pathways have extensively been discussed in the last decades. On the one hand, the hydrophilic route is described to enable penetration of small ionic and water-soluble molecules across polysaccharide strands traversing the cuticle, but on the other hand, most non-electrolytes, such as agrochemicals have lipophilic properties, which make them suitable for the lipophilic pathway to enter the plant (Jeffree, 1996; Popp *et al.*, 2005; Schreiber, 2005).

One of the most straightforward cases of non-electrolyte uptake into the cuticle is from an aqueous donor solution. These solutions may be derived from rain, fog, dew or released from arthropods or fungi onto the plant surface (Hess, 1999). Besides that, non-electrolytes may also be deposited onto the plant surface in the solid state, e.g. as atmospheric particulate matter or derived from antennae, feet or eggs of arthropods (Hess, 1999). When a non-electrolyte is deposited onto the plant surface, transport across the plant cuticle occurs.

The transport of lipophilic non-electrolytes across the plant cuticle can be described as a simple diffusion process along a gradient of chemical potential, where the cuticle behaves like a solution-diffusion membrane (Riederer and Schreiber, 1995). Diffusion across this membrane is described as a three-step process. First, the permeating molecule is absorbed by the cuticle, then penetrates across the cuticle by simple diffusion and is finally desorbed at

the opponent cuticle interface (Vieth, 1991). Under the assumption that the main transport limiting barrier for the uptake of non-electrolytes is established by cuticular waxes, all barrier-limiting steps in non-electrolyte transport and diffusion must be strongly connected to the molecular and physical nature of cuticular waxes. The organic compound penetration across semicrystalline cuticular waxes is mostly explained by the “brick and mortar” model shown in Figure 3 (Reynhardt and Riederer, 1991; Riederer and Schreiber, 1995; Merk *et al.*, 1997).

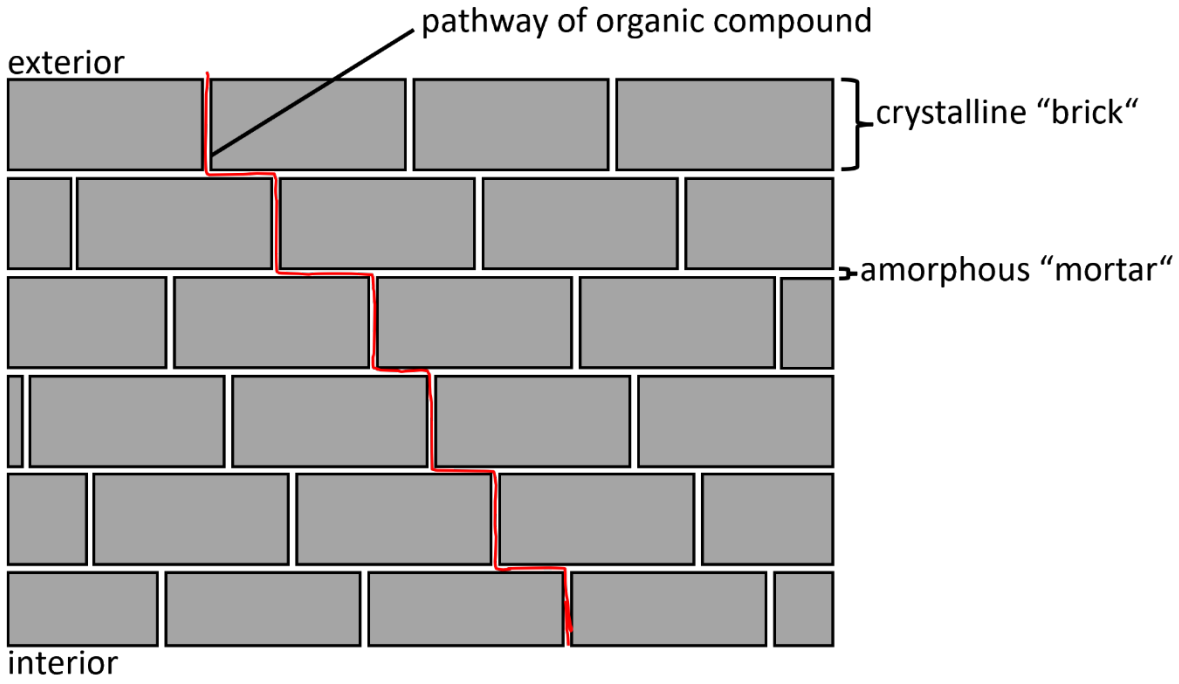

Figure 3. Illustration of the non-electrolyte transport across a semicrystalline cuticular wax according to (Riederer and Schreiber, 1995). Crystalline "bricks" represent regularly aligned impermeable crystalline domains, whereas amorphous “mortar” represents amorphous domains. Organic compound penetration (red line) is restricted to the amorphous domain.

Lipophilic compounds are only able to permeate the cuticular wax within its amorphous domains (zone B and D; see 1.2), whereas the crystalline wax fraction is inaccessible for non-electrolyte penetrants (zone A; see 1.2). Crystalline flakes in the wax are mainly responsible for a certain level of tortuosity, which consequently leads to an elongated pathway, compared to the actual thickness of the wax layer (Baur *et al.*, 1999). Several investigations have demonstrated that the solute permeability is strongly dependent on the amount and on the lateral arrangement of these flakes within cuticular waxes (Cussler *et al.*, 1988; Riederer and Schreiber, 1995). Furthermore, the amount and the spatial, like as the crystalline arrangement of these flakes strongly depend on the waxes aliphatic chain length distribution. Pure aliphatic compounds with no chain-length distribution only build crystalline zone A, while amorphous

zone B does not exist. Extending the chain-length distribution consequently leads to an increase of the amorphous Zone B, and therefore alters the ratio of crystalline and amorphous domains within the cuticular wax, leading to higher motional freedom and penetration rate for non-electrolytes (Riederer and Schreiber, 1995). Another aspect to be considered in terms of wax barrier properties is temperature. At room temperature the crystalline flakes representing zone A are regularly aligned in an orthorhombic manner, but with increasing temperature transition to the crystalline hexagonal and finally to the liquid state occurs (Reynhardt and Riederer, 1991, 1994; Ensikat *et al.*, 2006). Simultaneously, zones B and D only show one phase transition from amorphous to liquid state (Riederer, 1990). Consequently, the ratio of crystalline and amorphous volume fraction of cuticular waxes is drastically altered when temperature is increased, leading to decreasing tortuosity and less resistance against permeating solutes.

1.4 Theoretical background of cuticular transport

To comprehensively understand the transport mechanisms of non-electrolytes through the plant cuticle, the physical properties of the transport process as well as of the penetrating substance need to be considered. Under steady-state conditions Fick's first law relates the diffusive flux *J*, which is the amount of diffused mass per unit area and concentration,

$$J = -D\frac{\Delta c}{\Delta x} \tag{1}$$

where *D* is the diffusion coefficient and *Δc* is the difference in non-electrolyte concentration depending on the travelled pathlength *Δx*. Thereby, the flux goes from higher to lower concentration of the substance, which simply means solutes diffuse from high to low concentrations. The flux of a substance across a plant cuticle is described by,

$$J = P(c_{donor} - c_{receiver}) \tag{2}$$

where C_{donor} and $C_{receiver}$ are the concentrations at the inner and the outer CM side. When transport across a CM is characterized, the mass transfer coefficient called permeance *P* as a measure of velocity must be considered.

$$P = \frac{KD}{L} \tag{3}$$

Thereby, permeance of homogeneous membranes is directly correlated to the fundamental transport parameters of solubility *K* (partition coefficient), mobility *D* (diffusion coefficient) and the pathlength of diffusion *L* (thickness of the membrane). While permeance is a useful

parameter to describe cuticular penetration, its usefulness is limited for comparison of cuticular membranes differing in membrane thickness. Instead, the permeability coefficient *p* is a useful measure, only relating mobility and solubility without considering respective pathlengths, reflecting a material specific property.

$$p = KD = PL \tag{4}$$

Unfortunately, Fick's first law is only valid for homogenous membranes, which means with respect to the pathlength heterogeneity of CMs including barrier-responsible cuticular waxes, all above mentioned models to describe non-electrolyte transport across the cuticle are only partly applicable (Schönherr and Riederer, 1988).

To elucidate a substance specific solubility, the octanol/water partition coefficient K_{ow} is used. K_{ow} relates the equilibrium concentrations of a non-electrolyte in a boundary phase system consisting of the highly lipophilic n-octanol ($c_{octanol}$) and water (c_{water}) (5), solely being dependent on the substance specific lipophilicity (Sangster, 1997).

$$K_{ow} = \frac{c_{octanol}}{c_{water}} \tag{5}$$

A partition coefficient of 1.0 represents an equally distributed substance in both phases, whereas partition coefficients < 1 are found for water-soluble substances and partition coefficients > 1 are typical for rather lipophilic substances. Mostly K_{ow}-values are given in logarithmic scale as $logK_{ow}$. However, in plant research not the octanol/water coefficient, but mostly the cuticle/water partition coefficient K_{cw} or the wax/water partition coefficient K_{ww} is considered to describe partitioning. While K_{cw} values have shown to be very similar numerically to K_{ow} values, K_{ww} values were shown to be significantly lower by factors varying between 2 and 10 (Schreiber and Schönherr, 1992; Kirsch *et al.*, 1997; Burghardt *et al.*, 1998; Burghardt *et al.*, 2006). This might be explained by the fact that cuticular waxes form solid and partially crystalline aggregates, which in comparison to the amorphous cutin and liquid n-octanol offer only a few sorption sites for non-electrolytes (Schreiber, 2006). Wax-water partition coefficients of different non-electrolytes measured in reconstituted cuticular waxes ranged from 3.5 to 3500 (Schreiber, 2006).

Nonetheless, not only the characterization of non-electrolyte partitioning, but also investigating the impact of non-electrolyte mobility is crucial for determining permeability coefficients. To date, there is only one study, where the authors tried to calculate diffusion coefficients of water in CM, but no studies to elucidate mobilities of non-electrolytes in CM are available so far (Becker *et al.*, 1986). When Becker *et al.* (1986) calculated *D*, they used the

CM weight average thickness, but as already stated above, barrier properties of the CM are almost solely established by cuticular waxes. Consequently, calculation of *D* with thicknesses of whole CMs lead to overestimated diffusion coefficients. Furthermore, as already mentioned, CMs are very heterogeneous systems with unevenly distributed wax layers. Consequently, severe inconsistencies may be apparent when calculating thickness dependent diffusion coefficients (Schreiber and Schönherr, 2009).

To overcome these drawbacks in calculating *D*, several studies have been performed using reconstituted and evenly distributed cuticular waxes instead of isolated CMs (Schreiber and Schönherr, 1993; Schreiber, 1995; Schreiber and Riederer, 1996a; Kirsch *et al.*, 1997; Burghardt *et al.*, 1998; Burghardt *et al.*, 2006), which will be discussed in later sections.

1.5 Adjuvants and their Mode of Action (MoA)

Agrochemicals like AIs are supposed to reach their right target site, when applied to plants. Several MoA are known for different AIs. They can either stay at the plant surface or can also be equally distributed inside the plant to reach their specified target site (Stoytcheva, 2011). To circumvent uncontrolled environmental pollution, AIs are usually applied as formulations, which are mostly designed as complex mixtures of several substances. The composition of formulations strongly influences the physical properties of the AI, for example regarding the solubility or enhancing effects of foliar uptake. Adjuvants, as part of formulations, are described to have the most improving effects on agrochemical applications (Green, 2000). An adjuvant is any compound that can be added to a pesticide formulation in order to facilitate the mixing, application or the effectiveness of the respective AI (Tu *et al.*, 2001). Unfortunately, to date there is no comprehensive standard system to classify adjuvants, but however, several classification approaches in terms of terminology or chemistry have been established so far (Hazen, 2000; Cronfeld *et al.*, 2001).

Regarding their function and usage, adjuvants can be divided into two different categories (Kirkwood, 1994). The American society for testing and materials gave a more extensive classification for adjuvants and separated them into utility and activator adjuvants (Hazen, 2000). The former is defined as so called spray modifiers. Hence, this group of adjuvants is classified as modifiers for physical interactions of the AI with the plant cuticle surface like altering wetting, spreading or sticking properties of the pesticide (McMullan, 2000). The latter embraces activators, which are known to enhance the biological efficacy of the AI (Penner,

2000). In plant science, activator adjuvants may also be termed as accelerators, or plasticizer adjuvants which enhance the uptake of an AI into the plant by modifying the waxes physical properties somehow (Schönherr, 1993b, a; Schreiber, 2006). A simplified model of the plasticizing impact of adjuvants on the AI penetration pathway is shown in Figure 4.

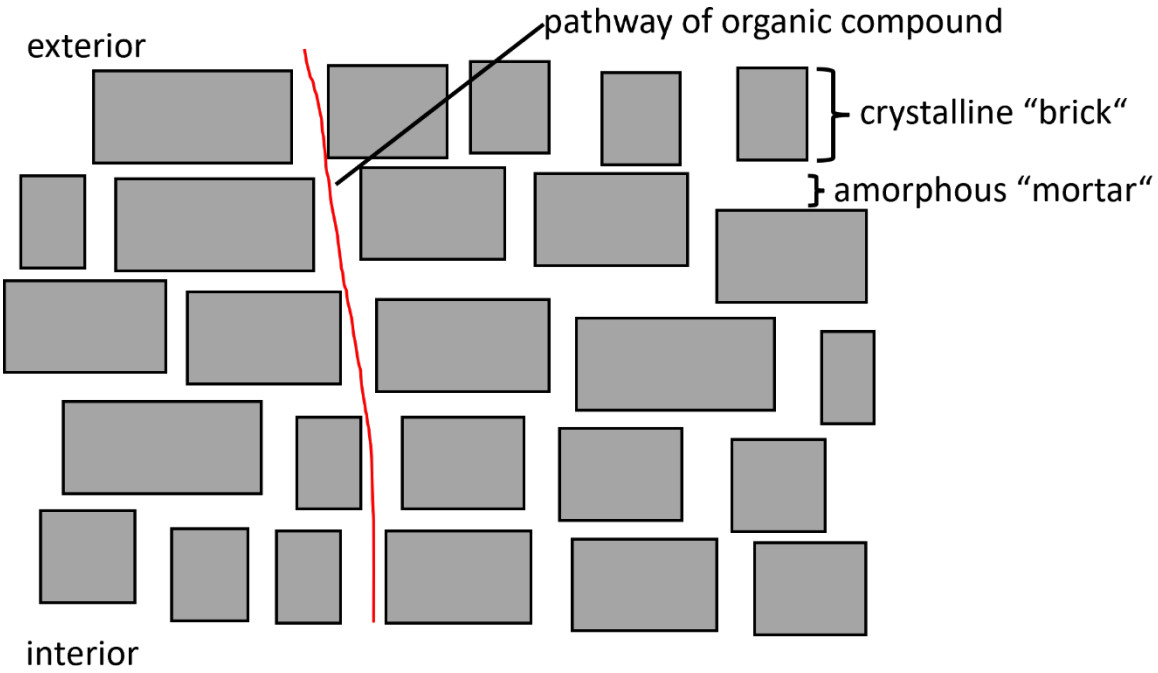

Figure 4. Illustration of the “brick and mortar” model of irregularly aligned crystallites in cuticular wax after adjuvant induced plasticization. The less tortuous pathway facilitates organic compound uptake, thereby increasing compound permeation across the waxy barrier.

Probably the most common group of activator adjuvants are surface active agents, also called surfactants (Penner, 2000). Although surfactants are mostly associated with activator properties, they may also be defined as utility agents having the ability to affect surface tension properties of pesticide formulations, thereby altering and facilitating the emulsifying, dispersing, spreading, sticking and wetting properties of pesticide formulations (Hess, 1999).

1.5.1 Surfactants

Surfactant molecules often contain a lipophilic long chain hydrocarbon chain as well as a hydrophilic polar group, which can either be charged (positive, negative, zwitterionic) or be of nonionic nature (Kirkwood, 1993). Due to their hydrophilic and lipophilic properties, surfactants may interact with the lipophilic plant surface and lipophilic pesticides as well as with hydrophilic herbicides and water. Therefore, surfactants are mostly allocated a “hydrophilic-lipophilic balance” value (HLB) (Griffin, 1954). Compounds of low HLB are well

soluble in lipophilic environments, whereas surfactants of high HLB are more soluble in water (Kirkwood, 1993). A surfactant's HLB therefore indicates the conditions under which the surfactant will perform best.

As already mentioned, an important aspect of surfactants is the reduction of surface tension for a specific pesticide formulation to increase the contact between the spray droplet and the cuticular surface. Surfactants show a characteristic behavior when dissolved in water. At low concentrations they accumulate at the air/water interface, which results in a decrease of the surface tension of water and that is why wetting of hydrophobic surfaces, like CMs gets enhanced. Additionally, surfactants show a typical phenomenon at the further described critical micelle concentration (cmc). With increasing surfactant concentration in water, surfactant molecules build aggregates and form micelles within the aqueous solution (Schick, 1987). Below the cmc, surfactants are dissolved as monomers, but as soon as the concentration in the aqueous solution reaches the cmc, all further added molecules tend to form micelles. Consequently, the concentration of surfactant monomers in the aqueous solution remains constant, irrespective of the amount of surfactant added (Schreiber, 1995). Many surfactant effects are encountered at aqueous concentration exceeding the cmc by far. Consequently, the MoA of surfactants are not only limited to surface tension reducing effects (Hess, 1999). Therefore, surfactants do not only manipulate physical surface properties of pesticide formulations. They may also positively affect the absorption of pesticides into the cuticle by modifying its wax characteristics. Unlike polydisperse AEs, monodisperse AEs are chemically pure compounds. For this reason, they are more adequate to study plasticizing effects on cuticular transport (Schönherr, 1993b, a; Riederer *et al.*, 1995; Burghardt *et al.*, 1998; Burghardt *et al.*, 2006) Monodisperse AEs consist of a lipophilic long-chain fatty alcohol with differing numbers of carbon atoms, and additionally a polar head with a variable amount of ethylene oxide units (EO) (-O-CH_2-CH_2-), while both units are interconnected via ether bonds (Figure 5).

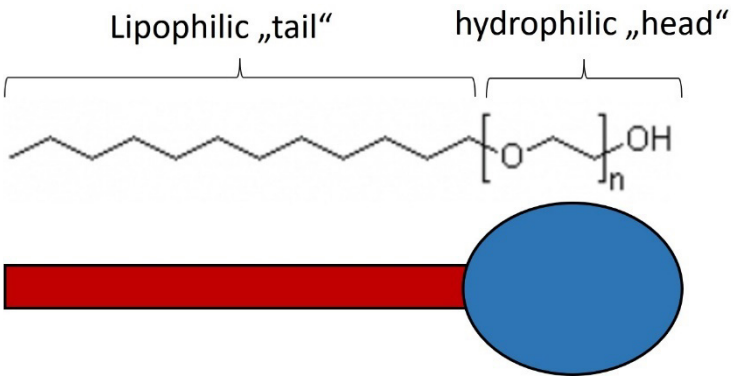

Figure 5. Illustration of an alcohol ethoxylate molecule, contributing a lipophilic "tail" of repeated ethylene groups and a hydrophilic head, contributing repeated ethoxylate units.

It was shown that the penetration level into and across the plant cuticle is dependent on the EO content. Coret *et al.* (1993) hypothesized permeation into the cuticle is highest for AEs with low EO content, while surfactants with high EO content increase the hydration state of the cuticle at a given relative humidity (RH) (Coret and Chamel, 1993; Coret and Chamel, 1995). It is obvious, that an increased hydration state of the cuticle may increase the diffusion of water and water-soluble AIs through the cuticle. Concerning the question, how surfactants with differing EO content lead to increased permeation of lipophilic AIs, Coret and Chamel used a differential scanning calorimetry (DSC) approach. They could show that waxes tended to have lower melting temperatures after surfactant absorption. Therefore, they hypothesized an increase in wax fluidity, which would lead to increased diffusion rates for lipophilic substances across the plant cuticle (Coret and Chamel, 1994; Coret and Chamel, 1995). Further evidence for unspecific plasticization effects of AE on cuticular waxes was gained with the aid of ESR- and ^{2}H-NMR experiments (Schreiber *et al.*, 1996b; Schreiber *et al.*, 1997).

As recent studies have hypothesized, not only the crystallinity of the wax is reduced by adding plasticizers, but at the same time the amorphicity of the wax is also increased (Fagerström *et al.*, 2014; Zhang *et al.*, 2016). Staiger *et al.* (2019) could show the same effects of AE on cuticular wax of *Schefflera elegantissima* (Staiger, 2022). Apart from the group of surfactants, there is another widely used group of accelerating adjuvants, which will be discussed in the next section.

1.5.2 Oils and oil derivatives

Besides surfactants, which are commonly used in pesticide formulations, oils or oil derivatives, are added to tank mixtures. All oil adjuvants are commonly highly hydrophobic. Therefore,

when an oil is used as admixture for aqueous pesticide formulations, a surfactant emulsifier must be added to satisfactorily distribute the solution to a uniformly mixed emulsion (Tu and Randall, 2003). The addition of surfactants to oil adjuvant mixtures does not only emulsify the oil in water-based spray solutions, but also lower the surface tension of the pesticides, which consequently leads to better retention and spreading on the plant surface (Gauvrit and Cabanne, 1993; Miller and Westra, 1998; Tu and Randall, 2003). In addition, oil adjuvants can be used as transporters to carry synthetic pesticides through the cuticle into the plant, primarily exhibiting plasticizing properties (Manthey *et al.*, 1989; Gauvrit and Cabanne, 1993; Santier and Chamel, 1996; Hess, 1999).

In agriculture treatment several oil classes like vegetable seed oil, petroleum oils or esterified seed oils are used as adjuvants (Miller and Westra, 1998). First evidence of using petroleum oils as adjuvants for pesticide formulations to enhance pesticide spreading properties was given very early (Saunders and Lonnecker, 1967). Later studies investigating petroleum oil as adjuvant showed a distinct surface tension decrease, increased wetting behavior and accelerated AI absorption (Bohannan and Jordan, 1995). Furthermore, petroleum oils can smooth epicuticular waxes and cause cuticle cracks, which consequently results in higher AI penetration rates (Foy and Smith, 1969). Within each type of petroleum oil, the composition can vary in molecular size, purity and viscosity (Krenek and King, 1987).

In contrast to petroleum oils, vegetable oils - also called seed oils consist of triglycerides and do not derive from fossil sources, but mostly from crop plants. They show wide variation in terms of fatty acid composition and chain length distribution (Hamilton, 1993). Like as petroleum oils, vegetable oils also decrease surface tension properties, but even though vegetable oils show great potential as additives in pesticide solutions, today's focus on oil adjuvants in agrochemistry lays on oil derivatives like esterified seed oils. Esterified seed oils are mostly formed by hydrolysis of seed oils into glycerol and fatty acids. The derived fatty acids are then esterified with alcohols, like methanol or ethanol, resulting in methyl- or ethyl esters such as methyl- or ethyl oleate (Nalewaja, 2002).

In comparison to seed oils, methylated seed oils comprise lower viscosity and exhibit better wax disrupting properties, while both characteristics may influence droplet spreading, retention and pesticide penetration (Nalewaja, 2002). One study investigated the influence of all three mentioned oil- and oil derivative types on cuticular penetration. Thereby, it was observed that the uptake of the AI primisulfuron was two-fold increased in combination with

methylated seed oils in contrast to petroleum oil (Bruce *et al.*, 1993). Furthermore, the absorption of the AI nicosulfuron was more increased in combination with methylated seed oils than with vegetable oil and petroleum oil (Nalewaja, 2002). It is assumed that methylated oil derivatives like methyl or ethyl oleate influence the cuticular wax structure and act as plasticizers (Hazen, 2000). One study hypothesized oil derivatives leading to severe liquefaction of cuticular waxes (Gauvrit and Cabanne, 1993). Another study could show a decrease of enthalpy of transition using DSC and decreasing crystallinity in cuticular wax modelling tristearin (Webster *et al.*, 2018). Staiger (2019) investigated the impact of methyl oleate on the waxy barrier. DSC and FTIR were used to evaluate the impact of methyl oleate on artificial cuticular model waxes as well as on cuticular wax of *Schefflera elegantissima*. With DSC, phase transitions from orthorhombic to hexagonal state were observed at lower transition enthalpy, which was interpreted as plasticization (Staiger, 2022).

1.5.3 Organophosphate esters

The third group of investigated accelerators used to enhance AI uptake into the plant are organophosphate esters. Tributyl phosphate (TBP) was repeatedly shown to act as plasticizing agent, which enhanced diffusion of 4-(2,4-dichlorophenoxy)butyric acid (2,4-DB) in cuticles across isolated cuticles of *Stephanotis floribunda* leaves and furthermore significantly reducing the activation energy of diffusion (Schönherr *et al.*, 2001; Shi *et al.*, 2005b). Besides TBP, the built-in accelerator Tris(2-ethylhexyl)phosphate (TEHP) was shown to substantially accelerate uptake rates of the herbicide pinoxaden both in wheat and barley leaves (Muehlebach *et al.*, 2011). However, TEHP did not increase desirable retention and spreading of pinoxaden but strongly enhanced the diffusion of PXD across isolated *Prunus laurocerasus* cuticular membranes (Arand *et al.*, 2018). Due to the low information density of TEHP-induced uptake acceleration of lipophilic AIs, further studies are needed to classify more precisely the influence on the wax structure and MoA of TEHP.

1.6 Basic methodologies used within this thesis

1.6.1 Fourier-transformed Infrared spectroscopy (FTIR)

Infrared spectroscopy (IR) is a widely used analytical method based on the interaction of infrared radiation with molecular functional groups. IR can be divided in near, -mid and -far infrared spectroscopy, each method offering different spectral ranges and associated

excitation energies. Especially mid infrared spectroscopy (MIR) is used in organic compound analysis, since its IR radiation between 2.5 nm and 15 nm wavelength induces most of organics specific functional group vibrations (Günzler and Gremlich, 2012). Several experiments characterizing the structural features of plant cuticle have already demonstrated the suitability of FTIR as a universal analytical tool in plant biology (Johnson *et al.*, 2007; Heredia-Guerrero *et al.*, 2014; Leide *et al.*, 2020; Liu *et al.*, 2020; Diarte *et al.*, 2021). The most important prerequisite for the interaction of IR radiation with molecular functional groups is a given intramolecular dipole moment, which only occurs if charge distribution is asymmetrical due to the vibrational atomic movement (Günzler and Gremlich, 2012). Depending on the respective dipole moment intensity, different intensity ratios of the molecular vibrations within a substance can be observed, which enables qualitative substance characterization. Inducing functional group vibrations largely depends on the respective wavelength of the IR radiation and the excitation energy associated with it. The molecular vibration modes of an exemplary -CH_2 functional group are given in Figure 6.

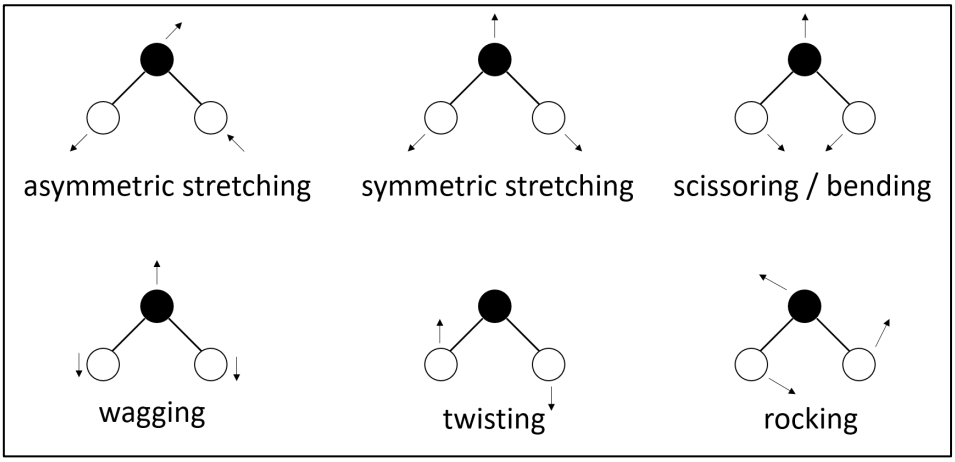

Figure 6. IR-induced vibration modes of CH_2 functional groups. Black circles represent C-atoms, whereas white circles show H-atoms and arrows indicate atomic movement directions within CH_2 functional groups.

In IR spectroscopy, usually not the wavelength, but rather its reciprocal, namely the wavenumber (cm^{-1}) is used as dimensional unit. An overview of relevant molecular vibrations with their respective ordinary wavenumber range is given in Figure 7**.**

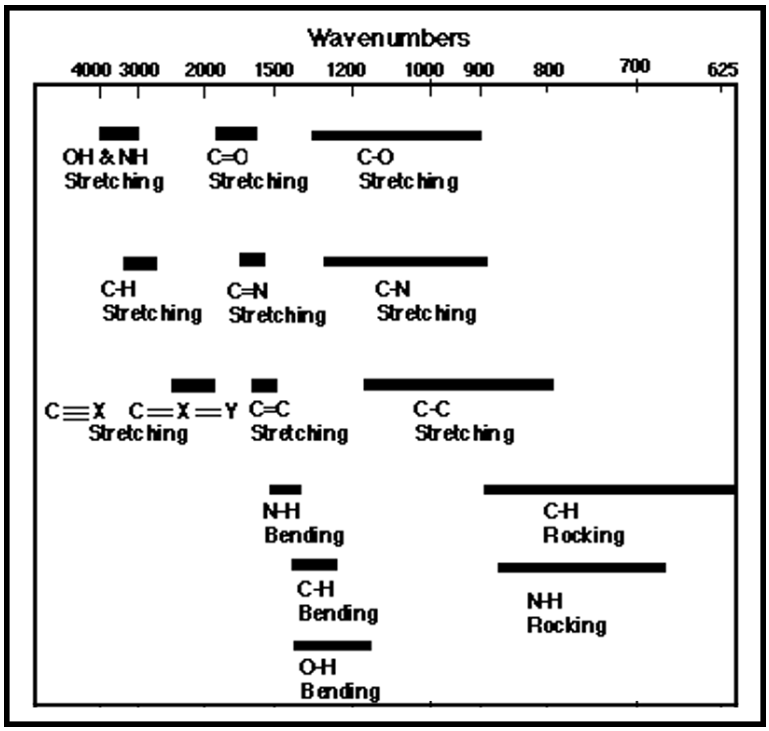

Figure 7. Typical molecular vibrations of organic functional groups and corresponding wavenumbers of absorbed IR-radiation. From (Günzler and Gremlich, 2012).

It can be seen that most vibration modes occur in the wavenumber region between 1500 and 625 cm^{-1}, also called the "finger print" region. The term fingerprint region is derived from the fact that respective intensities of specific bands in this region are unique for each substance, like the unique fingerprint of each human. However, discriminating analysis of single bands within the fingerprint region is difficult, since mostly strong overlapping of functional group vibrations occurs. In contrast to that, vibration modes occurring in the range of 2000 to 4000 cm^{-1} are mostly separated, which opens a way of characterizing single bands without interference.

An IR spectrum can be visualized as a function of the intensity of transmitted infrared light *I* versus the wavenumber of emitted infrared light. Thereby, transmittance *T* is described as

$$T = \frac{I}{I_0} = 10^{-abc} \tag{6}$$

where, I_0 is the monochromatic radiation intensity of emitted light, *a* is the substance specific absorption coefficient, *b* is the thickness of the measuring cell or the substance and *c* is the substance concentration. A decadic log transformation of *T* results in the respective substance-depending absorption *A* of emitted light,

$$A = log_{10}\frac{I_0}{I} = abc \tag{7}$$

giving a linear relationship of absorption and concentration according to the law of Lambert-Beer (Günzler and Gremlich, 2012) and thus enabling not only qualitative, but also quantitative substance analysis.

1.6.2 Attenuated Total Reflection Fourier-Transform Infrared-Spectroscopy (ATR-FTIR)

Nowadays, a common way of recording IR-spectra is via ATR-FTIR. It comprises substance specific surface information up to a specific penetration depth of the evanescent wave into the sample (Günzler and Gremlich, 2012). In contrast to transmission mode FTIR, also IR-impenetrable samples and substances with high IR-absorption can be analyzed (Günzler and Gremlich, 2012). An overview of the basic ATR-FTIR principles is given in Figure 8.

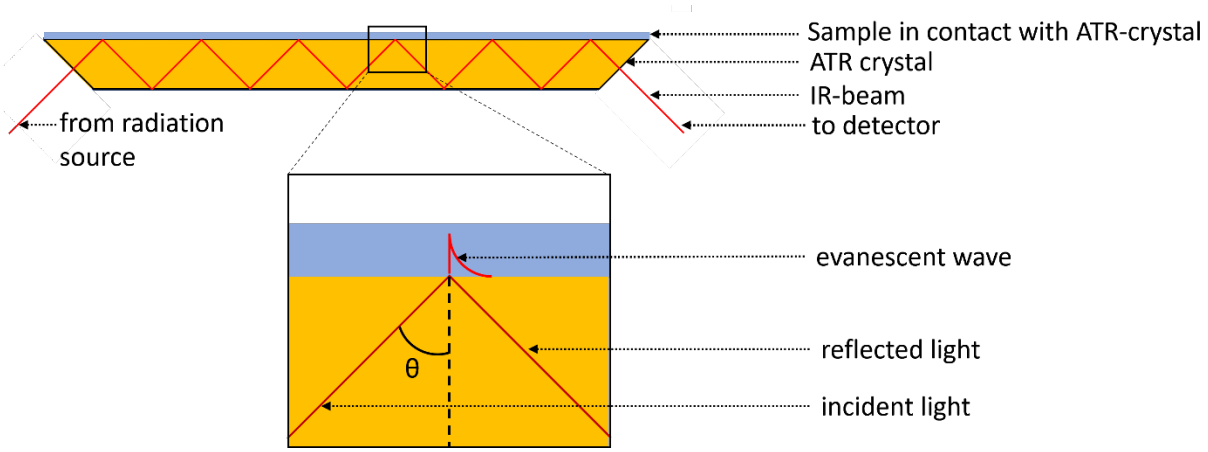

Figure 8. Schematic principle of ATR-FTIR, using a trapezoidal ATR crystal covered with a sample.

A sample is brought into intimate contact with an ATR crystal. Afterwards an IR-beam is generated and enters the ATR crystal. At the interface between the ATR crystal and the sample, total reflection occurs resulting in an evanescent wave penetrating the sample. The penetration depth d_p of the evanescent wave is defined as,

$$d_p = \frac{\lambda}{2\pi n_1 \sqrt{sin^2(\Theta) - (n_2/n_1)^2}} \tag{8}$$

where λ is the wavelength of the incident IR radiation, n_1 is the refractive index (RI) of the optically thicker medium (ATR crystal), n_2 refers to the RI of the optically thinner medium (sample) and Θ represents the incident angle of the IR-beam. Depending on the penetration depth d_p, different sampling rates can be achieved, consequently resulting in absorption

spectra with altered intensity values of respective vibration modes. d_p heavily depends on several factors. For example, d_p is influenced by the angle of incidence of the IR beam. An incident angle of 45° is commonly used, but smaller angles are also applied to achieve higher d_p values of the evanescent wave. Since the refractive index of a sample is usually constant, the respective crystal material used plays an important role. Higher penetration depths are achieved by using ATR crystals with low refractive indices, e.g. Zinc selenide (ZnSe; RI = 2.4), whereas lower penetration depths occur when using crystal materials with high refractive indices such as silicon (Si; RI = 3.4) or germanium (Ge; RI = 4.0).

Several studies characterizing CM or cuticular wax have been performed using ATR-FTIR, where the phase transition behavior and orthorhombic crystallinity of the wax have been studied in detail using the analysis of wax-specific functional groups. (Merk *et al.*, 1997; Ribeiro da Luz, 2006; Fernández *et al.*, 2011; España *et al.*, 2014; Heredia-Guerrero *et al.*, 2016; Bueno *et al.*, 2019). Phase transitions from solid to liquid state were indicated by sharp wavenumber shifts of symmetrical and asymmetrical CH_2 stretching vibrations corresponding to a transition from *all-trans* to *gauche* conformers of regularly aligned hydrocarbon chains within the waxes (Hastie and Roberts, 1994; Merk *et al.*, 1997). While early studies intuitionally derived midpoints of melting ranges empirically (Merk *et al.*, 1997), the midpoints of phase transitions were more elegantly determined by calculating midpoints obtained from fitting plots of wavenumber vs. temperature to a logistic equation (Patel *et al.*, 2001).

According to Zerbi *et al.* (1989), the determination of orthorhombic wax crystallinity may be achieved by relating the height ratios of the CH_2 scissoring or rocking doublet vibrations at either 1472 cm^{-1} and 1462 cm^{-1} or 730 cm^{-1} and 720 cm^{-1} (Zerbi *et al.*, 1989; Merk *et al.*, 1997).

Besides characterizing structural features via ATR-FTIR, a way was opened by Fieldson and Barbari (1993) to not only study static material properties, but instead to also use ATR-FTIR in a time-resolved manner to measure diffusion kinetics of small molecules in polymer membranes (Fieldson and Barbari, 1993). This approach aimed to determine sorption kinetics *in vitro* by determining the IR-absorption of a penetrant's specific functional vibration band, sorbed into an artificial membrane as a function of time (Fieldson and Barbari, 1993). Therefore, one side of a membrane polymer film was exposed to the respective penetrant, whereas the other side was in intimate contact with the ATR crystal. Spectra of diffusing penetrants were collected in real-time as the penetrants diffused towards the interface between polymer and the ATR crystal (Wang *et al.*, 2011a). Fieldson and Barbari investigated

water sorption in polyacrylonitrile (PAN) and observed sorption kinetics according to Fickian diffusion, consequently giving reliable diffusion coefficients (Fieldson and Barbari, 1993). Reported diffusion coefficients were in the same range as already reported values, determined by established methods like quartz spring balance sorption analysis (Stannett *et al.*, 1982), making this method quite reliable. Several other investigations based on the work of Fieldson and Barbari followed, since ATR-FTIR was also found to be suitable for substance diffusion analysis in pharmaceutics, dermatology and in polymer science. (Fieldson and Barbari, 1993; Pellett *et al.*, 1997a; Sammon *et al.*, 1998; Dias *et al.*, 2001; Moser *et al.*, 2001; Dias *et al.*, 2004; Döppers *et al.*, 2004; Pereira *et al.*, 2005; Dhoot *et al.*, 2009; Russeau *et al.*, 2009; Guo *et al.*, 2016; Santos *et al.*, 2017; Shahzad *et al.*, 2019). Mostly, penetration across artificial membranes or human skin was investigated, but since ATR requires intimate contact between the ATR crystal and the respective membrane substrate, several precautions had to be taken to gain satisfying absorption data. One study observed water diffusion in polypropylene (PP), using the hydrostatic pressure of the circulating penetrant to gain sufficient contact between PP and the ATR crystal. Santos *et al.* (2018) investigated water diffusion into polymethyl methacrylate and polyisobutylene (Santos *et al.*, 2017). To obtain satisfactory polymer adhesion on the ATR crystal they developed an anvil apparatus, which provided a constant pressure onto the fluid penetrant, consequently pressing the membrane polymer onto the ATR crystal (Santos *et al.*, 2017). However, polymerization or solidification of a substrate directly on an ATR crystal was found to be best for good adhesion. For this, especially spin coating showed to be suitable (Van Alsten and Lustig, 1992; Fieldson and Barbari, 1993; Sutandar *et al.*, 1994; Fieldson and Barbari, 1995; Yi *et al.*, 2002; Murphy *et al.*, 2003; Flavin *et al.*, 2006; Vasconcelos *et al.*, 2010).

1.6.3 Spin coating

Spin coating has proven to be very suitable to cast artificial membranes, whose liquid or solved precursors are coated onto the ATR crystal and only then polymerize, giving well adhering and equally distributed polymer layers of variable thickness (Fieldson and Barbari, 1993; Sutandar *et al.*, 1994; Fieldson and Barbari, 1995; Murphy *et al.*, 2003; Flavin *et al.*, 2006). A schematical overview of the spin coating process to coat ATR crystals with liquid polymer precursors is given in Figure 9.

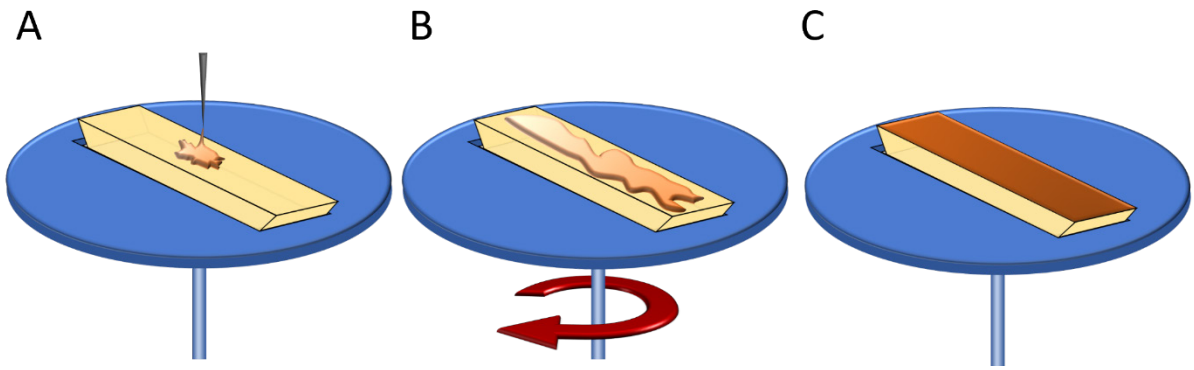

Figure 9. Spin coating process of fluid polymers onto an ATR crystal. (A) A liquid precursor is applied on an ATR crystal and (B) subsequent spin coating at variable spin velocities results in (C) equally distributed thin polymer layers.

The spin coating process can be divided in three distinct phases. During the first phase (Figure 9A) a non-polymerized fluid polymer precursor is pipetted onto the ATR crystal, which is situated in a special spin coating carrier chuck. The second step (Figure 9B) includes distribution phase of the fluid polymer with subsequent spin coating process. For the actual ATR crystal spinning, rotational speeds between 300 and 3000 rounds per minute (rpm) are commonly used, which is a layer thickness determining factor. During the last phase (Figure 9C), the polymer polymerizes. For sufficient adhesion of the polymer to be achieved, optional steps like temperature or vacuum treatment may be applied (Fieldson and Barbari, 1993). Even though spin coating has proven to be a suitable tool to generate equally distributed polymer films on ATR crystals, it requires a vast mass of coating material, because mostly over 90% of the material is spun away and only 10% or less remains on the substrate surface (Hsin-Fei, 2013). However, spin coating in combination with ATR-FTIR offers great opportunities to investigate diffusion processes in polymers. Hence, combining both methods was a crucial requirement for this thesis to characterize the penetration of water, adjuvant and model AI in cuticular model waxes.

1.7 Motivation and objectives of this work

The plant cuticle forms the main barrier against water loss, as well as against penetrating organic molecules. Therefore, the efficiency of this barrier mainly determines the uptake rate of active ingredients (AI) and mainly defines the AI bioefficiency under economic and ecological aspects. Many penetration studies have been performed on isolated cuticles to characterize the effectiveness of the cuticular barrier against the uptake of AIs (Riederer and

Schönherr, 1985; Bauer and Schönherr, 1992; Schreiber and Schönherr, 1992; Schönherr and Baur, 1994; Kirkwood, 1999; Buchholz, 2006). It was found that mainly the aliphatic fraction of cuticular waxes is responsible for the barrier function (Jetter and Riederer, 2016; Zeisler-Diehl *et al.*, 2018; Staiger *et al.*, 2019). Consequently, investigating the cuticular barrier based on model AI penetration in aliphatic reconstituted cuticular waxes rather than in isolated cuticles is mandatory. Unfortunately, the method used for this purpose only provided desorption kinetics with low temporal resolution, also requiring radioactively labeled penetrants (Schreiber and Schönherr, 1993; Schreiber *et al.*, 1996a; Schreiber *et al.*, 1996b; Kirsch *et al.*, 1997; Schreiber, 2006). Hence, determination of high-resolution sorption kinetics of a broader range of unlabeled organic molecules was desirable, which should be achieved by a new ATR-FTIR based approach developed in this work.

The determination of diffusion kinetics of organic substances is mainly important for basic plant research, which aims to understand the barrier mechanisms of the cuticle. Moreover, plant protection science pursues the approach to establish a fast and efficient screening method for the investigation of AI diffusion kinetics and precisely determining uptake enhancing properties of adjuvants. This in turn would reveal wax-adjuvant-AI interactions and is therefore indispensable from both ecological and economic points of view. Adjuvants are commonly formulated in the agricultural industry along with the AI to ensure efficient uptake and biodelivery (Kirkwood, 1993). Utility adjuvants, e.g., spray modifiers mainly affect the interaction between the AI and the cuticular surface (McMullan, 2000). Thereby wetting, spreading or sticking properties of the spray solution are modified to ensure adequate AI uptake. However, this work will solely investigate activator adjuvant properties such as physical modification of the barrier properties of cuticular model waxes (Penner, 2000). The modification is assumed to be a plasticization or softening of cuticular wax as induced by adjuvant – wax interactions, leading to e.g., decreasing crystallinity (Zhang *et al.*, 2016; Webster *et al.*, 2018) or increasing wax fluidity (Schreiber *et al.*, 1996b; Schreiber *et al.*, 1997) as well as ingress in amorphous parts of the wax and in crevices between crystalline domains, consequently causing irreversible effects on the wax structure (Fagerström *et al.*, 2014). Direct evidence about the MoA of activator adjuvants is missing and evidence on the relationship between chemical wax composition, structure and adjuvant efficacy is lacking. Accordingly, this work had the following objectives:

1. Establishment of a universally applicable ATR-FTIR based method to identify temperature dependent diffusion kinetics of AI modelling organic compounds in n-alkane dominated paraffin, serving as a cuticular model wax. HPB and CNP were chosen as model AIs both contributing different levels of lipophilicity and molar volume, thus reflecting a broad range of AIs.

2. Identification of diffusion kinetics of the widely used adjuvants methyl oleate, TEHP and three selected monodisperse alcohol ethoxylates C12E2, C12E4 and C12E6 with different degrees of ethoxylation into the two cuticular model waxes candelilla wax and carnauba wax using the new ATR-FTIR approach. Furthermore, the determination of the adjuvant-induced wax modification should be carried out simultaneously. This modification was to be characterized by a) determining alteration of orthorhombic crystallinity and b) measuring the adjuvant impact on wax molecule density, both indicating plasticization.

3. Characterization of the adjuvant diffusion kinetics depending on different proportions of aliphatic components within a basic cuticular model wax should be pursued. For this purpose, the diffusion kinetics of the mentioned adjuvants in n-alkane dominated candelilla wax blends were determined, contributing different proportions of policosanol (mainly octacosanol), as well as rice bran wax (mainly long-chain alkyl esters). Conclusion should be drawn on the relationship between chemical composition - structure - barrier properties.

4. Determination of mobility and solubility parameters of the AI modelling compound CNP, as well as of water after adjuvant induced wax modification to characterize the relationship of model AI mobility and sorption properties on the plasticization susceptibility of the n-alkane dominated candelilla wax compared to the alkyl ester dominated carnauba wax.

1.8 List of chemicals

Table 1. List of chemicals used in chapter 1 to 3

compound	purity (%)	chemical name	CAS	molecular weight (g mol^{-1})	molar volume[a] (cm^3 mol)	log K_{ow}	HLB[b]	company
heptyl parabene	99.0	heptyl 4-hydroxybenzoate	1085-12-7	236.31	237.40	4.83	n.d.	Sigma-Aldrich Chemie GmbH (Steinheim, Germany)
4-cyanophenol	95.0	4-hydroxybenzonitrile	767-00-0	119.12	108.92	1.6	n.d.	Sigma-Aldrich Chemie GmbH (Steinheim, Germany)
methyl oleate	99.0	methyl (z)-octadec-9-enoate	112-62-9	296.50	336.37	7.45	n.d.	Sigma-Aldrich Chemie GmbH (Steinheim, Germany)
TEHP	97.0	tris(2-ethylhexyl) phosphate	78-42-2	434.60	469.81	8.9	n.d.	Sigma-Aldrich Chemie GmbH (Steinheim, Germany)
C12E2	> 95.0	diethylene glycol monododecyl ether	3055-93-4	274.44	307.21	4.9	7.66	TCI Chemicals (prefecture Tokyo, Japan
C12E4	≥ 98.0	tetraethylene glycol monododecyl ether	5274-68-0	362.50	392.39	4.7	10.66	Sigma-Aldrich Chemie GmbH (Steinheim, Germany)
C12E6	≥ 98.0	hexaethylene glycol monododecyl ether	221-282-3	450.65	477.56	4.4	12.49	Sigma-Aldrich Chemie GmbH (Steinheim,

								Germany)
chloroform	> 99.8	trichlormethane	67-66-3	119.37	n.d.	1.97	n.d.	Carl Roth GmbH + Co. KG (Karlsruhe, Germany)
methanol	> 99.8	methyl alcohol	67-56-1	32.04	n.d.	- 0.77	n.d.	Carl Roth GmbH + Co. KG (Karlsruhe, Germany)
paraffin wax	n.d.	paraffin wax purum	8002-74-2	n.d.	n.d.	n.d.	n.d.	Sigma-Aldrich Chemie GmbH (Steinheim, Germany)
candelilla wax	n.d.	n.d.	8006-44-8	n.d.	n.d.	n.d.	n.d.	TER Chemicals Distribution Group (Hamburg, Germany)
carnauba wax	n.d.	n.d.	8015-86-9	n.d.	n.d.	n.d.	n.d.	Sigma-Aldrich Chemie GmbH (Steinheim, Germany)
rice bran wax	n.d.	n.d.	8016-60-2	n.d.	n.d.	n.d.	n.d.	Kahlwax (KAHL GmbH & Co. K.G., Trittau, Germany)
policosanol	n.d.	n.d.	142583-61-7	n.d.	n.d.	n.d.	n.d.	BOC Sciences (Shirley, NY, USA)
D_2O	≥ 99.90	deuterium oxide	7789-20-0	n.d.	n.d.	- 0.5	n.d.	Sigma-Aldrich Chemie GmbH (Steinheim, Germany)
BSTFA	> 99.0	n,o-bis-(trimethylsilyl) trifluoroacetamide	25561-30-2	257.40	n.d.	n.d.	n.d.	Macherey-Nagel GmbH & Co. KG, (Düren, Germany)
pyridine	99.9	pyridine	110-86-1	79.10	n.d.	0.7	n.d.	Carl Roth GmbH + Co. KG (Karlsruhe, Germany)

[a]calculated with Molinspiration Cheminformatics free web services, Slovensky Grob, Slovakia

[b]calculated according to Griffin (1954)

2 Chapter 1: Diffusion kinetics of organic compounds in cuticular model wax

This chapter is based on the following publication.

Kunz M, Staiger S, Burghardt M, Popp C, George N, Roberts K, Riederer M. (2022). Diffusion Kinetics of Active Ingredients and Adjuvants in Wax Films: An Attenuated Total Reflection-Infrared Spectroscopy Study of a Leaf Surface Model. *Agricultural Science and Technology* (doi: 10.1021/acsagscitech.2c00054)

Statement of individual author contributions and of legal second publication rights

	Reprinted with permission from (complete reference): **Kunz M, Staiger S, Burghardt M, Popp C, George N, Roberts K, Riederer M. (2022).** Diffusion Kinetics of Active Ingredients and Adjuvants in Wax Films: An Attenuated Total Reflection-Infrared Spectroscopy Study of a Leaf Surface Model. *Agricultural Science and Technology* (doi: 10.1021/acsagscitech.2c00054)

Participated in	**Author Initials**, Responsibility decreasing from left to right						
Study Design	M.K.	M.R	S.S.	M.B.	C.P.	N.G.	K.R.
Methods Development	M.K.	M.R	S.S.	M.B.	C.P.	N.G.	K.R.
Data Collection	M.K.	M.R	S.S.	M.B.	C.P.	N.G.	K.R.
Data Analysis and Interpretation	M.K.	M.R	S.S.	M.B.	C.P.	N.G.	K.R.
Manuscript Writing	M.K.	M.R	M.B.	S.S.	C.P.	N.G.	K.R.
Writing of Introduction	M.K.	M.R	M.B.	S.S.	C.P.	N.G.	K.R.
Writing of Materials and Methods	M.K	M.R	M.B.	S.S.	C.P.	N.G.	K.R.
Writing Discussion	M.K.	M.R	M.B.	S.S.	C.P.	N.G.	K.R.
Writing of First Draft	M.K.	M.R	M.B.	S.S.	C.P.	N.G.	K.R.

Explanations:

Figure 10 and Table 1 are not illustrated in the publication. Diffusion data of heptyl parabene and 4-cyanophenol at 29.0 °C and 37.0 °C were not included in the dissertation and activation energies derived from Arrhenius formalism were calculated using diffusion coefficients derived from diffusion kinetics recorded at 25.0, 32.5 and 40 °C, but not at 29.0 and 37.0 °C. Methyl oleate and C12E2 diffusion data in paraffin wax were not included in the dissertation.

I confirm that I have obtained permission from both the publishers and the co-authors for legal second publication and the correctness of the above mentioned assessment.

I also confirm my primary supervisor's acceptance.

Marcel Kunz Würzburg

_____

Doctoral Researcher's Name Date Place Signature

2.1 Introduction

2.1.1 Determination of diffusion kinetics in cuticular waxes

Understanding the physio-chemical properties of the cuticular barrier concerning pathways of organic molecules is of great importance for optimizing pesticide applications under economic and ecological constraints. The determination of mobility parameters helps to better understand cuticular uptake properties. Bauer and Schönherr (1992) presented "Unilateral Desorption from the Outer Surface" (UDOS) (Bauer and Schönherr, 1992) enabling the calculation of compound specific rate constants within the CM. However, to exclude disturbing influences of the CM matrix, which is only of minor importance for cuticular barrier properties, several attempts to elucidate diffusion coefficients have been performed solely on barrier forming reconstituted cuticular waxes (Schreiber and Schönherr, 1993; Schreiber and Riederer, 1996a; Kirsch *et al.*, 1997; Burghardt *et al.*, 1998; Burghardt *et al.*, 2006). Although it is known that mainly aliphatic wax compartments are crucial for the barrier constitution against water and organic compound penetration (Jetter and Riederer, 2016; Zeisler and Schreiber, 2016; Zeisler-Diehl *et al.*, 2018; Staiger *et al.*, 2019), the mentioned studies neglected these aspects and simply used wax extracts from whole leaves with no regard to wax compartmentation. Diffusion coefficient investigation of organic compounds mainly focused on *Hordeum vulgare* (barley), *Fagus sylvatica*, *Picea abies, Prunus laurocerasus, Gingko biloba, Juglans regia, Stephanotis floribunda* and *Chenopodium album* leaf wax (Schreiber *et al.*, 1996a; Kirsch *et al.*, 1997; Burghardt *et al.*, 1998; Šimáňová *et al.*, 2005; Burghardt *et al.*, 2006). Desorption kinetics of radioactively labelled organic compounds from films of reconstituted cuticular waxes were measured to determine diffusion coefficients. However, the initially used method lacks the robustness and ease desirable for routinely studying the mobilities of a wider range of organic solutes in waxes of different composition, at varying temperatures and in the presence of various chemicals such as adjuvants in pesticide formulations. To get a better understanding on how compound mobility is affected by the barrier forming VLCAs, a basic model wax was chosen solely contributing n-alkanes, namely paraffin wax.

2.1.2 ATR-FTIR based approach

A new approach based on Attenuated Total Reflection Fourier Transform Infrared Spectroscopy (ATR-FTIR) adapted from earlier work published by Fieldson and Barbari (1993) is presented here (Fieldson and Barbari, 1993). This approach studies the sorption of compounds from a solution contained in a reservoir into a thin wax film as a function of time. The intensities of individual vibrational absorption bands were recorded via ATR-FTIR, which is highly substance specific. Additionally, ATR-FTIR allowed to automatically record diffusion kinetics with high temporal resolution over extended periods of time. Even, the diffusion of substances with different characteristic absorption bands may be followed simultaneously in one experiment. Using similar ATR-FTIR-based approaches, several studies have so far successfully investigated the diffusion kinetics of water, solvents or organic compounds in rubbery or semicrystalline polymers (Pellett *et al.*, 1997a, b; Elabd *et al.*, 2003; Döppers *et al.*, 2004; Dhoot *et al.*, 2009; McAuley *et al.*, 2010). Usually, the type of diffusion observed was Fickian, solely driven by a diffusant concentration gradient between a donor reservoir and the polymer.

The preparation of thin and uniformly distributed wax films on ATR crystals was one of the main prerequisites for the development of the ATR-FTIR method. As it turned out, spin coating was well suited to produce wax films with the mentioned properties. However, because spin coating requires large amounts of liquid wax, well in excess of the amounts of cuticular wax that can be obtained by extracting isolated cuticles with chloroform (Riederer and Schneider, 1989), a commercially available model for plant cuticular waxes had to be used. Since many cuticular waxes consist of very long-chain alkanes (Holloway, 1994), a polydisperse paraffin wax mainly contributing barrier-forming alkanes was chosen to set base for developing the proposed method.

2.1.3 Heptyl parabene (HPB) and 4-cyanophenol (CNP) as model Active ingredients (AI)

4-cyanophenol (CNP) and heptyl parabene (HPB) were chosen as model diffusants since their molecular sizes and lipophilicities lay in the range of those of common AI molecules. Chemical structures of HPB and CNP are shown in Figure 10.

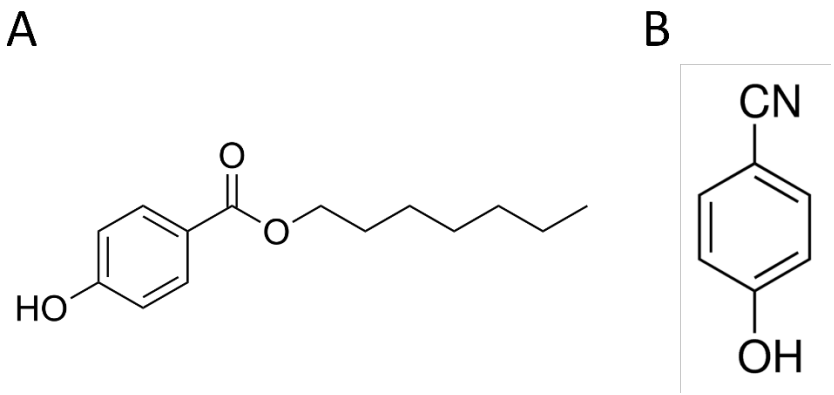

Figure 10. Chemical structures of (A) heptyl parabene and (B) 4-cyanophenol.

Parabenes are mostly utilized as preservatives to inhibit microbial growth and maintain product integrity in cosmetics and dermatologically relevant products (Darbre and Harvey, 2008). Parabenes such as HPB commonly show distinctive FTIR spectra, with their most prominent absorption band at around 1280 cm^{-1}, corresponding to a C-O stretching vibration. Contrastingly, the most prominent vibration mode of CNP is the cyano-stretching vibration at around 2230 cm^{-1}. Since the C≡N stretching absorption is occurring apart from the previously introduced fingerprint region, distinct absorption quantification became possible. CNP has already shown to be suitable for pharmaceutical and dermatological ATR-FTIR specific diffusion coefficient determinations (Pellett *et al.*, 1997a; McCarley and Bunge, 2003; Romonchuk and Bunge, 2006).

2.1.4 Objectives and research questions

The plant cuticle mainly establishes the barrier against water loss and uptake of organic compounds into the plant. (Schönherr, 1976; Riederer and Schreiber, 2001) To exclude interfering influences of the cuticular matrix during the study of substance mobility in the barrier-defining wax, the diffusion process must ideally be studied in barrier-forming wax constituents. Although one approach already exists that studied the desorption kinetics of organic molecules in reconstituted cuticular wax, this method lacks the robustness and simplicity that would be desirable for routinely studying the mobilities of a broader range of organic solutes in waxes of different compositions, at different temperatures, and in the presence of different chemicals used as adjuvants in pesticide formulations (Schreiber and Schönherr, 1993).

Consequently, the aim of this work was to (1) adapt the ATR-FTIR method developed for studying the diffusion of molecules in polymers to doing the same in thin wax films, (2) derive the diffusion coefficients of model diffusants differing in chemical structure, lipophilicity and size, and (3) investigate the effect of temperature on the diffusion of these compounds.

2.2 Material and methods

2.2.1 Material

All chemicals used in this chapter are listed in Table 1. Paraffin wax served as cuticular model wax. HPB was used as lipophilic model diffusant (10 g l^{-1} in 70 % methanol/water) and CNP represented a model diffusant with intermediate lipophilicity (saturated in pure water). BSTFA and pyridine were used for silylation of potentially polar compounds in paraffin wax for GC analysis.

2.2.2 ATR-FTIR experimental setup and data collection

The sorption kinetics of HPB and CNP in paraffin wax were determined by ATR-FTIR. Model diffusants were applied as aqueous solutions on top of thin wax layers of equal thickness deposited on an ATR crystal with the spin coating technique. Subsequently, diffusion towards the crystal-wax interface was measured by determining the absorption of IR-radiation induced by the increased concentration of diffusants entering the region of the wax defined by the evanescent wave of the IR beam over time. An ATR crystal was first covered with an equally distributed thin wax layer. Afterwards, the wax-covered ATR crystal was attached to a water-heated trough Gateway™ ATR top plate (Specac Ltd, Orpington, United Kingdom) (Figure 11).

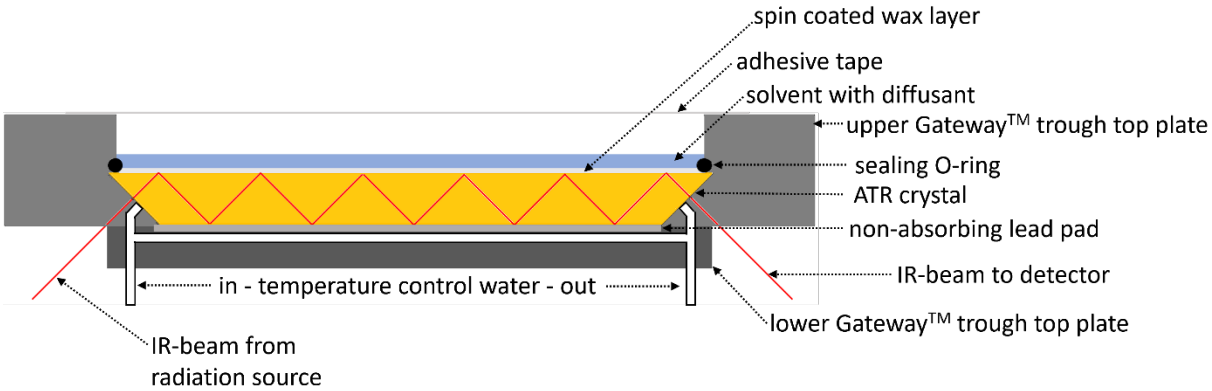

Figure 11. Experimental ATR-FTIR setup to measure diffusion kinetics of organic compounds in spin-coated paraffin wax.

Flexible tubes from a thermostat (Thermo Scientific Haake DC30-K20, Karlsruhe, Germany) were connected to the inlet and outlet ports of the top plate to establish water circulation, enabling temperature adjusted measurements. Subsequently, the top plate was placed into a Gateway^{TM} ATR-FTIR spectrometer accessory (Specac Ltd, Orpington, United Kingdom). After an equilibration time of five minutes, absorption spectra were recorded with a Fourier-transform infrared spectrometer (FTIR, Bruker Tensor 27 with liquid N_2-cooled MCT-detector, Bruker, Ettlingen, Germany) within a wavenumber range of 4000 to 500 cm^{-1}. The resolution was set to 2 cm^{-1} with 120 scans for each averaged spectrum. The Gateway^{TM} unit and the FTIR-spectrometer were purged with dry CO_2 -free air (K-MT-LAB 3, Parker Hannifin, Kaarst, Germany). To control the FTIR-apparatus and collect absorption spectra, the software OPUS 7.2 (Bruker, Ettlingen, Germany) was used. After gathering background spectra of the model wax, aqueous organic compound solutions (5 ml) were applied on top of the ATR crystal. It was essential that the apparatus was leakproof and that the crystal top surface was entirely covered. The trough was sealed either with adhesive tape or with an aluminum plate with a sealing ring to prevent solvent evaporation. After applying the compound solutions onto the ATR crystal, spectra were recorded every 5 to 7.5 minutes over a time range of 67 hours.

2.2.3 Preparation of wax samples

The paraffin wax and a trapezoidal ATR crystal (ZnSe 72 x 10 x 6 mm, Specac Ltd, Orpington, United Kingdom) were heated to 85 °C using a heating module (Pierce Reacti-Therm, Pierce Chemical, Dallas, TX, USA). The ATR crystal was attached to a POLOS^{TM} spin coater SPIN150i-NPP (SPS-Europe GmbH, Ingolstadt, Germany), and a small amount of liquid wax was then drawn up into a Pasteur pipette and subsequently applied on top of the preheated ATR crystal until its surface was fully covered. Subsequent spin coating of the ATR crystal was performed for 15 seconds at 1000 rpm, followed by a wax solidification phase for 10 seconds at 500 rpm.

2.2.4 Determination of wax film thickness

To determine the coated wax layer thickness *L* on the crystal surface, the ATR crystal was weighed with a microbalance (Model SBA31, Scaltec GmbH, Göttingen, Germany) before and after spin coating. The resulting mass difference corresponded to the mass of the wax. Equation (9) was used to determine the wax thickness considering its assumed density (0.9 g l^{-1}) (Büscher, 1960).

$$L = \frac{(m_{cc} - m_{bc}) * \delta_w}{A_c} \quad (9)$$

In equation (9), m_{cc} corresponds to the coated ATR crystal mass and m_{bc} corresponds to the mass of the bare ATR crystal, respectively. δ_w represents the wax density, and A_c represents the ATR crystal surface area.

2.2.5 Determination of diffusion coefficients by ATR-FTIR

The diffusion coefficients of HPB and CNP in paraffin wax were determined. Therefore, the increasing compound concentration, rising at the ATR crystal-wax interface, was directly measured during the sorption process. Since the Lambert-Beer law applies to ATR-FTIR measurements, the concentration of organic compounds in the wax is directly proportional to the level of the respective infrared radiation absorption of the functional groups within the evanescent wave. The absorption band of a C-O stretching vibration (1280 cm^{-1}) was integrated at each recorded IR-spectrum during the diffusion experiments with HPB (Chai and Isa, 2013). CNP diffusion was determined using a C≡N stretching vibration (2230 cm^{-1}) typical for nitriles (Pellett *et al.*, 1997a). The estimated refractive index for paraffin wax was 1.5 (Johnson, 1954). The ATR crystal was made of ZnSe with a refractive index of 2.43 and an incident angle of radiation of 45°. Due to its trapezoidal shape, IR-radiation gets reflected six times, resulting in high-resolution absorption spectra. Equation (10) was used for determining diffusion coefficients from diffusion kinetics recorded by ATR-FTIR (Fieldson and Barbari, 1993).

$$\frac{A_t - A_0}{A_{eq} - A_0} = 1 - \frac{8\gamma}{\pi[1 - exp(-2\gamma L)]} * \sum_{n=0}^{\infty}\left[\frac{exp(g)[f\, exp(-2\gamma L) + (-1)^n(2\gamma)]}{(2n+1)(4\gamma^2 + f^2)}\right] \quad (10)$$

where

$$g = \frac{-D(2n+1)^2\pi^2 t}{4L^2}$$

and

$$f = \frac{(2n+1)\pi}{2L}$$

Equation (10) is an exact solution for diffusion processes according to Fickian diffusion kinetics recorded via ATR-FTIR. The absorption at the time (A_t) resembles the compound concentration at time t, A_{eq} is the absorption (concentration) at equilibrium state and A_0 is the initial absorption (concentration). The diffusion coefficient D of a diffusant can be calculated in dependence of time t, the reciprocal of the evanescent wave penetration depth γ and the wax layer thickness L (Fieldson and Barbari, 1993). Using a six reflection ATR crystal, the averaged absorption along the whole ATR crystal is recorded. When determining diffusion coefficients in the model wax, the averaged absorption generated by all occurring reflections at the crystal-diffusant interface along the wax layer is measured. The evanescent wave penetration depth determines the minimum necessary thickness of the wax layer.

2.2.6 Data evaluation of ATR-FTIR absorption spectra

Absorption spectra were imported in OriginPro 9 (OriginLab Corporation, Northampton, MA, USA) and only the relevant vibrational regions of HPB (C-O stretching ~ 1280 cm^{-1}) and CNP (C≡N stretching ~ 2230 cm^{-1}) were considered, respectively. A script was written for performing baseline fits for each spectrum, setting the same anchor points for each time point. Levenberg-Marquardt linear-least-square regression analysis of integrated absorptions within a specific time range was conducted with OriginPro 9, using equation (10), where D was the only adjustable parameter. The coefficient of determination (r^2) was used to determine the model's accuracy compared to the experimental data until reaching A_{eq}.

2.2.7 Temperature dependence of diffusion

Temperature adjusted diffusion experiments were conducted by setting respective temperatures with a thermostat (Thermo Scientific Haake DC30-K20, Karlsruhe, Germany). Thermostabilized water circulation within the ATR-top plate enabled the investigation of temperature dependent diffusion kinetics of HPB and CNP in the model wax. Diffusion experiments were conducted at 25.0 °C, 32.5 °C and 40.0 °C. Ln-linear relationships of diffusion coefficients and temperature were investigated by plotting ln D versus the reciprocal of absolute temperature, according to the Arrhenius equation (Cussler, 2009)

$$D = D_0 e(-\frac{E_a}{RT}) \tag{11}$$

where D_0 is the pre-exponential factor, E_a is the activation energy of diffusion, T is the absolute temperature in Kelvin and R is the universal gas constant.
Activation energies and diffusion coefficients were calculated by the slopes of regression.

2.2.8 Determination of melting points and orthorhombic crystallinity of wax

A model wax solution (200 µl) (1 g l^{-1} in chloroform) was applied on a silicon ATR crystal embedded in an ATR-FTIR measure cell (Bio-ATR II®, Bruker, Ettlingen, Germany). The water inlet and outlet ports of the cell were connected to a thermostat (Thermo Scientific Haake DC30-K20, Karlsruhe, Germany) and the ATR-FTIR measure cell was heated up to 90 °C to ensure that chloroform was fully evaporated. The crystal was then cooled to 20 °C and infrared spectra were recorded in a wavenumber range of 4000 to 670 cm^{-1} from 20 °C to 92 °C with 1 minute equilibration time for each averaged spectrum. The Bio-ATR II® unit was purged with dry CO2-free air (K-MT-LAB 3, Parker Hannifin, Kaarst, Germany). Resolution was set to 2 cm^{-1} with an acquisition time of 32 scans. OPUS 7.2 software (Bruker, Ettlingen, Gemany) was used to analyze spectra and to control the spectrometer (Tensor 27, Bruker, Ettlingen, Germany) and the thermostat. Determination of melting points was performed by plotting respective wavenumber maxima of wax specific CH_2 asymmetrical (~ 2915 cm^{-1}) stretching vibration versus corresponding temperatures (°C). Non-linear regression was performed with OriginPro 9 (OriginLab Corporation, Northampton, MA, USA) using logistic regression according to Patel *et al.* (2001) For the determination of crystallinity according to Zerbi *et al.* (1989), spectra were recorded and OriginPro 2019 (OriginLab, Northampton, USA) was used to determine maximum intensities of the two rocking bands at 720 and 730 cm^{-1}.

2.2.9 Scanning electron microscopy (SEM)

Microscope slides (Paul Marienfeld GmbH & Co. KG, Lauda-Königshofen, Germany) were spin-coated with model wax under the same spinning conditions as ATR crystals. Cut slices of spin-coated microscope slides were placed on aluminum stubs using double-sided adhesive tape. These stubs were then sputter-coated with gold-palladium (10 nm to 15 nm) (150 s, 25 mA, partial argon pressure 0.05 mbar, SCD005 sputter coater, Bal-Tec, Pfäffikon, Switzerland). The surface morphology of the paraffin wax layers was investigated by using scanning electron microscopy (SEM, JEOL JSM-7500F, JEOL GmbH, Freising, Germany). The SEM was equipped with a field emission gun and a lower secondary electron image (LEI) detector. The

acceleration potential was set to 5 kV, and a working distance greater than 10 mm was applied.

2.2.10 Gas-chromatographic analysis (GC)

Paraffin wax (5 mg) was dissolved in chloroform (100 ml). For detecting any polar compounds, the solution (0.1 ml) was derivatized with BSTFA (10 µL) and pyridine (10 µL) at 70 °C for 30 min using a heating module (Pierce Reacti-Therm, Pierce Chemical, Dallas, TX, USA). The mixture was then dissolved in chloroform (100 µl) and used for gas chromatography (GC). GC-mass spectrometry (GC-MS; 6890 N, GCSystem; Agilent Technologies, Santa Clara, CA, USA) was used to identify wax compounds. Helium was used as a carrier gas. An MS detector (m/z 50–750, MSD 5977A, Agilent Technologies) was applied. On-column injection with a capillary column (30 m × 0.32 mm, DB-1, 0.1 µm film: J&W Scientific, Agilent Technologies) was used for paraffin wax compound identification. The liquid paraffin wax samples were injected at 50 °C, and the temperature was held for 2 minutes. The temperature was then increased to 200 °C at a heating rate of 40 °C min^{-1} and hold for 2 min. The temperature was then increased to 320 °C at a heating rate of 3 °C min^{-1} and hold for 30 min. Identification was undertaken using Wiley 10th/NIST 2014 mass spectral library (John Wiley & Sons, Hoboken, NJ, USA) reference specimen or spectra interpretation. Quantification was undertaken using GC flame ionization detection (GC-FID, 6850N, Agilent Technologies, Santa Clara, CA, USA). Similar GC conditions were used to separate compounds, except that hydrogen gas was used as the carrier gas.

2.3 Results

2.3.1 Chemical composition of paraffin wax

The paraffin wax used mainly consisted of n-alkanes (82.7 % of total wax (Figure 12A)) with chain lengths ranging from C_{21} to C_{47} (Figure 12B, n=6).

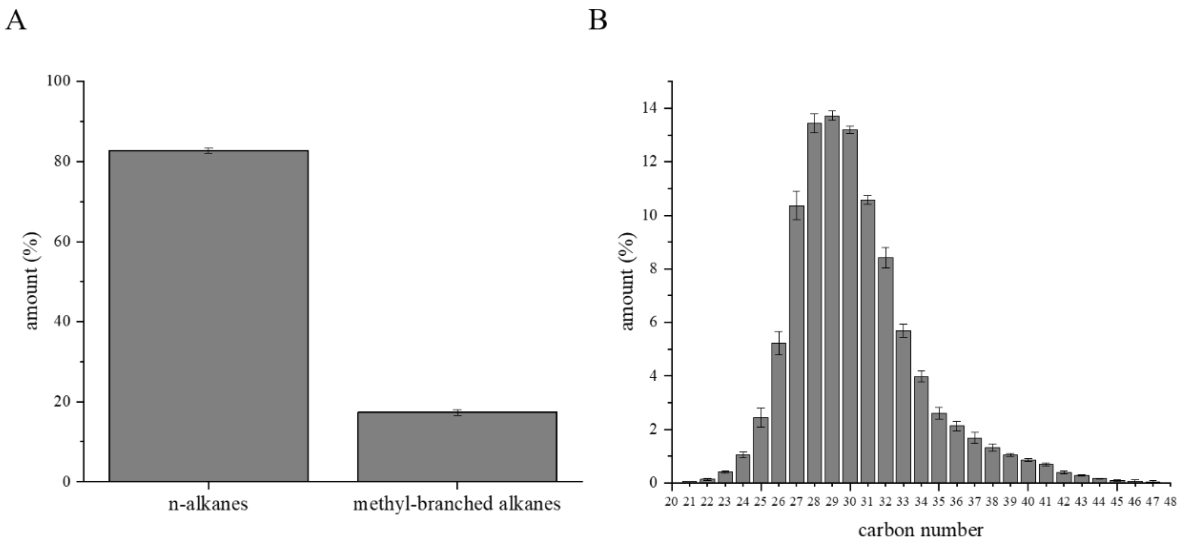

Figure 12. Comparison of polydisperse paraffin wax fractions (A) and its chain-length distribution of n-alkane portion (B) Data is given as mean proportion (%), and error bars represent standard deviation.

C_{28}, C_{29} and C_{30} were most prominent, with each around 14 %, whereas n-alkanes with chain lengths shorter than 27 carbons or longer than 32 carbons contributed to less than 6 % to the total n-alkane fraction, respectively. A fraction of 17.3 % of the wax were branched, mainly iso- and anteiso-methyl long-chain alkanes (Figure 12A) following the same chain length distribution as observed for n-alkanes. The weighted average chain length of both n-alkanes and branched alkanes was 30.32 (Huang *et al.*, 2017). Melting range analysis and temperature dependent determination of orthorhombic crystallinity according to Zerbi *et al.* (1989) was performed (Figure 13).

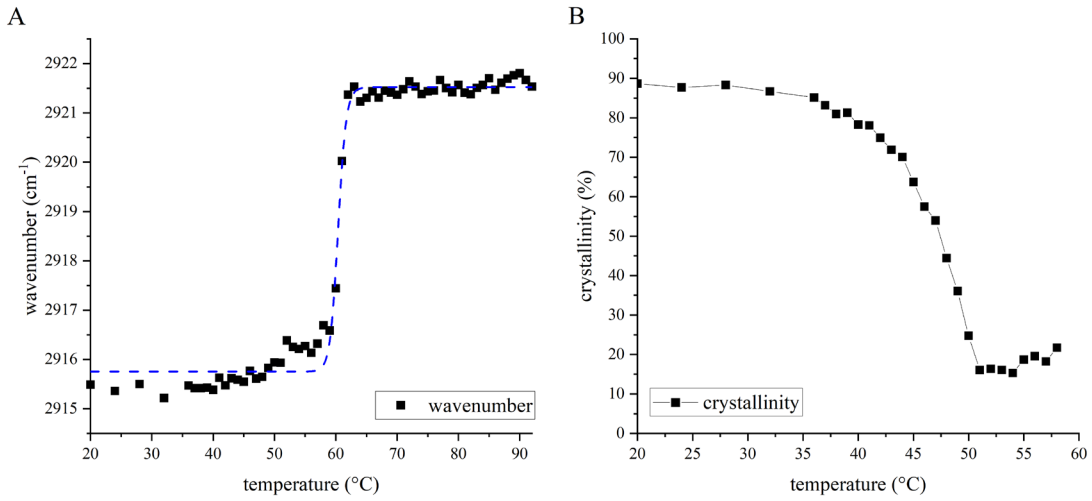

Figure 13. Paraffin wax specific melting behavior and logistic fit (blue dashed curve) from 20 to 92 °C (A) and decrease of orthorhombic crystallinity from 20 to 60 °C.

The mid of melting range of the paraffin wax was determined to be 60.4 °C according to the best fit of a logistic regression analysis (r^2 = 0.99) (Figure 13A). The orthorhombic crystallinity of the paraffin wax decreased from 88 % to 78 % within in a temperature range from 20 °C to 40 °C, (Figure 13B).

2.3.2 Paraffin wax film preparation

Before coating, ATR crystal surfaces are shining (Figure 14A), whereas after spin-coating with paraffin wax the surfaces were uniformly cloudy and matt (Figure 14B). SEM images of spin-coated object slides showed that the wax was equally and smoothly distributed also on a microscopic scale (Figure 14C and D).

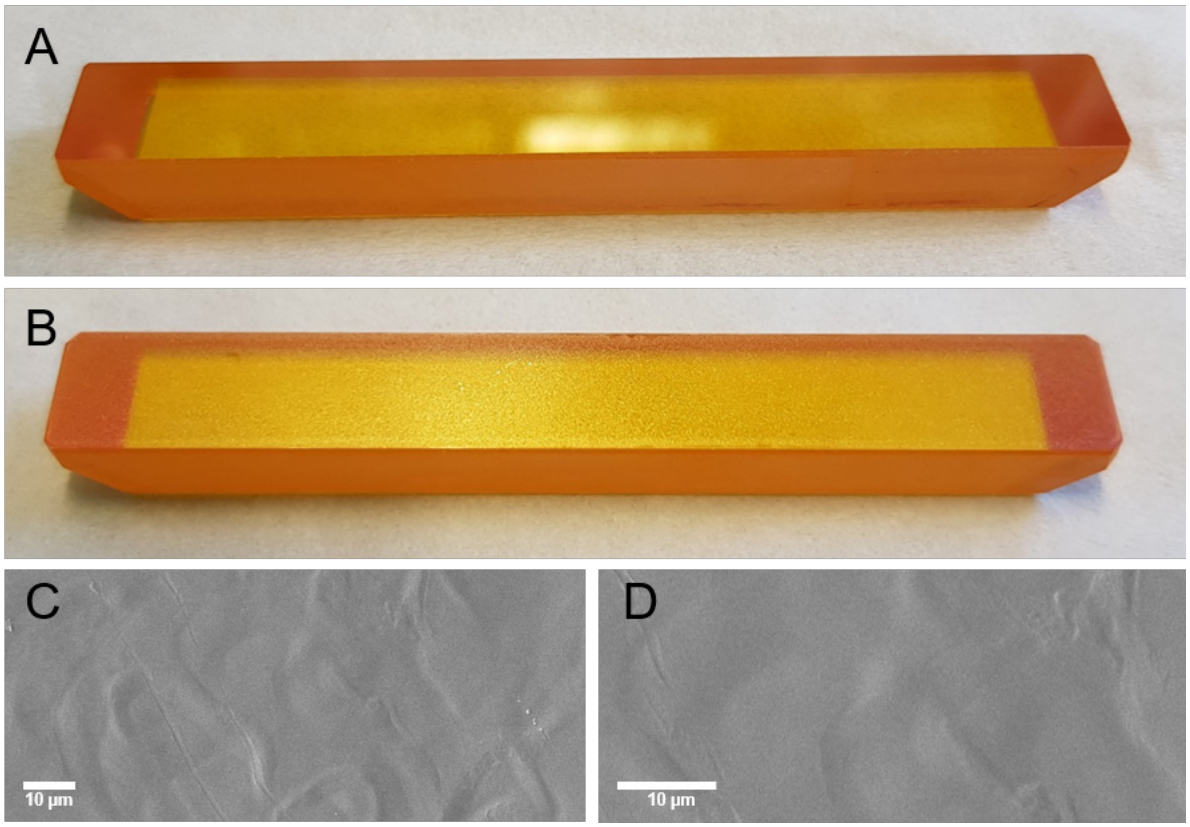

Figure 14. (A) Image of a bare ZnSe ATR crystal. (B) Image of a with paraffin spin coated ATR crystal. (C, D) images of with paraffin wax spin-coated object slides at different resolutions.

Under constant spin-coating conditions, the thickness of the paraffin wax films on ATR crystals did not vary by more than 17.1 %, with an average wax layer thickness of 7.9 ± 0.6 µm.

2.3.3 HPB and CNP diffusion kinetics in paraffin wax

The ATR-FTIR specific absorption of HPB and CNP diffusing from an external reservoir into the wax film on top of the ATR crystal was measured at short time intervals up to a total of 67 h at 25.0 °C, 32.5 °C and 40.0 °C. The intensities of the C-O stretching specific vibrational band of HPB and the C≡N stretching specific vibrational band of CNP were recorded in the wax layer immediately adjacent to the crystal surface defined by the penetration depth of the evanescent wave. The penetration depth calculated according to equation (8) amounted to 1.48 µm and 0.85 µm at 1280 and 2230 cm^{-1}, the peak maxima of the C-O and C≡N bands, respectively. The intensities of the bands increased with time as increasing amounts of the diffusants had entered and diffused across the wax films (Figure 15; diffusion at 25 °C).

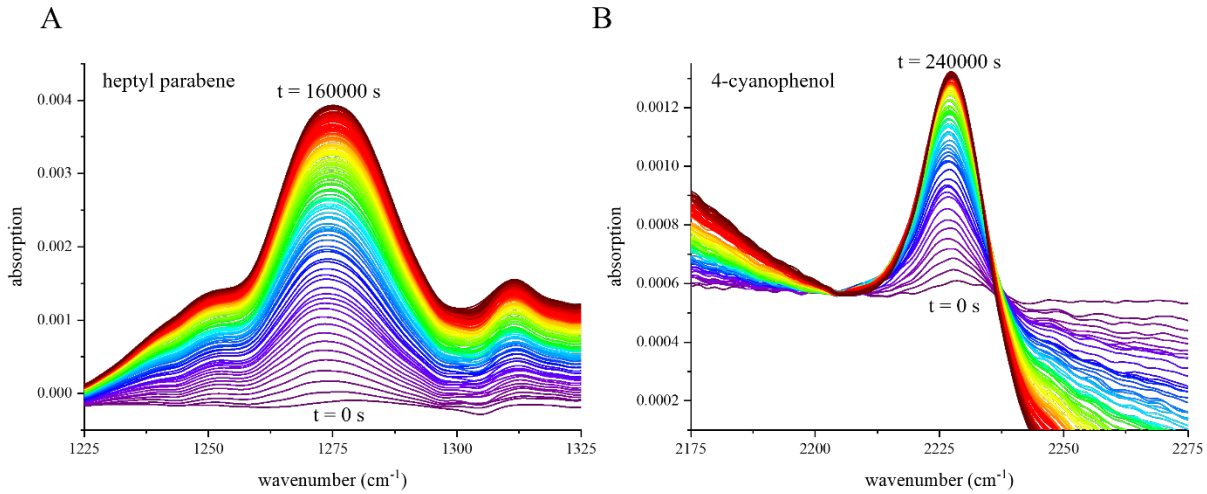

Figure 15. ATR-FTIR vibration bands of (A) heptyl parabene at ~1280 cm^{-1} and (B) 4-cyanophenol at ~2230 cm^{-1}, recorded during respective penetration in spin-coated paraffin wax at 25 °C. Penetration processes were conducted until 160000 s and 240000 s, respectively.

The curves of the integrated HPB specific C-O absorption at ~1280 cm^{-1} (Figure 15A) and CNP specific C≡N absorption at ~2230 cm^{-1} (Figure 15B) initially increased steeply with time and later levelled off into approximately linear time-courses of increase until the end of the experiments.

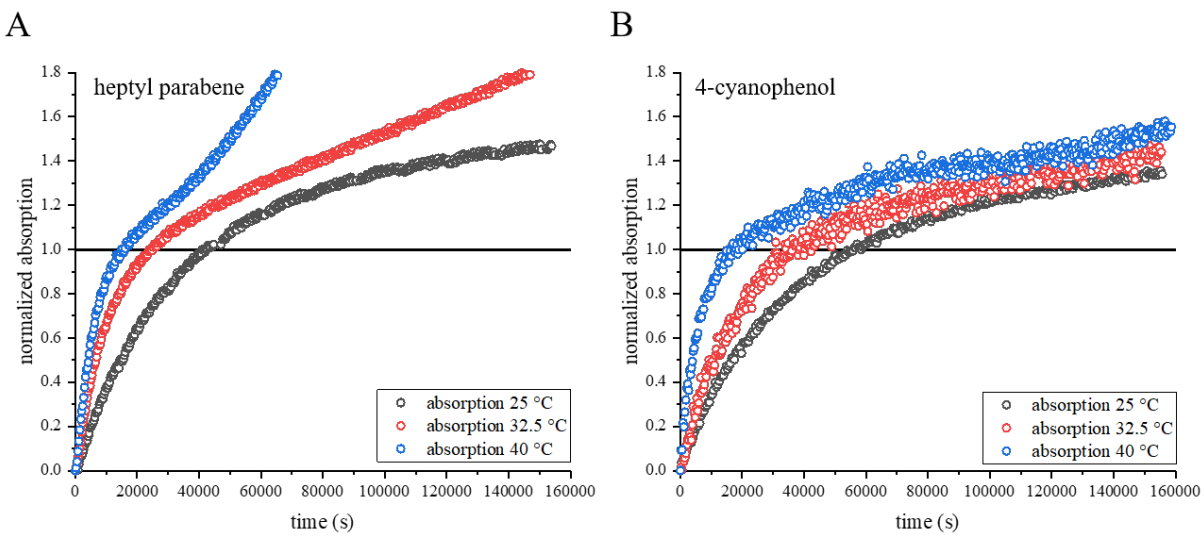

Figure 16. Normalized integrated absorptions of (A) heptyl parabene and (B) 4-cyanophenol diffusion in paraffin wax at 25 °C, 32.5 °C and 40 °C, recorded via ATR-FTIR. Respective integrated absorptions were normalized to estimated pseudo-equilibria of Fickian diffusion, represented by the solid black line at normalized absorption = 1.0.

The concentration of the diffusants in the wax layer defined by the evanescent wave and its increase with time was higher at increased temperatures. However, no sorption equilibria were obtained directly from the time-courses observed in our system (Figure 16). Therefore, an assumption-free rule had to be established to derive the sorption equilibrium of the Fickian portion of the sorption kinetics. For this purpose, equation (10) describing Fickian diffusion was repeatedly fitted to the initial parts of the curves stepwise omitting later data points until a maximum r^2 of the fit was reached. The curve fits generated in this way reproduced the respective first sections of the sorption kinetics and delineate the pseudo-equilibria achievable by Fickian diffusion (Figure 17).

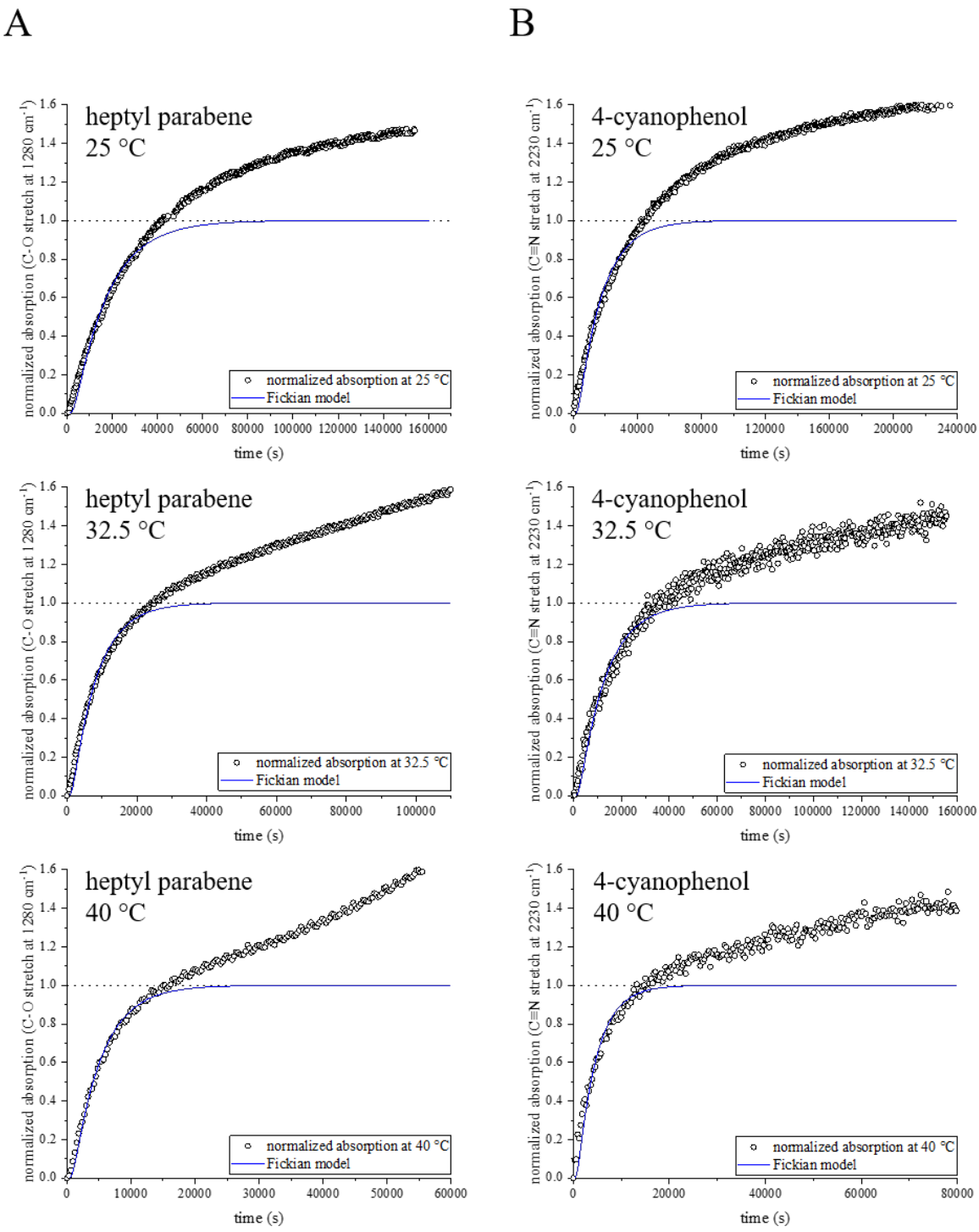

Figure 17. Normalized integrated absorption of heptyl parabene and 4-cyanophenol at 25 °C, 32.5 °C and 40 °C, recorded via ATR-FTIR. Integrated absorptions were normalized to assumed pseudo-equilibria, represented by a dashed line at normalized absorption = 1.0. The blue line represents non-linear regression fit with a the Fickian diffusion model until reaching respective pseudo-equilibria at normalized absorption = 1.0.

The diffusion coefficients at 25 °C in the model wax obtained by this method are 1.73 x 10^{-15} m^2 s^{-1} for HPB diffusion and 1.48 x 10^{-15} m^2 s^{-1} for CNP, both log-linearly increasing with temperature (Table 2).

Table 2. Diffusion coefficients and respective statistical data for heptyl parabene and 4-cyanophenol diffusion in paraffin wax

compound	temp (° C)	D (10^{16} x m^2 s^{-1})	95% UCL x 10^{16}	95% LCL x 10^{16}	r^2	wax layer thickness (µm)
heptyl parabene	25.0	17.3	17.6	17.0	0.98	8.0
	32.5	39.5	40.5	38.6	0.98	8.3
	40.0	66.4	68.7	64.7	0.99	8.5
4-cyanophenol	25.0	14.8	15.2	14.4	0.97	7.4
	32.5	24.1	24.8	23.4	0.96	8.2
	40.0	47.7	49.8	45.0	0.96	6.8

Plotting ln D vs. 1/T yielded linear Arrhenius plots for HPB and CNP diffusion (Figure 18).

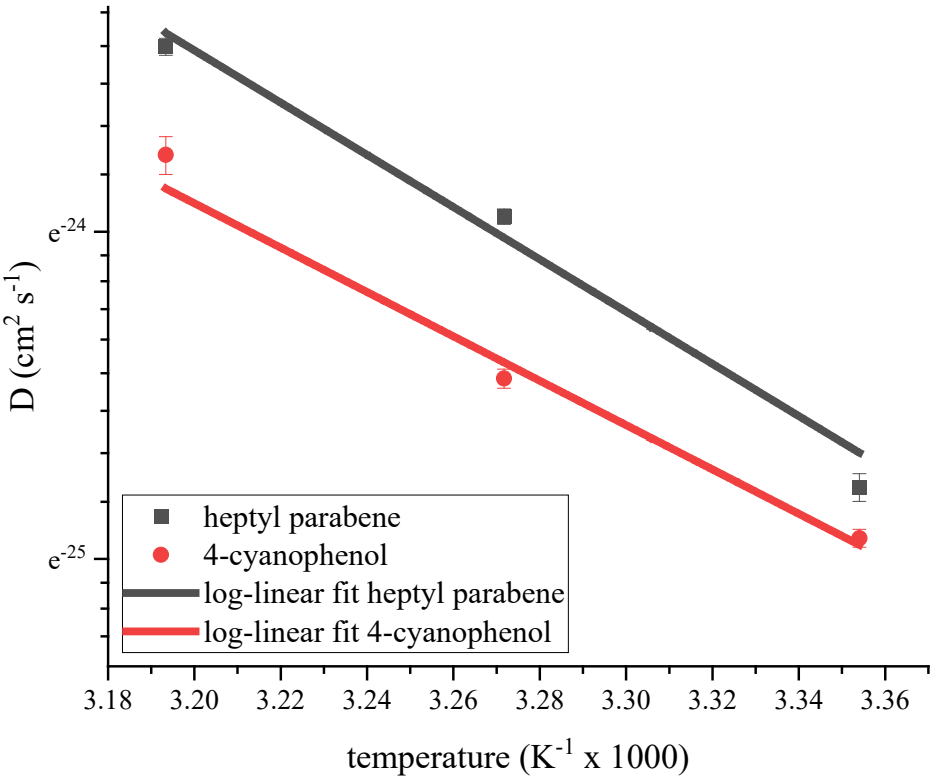

Figure 18. Natural logarithms of *D* versus reciprocal of absolute temperature for heptyl parabene and 4-cyanophenol diffusion in paraffin wax. Error bars indicate respective 95% UCL and LCL of equation (3).

Respective activation energies of diffusion (E_a) were estimated according to equation (11) resulting in 66.2 ± 7.4 kJ mol^{-1} (r^2 = 0.97) and 56.4 ± 9.8 kJ mol^{-1} (r^2 = 0.95) for HPB and CNP.

2.3.4 Solvent uptake into the model wax

Solvent molecules may enter and diffuse across the wax layers simultaneously with the solute molecules. To investigate this process, the water- and methanol-specific OH stretching vibrations, both occurring simultaneously at ~ 3400 cm^{-1} were quantified during HPB (Figure 19A) and CNP (Figure 19B) diffusion experiments at the different temperatures.

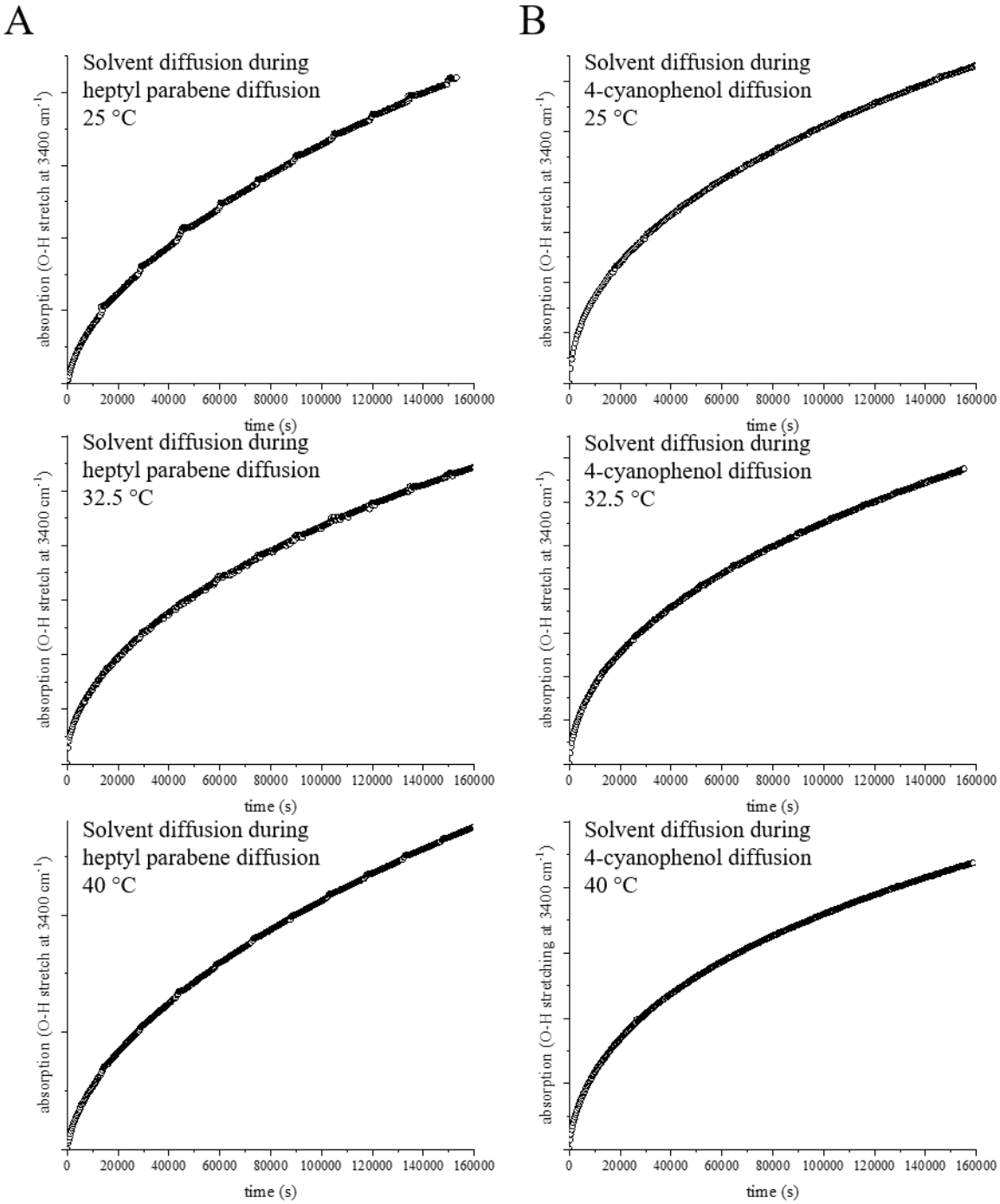

Figure 19. Integrated absorption of solvent specific OH-stretching vibration during diffusion of (A) heptyl parabene and (B) 4-cyanophenol in paraffin wax at 25, 32.5 and 40 °C, recorded via ATR-FTIR.

The shapes of the time courses resembled those found for the organic model compounds studied here. After an initial steep slope, the curves transitioned to linear sections whose slope was constant over the duration of the experiment. This indicates a constant flux of solvent from the reservoir into the spatial compartment covered by the evanescent wave of the ATR-FTIR setup.

2.4 Discussion

AI diffusion across the plant cuticle is the rate limiting step for the foliar uptake of systemic pesticides. Therefore, characterizing and mechanistically understanding the diffusive movement of the penetrating AI molecules in the wax barrier of the cuticle is a prerequisite for optimizing pesticide application under economic and ecological restraints. A high-resolution ATR-FTIR-based system for the accurate determination of organic compound diffusion kinetics in a cuticular model wax was established.

2.4.1 Paraffin wax as cuticular model wax

Thin wax films of constant and uniform thickness mimicking the waxy cuticular diffusion barrier are a prerequisite for determining the diffusion kinetics of organic compounds in a wax with the ATR-FTIR-based method described here. Such films can be produced routinely using the spin coating approach (Figure 14). A disadvantage of this method, however, is that a relatively large amount of wax is required for each crystal coating (approximately 0.5 ml of molten wax). Such amounts of wax significantly exceed the quantities of cuticular wax which can be obtained by extracting isolated cuticles with chloroform (Riederer and Schneider, 1989). Therefore, a commercially available model for plant cuticular waxes had to be used. Since many cuticular waxes consist of very-long-chain alkanes (Holloway, 1994) a polydisperse paraffin wax with a weighted average chain length of 30.32 carbon atoms (Figure 12) was chosen.

2.4.2 Diffusion kinetics

This study aimed to translate ATR-FTIR approaches developed for the determination of diffusion kinetics in polymers (Fieldson and Barbari, 1993; Fieldson and Barbari, 1995; Pellett *et al.*, 1997a, b; Sammon *et al.*, 1998; Dias *et al.*, 2001; Elabd *et al.*, 2003; Döppers *et al.*, 2004; Dhoot *et al.*, 2009; McAuley *et al.*, 2010) to quantitatively characterize the movement of

organic model compounds in a wax representing a model for plant cuticular waxes. The time-courses recorded for two model compounds at three temperatures each consistently deviated from kinetics to be expected from simple Fickian diffusion (Figure 17). While at the beginning of the diffusion experiments the concentrations of the diffusants in the wax increased as to be expected during Fickian diffusion, the curves transitioned to linear sections with smaller slopes but extending without showing signs of reaching an equilibrium over the whole course of the experiments (67 h). Thus, the observed kinetics may result from two independent mechanisms acting on different timescales. (1) Fickian diffusion as a faster mechanism leading to the movement of diffusant into the wax until the sorption equilibrium between the wax and the outside reservoir is reached and the driving force for the uptake of diffusant into the wax ceases, and (2) a mechanism becoming relevant only after the diffusant has reached its equilibrium concentration in the wax and being independent of the concentration gradient driving Fickian diffusion kinetics of water and organic compounds in various substrates such as rubbery membranes, semicrystalline polymers or even natural substrates like the human skin (Fieldson and Barbari, 1995; Pellett *et al.*, 1997b; Elabd *et al.*, 2003). McAuley *et al.* (2010) determined a diffusion coefficient of 6.3 x 10^{-11} m^2 s^{-1} for CNP diffusion in rubbery silicone membranes (McAuley *et al.*, 2010). Diffusion kinetics of other organic model compounds comprising similar molar volumes as HPB were also investigated. For example, methyl nicotinate and butyl parabene diffusion in silicone membranes revealed diffusion coefficients of 3.6 x 10^{-11} m^2 s^{-1} and 10 x 10^{-11} m^2 s^{-1}, respectively (McAuley *et al.*, 2009). Silicone membranes typically appear in a rubbery state which explains the comparably high diffusion coefficients exceeding those observed here for the diffusion in wax by about four orders of magnitude. In contrast to rubbery polymers, semicrystalline polymers are often used as barrier coatings in packaging and separation applications (Vieth, 1991). Compound mobilities in semicrystalline polymers such as polyethylene (PE), polyethylene terephthalate (PET) or polyvinyl alcohol (PVA) membranes, determined by ATR-FTIR, are considerably lower than those in rubbery polymers (Sammon *et al.*, 1998; Döppers *et al.*, 2004; Dhoot *et al.*, 2009). Dhoot *et al.* (2009) investigated eugenol diffusion in linear-low-density-polyethylene (LLDPE) and found a diffusion coefficient of 3 x 10^{-14} m^2 s^{-1} (Dhoot *et al.*, 2009). Furthermore, Sammon *et al.* (1998) determined diffusion coefficients for water in semicrystalline PET in the range of 5 x 10^{-14} m^2 s^{-1} and 8 x 10^{-13} m^2 s^{-1}, increasing from 25 % to 5 % crystallinity, showing the diffusion coefficient being strongly dependent on the polymer crystallinity level (Sammon *et*

al., 1998). Again, the diffusion coefficients of HPB and CNP in the model wax are lower than those for comparable diffusants in semicrystalline polymers but in this case only by about one order of magnitude. This can be explained by the high degree of orthorhombic crystallinity of the model wax within the temperature range of our experiments (Figure 13B).

The presented results underline the excellent barrier properties of paraffin wax films with degrees of orthorhombic crystallinity comparable to those of plant cuticular waxes (Merk *et al.*, 1997) thus making them an ideal model system to study diffusion. The diffusion coefficients reported here may be compared to diffusion coefficients of organic compounds in reconstituted cuticular waxes previously published. The presented values for the two compounds diffusing in paraffin wax are significantly higher than those published earlier (Schreiber, 2006). The discrepancy may be due to differences in wax composition and film structure as well as the fact that earlier work relied on a desorption approach which may restrict the availability for desorption of certain parts of the diffusants. Further work will have to focus on the effects these variables have on the diffusion coefficients measured.

2.4.3 Temperature dependence of Fickian diffusion

Hot environments and high irradiation levels lead to increased leaf temperatures, resulting in increased compound mobilities within the cuticle (Kappen, 1981; Baur and Schönherr, 1995). Earlier investigations of organic compound desorption from isolated cuticles via unilateral desorption from the outer surface (UDOS) have shown the mobility of organic compounds being strongly dependent on temperature (Baur and Schönherr, 1995; Baur *et al.*, 1997a; Buchholz and Schönherr, 2000).

Diffusion kinetics of organic molecules in isolated cuticles at different temperatures revealed activation energies in the range from 75 to 189 kJ mol^{-1} depending on plant species and diffusant size (Baur and Schönherr, 1995; Baur *et al.*, 1997a; Buchholz and Schönherr, 2000). Thermal effects on the mobility properties of organic compounds in cuticles are difficult to interpret since the different components of the cuticle (cutin matrix, cuticular waxes, polysaccharides) interact and may undergo differential changes due to temperature (López-Casado *et al.*, 2007). The method presented here allows to study the effect of temperature on the barrier properties of the wax fraction separately from other effects. Using the ATR-FTIR-based method, temperature-dependent Fickian diffusion kinetics of the model compounds HPB and CNP sorption in the cuticular model wax could be measured at three different

temperatures from 25 °C to 40 °C. Plotting ln *D* vs. 1/T yielded linear Arrhenius plots for HPB and CNP diffusion (Figure 18). This indicates that within this temperature interval the model wax did not undergo structural changes on the molecular level as sensed by the diffusing molecules. Diffusion coefficients increased by factors of 3.20 and 3.84 from 25 °C to 40 °C (Table 2) and the activation energies estimated according to equation (11) were 66.2 ± 7.4 kJ mol^{-1} (r^2 = 0.97) and 56.4 ± 9.8 kJ mol^{-1} (r^2 = 0.95) for HPB and CNP, respectively. The activation energies are of the same order of magnitude as those obtained by desorption experiments from isolated cuticles underlining the suitability of the paraffin wax used here as a model for cuticular wax (Baur and Schönherr, 1995; Baur *et al.*, 1997a; Buchholz and Schönherr, 2000). Further studies characterizing temperature effects on the diffusion of organic molecules in cuticular model waxes closer to biological systems, comprising broader variations of VLCAs, such as n-alcohols or fatty acid esters, will lead to a better understanding of temperature effects on the cuticular penetration barrier.

2.4.4 Deviations to the Fickian diffusion model

In the previous sections it was suggested that the curves describing the time-course of the uptake of the organic model compounds into the model wax (Figure 17) consist of an initial part dominated by Fickian diffusion and a later part becoming visible only after the diffusant has reached its equilibrium concentration in the wax. These pseudo-equilibria can be deduced by fitting equation (10) to the initial parts of the curves. However, the intensities of the characteristic vibrational bands for the two model compounds linearly increase beyond the pseudo-equilibria even though at a much slower rate. This implies that the mechanism leading to slowly increasing amounts of the model compounds within the range of the evanescent wave is independent of the concentration gradient driving Fickian diffusion.

A similar deviation of the experimental kinetics from the Fickian model has been described by McCarley *et al.* (2003) who investigated CNP diffusion from solutions into silicone membranes using an analogous ATR-FTIR setup (McCarley and Bunge, 2003). The authors point out that the solvent is also taken up into the polymer and diffuses across it simultaneously with the solvent. Using ATR-FTIR imaging, McAuley *et al.* (2010) demonstrated that small discrete solvent pools become apparent between the polymer and the outer surface of the ATR crystal within the reach of the evanescent wave (McAuley *et al.*, 2010). Condensed water or other polar solvents on the surface of the ATR crystal is favored by the hydrophilicity of ZnSe

surfaces (Lohar *et al.*, 2014). Diffusant molecules re-dissolve in the condensed solvent and build up appreciable concentrations in the solvent pools when they are readily soluble in the solvent. If the diffusant concentration in the solvent pools in the vicinity of the crystal surface is much smaller than in the reservoir the diffusant will permeate the polymer (or the wax film) at a constant flux rate leading to an increase of the signal detected by the ATR-FTIR system (McAuley *et al.*, 2010).

For testing whether in our system appreciable amounts of solvent occur within the range of the evanescent wave the intensities of the solvent-specific OH-stretching vibrations were monitored in all experiments (Figure 19) simultaneously with the characteristic bands of the diffusants (Figure 17). Quite like the diffusant kinetics the curves rise steeply at the beginning but also transition to continuous slower increases over the whole remaining time of the experiment (Figure 19). No indications of the onset of pseudo-equilibria are detectable. Hence, it was hypothesized that the extended linear increase of the solvent signal signifies the buildup of condensed solvent in a microscopic scale in between the surface of the ZnSe crystal and the model wax film. With increasing volumes of solvent condensing increasing amounts of diffusant will dissolve in the solvent pools leading to increasing intensities of the diffusant-characteristic bands at experimental times when the Fickian diffusion governed equilibrium has long been reached.

It was concluded that the ATR-FTIR-based approach for measuring the diffusion of organic molecules in model wax can be used to derive valid Fickian diffusion coefficients from the initial parts of the sorption kinetics while the undefined absorption increases of the curves result from the special properties of the experimental system used and do not reflect properties of the wax *per se*. Although the diffusion kinetics determined using the ATR-FTIR based method provide insight into the extraordinarily barrier nature of cuticular waxes, the results shown here should first be considered as proof of principle. Due to the extraordinarily low mobility of organic compounds in cuticular waxes, as was shown here for the model paraffin wax, elucidating diffusion kinetics of unformulated AIs is irrelevant in plant protection science. Instead, enhancement of uptake is essential for effective biodelivery and may be achieved by increasing AI mobility by using accelerating adjuvants. Subsequent chapters will therefore directly address adjuvant uptake and influenced model AI uptake in cuticular model waxes using the established ATR-FTIR based method. In addition to deciphering diffusion kinetics, the ATR-FTIR based tool introduced here offered the best prerequisites to

simultaneously characterize modifications in the wax and to draw conclusions on the plasticization and the acceleration of the AI uptake in the later sections.

3 Chapter 2: Adjuvant diffusion in cuticular model waxes and plasticization events

3.1 Introduction

3.1.1 Cuticular model waxes used within this study

Cuticular waxes are usually very heterogeneous mixtures of aliphatic components contributing broad chain length distributions and functional group variations (Jetter *et al.*, 2008). Additionally, cyclic components may also be present, but several studies rejected their role as barrier forming elements (Jetter and Riederer, 2016; Staiger *et al.*, 2019). To investigate the adjuvant impact on the barrier properties, cuticular model waxes had to be chosen which, on the one hand, mainly consist of barrier defining VLCAs and on the other hand, represent heterogeneous systems contributing alterations in polarity, chain length distribution and functional group variation. Based on these prerequisites, candelilla wax was chosen representing a simplistic basis of a heterogeneous mixture of various VLCAs such as n-alkanes, n-alcohols and free fatty acids. Furthermore, carnauba wax was investigated, also being dominated by VLCAs, but unlike candelilla wax mainly contributing long-chain alkyl esters and n-alcohols.

3.1.2 Accelerators used within this study

The characterization of cuticular barrier properties in terms of wax chemistry and structure are important in crop protection science. Usually, pesticides can only reach their specific sites of action in the plant via the cuticular route (Riederer and Schönherr, 1985). Due to the excellent barrier properties of the cuticle and especially the cuticular waxes, pesticide molecules are formulated together with emulsifiers or adjuvants (Falk, 1994). They help reduce the surface tension of the spray solution, act as emulsifiers themselves, form micelles, increase spray retention, promote rain fastness (McMullan, 2000), and most importantly, modify the cuticle structure thus accelerating the uptake rate of an AI into the cuticle, which terms them accelerators (Penner, 2000). One major group of accelerating adjuvants mostly used for pesticide formulations are surfactants or alcohol ethoxylates (AE) (Kirkwood, 1994). Usually, polydisperse surfactants are used in pesticide formulations to enhance AI uptake rates into the plant. They contribute varying molecular structures and physical-chemical

properties (Miller and Westra, 1998; Hess, 1999; Asmus *et al.*, 2016). Polydisperse AEs showed a wax-disrupting effect (Perkins *et al.*, 2005). Electron spin resonance spectroscopy (ESR) revealed an unspecific effect of AEs, creating a liquid environment surrounding AI within the wax (Schreiber *et al.*, 1996b). Furthermore, a softening of cuticular waxes by AE treatment has been observed via AFM (Grant *et al.*, 2008). However, there is no clear evidence on the MoA of accelerator adjuvants (Hess, 1999). It must be noted that the compositional complexity of polydisperse AEs renders mechanistic studies on the MoA difficult (Schönherr *et al.*, 1991). In contrast, monodisperse AEs are pure substances and are therefore more suitable for basic studies on the MoA in cuticular model waxes (Burghardt *et al.*, 1998; Burghardt *et al.*, 2006). Consequently, the monodisperse AEs C12E2, C12E4 and C12E6 contributing the same hydrocarbon chain length, but differing in respective ethoxylation degrees (EO) were used within this study. Coret *et al.* (1993) stated permeation into the cuticle is highest for AEs with low EO content, while surfactants with high EO content increase the hydration state of the cuticle at a given relative humidity (RH) (Coret and Chamel, 1993; Coret and Chamel, 1995). Moreover, Burghardt *et al.* (2006) showed the maximum AE concentration within a cuticular wax linearly affects organic compound mobility (Burghardt *et al.*, 2006). This is in concordance with previous results (Riederer *et al.*, 1995; Burghardt *et al.*, 1998) suggesting AEs exhibiting a common intrinsic effect, only depending on the AE amounts sorbed in the wax.

However, no data on diffusion kinetics of wax penetrating AEs with different EO content have been provided so far, which is necessary for understanding the actual MoA. Moreover, there are no studies describing the effects of monodisperse AEs on cuticular waxes depending on their respective VLCA compositions. Besides monodisperse AEs, also TEHP and methyl oleate were used in this study, both being extensively used in pesticide formulations. Literature data on the MoA of TEHP is rare. TEHP was shown to drastically enhance uptake rates of the herbicide pinoxaden (Muehlebach *et al.*, 2011). Furthermore, Arand *et al.* (2018) showed pinoxaden penetration rate across isolated cuticles of *Prunus laurocerasus* was drastically increased by TEHP (Arand *et al.*, 2018). They explained their finding with TEHP entering the cuticle, leading to unspecified modification of the cuticle structure. However, evidence on the MoA is still lacking. Contrastingly, data on wax modification induced by oil derivatives is well available and provides basic understanding of their respective MoA (Gauvrit and Cabanne, 1993; Hamilton, 1993; Nalewaja, 2002; Zhang *et al.*, 2016; Webster *et al.*, 2018). Especially the esterified seed oil methyl oleate is most extensively used in pesticide formulations. Gauvrit

and Cabanne (1993) showed oil adjuvants impregnating cuticular waxes within a few seconds, proposing an intrinsic wax modification (Gauvrit and Cabanne, 1993). Hazen (2000) suggested that esterified seed oils may act as plasticizers or wax disruptors, promoting the uptake of AIs in the plant (Hazen, 2000) and Webster *et al.* (2018) observed decreasing α-crystallite level in tristearin, correlating with increasing amounts of methyl oleate and other esterified fatty acids, again suggesting a wax disrupting effect (Webster *et al.*, 2018). However, no discrimination of methyl oleate affecting waxes with altering amount of different VLCA fractions was done yet. Even though there is one study reporting polysorbates and Span 65 affecting crystallinity levels in carnauba wax (Zhang *et al.*, 2016), there was no effort made on investigating methyl oleate induced modification of cuticular wax crystallinity.

3.1.3 Objectives and research questions

In Chapter 1 the diffusion kinetics of the organic compounds HPB and CNP representing models for AIs, were successfully determined in the cuticular model wax paraffin via ATR-FTIR. It was shown that the applied ATR-FTIR method was suitable for analyzing diffusion of different molecules based on their IR vibrational spectra and that the method provides high resolution diffusion kinetics over extended time periods. However, due to very low mobilities of AIs in cuticular waxes, as was indicated by respective diffusion coefficients in the range of 10^{-15} m^2 s^{-1} (chapter 1), they are usually formulated together with accelerating adjuvants. This adjuvant class was shown to drastically enhance AI uptake rates in the plant, leading to increased bioavailability. It was suggested that accelerators modify the wax barrier somehow, but evidence on their specific MoA is lacking. Consequently, the aim of this study was to determine accelerator diffusion kinetics, while simultaneously characterizing the modification of structural properties in cuticular model waxes dominated either by n-alkanes or very-long chain alkyl esters by ATR-FTIR.

Diffusion kinetics of the accelerating adjuvants methyl oleate, TEHP and three selected monodisperse AEs C12E2, C12E4 and C12E6 should be characterized to decipher self-accelerating properties. Furthermore, simultaneously recorded modifications of the wax structure, such as decreasing orthorhombic crystallinity, influence on internal hydrogen bonding, and impaired molecular density should serve as indicators for plasticization processes.

3.2 Material and methods

3.2.1 Chemicals

All chemicals used in this study are listed in Table 1. Candelilla wax and carnauba wax served as cuticular model waxes. Methyl oleate, TEHP and the three selected monodisperse AEs C12E2, C12E4 and C12E6 represented accelerator adjuvants used for diffusion studies in cuticular model waxes (Figure 20).

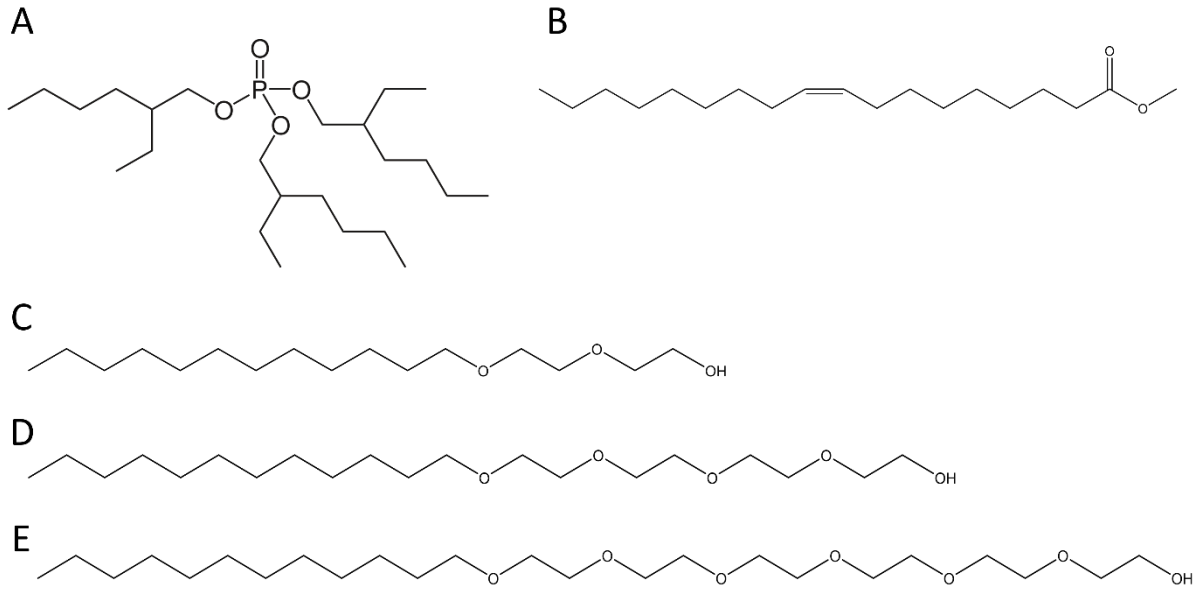

Figure 20. Chemical structures of (A) TEHP, (B) methyl oleate, (C) C12E2, (D) C12E4 and (E) C12E6.

BSTFA and pyridine were used for silylation of polar compounds in candelilla and carnauba wax for GC analysis.

3.2.2 ATR-FTIR experimental setup and data collection for adjuvant diffusion

The diffusion kinetics of methyl oleate, C12E2, C12E4, C12E6 and TEHP in candelilla and carnauba wax were determined by ATR-FTIR. Pure adjuvants were applied on top of wax layers, equally distributed on an ATR crystal with the spin coating technique. The adjuvant diffusion towards the crystal-wax interface resulted in increasing molecular concentrations within the evanescent wave over time, leading to increasing IR absorptions induced by respective vibration modes. A carbonyl (C=O) stretching vibration at 1736 cm^{-1} was considered for determining methyl oleate diffusion kinetics. AE (C12E2, C12E4 and C12E6) diffusion kinetics were evaluated using a C-O-C stretching vibration at 1100 cm^{-1}, respectively, and TEHP diffusion kinetics were determined using a P-O-C stretching vibration at 1013 cm^{-1}. The

corresponding absorption bands were integrated for each spectrum and assigned to the respective measurement time.

The same experimental setup as described in 2.2.2 was used. Exceptions were: FTIR absorption spectra were recorded with another Fourier-transform infrared spectrometer (FTIR, Bruker Invenio R with liquid N2-cooled MCT-detector, Bruker, Ettlingen, Germany). 16 scans instead of 120 scans were used for each averaged IR-spectrum. For controlling the FTIR-apparatus and to collect absorption spectra, the software OPUS 8.2 instead of OPUS 7.2 (Bruker, Ettlingen, Germany) was used. Background spectra of bare ATR crystals were used, instead of with wax coated ATR crystals. Approximately 100 µl to 300 µl of the respective liquid adjuvants were applied on top so that the ATR crystal surface was fully covered. IR-absorption spectra were recorded every 20 seconds to 2 minutes over a maximum time range of 16 hours.

3.2.3 Preparation of wax samples

Candelilla wax or carnauba wax as well as a trapezoidal ATR crystal (ZnSe 72 x 10 x 6 mm, Specac Ltd, Orpington, United Kingdom) were heated up to 120 °C using a heating module (Labnet Dry Bath, Labnet International Inc., Corning, NY, USA). The ATR crystal was attached to a POLOS^{TM} spin coater SPIN150i-NPP (SPS-Europe GmbH, Ingolstadt, Germany). A small amount of liquid wax was then drawn up into a glass pipette and subsequently applied on top of the preheated ATR crystal until its surface was fully covered. Subsequent spin coating of the ATR crystal was performed for 15 seconds at 2000 rpm for candelilla wax and at 2250 rpm for carnauba wax, followed by a wax solidification phase for 10 to 30 seconds at 500 rpm. Solidified wax at the long or bottom sides of the ATR crystal was wiped with chloroform.

3.2.4 Determination of wax film thickness, diffusion coefficients and data evaluation of ATR-FTIR absorption spectra

Determination of wax film thicknesses and diffusion coefficients were determined according to 2.2.4, 2.2.5. Data evaluation was performed as previously described in 2.2.6.

3.2.5 Determination of candelilla wax and carnauba wax melting behavior and orthorhombic crystallinity

Determination of melting behavior and orthorhombic crystallinity was performed according to 2.2.8. Orthorhombic crystallinity was determined using the height ratios of wax specific CH_2

scissoring vibrations at 1472 cm^{-1} and 1462 cm^{-1}, according to Zerbi *et al.* (1989). The determination of orthorhombic crystallinity below a certain value (about 72%) was not possible due to merging doublet bands, thus eliminating the discrimination of respective absorption contributions.

3.2.6 Gas-chromatographic analysis (GC)

5 mg of candelilla wax and carnauba wax were dissolved in 100 ml chloroform. 0.1 ml of the solutions were derivatized with 10 µL BSTFA and 10 µL pyridine at 70 °C for 30 min using a heating module (Pierce Reacti-Therm, Pierce Chemical, Dallas, TX, USA). The mixture was then dissolved in 100 µl chloroform and used for gas chromatography (GC). GC-mass spectrometry (GC-MS; 6890 N, GCSystem; Agilent Technologies, Santa Clara, CA, USA) was used to identify wax compounds. Helium was used as a carrier gas. A MS detector (m/z 50–1000, MSD 5977A, Agilent Technologies) was applied. Due to the high boiling points of long-chain esters, on-column injection was performed using a capillary high-temperature column (30 m × 0.32 mm, DB-1HT, 0.1 µm film: J&W Scientific, Agilent Technologies). The liquid sample was injected at 50 °C and the temperature was hold for 1 min. The temperature was then increased to 120 °C at a heating rate of 10 °C min^{-1} and hold for 1 min. The temperature was then increased to 240 °C at a heating rate of 7.5 °C min^{-1} and hold for 1 min. The temperature was then increased to 390 °C at a heating rate of 4 °C min^{-1} and hold for 10 min. Identification was undertaken using Wiley 10th/NIST 2014 mass spectral library (John Wiley & Sons, Hoboken, NJ, USA) reference specimen or spectra interpretation. Quantification was undertaken using GC flame ionization detection (GC-FID, 6850N, Agilent Technologies, Santa Clara, CA, USA). Similar GC conditions as before were used to separate compounds, except that hydrogen gas was used as the carrier gas.

3.3 Results

3.3.1 Wax analysis

Wax analysis revealed that candelilla wax consisted of 84.7 % barrier-forming VLCAs (Figure 21A, n=6).

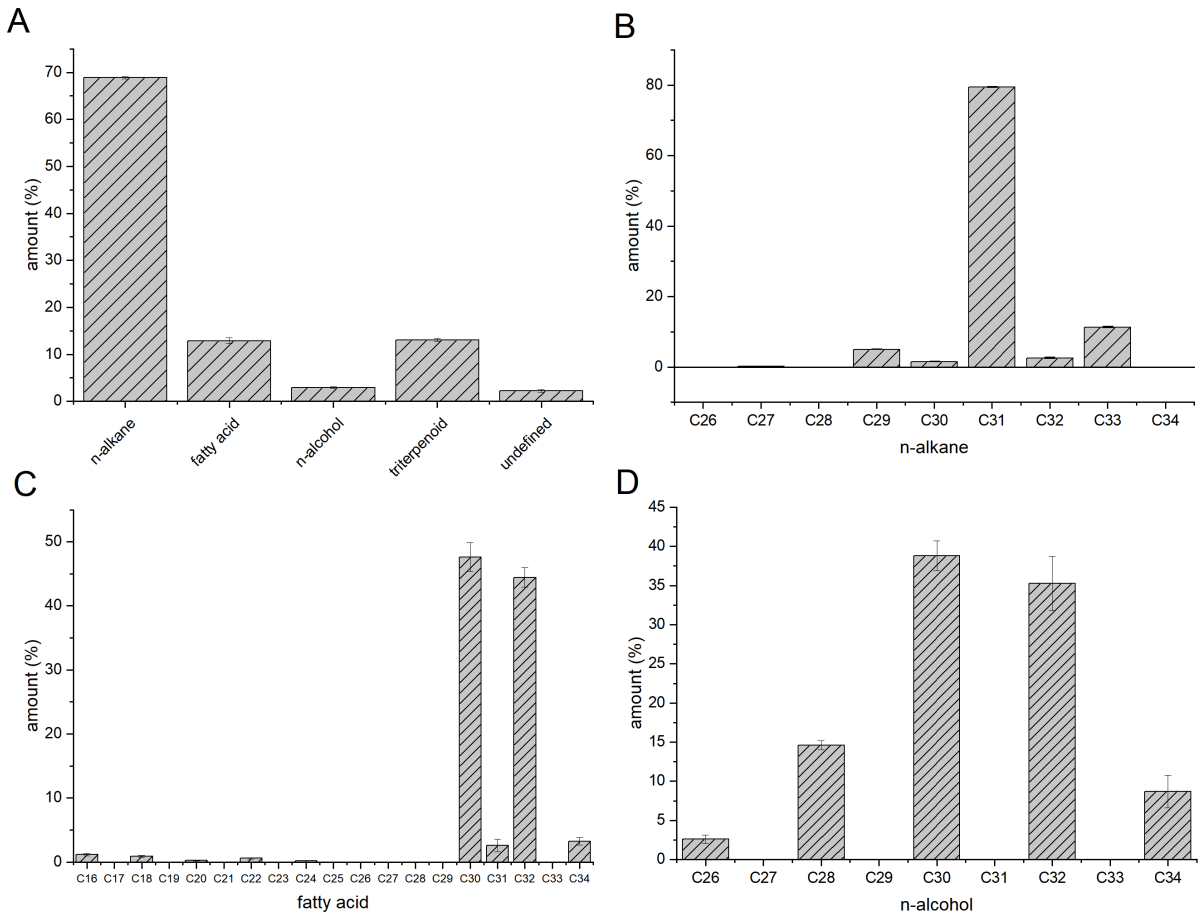

Figure 21. (A) Chemical composition of major compound groups in candelilla wax and carbon chain length distribution of (B) n-alkanes, (C) free fatty acids and (D) n-alcohols in candelilla wax.

The VLCA fraction was dominated by n-alkanes (68.9 ± 0.2 %) (Figure 21A). Minor amounts of fatty acids (12.9 ± 0.6 %), n-alcohols (2.9 ± 0.2 %) and triterpenoids (11.2 ± 0.3 %) were found. N-alkanes were dominated by C31 (79.4 ± 0.1 %), with minor amounts of n-alkanes with chain lengths ranging from C27 to C33 (Figure 21B). Odd-numbered n-alkanes were most prominent. The fatty acid fraction was dominated by C30ac (47.6 ± 2.3 %) and C32ac (44.4 ± 1.5 %) (Figure 21C). The n-alcohol fraction consisted solely of even-numbered n-alcohols ranging from C26ol to C34ol with C30ol (38.8 ± 1.9 %) being most prominent (Figure 21D). The melting behavior of candelilla wax was analyzed via ATR-FTIR (Figure 22).

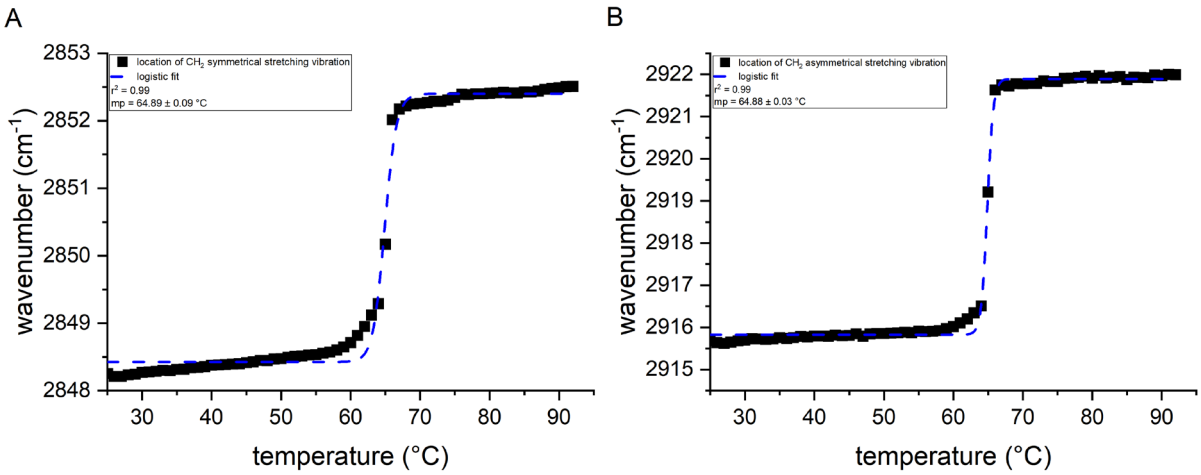

Figure 22. Wavenumber shift of (A) asymmetrical and (B) symmetrical CH_2-streching modes, indicating melting range of candelilla wax and logistic fit.

Candelilla wax asymmetrical (Figure 22A) and symmetrical (Figure 22B) CH_2-stretching vibrations each showed one defined wavenumber shift with their midpoint at approximately 65 °C, indicating a phase transition from solid to liquid state. Carnauba wax chemical composition was analyzed as well (Figure 23, n=3).

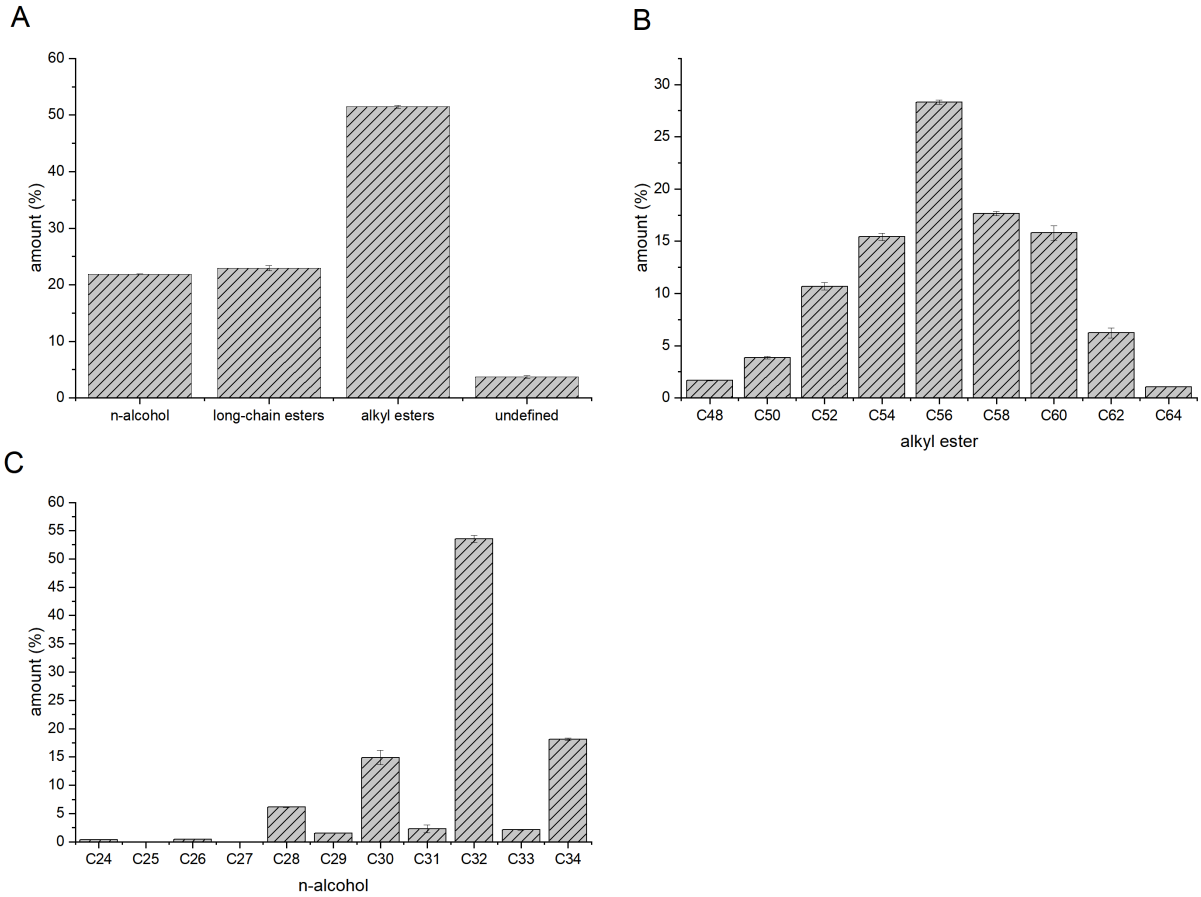

Figure 23. (A) Chemical composition of carnauba wax and carbon chain length distribution of (B) alkyl ester fraction and (C) n-alcohol fraction.

In contrast to candelilla wax, which was dominated by n-alkanes and free fatty acids, carnauba wax consisted mainly of long-chain alkyl esters (51.5 ± 0.3 %), other long-chain esters (22.9 ± 0.5 %), which were not identified more specifically, but according to literature, mainly consist of aromatic compounds (Basson and Reynhardt, 1988), as well as of n-alcohols (21.8 ± 0.0) (Figure 23A). Alkyl ester composition followed a Gaussian manner with C56 being most prominent. Carbon chain lengths of the alkyl ester fraction ranged from C48 up to C64 (Figure 23B). N-alcohols were at least present (21.9 ± 0.0 %) (Figure 23C). Carbon chain lengths ranged from C24 to C34 with C32 being dominant. Other VLCAs such as free fatty acids or n-alkanes were not found.

Carnauba wax melting behavior was also analyzed by ATR-FTIR (Figure 24).

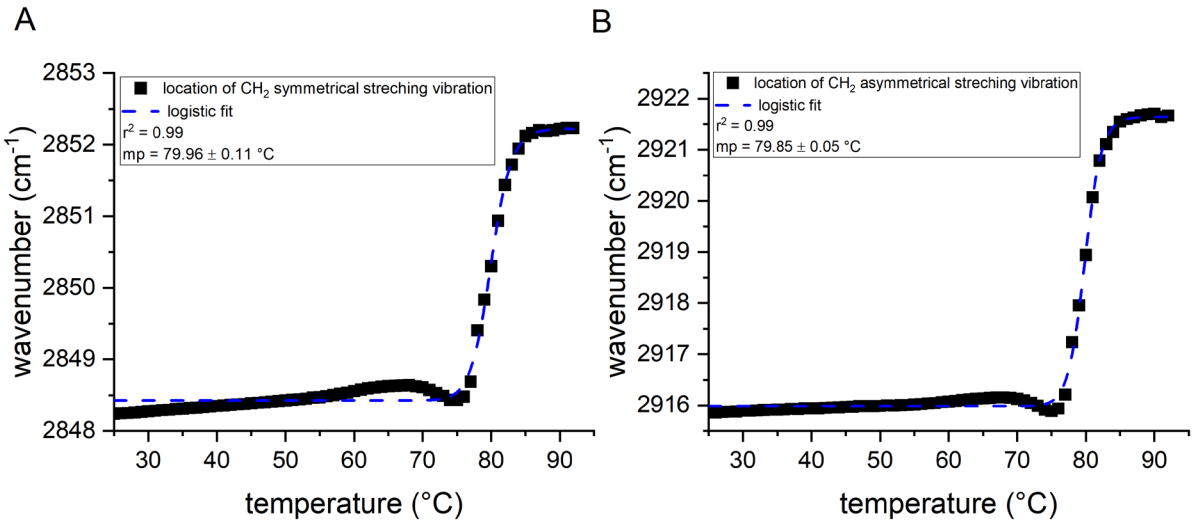

Figure 24. Wavenumber shift of (A) asymmetrical and (B) symmetrical CH_2-streching modes, indicating melting range of carnauba wax and logistic fit.

Carnauba wax asymmetrical (Figure 24A) and symmetrical (Figure 24B) CH_2-stretching vibrations each showed one defined wavenumber shift at approximately 80 °C, indicating a phase transition from solid to liquid state.

In conclusion, candelilla wax and carnauba wax both consisted mainly of barrier-forming VLCAs but contributed entirely different VLCA fractions (alkane-dominated candelilla wax and alkyl ester dominated carnauba wax). Furthermore, both waxes showed one defined transition from solid to liquid state, but melting points differed by approximately 15 °C.

3.3.2 Methyl oleate diffusion in candelilla and carnauba wax

The presented ATR-FTIR method allowed the observation of different molecular vibrations specific to diffusing adjuvants entering the wax over time. The diffusion of methyl oleate was characterized by relating the integrated IR absorption of the C=O stretching vibration specific to methyl oleate (1736 cm^{-1}) to the experimental time scale, revealing its diffusion kinetics in real time (Figure 25).

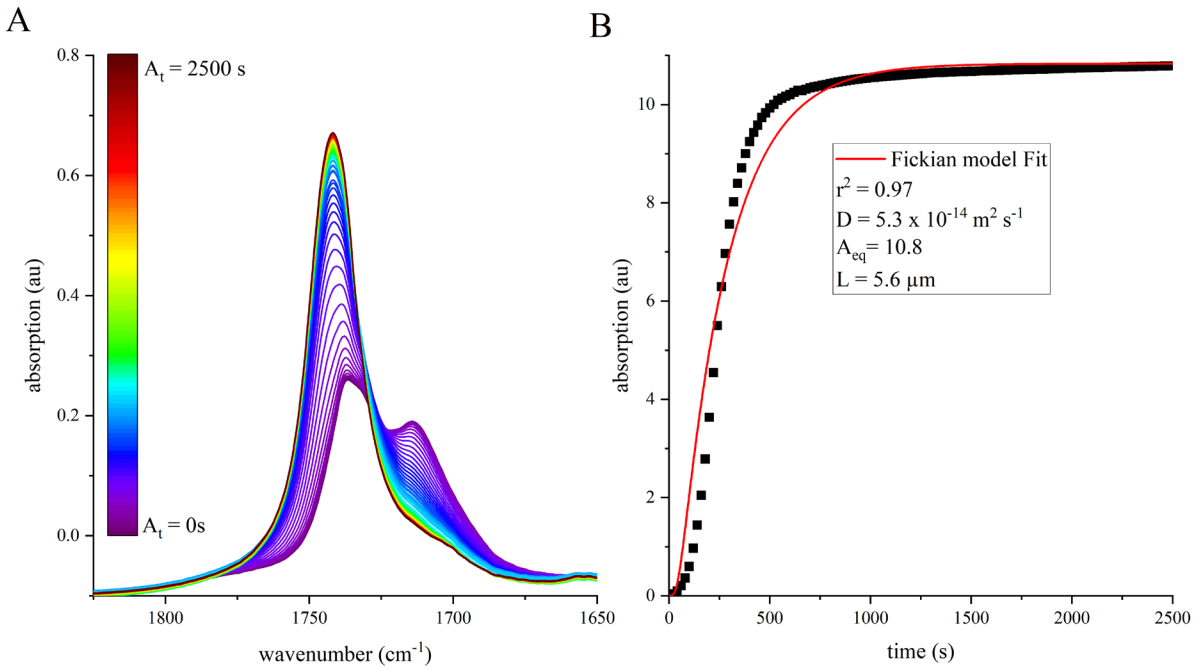

Figure 25. (A) ATR-FTIR specific absorption of monomeric (~1736 - 1742 cm^{-1}) and dimeric (1714 cm^{-1}) C=O vibration bands recorded during diffusion of methyl oleate in spin coated candelilla wax. Absorption recorded at time *t* is indicated by A_t. (B) Deconvoluted and integrated absorption of methyl oleate specific C=O vibration (1736 – 1742 cm^{-1}) in spin coated candelilla wax recorded during diffusion up to 2500s and the applied Fickian model fit is shown.

The initial absorption at 1736 cm^{-1} represented the carbonyl stretching vibration of the monomeric free long-chain fatty acids of the wax, whereas the vibration at 1714 cm^{-1} corresponded to the carbonyl groups of the fatty acids present dimeric via hydrogen bonds (Figure 25A, A_t = 0s).

External application of methyl oleate to the candelilla wax layer resulted in an increasing IR-absorption of the monomeric (1736 cm^{-1}) C=O stretching vibration over time, which was attributed to diffusing methyl oleate molecules toward the evanescent wave. At the same time, an absorption decrease of the dimeric vibrational band of the wax-specific components was observed, indicating a break of the intermolecular hydrogen bonds within the wax structure. Since both monomeric and dimeric C=O vibrational modes coexisted during the diffusion of methyl oleate, but only the IR-absorption increase of the monomeric vibration was relevant to the determination of methyl oleate diffusion kinetics, Gaussian peak deconvolution was performed. To determine methyl oleate specific diffusion kinetics, initial wax specific absorption of monomeric (1736 cm^{-1}) and dimeric (1714 cm^{-1}) C=O vibrations were subtracted from all deconvoluted absorptions, separating methyl oleate specific

absorption levels over the experimental time range (Figure 25B). Wax layer thickness was 5.6 µm and according to equation (10), the diffusion coefficient of methyl oleate in candelilla wax was determined to be 5.3 x 10^{-14} m^2 s^{-1} (Figure 25B).

The methyl oleate diffusion kinetics in carnauba wax were also investigated (Figure 26).

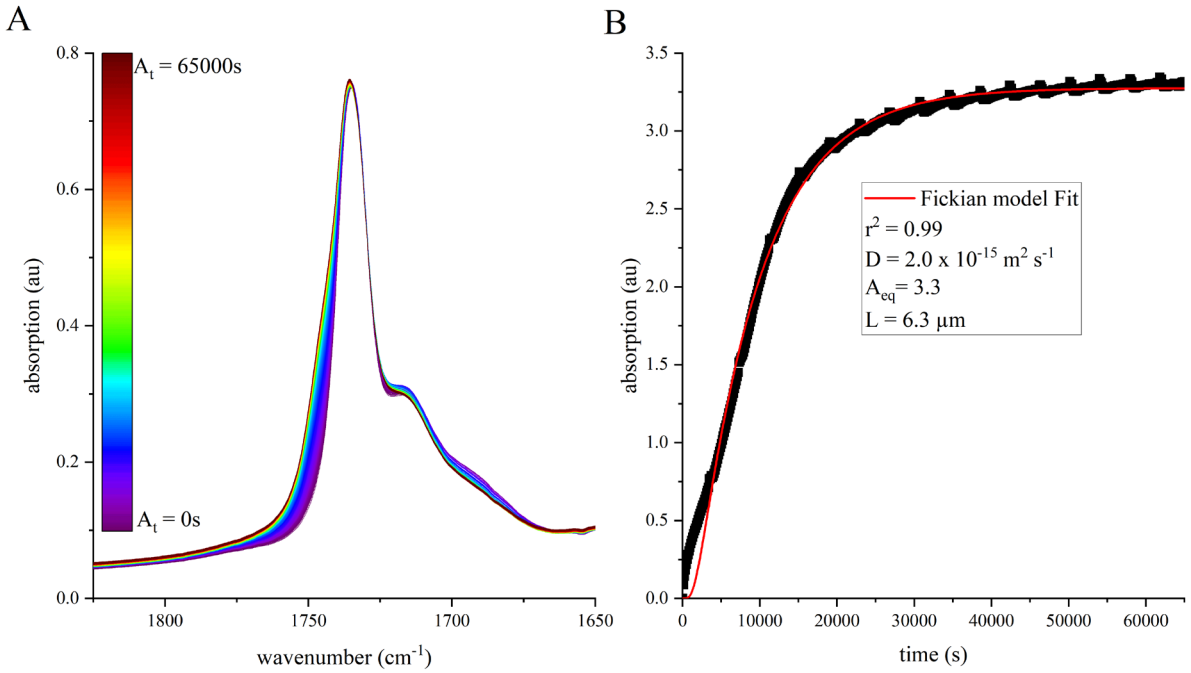

Figure 26. (A) ATR-FTIR specific absorption of monomeric (~1736 - 1742 cm^{-1}) and dimeric (1714 cm^{-1}) C=O vibration bands recorded during diffusion of methyl oleate in spin coated carnauba wax. Absorption recorded at time *t* is indicated by A_t. (n=1) (B) Integrated absorption of methyl oleate specific C=O vibration (1736 – 1742 cm^{-1}) in spin coated carnauba wax was recorded during diffusion up to 65000s and the applied Fickian model fit is shown.

In contrast to the diffusion in candelilla wax, the increase of methyl oleate specific IR-absorption of the monomeric C=O stretching vibration was less intense (Figure 26A). A broadening towards higher wavenumbers was observed instead of a constantly rising absorption band. Increasing absorption was attributed to diffusing methyl oleate molecules towards the evanescent wave. Initially observed absorption was subtracted to compensate for carnauba wax specific C=O stretching vibration (Figure 26B). Wax layer thickness was determined to be 6.3 µm and the diffusion coefficient was calculated to be 2.0 x 10^{-15} m^2 s^{-1}, which indicated a 26.5 times lower diffusion process as observed for methyl oleate in candelilla wax.

3.3.3 Methyl oleate effect on orthorhombic crystallinity in candelilla and carnauba wax

Beyond the determination of the diffusion kinetics of methyl oleate, the influence on wax structural properties were characterized simultaneously by ATR-FTIR. The methyl oleate-induced change in the intensity ratio of the orthorhombic crystallinity bands revealed modification of orthorhombic crystallinity. The quotient of the IR-absorption height induced by wax specific CH_2 scissoring vibrations occurring at 1472 cm^{-1} and 1462 cm^{-1} represented the level of wax specific orthorhombic crystallinity. Candelilla wax specific orthorhombic crystallinity was determined during methyl oleate diffusion over a time range of 2500 s (Figure 27).

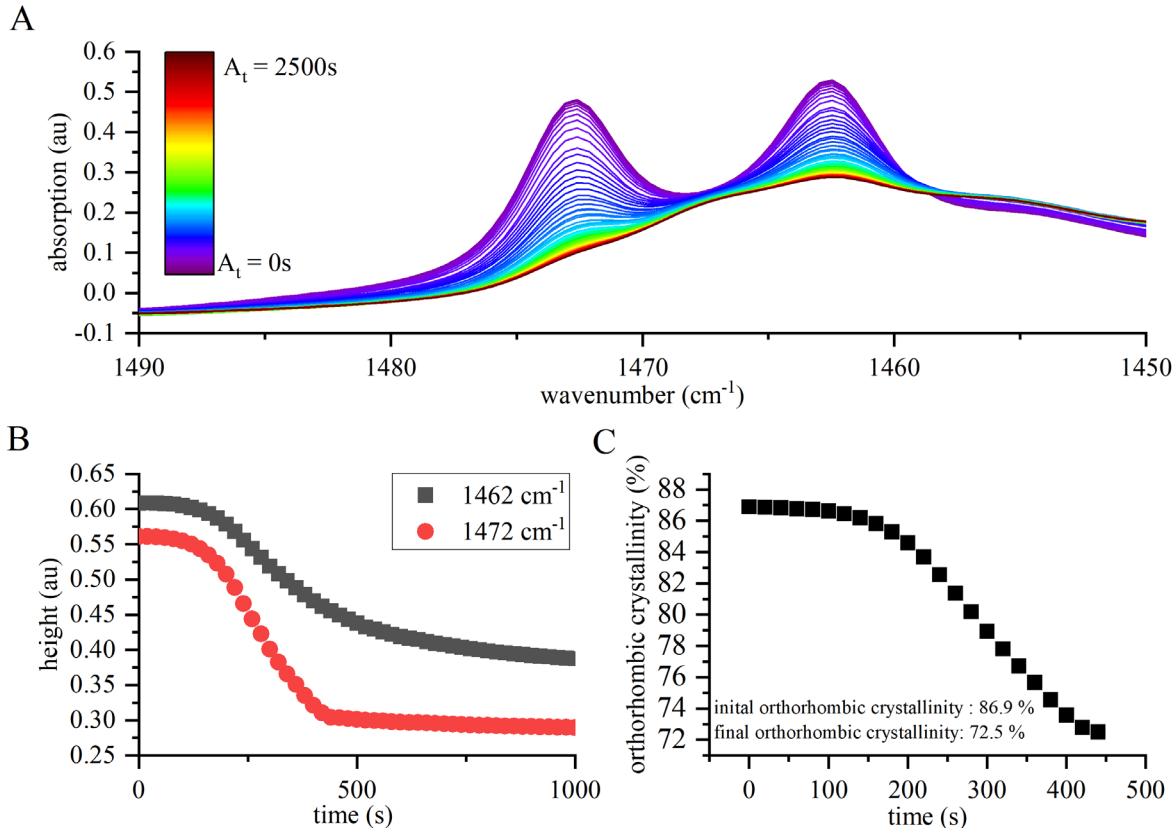

Figure 27. (A) ATR-FTIR specific absorption of scissoring mode vibrations at 1472 cm^{-1} and 1462 cm^{-1} of spin-coated candelilla wax specific CH_2 groups recorded via ATR-FTIR during diffusion of methyl oleate. Spectra were recorded during the experimental diffusion period between 0 and 2500 s. (B) Relative heights of candelilla wax specific CH_2 scissoring vibration mode occurring as doublet at 1462 cm^{-1} and 1472 cm^{-1}. Heights were plotted versus experimental time. (C) Change of methyl oleate induced orthorhombic crystallinity of candelilla wax over time.

As was observed, initial absorption levels of both bands drastically decreased during diffusion of methyl oleate in candelilla wax (Figure 27A), indicating a drastic decrease of wax molecule density within the evanescent wave.

Even though both bands drastically decreased, height levels of both bands were determined over the experimental time scale (Figure 27B) and accordingly height ratios revealed the methyl oleate induced change of orthorhombic crystallinity according to Zerbi *et al.* (1989) (Figure 27C). Orthorhombic crystallinity decreased from 86.9 % to 72.5 % over the experimental time scale.

Altered orthorhombic crystallinity of carnauba wax was determined during methyl oleate diffusion over a time range of 65000s (Figure 28).

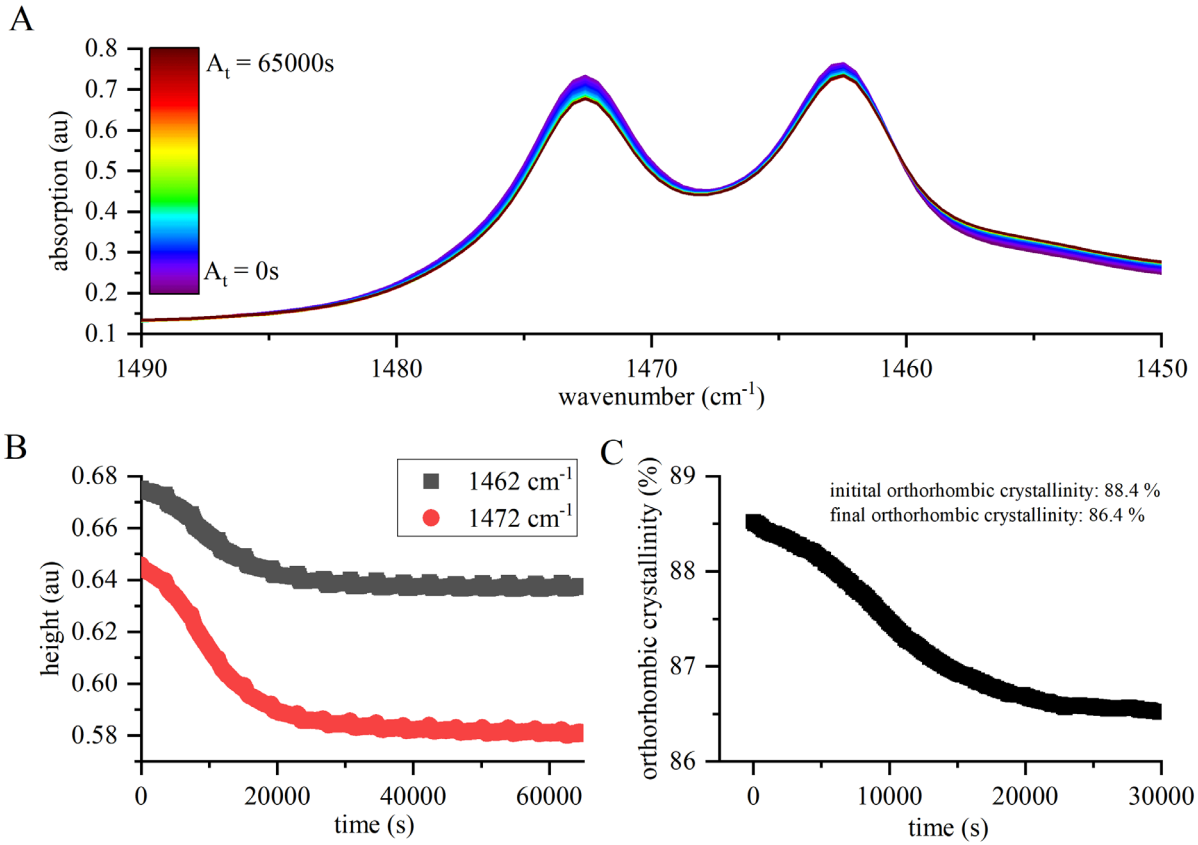

Figure 28. (A) ATR-FTIR specific absorption of scissoring mode vibrations at 1472 cm^{-1} and 1462 cm^{-1} of spin-coated carnauba wax specific CH_2 groups recorded via ATR-FTIR during diffusion of methyl oleate. Spectra were recorded from 0s to 65000s of experimental diffusion time. (B) Relative heights of carnauba wax specific CH_2 scissoring vibration mode occurring as doublet at 1462 cm^{-1} and 1472 cm^{-1}. Height levels were plotted versus experimental time and (C) decreasing wax specific orthorhombic crystallinity was determined.

As was observed, the impact on orthorhombic crystallinity affected by methyl oleate was drastically lower for carnauba wax (Figure 28A) than for candelilla wax (Figure 27A). The absorption of both bands of the scissoring mode doublet slightly decreased, and height levels were determined (Figure 28B). Relating height ratios revealed decreasing orthorhombic crystallinity over time (Figure 28C). Orthorhombic crystallinity decreased from 88.4 % to 86.4

%. Relating methyl oleate induced change of orthorhombic crystallinity both in candelilla and carnauba wax, it became obvious that candelilla wax orthorhombic crystallinity decreased 7.2 times more than carnauba wax orthorhombic crystallinity within a ~60 times shorter time range.

3.3.4 Diffusion of TEHP in candelilla and carnauba wax

The diffusion kinetics of TEHP in candelilla wax were obtained by plotting the integrated IR absorption of the P-O-C stretching vibration specific (~1000 cm^{-1}) to the experimental time (Figure 29).

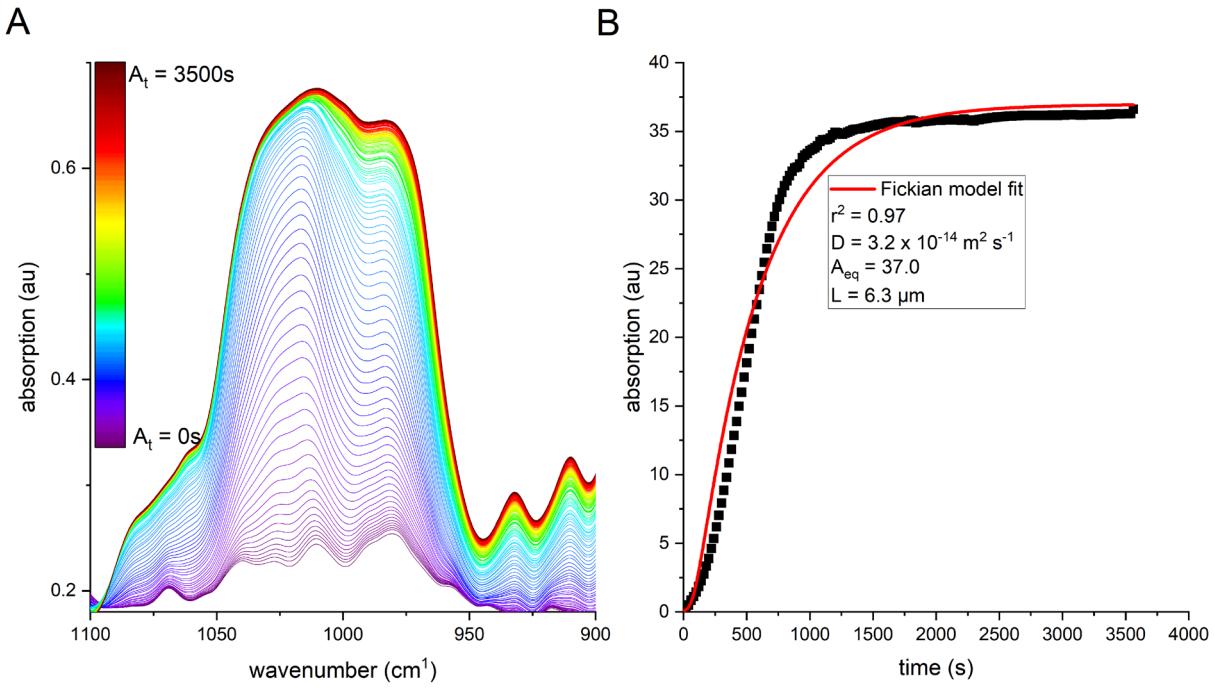

Figure 29. (A) ATR-FTIR specific absorption of P-O-C stretching vibration was recorded during diffusion of TEHP in spin coated candelilla wax. Absorption recorded at time *t* is indicated by A_t. (B) Integrated absorption of TEHP specific P-O-C vibration (1000 cm^{-1}) in spin coated candelilla wax recorded during diffusion up to 3500s and the Fickian model fit is shown.

Applying TEHP to the candelilla wax layer resulted in an increasing absorption of the monomeric P-O-C stretching vibration over time, which was attributed to diffusing TEHP molecules towards the evanescent wave (Figure 29A). TEHP diffusion kinetics were obtained from plotting integrated absorption over the experimental time (Figure 29B). Wax layer thickness was 6.3 µm and the diffusion coefficient was 3.2 x 10^{-14} m^2 s^{-1}. Diffusion kinetics of TEHP in spin coated carnauba wax were also recorded (Figure 30).

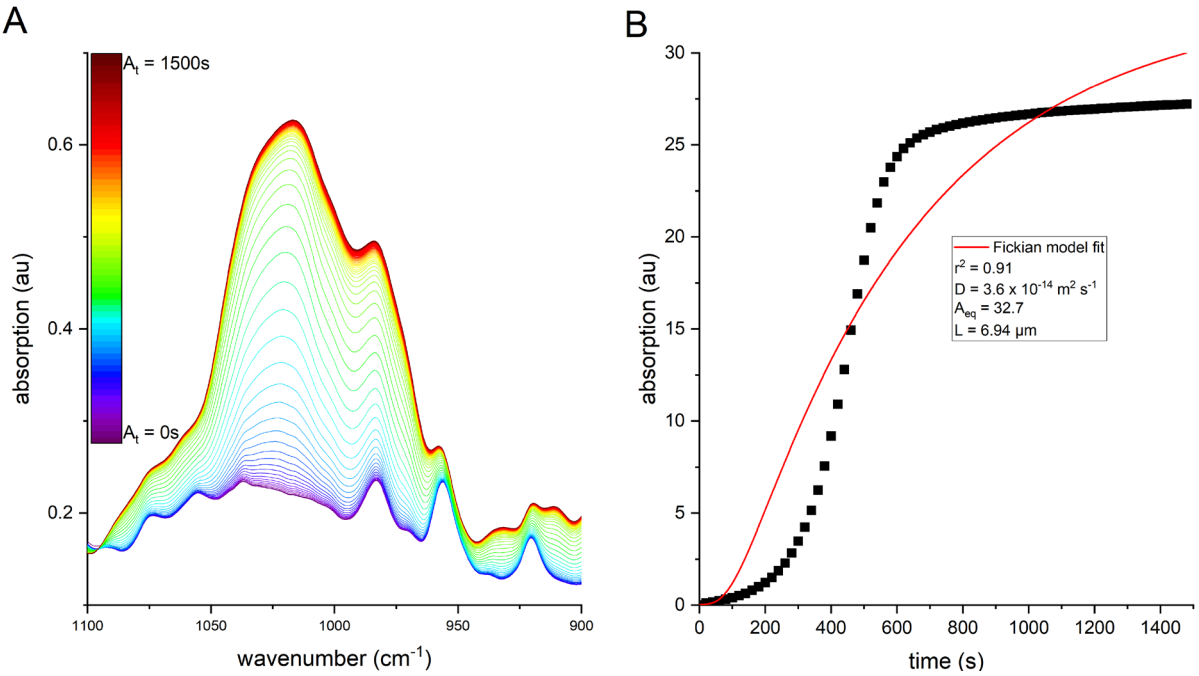

Figure 30. (A) ATR-FTIR specific absorption of P-O-C stretching vibration was recorded during diffusion of TEHP in spin coated carnauba wax. Absorption recorded at time *t* is indicated by A_t. (B) Integrated absorption of TEHP specific P-O-C vibration (1000 cm^{-1}) in spin coated carnauba wax recorded during diffusion up to 1500s and the Fickian model fit is shown.

A drastic increase of TEHP specific P-O-C stretching vibration was observed after initial deposition on the carnauba wax layer (Figure 30A). However, the Fickian model was not able to accurately describe the experimentally determined diffusion kinetics obtained from integrated P-O-C stretching absorptions over time (Figure 30B). A severe initial lag-phase was observed, which did not match Fickian diffusion kinetics. Consequently, the calculated diffusion coefficient hardly represented the experimental data. Instead, altering diffusion coefficients representing the diffusion time course rather than a constant diffusion coefficient became apparent.

3.3.5 TEHP effect on orthorhombic crystallinity in candelilla and carnauba wax

Candelilla wax specific orthorhombic crystallinity was determined during TEHP diffusion over a time range of 3500s analogous to 3.3.4 (Figure 31).

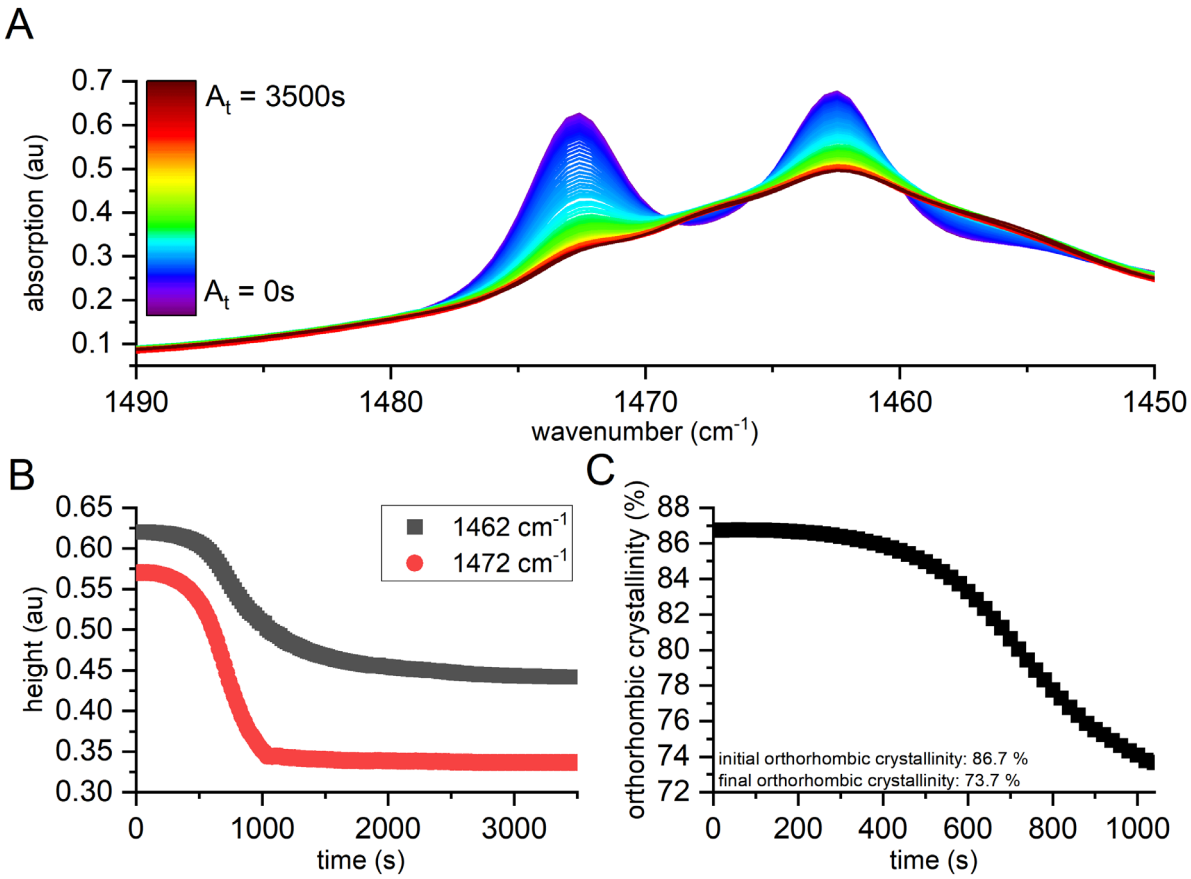

Figure 31. (A) ATR-FTIR specific absorption of scissoring mode vibrations at 1472 cm^{-1} and 1462 cm^{-1} of spin-coated candelilla wax specific CH_2 groups recorded via ATR-FTIR during diffusion of TEHP. Spectra were recorded from 0s to 3500s of experimental diffusion time. (B) Relative heights of candelilla wax specific CH_2 scissoring vibration mode occurring as doublet at 1462 cm^{-1} and 1472 cm^{-1}. Heights were plotted versus experimental time. (C) Change of TEHP induced orthorhombic crystallinity of candelilla wax over time.

Initial absorption levels of both CH_2 scissoring vibration bands drastically decreased during TEHP diffusion in candelilla wax (Figure 31A), indicating decreasing wax molecule density within the evanescent wave. Height levels of both bands were determined over the experimental time scale (Figure 31B) and height ratios were calculated according to Zerbi *et al.* (1989). Drastic decrease of orthorhombic crystallinity, just as was observed during methyl oleate diffusion became apparent (Figure 31C). Orthorhombic crystallinity decreased from 86.7 % to 73.7 % over the experimental time scale.

Carnauba wax specific orthorhombic crystallinity was determined during TEHP diffusion over a time range of 1500s (Figure 32).

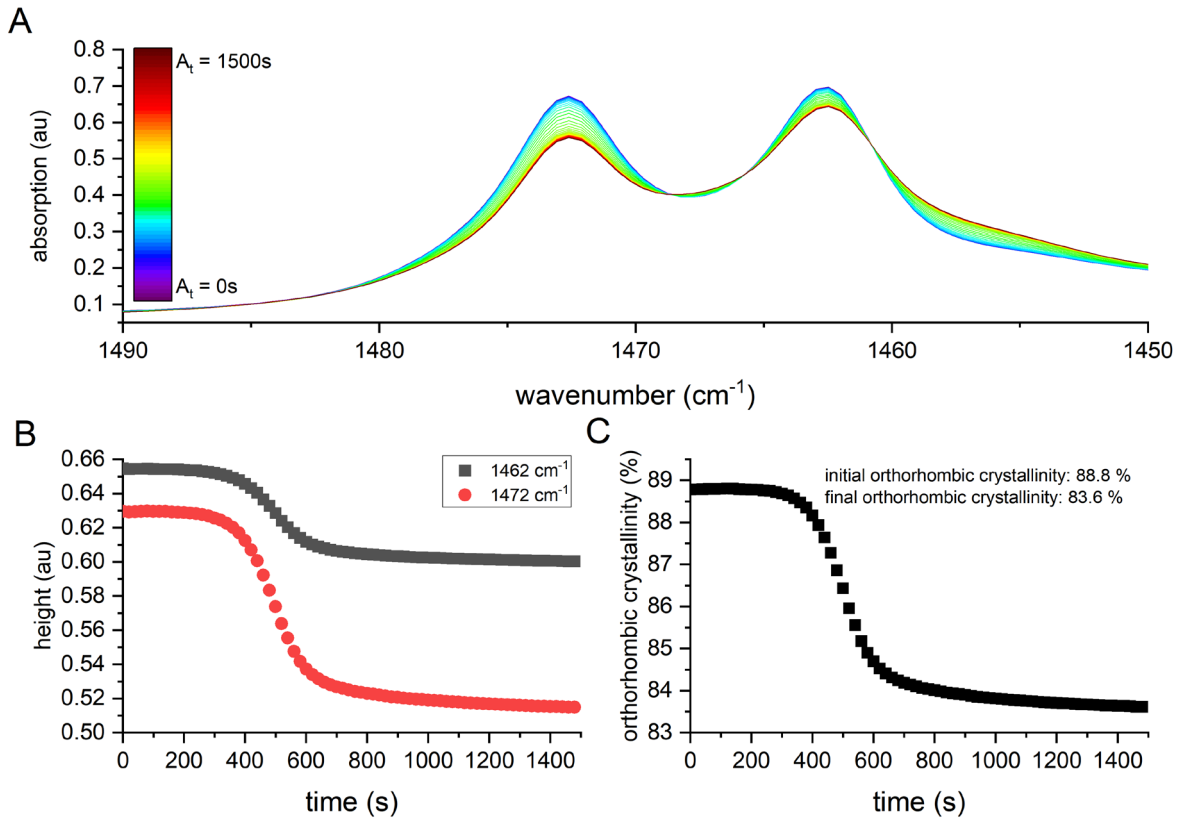

Figure 32. (A) ATR-FTIR specific absorption of scissoring mode vibrations at 1472 cm^{-1} and 1462 cm^{-1} of spin-coated carnauba wax specific CH_2 groups recorded via ATR-FTIR during diffusion of TEHP. Spectra were recorded from 0s to 1500s of experimental diffusion time. (B) Relative heights of candelilla wax specific CH_2 scissoring vibration mode occurring as doublet at 1462 cm^{-1} and 1472 cm^{-1}. Heights were plotted versus experimental time. (C) Change of TEHP induced orthorhombic crystallinity of carnauba wax over time.

TEHP treatment of carnauba wax resulted in decreasing absorptions of CH_2 scissoring mode vibrations (Figure 32A). Both bands of the scissoring mode doublet slightly decreased, and height levels were determined (Figure 32B) and height ratios revealed decreasing orthorhombic crystallinity over time (Figure 32C). The orthorhombic crystallinity decreased from 88.8 % to 83.6 %, which, in contrast to candelilla wax, was only a minor. In contrast to the decrease in orthorhombic crystallinity induced by methyl oleate, the decrease in orthorhombic crystallinity induced by TEHP occurred in a roughly comparable time scales both in candelilla wax and carnauba wax.

3.3.6 Diffusion of monodisperse alcohol ethoxylates in candelilla and carnauba wax

Diffusion kinetics of the three selected monodisperse AEs in spin coated candelilla wax were determined from 0 to 6500s (C12E2), 7500s (C12E4) and 9000s (C12E6) (Figure 33).

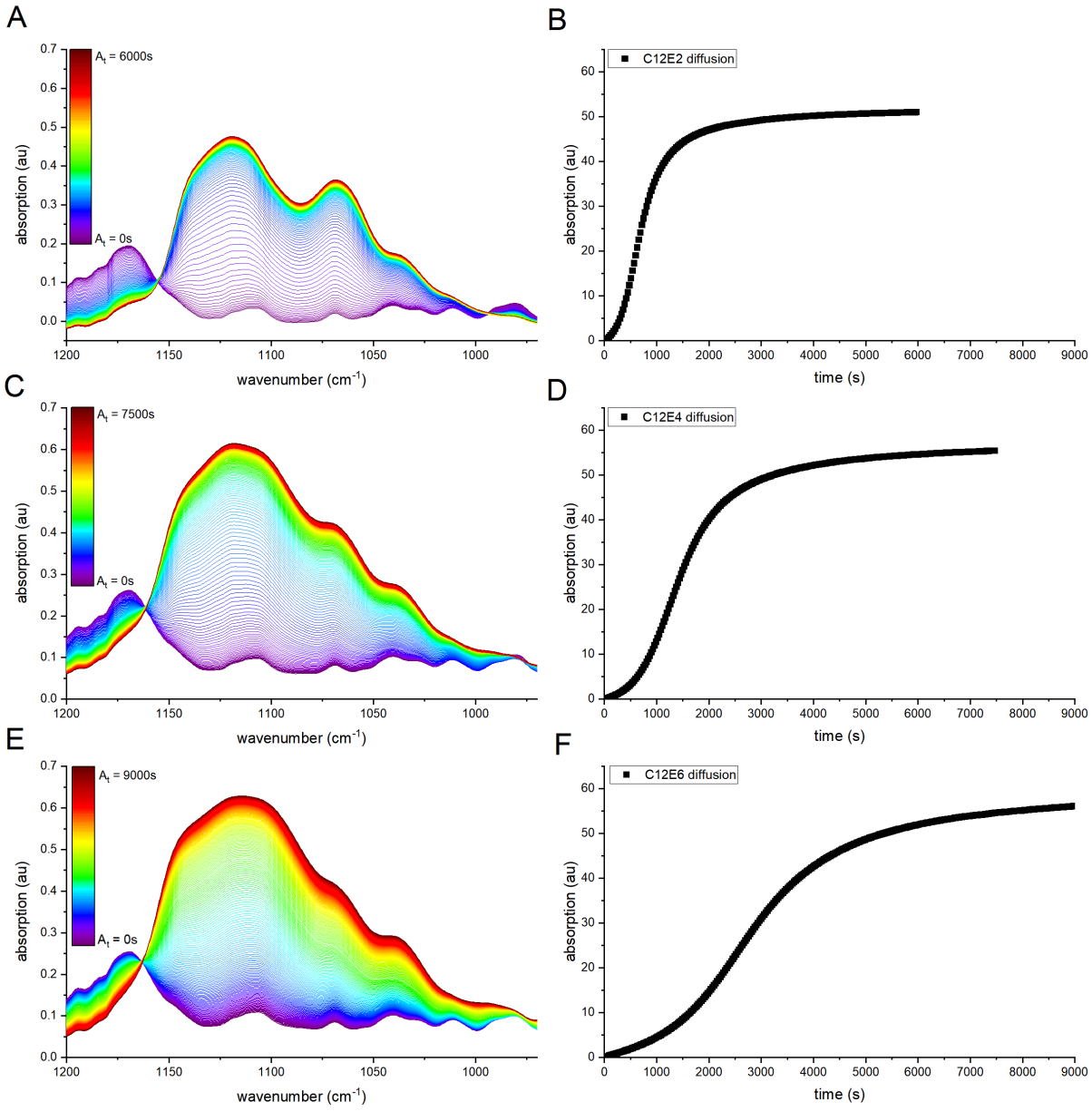

Figure 33. Diffusion of monodisperse alcohol ethoxylates in spin coated candelilla wax as indicated by increasing IR-absorption of C-O-C stretching vibration at 1100 cm^{-1} corresponding to ether-functional groups of (A) C12E2, (C) C12E4 and (E) C12E6. Respective absorption levels were integrated for each recorded spectrum of (B) C12E2, (D) C12E4 and (F) C12E6 diffusion.

The diffusion of AEs in candelilla wax was indicated by an increase in C-O-C stretching vibrations in the range between 1150 cm^{-1} and 1000 cm^{-1} (Figure 33A, C, E). To accurately determine respective diffusion kinetics, the absorption bands of each recorded spectrum were integrated and plotted against experimental time (Figure 33B, D, F). It was found that the degree of ethoxylation had a drastic effect on respective diffusion kinetics. The lipophilic C12E2 reached an equilibrium level after about 2500 s (Figure 33B) accommodated with a slight initial lag phase. In contrast, the diffusion kinetics of C12E4 exhibited a more

pronounced initial lag phase (Figure 33D). As a result, the experimental data entirely deviated from the proposed Fickian model (model fit not shown). Diffusion kinetics reached an equilibrium level after about 5000 seconds, indicating a slower diffusion process as observed for C12E2. The sigmoidal diffusion kinetics of C12E6 also entirely deviated from Fickian diffusion and exhibited a pronounced initial lag phase (Figure 33F). An approximate equilibrium of the diffusion kinetics was reached after 9000 seconds, revealing slower diffusion kinetics as observed for C12E2 and C12E4. Conclusively, it was observed that the number of ethoxylate units of monodisperse AEs was negatively correlated with their mobility in candelilla wax. This effect did not depend on the number of ethylene groups, but rather on respective ethoxylation levels. To investigate whether this assumption can be established as a rule for VLCA-dominated cuticular waxes *per se*, regardless to their chemical composition, diffusion kinetics were also recorded for C12E2, C12E4 and C12E6 in the alkyl ester dominated carnauba wax (Figure 34A, C, E).

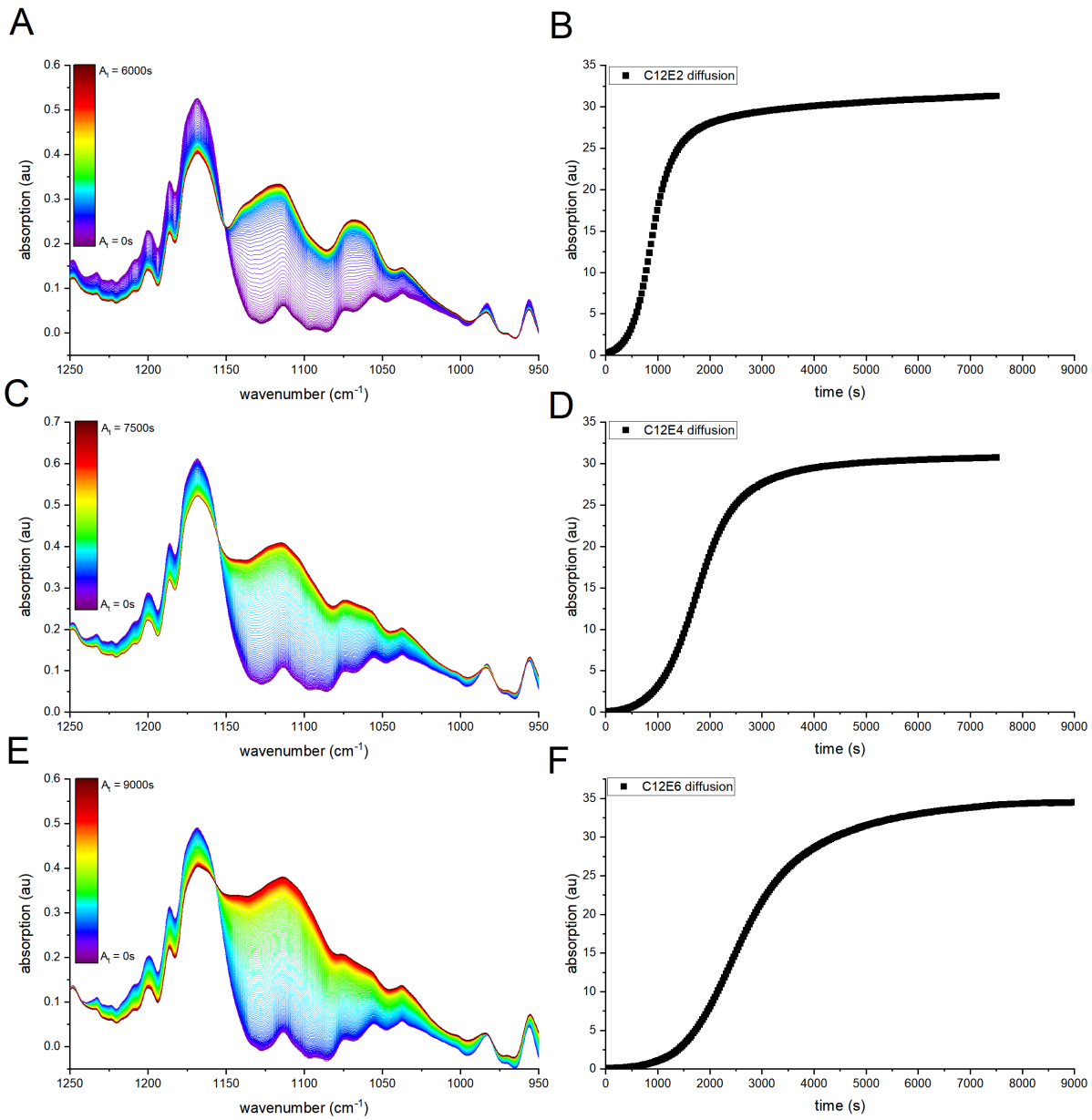

Figure 34. Diffusion of monodisperse alcohol ethoxylates in spin coated carnauba wax as indicated by increasing IR-absorption of C-O-C stretching vibration at 1100 cm^{-1}, corresponding to ether-functional groups of (A) C12E2, (C) C12E4 and (E) C12E6. Respective absorption levels were integrated for each recorded spectrum of (B) C12E2, (D) C12E4 and (F) C12E6 diffusion.

As expected, the diffusion kinetics of C12E2 in carnauba wax reached an equilibrium level most rapidly, after about 2500s (Figure 34B), whereas C12E4 (Figure 34D) and C12E6 (Figure 34F) showed delayed equilibria levels after about 4000 and 9000 seconds, respectively. The diffusion kinetics of C12E4 and C12E6 were accompanied by strong initial lag phases that transformed Fickian kinetics into sigmoidal diffusion curves, eliminating the possibility of calculating constant diffusion coefficients.

When comparing the uptake of the monodisperse AEs in candelilla and carnauba wax, only slight differences were seen in the diffusion kinetics (longer lag phase and sigmoidal course with higher degree of ethoxylation). However, the absolute absorptions, representing AE solubilities, differed enormously within both investigated waxes. While the diffusion curves in candelilla wax reached final absorptions between 51 and 56 au, these were only between 31 and 34 au when the diffusion kinetics reached equilibria levels in carnauba wax. Hence, AE solubilities in candelilla wax almost doubled those in carnauba wax.

3.3.7 Monodisperse alcohol ethoxylate effect on orthorhombic crystallinity in candelilla and carnauba wax

The effect of the three monodisperse AEs C12E2, C12E4 and C12E6 on orthorhombic crystallinity during diffusion in candelilla and carnauba wax was simultaneously determined via ATR-FTIR according to Zerbi *et al.* (1989) (Figure 35).

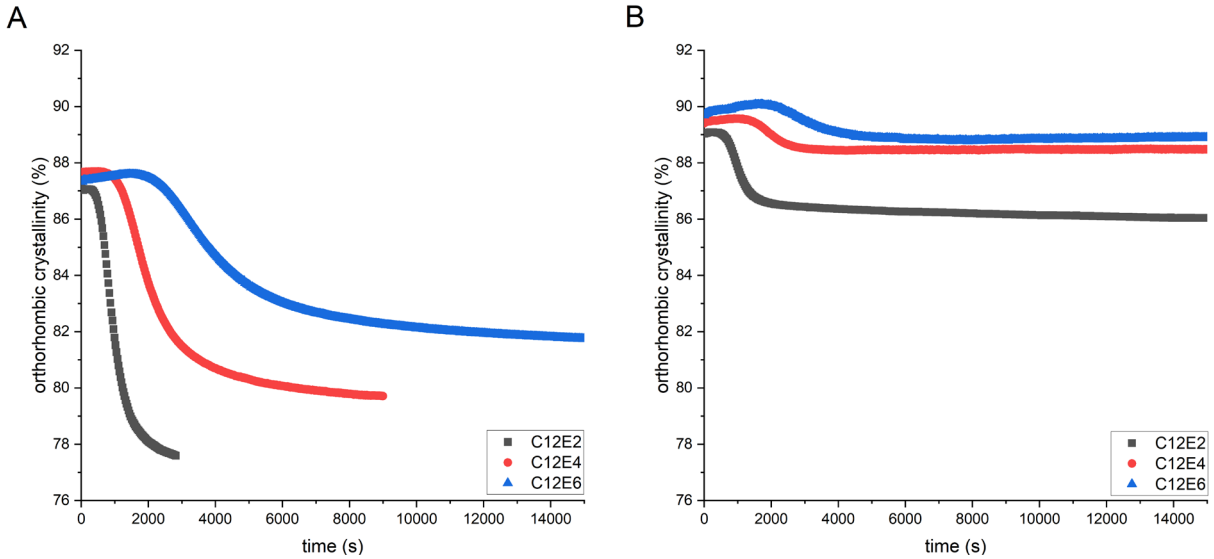

Figure 35. Effect of diffusing alcohol ethoxylates C12E2, C12E4 and C12E6 on orthorhombic crystallinity of (A) candelilla wax and (B) carnauba wax.

Both the time course and the level of orthorhombic crystallinity reduction correlated with respective ethoxylation levels of the investigated AEs. It was found that the lipophilic C12E2 most drastically decreased orthorhombic crystallinity in candelilla wax. A reduction of orthorhombic crystallinity from 87.0 to 77.6% was detected already after 2800 seconds. In contrast, the reduction of orthorhombic crystallinity induced by C12E4 diffusion stagnated at 79.6 % after 9000 seconds. C12E6 induced the lowest reduction of orthorhombic crystallinity

in candelilla wax (81.7 %). Reaching an approximate end point of the reduction in orthorhombic crystallinity required 15000 seconds.

In contrast to candelilla wax, the initial orthorhombic crystallinity was about 2% higher in carnauba wax (Figure 35B). Diffusion of C12E2 led to decreasing orthorhombic crystallinity until stagnation at about 86.5 % after 2500 seconds, whereas diffusion of C12E4 affected orthorhombic crystallinity to stagnate at approximately 88.5 % after 4000 seconds and diffusion of C12E6 decreased the orthorhombic crystallinity to 88.8 % after 6000 seconds. Table 3 shows decreasing orthorhombic crystallinities in candelilla and carnauba wax accommodated by AE diffusion.

Table 3. Alcohol ethoxylate induced decrease of candelilla and carnauba wax orthorhombic crystallinity.

	orthorhombic crystallinity decrease (%)	
alcohol ethoxylate	candelilla wax	carnauba wax
C12E2	9.5	2.5
C12E4	8.0	1.0
C12E6	5.7	0.9

The orthorhombic crystallinity decrease was more intense in candelilla wax than in carnauba wax during diffusion of each AE. AE ethoxylation level strongly correlated with decreasing orthorhombic crystallinity both in candelilla and carnauba wax even though exhibiting different absolute intensities.

3.4 Discussion

This study aimed to investigate accelerator diffusion kinetics in two cuticular model waxes and, based on this, to derive insights on self-accelerating mechanisms. For this purpose, pure adjuvants, instead of adjuvant-containing formulations were used, simulating the adjuvant uptake from highly concentrated residues after spray-droplet evaporation (Ramsey *et al.*, 2005). Lipophilic accelerator adjuvants were already shown to accumulate within lipophilic cuticles, rather than being desorbed into the underlaying plant tissue (Santier and Chamel, 1996). Hence, the proposed system only providing barrier-forming lipophilic wax layers and thus excluding any desorption medium appeared reasonable to mimic the real-world situation of accelerator adjuvant uptake.

Using the presented ATR-FTIR-based method, high resolution diffusion kinetics have been recorded simultaneously with wax-specific modifications such as decreasing orthorhombic crystallinity, change in wax molecule density or impact on intermolecular hydrogen bonds. Consequently, investigating both diffusion and wax modification within one attempt should provide plasticization effectiveness of the respective adjuvants, required for sufficient AI uptake.

3.4.1 Methyl oleate diffusion and modification of candelilla and carnauba wax

Typically, Fickian diffusion processes are described for rubbery polymers whose structural formation is immediately adjusted to penetrating molecules, leading to no significant resistance to diffusion (Piringer and Baner, 2008). Diffusion processes of organic compounds and accelerators in general are depicted to follow Fickian diffusion kinetics in cuticular waxes (Schreiber and Riederer, 1996a). It was shown that the diffusion kinetics of methyl oleate in candelilla wax could be largely explained by the Fickian diffusion model exhibiting a constant diffusion coefficient of 5.3×10^{-14} m^2 s^{-1} (Figure 25B). Diffusion coefficients of non-accelerating CNP and heptyl parabene in paraffin wax were one order of magnitude lower (chapter 1) and furthermore diffusion coefficients in reconstituted cuticular waxes derived from desorption kinetics were also orders of magnitude lower. (Schreiber and Schönherr, 1993; Schreiber and Riederer, 1996a; Kirsch *et al.*, 1997; Burghardt *et al.*, 1998; Burghardt *et al.*, 2006; Schreiber, 2006). Hence an acceleration mechanism enhancing the uptake of methyl oleate in candelilla wax was suspected as was already described by several authors (Gauvrit and Cabanne, 1993; Santier and Chamel, 1996; Hazen, 2000; Webster *et al.*, 2018).

Providing high temporal resolution diffusion data via ATR-FTIR, an initial lag phase of methyl oleate penetration in candelilla wax was observed, reflecting a slight discrepancy to the Fickian model (Figure 25B). This lag phase indicated an initially low rate of methyl oleate diffusion into the wax, rapidly transforming to an exponential phase after reaching a critical concentration and finally persisting until an equilibrium level was reached. Reaching a critical concentration during the initial diffusion phase is thought to trigger severe structural modifications, which in turn lead to a cascade of additional self-accelerating methyl oleate molecules entering the wax. Further penetration of methyl oleate molecules is thought to enhance this wax modification over the experimental time.

To comprehensively characterize the observed diffusion kinetics of methyl oleate, evidence for wax modification had to be found. Gauvrit and Cabanne (1993) showed oil adjuvants like methyl oleate impregnating cuticular waxes within a few seconds, proposing an intrinsic wax modification (Gauvrit and Cabanne, 1993). Hazen (2000) suggested that esterified seed oils may act as plasticizers or wax disruptors (Hazen, 2000) and Webster *et al.* (2018) observed decreasing α-crystallite level in tristearin, correlating with increasing amounts of methyl oleate and other esterified fatty acids, again suggesting a wax disrupting effect (Webster *et al.*, 2018). However, since tristearin is a triglyceride consisting of glycerol and stearic acid, the transferability to cuticular waxes dominated by long-chain aliphatic molecules remained questionable and furthermore, no correlation of methyl oleate diffusion kinetics with decreasing crystallinity levels have been reported yet. As was observed here, the self-accelerated diffusion kinetics of methyl oleate were accommodated with simultaneously recorded decrease in orthorhombic crystallinity, both following similar time courses (Figure 25; Figure 27C). A direct effect of exponential methyl oleate diffusion on the orthorhombic crystallinity decrease can be assumed and, conversely, the crystallinity decrease as an indication of plasticization implies a feedback exponentializing on diffusion kinetics.

Fitting methyl oleate diffusion data to the Fickian model revealed Fickian diffusion kinetics in carnauba wax. The diffusion coefficient in carnauba wax was drastically lower than that observed in candelilla wax differing by one order of magnitude (2.0×10^{-15} m^2 s^{-1}) (Figure 26B). In addition, no initial lag phase was observed, which explained the lack of reaching a critical methyl oleate concentration. During methyl oleate diffusion, candelilla wax orthorhombic crystallinity decreased 7.2 times more than carnauba wax orthorhombic crystallinity, implying methyl oleate induced plasticization was drastically lower in the alkyl-ester dominated carnauba wax. Besides characterizing the methyl oleate induced effect on orthorhombic crystallinity, a decrease of wax molecular density was observed in candelilla and carnauba wax. This effect was clearly more pronounced for candelilla wax (Figure 27C) than for carnauba wax (Figure 28C), confirming a more intense plasticization of the n-alkane dominated wax.

ATR-FTIR also provided deeper insights on the modification of intermolecular interactions of wax molecules. An intense IR absorption decrease of the C=O stretching vibration assigned to dimeric fatty acids in candelilla wax was observed (Figure 25). Therefore, breaking of the intermolecular hydrogen bonds between the fatty acids triggered by the diffusion of methyl oleate is suggested. Intermolecular hydrogen bond formation between wax molecules and

adjuvant molecules contributes significantly to the plasticization potential (Zhang *et al.*, 2016). Due to the carbonyl group in methyl oleate, this molecule can act as a hydrogen bond acceptor (Lommerse *et al.*, 1997), which in turn leads to H-bonds forming between free fatty acids in candelilla wax and methyl oleate, finally triggering amplified plasticization. In contrast, the majority of OH-groups of the n-alcohol moiety in carnauba wax is assumed to already be bonded to corresponding carbonyl groups of alkyl esters, which is in concordance to previous results showing that hydrogen bonding in plant waxes prevents phase separation of shorter and longer chain distributions (Reynhardt, 1997) and therefore do not offer themselves as hydrogen bond donor for penetrating methyl oleate.

Based on the model developed by Reynhardt (1997) assuming long chain alkyl esters being parallel orientated to shorter chains and run through two adjacent layers of short chains being interconnected via hydrogen bonds (Reynhardt, 1997), Bueno *et al.* (2018) proposed long-chain esters acting as reinforcing rods connecting two or more crystallites, strengthening the mechanical stability of the wax and leading to higher melting ranges than those observed for waxes lacking alkyl esters (Bueno *et al.*, 2019). Several authors stated apolar polyethylene chains of surfactant molecules may be incorporated into wax crystallites, whereas the protruding polar heads will be situated in the amorphous domain leading to increase of fluidity (Fagerström *et al.*, 2014; Zhang *et al.*, 2016). In this study, a comparable situation is proposed for methyl oleate (Figure 36A), whose apolar C18-hydrocarbon chain is assumed to be integrated into crystalline zone A, while its polar methyl ester group is probably situated within amorphous zones B and D. A model simulation of methyl oleate showing its polarity distribution is shown in Figure 36B.

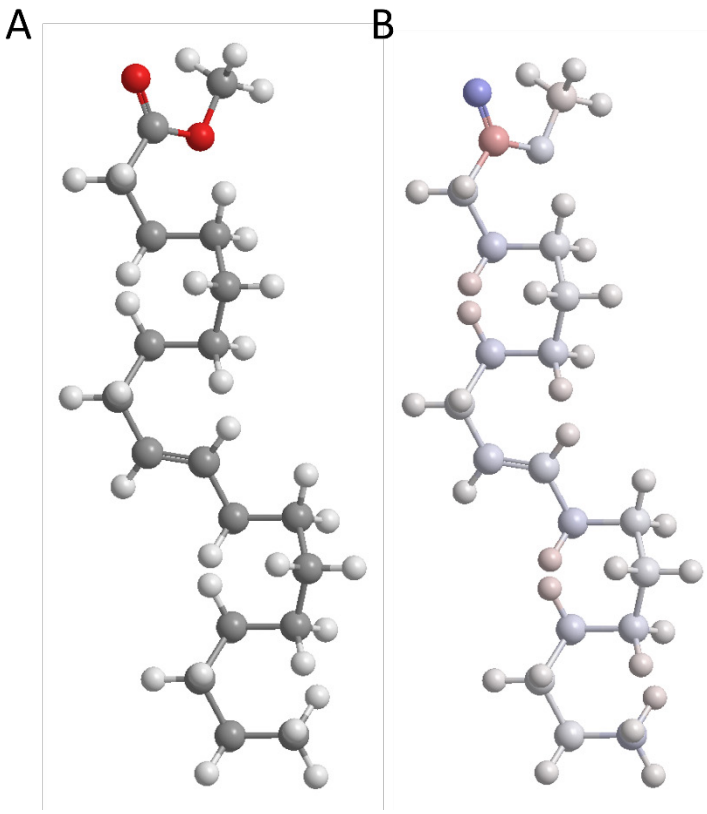

Figure 36. Ball-and-Stick model of a methyl oleate molecule (A). Colors of ball represent atoms: red = oxygen, grey = carbon, white = hydrogen. (B) Charge distribution according to the extended-Huckel-method (Hoffmann, 1964), where blue shade represents the level of negative charge and red shade represents level of positive charge. Calculated with Chem3d 20.1.

Due to the small size of the methyl ester function, minor interactions with adjacent crystallites are assumed, leading to negligible disentanglement of alkyl ester bridges in carnauba wax.

Dorset *et al.* (1995) stated the c-axis of orthorhombically aligned wax molecules is proportional to their average molecule chain length (Dorset, 1995). Therefore, alkyl ester dominated carnauba wax contributing carbon chain length ranging from C48 to C64 (Figure 23) presumably provides orthorhombic crystallites with longer c-axis than C31-dominated candelilla wax (Figure 21). Hence, the large resulting orthorhombic unit cells of carnauba wax give hints for the high plasticization resistance compared to candelilla wax.

Since it was repeatedly postulated that temperature and accelerators have a similar effect on the cuticular barrier (Schreiber *et al.*, 1996b; Buchholz, 2006), the assumption seems reasonable that barrier-forming waxes with high melting ranges are more resistant to elevated temperature and to adjuvant-induced structural modifications. Hence, carnauba wax contributing a significant proportion of long chain alkyl esters and showing a 15 °C higher

melting point than candelilla wax (Figure 22; Figure 24) was less susceptible against methyl oleate diffusion accompanied by less intense decrease of orthorhombic crystallinity.

3.4.2 TEHP diffusion and modification of candelilla and carnauba wax

TEHP is usually used as flame retardant and plasticizing agent for technical approaches, providing excellent softening properties (Van Esch and Organization, 2000). In agrochemistry, TEHP was shown to drastically enhance uptake rates of the herbicide pinoxaden (Muehlebach *et al.*, 2011). Arand *et al.* (2018) showed pinoxaden penetration rate across isolated cuticles of *Prunus laurocerasus* was drastically increased by TEHP treatment (Arand *et al.*, 2018). They explained their finding with TEHP entering the cuticle and modifying the cuticular pathway somehow. However, other approaches using TEHP as an accelerating adjuvant have not been published, so its MoA remained unknown. Consequently, data on the wax-modifying effect of TEHP, e.g., decreasing crystallinity depending on chemical compositions or structural properties, is lacking to date. Within this study, drastic TEHP uptake was shown into both investigated candelilla and carnauba wax (Figure 29; Figure 30). Analogous to methyl oleate (3.4.1), TEHP diffusion kinetics in candelilla wax slightly deviated from the Fickian model, exhibiting an initial lag phase. Due to the slight discrepancies, a still meaningful diffusion coefficient of 3.2×10^{-14} m^2 s^{-1} was derived, being in the same order of magnitude as the diffusion coefficient of methyl oleate in candelilla wax. Like methyl oleate, the penetrating TEHP molecules reached critical concentrations in the wax, inevitably leading to self-accelerating exponential diffusion. It was shown that orthorhombic crystallinity of candelilla wax was drastically decreased during TEHP uptake, indicating severe wax plasticization (Figure 31C). Decreasing orthorhombic crystallinity followed the same time course as diffusing TEHP did (Figure 30). As was observed for methyl oleate diffusion, TEHP uptake induced decreasing wax molecule density.

In contrast to Fickian diffusion kinetics of TEHP in candelilla wax, the diffusion kinetics of TEHP in carnauba wax entirely deviated from the Fickian model (Figure 30B). Hence, sigmoidal rather than exponential diffusion kinetics were observed (Figure 30B). Comparable results were already reported for desorption kinetics of the lipophilic 2,4-DB from isolated cuticles of *Stephanotis floribunda* leaves treated with the chemically related tributyl phosphate (TBP) (Shi *et al.*, 2005b). *Stephanotis floribunda* cuticular waxes consisted to 19.3 % of alkyl esters and 23.5 % n-alcohols (Šimáňová *et al.*, 2005) probably rendering the same MoA as was observed

in carnauba wax. However, studies investigating diffusion kinetics of TBP in cuticular waxes are lacking and consequently no prediction of TEHP diffusion curves could be made here. In literature, sigmoidal diffusion curves indicate a limitation of diffusion kinetics at the polymer interface (Zaki *et al.*, 2009). This effect is amplified by the lack of strong interactions between penetrants and substrate, resulting in weak sorption processes. To comprehensively interpret non-Fickian sigmoidal diffusion curves, Zaki *et al.* (2009) introduced another coefficient in addition to the diffusion coefficient, the so-called surface mass transfer coefficient, which is a measure of the surface resistance of a polymer to penetrating molecules (Zaki *et al.*, 2009). They found that the diffusion of amyl acetate into polypropylene depended significantly on the concentration of the amyl acetate solution. As a result, higher surface mass transfer coefficients were found for higher concentrated amyl acetate solutions than for low-concentration ones. Within this study, pure TEHP accompanied by weak adsorption to the wax surface potentially led to initial blocking of penetrating molecules on the surface, resulting in high mass transfer coefficients, consequently leading to a slow initial sorption phase. Additionally, due to the higher mechanical stability of carnauba wax than that of candelilla wax (see 3.4.1), it became obvious that a far greater number of TEHP molecules entering the wax was necessary to reach a critical concentration, which in turn initiated a plasticizing effect within the wax, as well as leading to self-accelerating, exponential diffusion kinetics. Therefore, based on the finding for TEHP diffusion, accelerator uptake kinetics are proposed to depend on (1) the initial level of adjuvant-wax interaction and (2) on the necessary level of critical adjuvant concentration within the wax, both together resulting in either Fickian or sigmoidal diffusion curves, and strictly being dependent on chemical compositions and structural wax properties.

To date, no study has rationally investigated the MoA of TEHP on very-long chain alkyl ester-containing waxes. Therefore, only assumptions about the MoA can be made here. Looking at the structural arrangement of a TEHP molecule (Figure 37A), it becomes obvious that the ethylene groups contribute low levels of polarity, whereas the centrally located phosphate group exhibits high intramolecular polarity (Figure 37B).

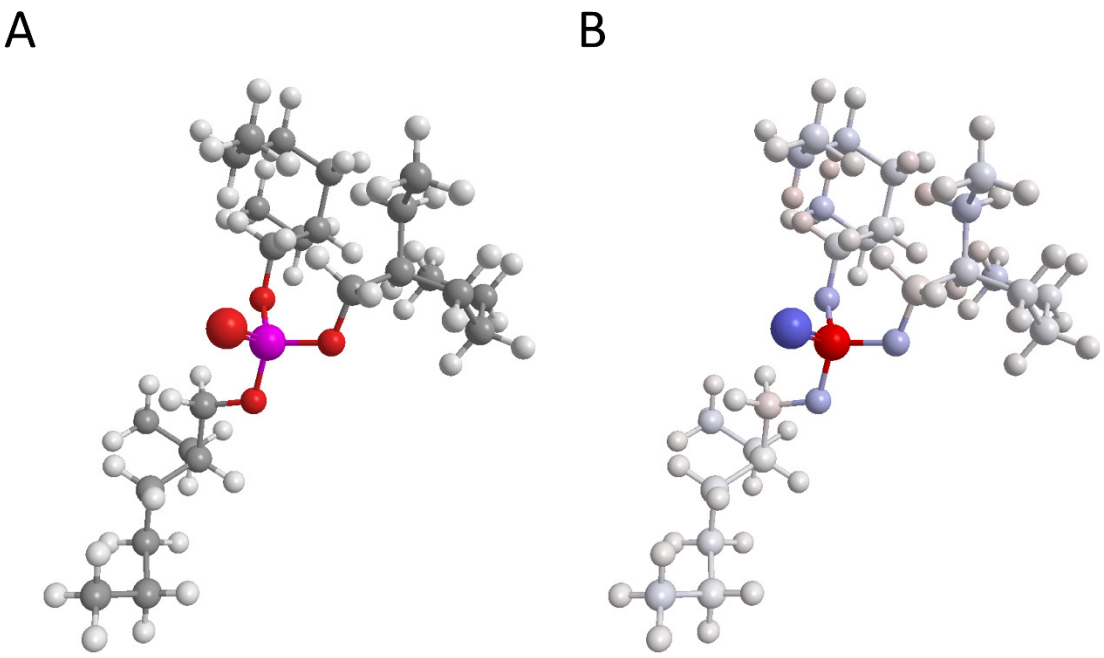

Figure 37. Ball-and-Stick model of a TEHP molecule. (A) Colors of ball represent atoms: purple = phosphorus, red = oxygen, grey = carbon, white = hydrogen. (B) Charge distribution according to the extended-Huckel-method (Hoffmann, 1964), where blue shade represents the level of negative charge and red shade represents level of positive charge. Calculated with Chem3d 20.1.

The polar group is assumed to intercalate into amorphous regions between two apolar crystallites in the wax. Consequently, due to the isometric conformation, the ethylene chains of TEHP push apart the crystallites linked by alkyl esters, eventually releasing the alkyl esters from their anchors instead of being integrated into adjacent crystallites as previously proposed for long-chain aliphatic molecules (Zhang *et al.*, 2016). The assumed ability of TEHP, disrupting crystallite connections, explains the strikingly faster diffusion kinetics and greater decrease in orthorhombic crystallinity and wax molecule density in carnauba wax compared to methyl oleate, which is ineffective at disentangling adjacent crystallites (3.4.1).

Further studies especially investigating the accelerator impact on alkyl ester rich cuticular waxes with respect to crystallographic data (XRD and electron diffractometry) are mandatory to draw conclusions on the uptake process and therefore on the time-dependent efficiency of plasticization.

3.4.3 Diffusion of monodisperse alcohol ethoxylates and modification of candelilla and carnauba wax

Former studies reported constant Fickian diffusion coefficients of monodisperse AEs in reconstituted cuticular waxes (Burghardt *et al.*, 1998; Burghardt *et al.*, 2006). The reported diffusion coefficients were derived from desorption kinetics rather than from sorption kinetics. Hence, the investigated waxes were presumably already in a plasticized state at the time of measurement. As plasticization leads to decreasing tortuosity of the penetration pathway (Buchholz, 2006), significantly lower resistance against desorbing AEs was obvious and explaining the apparent Fickian diffusion kinetics.

Within this study, however, diffusion kinetics were recorded from initial AE uptake into unplasticized waxes. As a result, non-Fickian sigmoidal diffusion kinetics were observed, rejecting Fickian diffusion processes during initial AE sorption in VLCA-dominated cuticular model waxes. Consequently, AE mobilities varied eventually depending on state-of-diffusion related wax plasticization levels, thereby causing continuously altering diffusion coefficients. As was shown here, the diffusion kinetics were retained with increasing ethoxylation level both during AE diffusion in candelilla and carnauba wax, thereby exhibiting increasing sigmoidal characteristics (Figure 33; Figure 34). The derived decrease in AE mobility is consistent with the results published by Coret *et al.* (1993) who observed AE diffusion kinetics negatively correlating with increasing ethoxylation levels (Coret and Chamel, 1993).

Several aspects of AE specific features must be considered to understand delayed mobility with increasing ethoxylation: First, molar volumes of monodisperse AEs increase with increasing EO content. Therefore, AE diffusion kinetics were negatively corelated with the respectively raising molar volumes. This is in line with previously reported results, showing organic compound mobility log-linearly decreased with rising molar volume in reconstituted cuticular waxes (Schreiber and Schönherr, 1993; Kirsch *et al.*, 1997). Second, the interaction of AEs with lipophilic waxes decreases with increasing hydrophilicity. The hydrophilicity of an AE increases with increasing EO content, which is defined by the HLB value (Griffin, 1954). As was stated by Hess and Foy (2000), HLB values below 8 (HLB of C12E2 = 7.66) are typical for lipophilic AEs, whereas HLB above 11 (HLB of C12E6 = 12.49) are mostly characteristic for hydrophilic AEs (Hess and Foy, 2000). Hence, according to the HLB values of the investigated AEs, delayed diffusion kinetics with raising EO content were not surprising.

Nevertheless, it was remarkable that with increasing ethoxylation level, a more pronounced initial lag phase occurred during initial diffusion. Hence, the presented results led to the assumption of mandatory critical accelerator concentrations triggering self-accelerated exponential AE uptake and wax modification events as was also observed for methyl oleate and TEHP diffusion in both examined waxes.

Besides determining mobility properties of monodisperse AEs from diffusion kinetics, also solubilities represented by equilibrium absorptions must be considered to comprehensively understand the MoA of AEs and their effect on AI mobility. Equilibrium absorptions between 51 and 56 au were found in candelilla wax. Contrastingly, final absorptions only ranged between 31 and 34 au in carnauba wax (Figure 33; Figure 34). Burghardt *et al.* (2006) already showed the maximum AE concentration within a cuticular wax linearly affects organic compound mobility (Burghardt *et al.*, 2006). Accordingly, AEs exhibiting a common intrinsic effect, only depending on the AE amounts absorbed in the wax, but not on respective EO contents appeared likely, as was previously demonstrated (Riederer *et al.*, 1995; Burghardt *et al.*, 1998). In accordance, the results presented here suggest higher effects on compound mobility in candelilla wax than in carnauba wax.

It should be noted that comparing equilibrium IR-absorptions of AEs with different ethoxylation levels is limited. The AE ethoxylation grade relates its dipole moment, consequently defining its concentration-to-IR-absorption ratio. Hence, similar equilibrium absorptions of different AEs in the same investigated model wax may not mistakenly be interpreted as similar equilibrium concentrations. AEs with higher EO content are thought to induce strikingly higher IR-absorption per molecule due their higher dipole moment (Günzler and Gremlich, 2012). Therefore, the equilibrium concentration of C12E6 will inevitably be lower than that of C12E4 and C12E2 even though showing similar equilibrium absorptions. Since the Lambert-Beer law applies to ATR-FTIR measurements, the individual linear correlation of IR absorption and concentration for each AE allows an external calibration to be established in future studies. Conclusions will then be drawn about the amount of AE absorbed in the wax as a function of the degree of ethoxylation.

Several approaches have already been pursued to investigate the AE-induced wax modification (Schreiber *et al.*, 1996b; Schreiber *et al.*, 1997; Zhang *et al.*, 2016). Nonspecific plasticization events have been detected using ESR and ^{2}H-NMR. Zhang *et al.* (2016) demonstrated a reduction of carnauba wax crystallinity using XRD. They found that the

nonionic surfactant polysorbate 60 reduced crystallinities by about 10 %. However, it must be noted that preformulated wax/polysorbate mixtures were used to characterize the impact on crystallinity. Therefore, meaningful conclusions about the influence on crystallinity during the natural penetration process of AEs into the wax were lacking. It can be assumed that the recrystallization of carnauba wax was clearly impaired due to the high polysorbate content (up to 30 %) and consequently does not happen in this way in plants.

Within this study, AE-induced orthorhombic crystallinity decrease was found to range between 5.7 and 9.5 %, and 0.9 and 2.5 % in candelilla and carnauba wax, respectively (Figure 35; Table 3). It must be assumed that the impact on orthorhombic crystallinity mainly depends on two factors, namely (1) the structural integrity and mechanical stability of the investigated waxes and (2) the AE ethoxylation level determining its lipophilicity and respective AE uptake rates and final equilibrium concentrations:

First, the wax chemical composition inevitably determines its structural stability and relates its barrier function against penetrating plasticizers. As observed here, candelilla wax consisting predominantly of n-alkanes and therefore being stabilized mainly by van der Waals forces (Dorset, 1995), showed drastic decrease of orthorhombic crystallinity during AE-diffusion. In contrast, carnauba wax, contributing n-alcohols and alkyl esters, can introduce more hydrogen bonds (Reynhardt, 1997), strengthening its structural integrity while being less impaired by penetrating AEs.

Second, as was already discussed, the level of ethoxylation relates the AE lipophilicity and inevitably determines the interaction intensity with cuticular waxes and its uptake rate. Consequently, as was shown within this study, more lipophilic AEs faster penetrated both investigated model waxes, thereby stronger influencing orthorhombic crystallinity as a measure of plasticization (Figure 35). Under the assumption of a common intrinsic activity, independent of the degree of ethoxylation (Riederer *et al.*, 1995; Burghardt *et al.*, 1998), the internal AE concentration correlates linearly with the AI mobility, which allows the assumption of a correlation between AE concentration and plasticization intensity (here effect on orthorhombic crystallinity). In this work, however, no striking differences were found between respective equilibrium absorptions of the studied AEs in one wax. Considering different AE dipole moments, differences in equilibrium concentrations (C12E2 > C12E4 > C12E6) appeared likely.

4 Chapter 3: Influence of the aliphatic wax composition on adjuvant diffusion

4.1 Introduction

4.1.1 Objectives and research questions

Until now, mostly isolated cuticles have been used for *in vitro* experiments to determine the diffusion kinetics of adjuvants, as well as the adjuvant-induced modification of the cuticular barrier (Becker *et al.*, 1986; Riederer and Schönherr, 1990; Schönherr and Baur, 1996; Baur *et al.*, 1997b; Baur, 1999; Schönherr *et al.*, 2001). However, no discrimination was made between cuticular waxes according to individual contribution of barrier-forming VLCAs and related structural properties. Some studies have also investigated the diffusion and permeation parameters of adjuvants in reconstituted cuticular wax (Schreiber, 1995; Burghardt *et al.*, 1998; Šimáňová *et al.*, 2005; Pambou *et al.*, 2018). However, no differentiation of the MoAs depending on the wax chemistry has been made. To perform large-scale *in vitro* adjuvant screening in cuticular waxes, the isolatable amount of wax is simply too small (Riederer and Schneider, 1989). In addition, impurities are usually present in cuticular waxes and may co-elute from the cutin matrix during the isolation process, leading to erroneous results. Furthermore, cuticular waxes form very heterogeneous mixtures of many different aliphatic (alkanes, alcohols, free fatty acids, aldehydes, alkyl esters) and cyclic molecules (triterpenoids, tocopherols, sterols) with often non-negligible amounts of unidentifiable components (Jetter *et al.*, 2008). Therefore, mainly aliphatic cuticular model waxes contributing the lowest possible chemical variability as well as the highest possible purity should be used for adjuvant activity screenings. Previous studies have already followed the development of cuticular model waxes. Carreto *et al.* (2002) designed a binary model wax consisting of 1-tetradecanol and 1-octadecanol as a goal to mimic properties of epicuticular waxes (Carreto *et al.*, 2002). Schreiber (1995) used tetracosanoic acid as a cuticular model, which is a typical aliphatic constituent of cuticular waxes (Schreiber, 1995). In addition, Coward (2010) proposed nonacosan-10-ol as an epicuticular model wax (Coward, 2010). Fagerström *et al.* (2013) first developed a model wax consisting of 1-docosanol and dotriacontane, which was based on the intracuticular wax of *Clivia miniate*. The model wax was used to investigate water permeability *in vitro* and surfactant induced plasticizing effect on transpiration (Fagerström *et al.*, 2013;

Fagerström *et al.*, 2014). A recent study went one step further and aimed to establish a quaternary model wax based on the aliphatic components of *Schefflera elegantissima* wax (Seufert, 2020). Nevertheless, in each case an attempt was made to find a model wax valid for all plants. The variability of chemical compositions of barrier-forming intracuticular waxes is almost infinite. Therefore, the assumption of establishing a model wax being representative for all plants appears naive. Consequently, instead of establishing a universal model wax, the aim of this study was to prepare wax blends contributing candelilla wax as basic matrix, mixed with different amounts of either n-alcohol dominated policosanol or long-chain alkyl ester dominated rice bran wax. The aim was to investigate adjuvant diffusion kinetics as affected by altering individual VLCA-compositions by ATR-FTIR.

Policosanol is a mixture of long-chain n-alcohols derived from sugarcane wax (Marinangeli *et al.*, 2007). In some cases, policosanol is also obtained from wheat germ or rice. Policosanol is said to lower blood lipid levels and is contained in dietary supplements (Gouni-Berthold and Berthold, 2002). The main component of policosanol is 1-octacosanol; the other components differ in the chain length of the aliphatic alcohol (Gouni-Berthold and Berthold, 2002). In addition, to obtain evidence from alkyl esters on the diffusion kinetics and plasticization modes of accelerating adjuvants, rice bran wax was added to candelilla wax at different ratios. Rice bran wax is a natural wax ester derived from rice bran (Kodali, 2009). The rice bran is extracted with hexane to obtain rice bran oil, which contains 2 to 3% rice bran wax. The wax is separated from the oil by overwintering and further refined to achieve suitability for food or industrial applications (Kodali, 2009). As was observed by Tada *et al.* (2014), ester functions of rice bran wax alkyl esters are centrally located (Tada *et al.*, 2014) just representing typical alkyl ester constituents of plant cuticular wax alkyl esters (Sümmchen *et al.*, 1995; Lai *et al.*, 2007; Guo *et al.*, 2018).

Diffusion kinetics of the previously introduced adjuvants methyl oleate and TEHP, as well as of the monodisperse AEs C12E2, C12E4 and C12E6 were recorded in candelilla wax blends contributing up to 50 % policosanol or rice bran wax, respectively.

Plasticization intensity and diffusion kinetics differing from those observed in pure candelilla wax, depending on the structural integrity of the respective wax mixtures were assumed. Due to the high complexity of individual crystalline arrangements of the wax structures, depending on respective compositions, it was expected that no clear improvements or deteriorations of the wax barrier with increasing alcohol or alkyl ester content would be detectable.

Nevertheless, it was investigated whether trends in the respective diffusion kinetics of the investigated adjuvants allowed any conclusions to be drawn about the modification of the wax barrier, depending on respective n-alcohol or alkyl ester contributions.

4.2 Material and methods

4.2.1 Chemicals

All chemicals used in this study are listed in Table 1. Candelilla wax, policosanol and rice bran wax served as cuticular model wax components. Methyl oleate, TEHP and the three selected monodisperse AEs C12E2, C12E4 and C12E6 represented accelerator adjuvants used for diffusion studies in cuticular model waxes. BSTFA and pyridine were used for silylation of polar compounds in candelilla and carnauba wax for GC analysis.

4.2.2 ATR-FTIR experimental setup and data collection for adjuvant diffusion

The ATR-FTIR experimental setup was used as previously described in 3.2.2.

4.2.3 Preparation of wax layers

Candelilla wax pellets and policosanol powder or candelilla wax pellets and rice bran wax platelets were weighed using a microbalance and mixed according to respective compositions. Melting solid wax mixtures at 120 °C using a heating module (Labnet Dry Bath, Labnet International Inc., Corning, NY, USA) and thoroughly mixing liquid compounds generated equally distributed wax solutions. Trapezoidal ATR crystals (ZnSe 72 x 10 x 6 mm, Specac Ltd, Orpington, United Kingdom) were heated up to 120 °C using a heating module (Labnet Dry Bath, Labnet International Inc., Corning, NY, USA) and attached to a POLOS^{TM} spin coater SPIN150i-NPP (SPS-Europe GmbH, Ingolstadt, Germany). A small amount of liquid wax was then drawn up into a glass pipette and subsequently applied on top of the preheated ATR crystal until its surface was fully covered. Subsequent spin coating of the ATR crystal was performed for 15 seconds at 2000 rpm for Candelilla wax blends, followed by a wax solidification phase for 10 to 30 seconds at 500 rpm. Solidified wax at the long or bottom sides of the ATR crystal was wiped with chloroform.

4.2.4 Determination of wax film thickness, diffusion coefficients and data evaluation of ATR-FTIR absorption spectra

Determination of wax film thicknesses and diffusion coefficients were determined according to 2.2.4, 2.2.5. Data evaluation was performed as previously described in 2.2.6.

4.2.5 Determination of candelilla wax blends melting behavior via ATR-FTIR

Determination of candelilla wax blends melting behavior was performed according to 2.2.8.

4.2.6 Determination of phase transitions by differential scanning calorimetry (DSC)

Differential scanning calorimetry (DSC) was used to determine phase transition temperatures of candelilla wax blends with a DSC 1 calorimeter (Mettler Toledo, Greifensee, Switzerland). Weight fraction of wax mixtures (candelilla wax + policosanol / rice bran wax) were prepared and 5 to 7 mg of each wax blend were weight into 40 µl volume aluminum crucibles. Three cycles of heating and cooling from 20 to 120 °C or 120 °C to 20 °C were performed. The heating and cooling rates were 1 °C min^{-1}. For phase transition analysis, the third cycle was used, respectively.

4.2.7 Gas-chromatographic analysis (GC)

5 mg of policosanol or rice bran wax were dissolved in 100 ml chloroform. 0.1 ml of the solutions were derivatized with 10 µL BSTFA and 10 µL pyridine at 70 °C for 30 min using a heating module (Pierce Reacti-Therm, Pierce Chemical, Dallas, TX, USA). The mixture was then dissolved in 100 µl chloroform and used for gas chromatography (GC). GC-mass spectrometry (GC-MS; 6890 N, GCSystem; Agilent Technologies, Santa Clara, CA, USA) was used to identify wax compounds. Helium was used as a carrier gas. A MS detector (m/z 50–1000, MSD 5977A, Agilent Technologies) was applied. Due to the high boiling points of long-chain esters, on-column injection with a capillary high-temperature column (30 m × 0.32 mm, DB-1HT, 0.1 µm film: J&W Scientific, Agilent Technologies) was used. The liquid sample was injected at 50 °C and the temperature was hold for 1 min. The temperature was then increased to 120 °C at a heating rate of 10 °C min^{-1} and hold for 1 min. The temperature was then increased to 240 °C at a heating rate of 7.5 °C min^{-1} and hold for 1 min. The temperature was then increased to 390 °C at a heating rate of 4 °C min^{-1} and hold for 10 min. Identification was undertaken using Wiley 10th/NIST 2014 mass spectral library (John Wiley & Sons, Hoboken, NJ, USA) reference

specimen or spectra interpretation. Quantification was undertaken using GC flame ionization detection (GC-FID, 6850N, Agilent Technologies, Santa Clara, CA, USA). Similar GC conditions as before were used to separate compounds, except that hydrogen gas was used as carrier gas.

4.3 Results

4.3.1 Wax analysis

Policosanol almost entirely consisted of n-alcohols (95.1 ± 0.3) (Figure 38A, n=6).

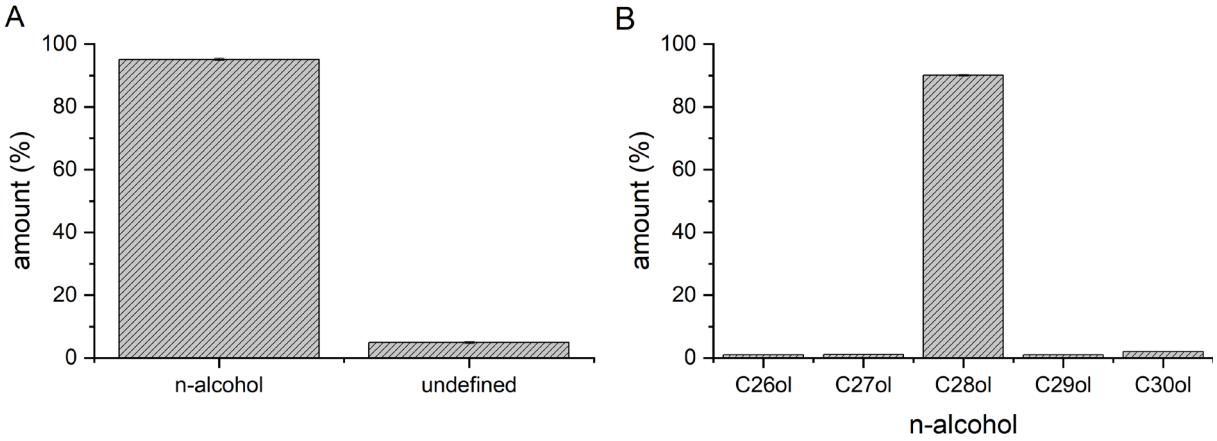

Figure 38. (A) Chemical composition of policosanol and (B) carbon chain length distribution of n-alcohol fraction.

The n-alcohol fraction was dominated by C28ol (90.0 ± 0.3 %) with only minor amounts of C26ol to C30ol (Figure 38B). Rice bran wax mainly consisted of long-chain alkyl esters (87.9 ± 1.3 %) (Figure 39A, n=6))

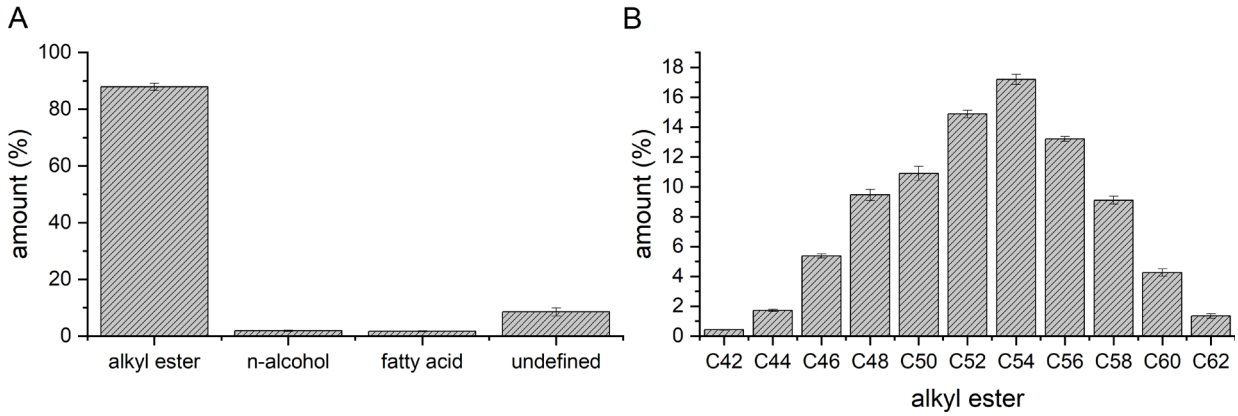

Figure 39. (A) Chemical composition of rice bran wax and (B) carbon chain length distribution of alkyl-ester fraction.

The carbon chain length of the alkyl ester fraction ranged from C42 to C62 with C54 being most prominent (17.2 ± 0.3 %) (Figure 39B).

4.3.2 Fourier-transform infrared spectroscopy

Phase transitions of candelilla/policosanol wax mixtures were recorded via ATR-FTIR (Figure 40).

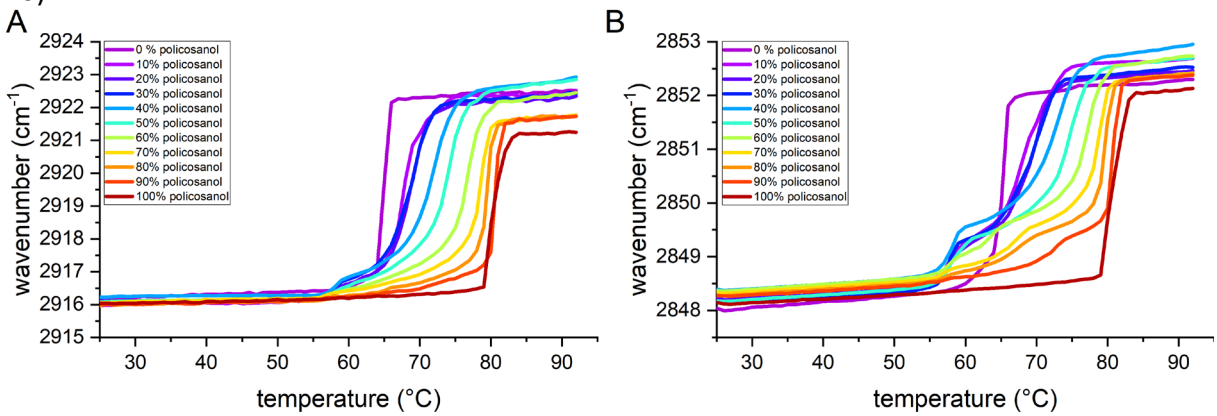

Figure 40. Shift of CH_2-streching modes (A) symmetrical and (B) asymmetrical, indicating melting range of candelilla/policosanol blends.

All mixtures showed one clear phase transition, indicated by a shift of the CH_2 asymmetrical vibration (Figure 40) from lower to higher wavenumbers. Increasing the amount of policosanol by 10 % in each of the candelilla/policosanol blends resulted in a constant shift in the melting range to higher temperatures. This effect was observed both for the CH_2- asymmetrical as well as for the CH_2 symmetrical stretching vibration of the wax mixtures. Applying the logistic model to each temperature curve of respective CH_2 symmetrical stretching vibrations (Appendix 1) revealed midpoint of respective melting ranges (Figure 41).

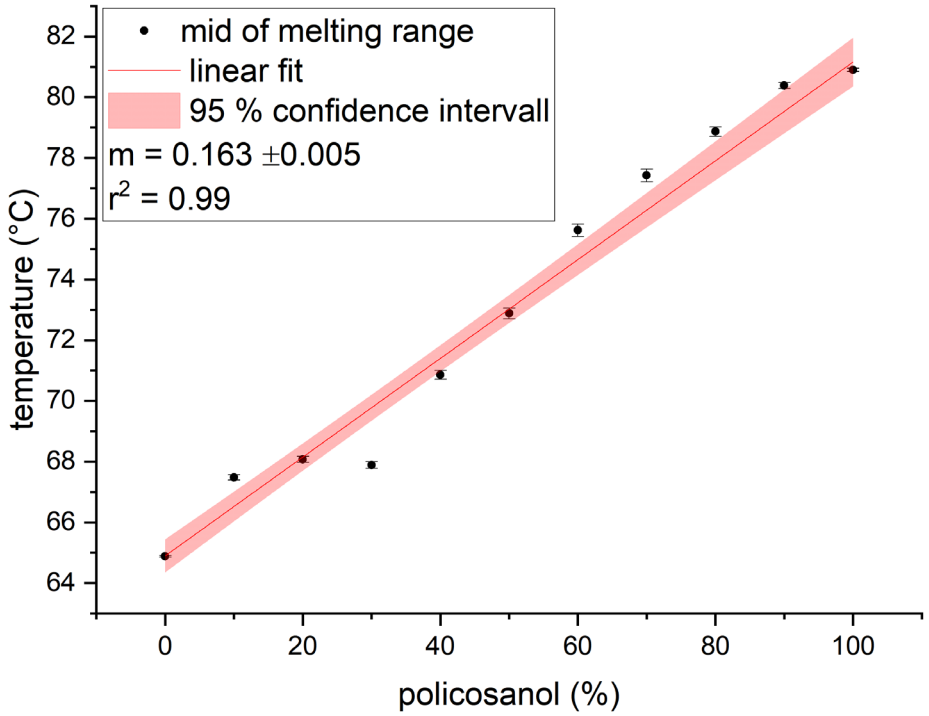

Figure 41. Mid points of candelilla wax/policosanol blends melting ranges determined via logistic fit of CH_2 asymmetric vibration modes (ATR-FTIR) and linear fit. Errors are given as standard deviations to the model fit.

Melting ranges were also determined for candelilla/rice bran mixtures via ATR-FTIR (Figure 42).

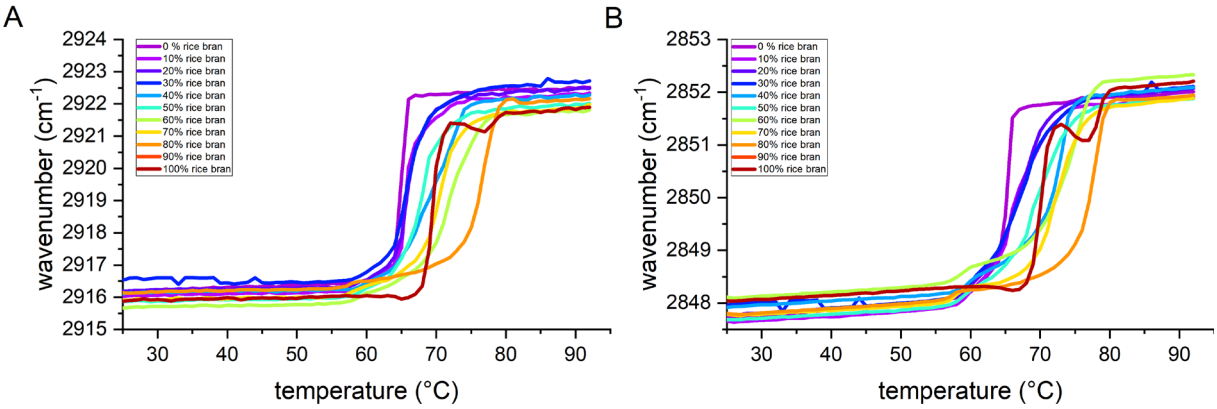

Figure 42. Shift of CH_2-streching modes (A) symmetrical and (B) asymmetrical, indicating melting range of candelilla/rice bran wax blends.

At first glance, a direct correlation of rice bran wax content and melting range increase failed both for the asymmetrical (Figure 42A) and the symmetrical CH_2 stretching vibration modes (Figure 42B). However, when applying the logistic model to each curve (Appendix 1), a linear correlation of rice bran wax content and melting range mid points was observed (Figure 43).

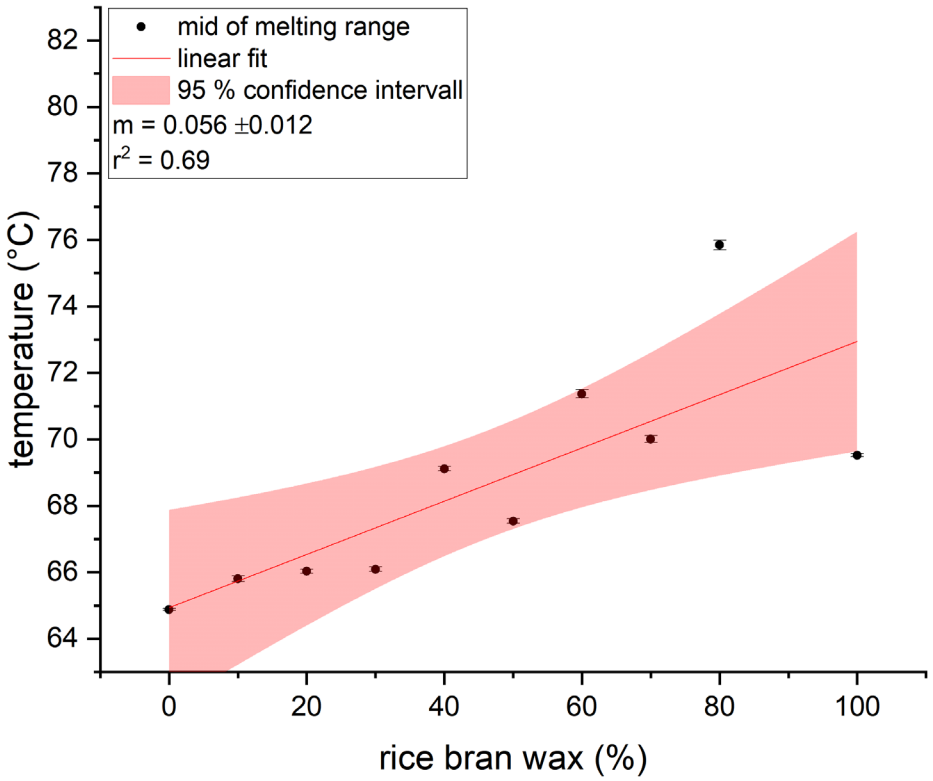

Figure 43. Mid points of candelilla wax / rice bran wax blend melting ranges determined via logistic fit of CH_2 asymmetric vibration modes (ATR-FTIR). Errors are given as standard deviations to the model fit.

A higher variability of melting points was observed at higher rice bran wax concentrations. The apparent effect of policosanol on melting temperature was higher than that of rice bran wax, which was confirmed by the higher slope.

4.3.3 Differential Scanning Calorimetry

Figure 44 depicts DSC heating (left) and cooling (right) thermograms of candelilla/policosanol and candelilla/rice bran wax blends during 3rd recorded cycles, respectively.

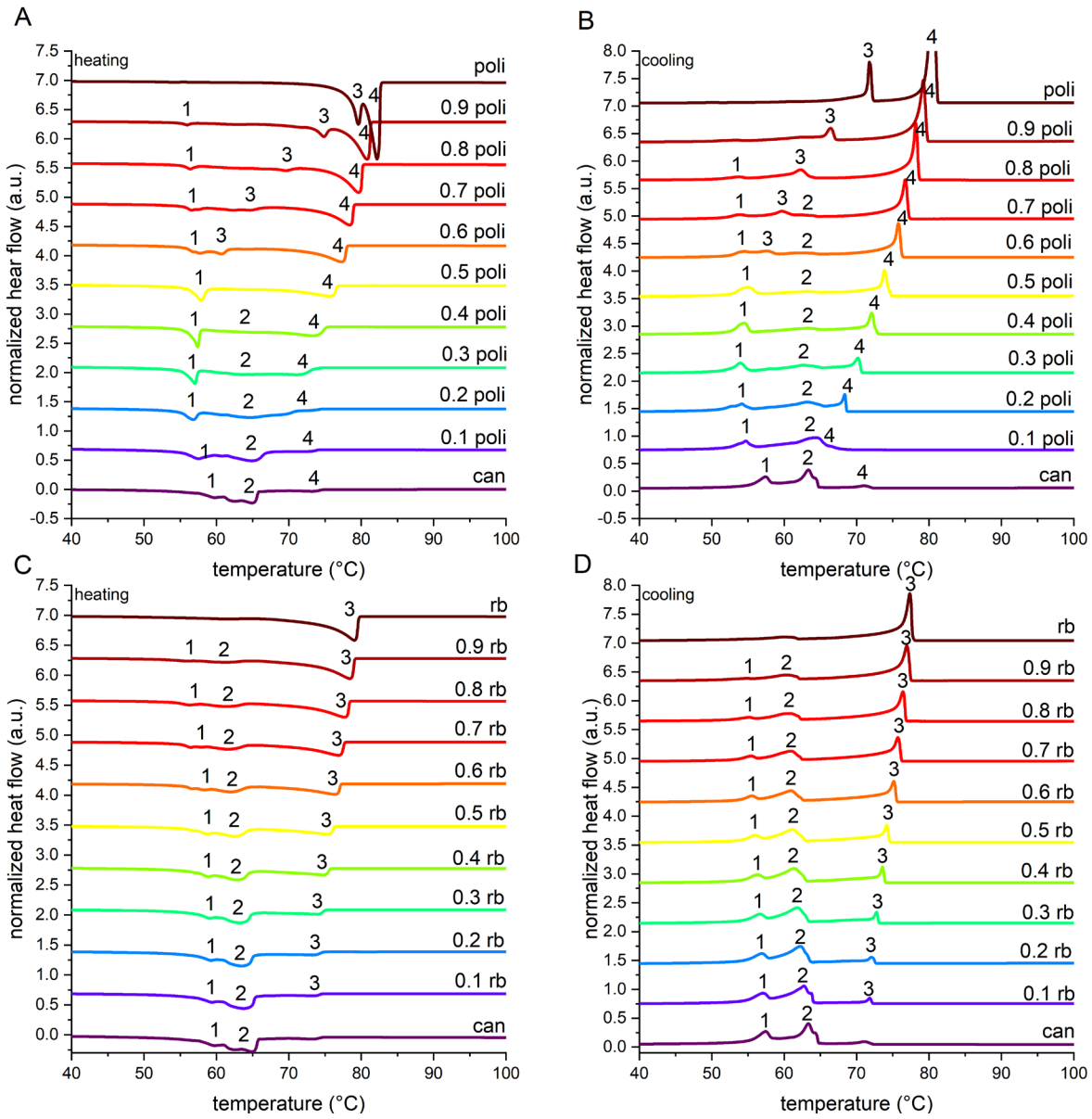

Figure 44. DSC heating (A and C) and cooling thermograms (B and D) of wax mixtures containing candelilla wax and policosanol (poli) or candelilla wax and rice bran wax (rb).

Pure candelilla wax showed broad DSC transition peaks with indefinite start and blunt maxima during heating. The bulk peaks were considered to mainly reflect complex phase transitioning of mainly hentriacontane and other aliphatic components (Figure 44A). However, during cooling two differentiable phase transitions occurred (Figure 44B). The first transition (signal 1) shifted to lower temperatures when adding 10 % policosanol, while further increasing policosanol content did not alter the peak position neither during heating nor during cooling. The second transition (signal 2) was almost unaffected by increasing policosanol content (signal 2). However, signal 2 vanished completely at 50 % policosanol content during heating and at 70 % policosanol content during cooling.

Just like candelilla wax, pure policosanol exhibited two transitions both during heating and cooling (Figure 44A, B). The first policosanol-specific peak (signal 3) was first visible at 60 % policosanol content, whereas the second transition (signal 4) was assigned to both n-alcohol phase transitions in policosanol and candelilla during heating and cooling, respectively.

In contrast to policosanol, rice bran wax melting was indicated by one broad transition (signal 3) both during heating and cooling (Figure 44C, D). This phase transition constantly shifted to higher temperatures with increasing rice bran wax content. Contrastingly, candelilla wax phase transitions (peak 1 and 2) were only marginally affected but were slightly shifted to lower temperatures with increasing rice bran wax content.

4.3.4 Adjuvant diffusion in candelilla/policosanol and candelilla/rice bran wax blends

Diffusion kinetics of methyl oleate in candelilla wax blends contributing up to 50 % policosanol (Figure 45A) or rice bran wax (Figure 45B) were measured via ATR-FTIR. Analogous to 3.3.2, methyl oleate diffusion kinetics were analyzed by integrating C=O stretching vibration (at 1736 cm^{-1}) of corresponding methyl ester-groups and plotting respective integrated absorptions versus the experimental time.

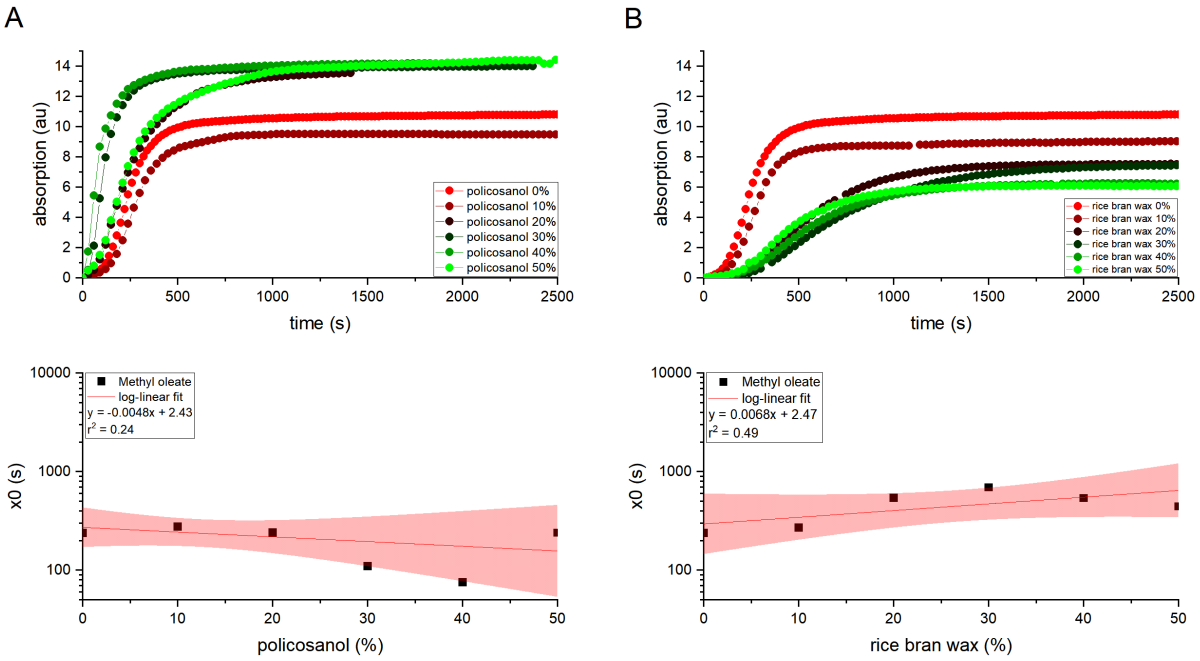

Figure 45. Methyl oleate diffusion kinetics in candelilla wax blends with up to 50 % (A) policosanol or (B) rice bran wax. Respective time points of half-maximal absorption (x0) were determined with non-linear regression of the logistic model and linear fits (red line) were performed on log (x0) vs. policosanol or rice bran wax content. Red shades represent 95 % confidence intervals.

The time courses of the diffusion curves of methyl oleate in candelilla wax/policosanol mixtures reached equilibrium absorption more rapidly with increasing policosanol content. Moreover, equilibrium absorptions increased with increasing policosanol content. In contrast, the time courses of the diffusion curves reached an equilibrium state later with increasing rice bran wax content, which also reflected lower absolute absorptions.

The diffusion kinetics obtained showed initial lag times for both policosanol and rice bran wax mixtures that deviated strictly from the proposed Fickian diffusion model (equation (10)). Therefore, Fickian diffusion kinetics were revised. Instead, with the aim of analyzing the obtained diffusion curves in some way, the logistic model was applied to the experimental data to finally evaluate the time points of the half-maximum absorption values (x0). Log-linear regression of x0 versus policosanol content revealed decreasing times required for half-maximal absorptions (Figure 45A). In contrast, increasing rice bran wax content led to increasing time required for reaching half-maximal methyl oleate absorptions (Figure 45B).

Diffusion kinetics of TEHP in candelilla wax blends contributing up to 50 % policosanol (Figure 46A) or rice bran wax (Figure 46B) were measured via ATR-FTIR. Analogous to 3.3.4, TEHP diffusion kinetics were analyzed by integrating P-O-C stretching vibration (at 1000 cm^{-1}) and plotting respective integrated absorptions versus the experimental time.

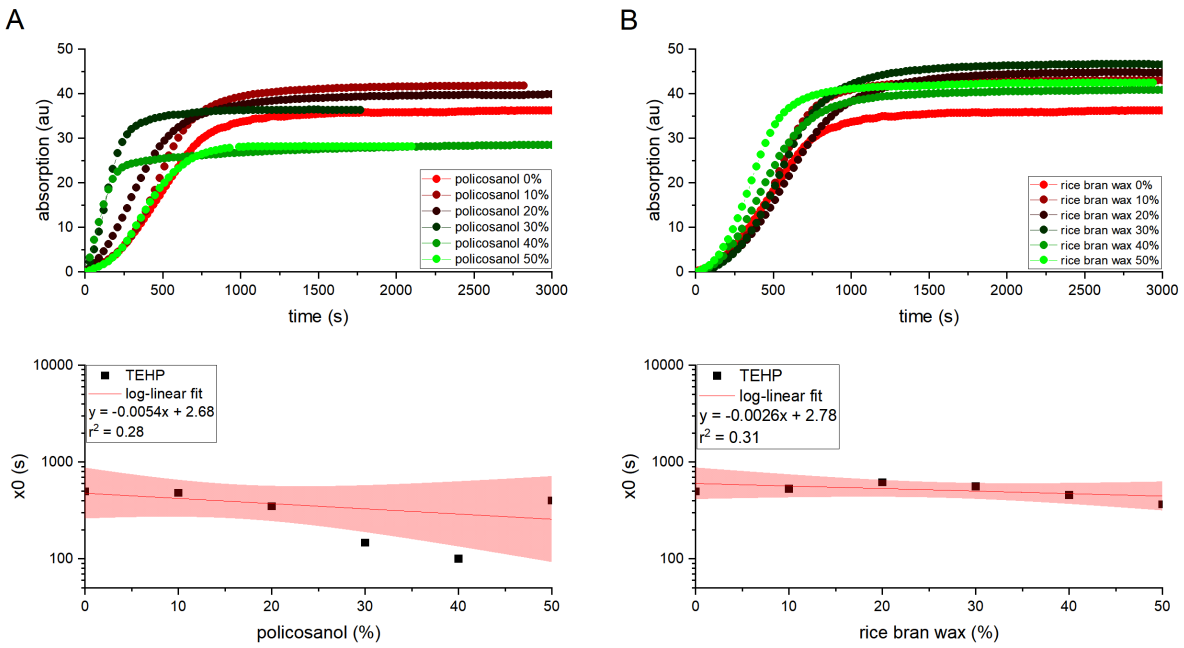

Figure 46. TEHP diffusion kinetics in candelilla wax blends with up to 50 % (A) policosanol or (B) rice bran wax. Respective time points of half-maximal absorption (x0) were determined with non-linear regression of the logistic model and linear fits (red line) were performed on log (x0) vs. policosanol or rice bran wax content. Red shades represent 95 % confidence intervals.

It was observed that the time courses reached equilibrium levels faster with increasing policosanol content (Figure 46A), although no trend for absolute absorption values was detected. The times of half-maximal absorption (x0) tended to decrease with increasing policosanol content, with x0 increasing again at 50% policosanol content. A log-linear regression showed that a higher overall policosanol content led to an acceleration in reaching half-maximal absorptions (Figure 46A). A similar trend was observed for the time points at which half-maximal absorption was reached with increasing rice bran wax content (Figure 46B). However, the effect was less pronounced, and the variance of individual x0-values was lower than for candelilla/policosanol blends.

Furthermore, diffusion curves of monodisperse AEs C12E2, C12E4 and C12E6 in candelilla/policosanol (Figure 47A) and candelilla/rice bran wax blends (Figure 47B) were recorded via ATR-FTIR. Analogous to 3.3.6, AE diffusion kinetics were analyzed by plotting integrated C-O-C stretching vibrations (at 1100 cm^{-1}) versus time.

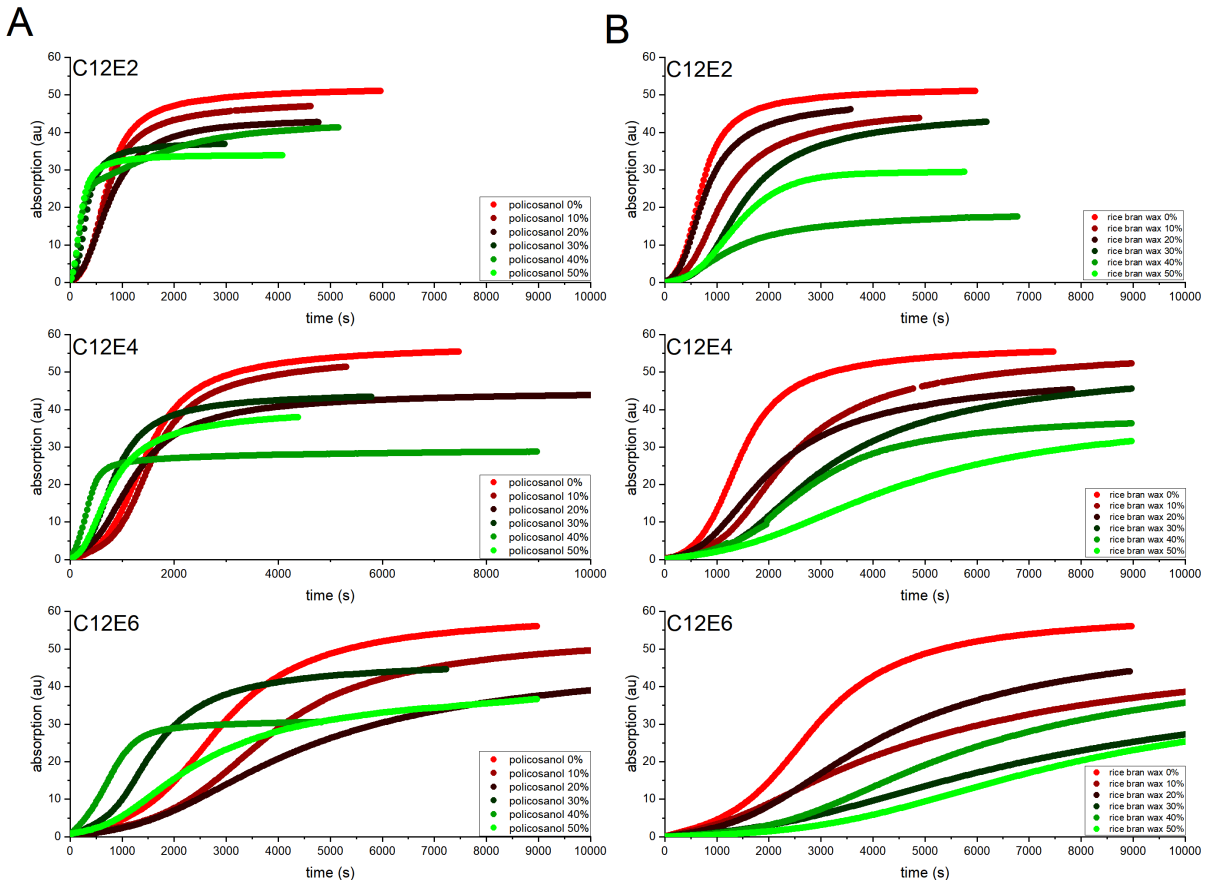

Figure 47. Diffusion of monodisperse alcohol ethoxylates C12E2, C12E4 and C12E6 in candelilla wax blends containing either 0 % to 50 % (A) policosanol or (B) rice bran wax.

Slower AE diffusion kinetics occurred with increasing ethoxylation levels both during diffusion in candelilla/policosanol and candelilla/rice bran wax blends. Comparing the respective

alcohol ethoxylate diffusion curves in both policosanol and rice bran wax blends, it is evident that the diffusion process in the latter was slower in each case.

Apparently, no trends of the diffusion kinetics as a function of the respective policosanol or rice bran wax contents were observed. Nevertheless, an increasing variance of the diffusion kinetics with increasing ethoxylation levels within the candelilla/policosanol blends was observed (Figure 47A). The variance of diffusion kinetics in candelilla/rice bran wax blends was high for all AEs studied and time courses of diffusion were slower with increasing rice bran wax content (Figure 47B).

Due to the mostly sigmoidal diffusion patterns, no Fickian diffusion could be detected. Thus, equation (10) could not be applied to the diffusion kinetics. Nevertheless, the logistic model was used to determine the times of half-maximal absorption (x0) in each case, irrespective to absolute absorptions (Figure 48).

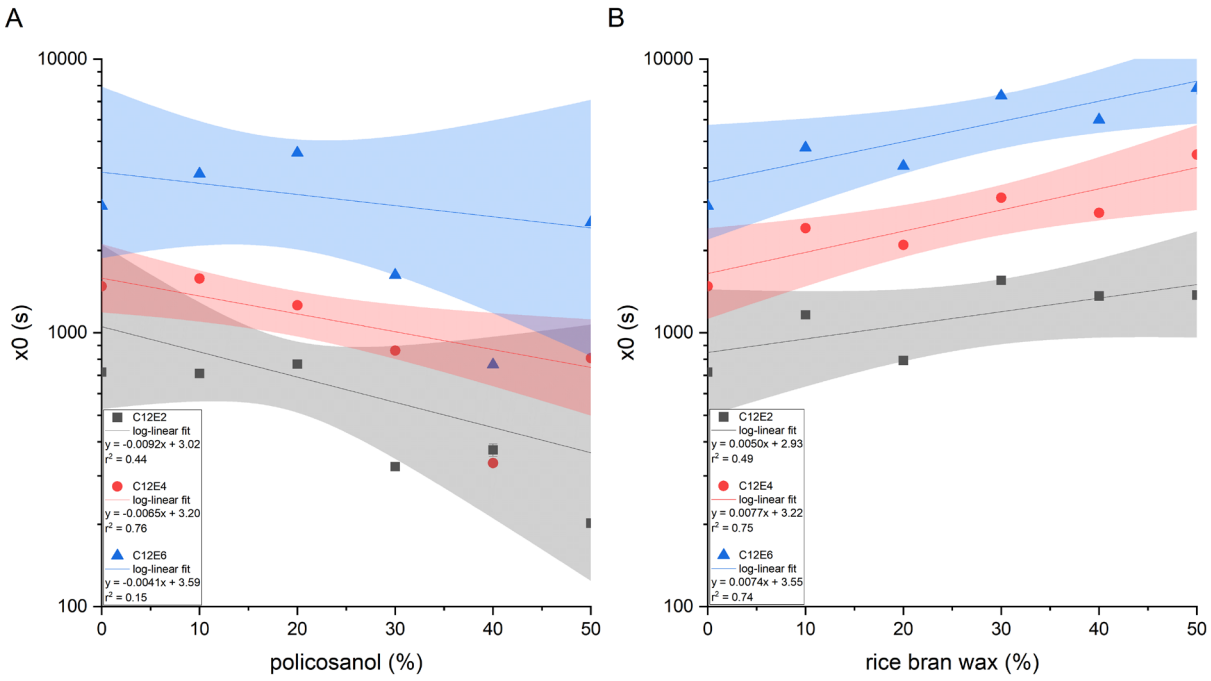

Figure 48. Half-maximal absorptions (x0) of the monodisperse alcohol ethoxylates C12E2, C12E4 and C12E6 in (A) candelilla/policosanol mixtures and (B) candelilla/rice bran wax mixtures. Log-Linear fits with corresponding confidence intervals (95 %) were performed, revealing either (A) positive or (B) negative correlations of half-maximal absorptions (x0) and wax admixture.

Log-linear correlations were found between the times of half-maximal absorption and the policosanol concentration (Figure 48A). The respective negative slopes of log-linear fits differed only marginally and indicated faster diffusion kinetics with increasing policosanol content. Respective intercepts differed by approximately 0.3 every two ethoxylate units,

indicating slower diffusion with increasing ethoxylation level. The coefficients of determination differed, in some cases enormously. In particular, x0 of C12E4 and C12E6 in 40% policosanol were outside the 95% confidence intervals, resulting in quite low coefficients of determination.

A similar relationship was found for the diffusion of AEs in candelilla/rice bran wax blends (Figure 48B). Again, the intercepts increased by about 0.3 per two ethoxylate units. The absolute values of the respective slopes again differed only marginally, but in contrast to diffusion in candelilla/policosanol blends, being all positive. The positive slopes indicate slower diffusion kinetics with increasing rice bran content. All values ranged within the respective 95% confidence intervals, resulting in meaningful coefficients of determination.

Wax layer thickness analysis was performed to check for potential dependencies between rice bran wax or policosanol content and half-maximal absorptions (Figure 49).

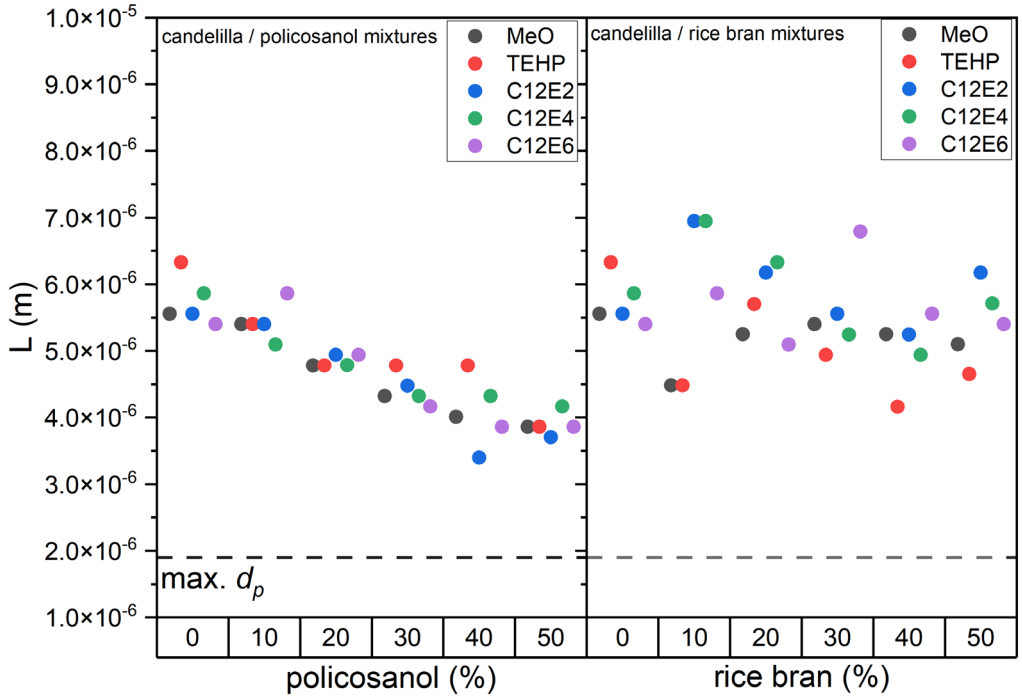

Figure 49. Wax layer thicknesses of candelilla wax mixtures ranging from either 0 to 50 % policosanol or rice bran wax used for adjuvant diffusion experiments. Dashed line indicates maximum evanescent wave penetration depth at 1740 cm^1, representing the maximum wavenumber of investigated adjuvant vibration modes (C=O stretching of methyl oleate).

Candelilla/policosanol wax layer thicknesses ranged from 3.40 x 10^{-6} m to 6.33 x 10^{-6} m. A linear trend showing decreasing wax layer thickness with increasing policosanol content was observed. Candelilla/rice bran wax layer thicknesses ranged from 4.19 x 10^{-6} m to 6.94 x 10^{-6}

m. No trend was observable for either higher or lower wax layer thicknesses with respect to the rice bran wax contents.

4.4 Discussion

This study aimed to investigate diffusion kinetics of self-accelerating adjuvants in aliphatic cuticular model waxes dominated either by n-alcohols or long chain alkyl esters. For this purpose, diffusion kinetics in wax mixtures consisting of either candelilla/policosanol (increasing content of octacosanol) or candelilla/rice bran wax (increasing content of very-long-chain alkyl esters) were recorded by ATR-FTIR. It was hypothesized that an increasing alcohol content leading to phase separation would largely lead to deteriorated barrier functions of the wax blends, whereas an increased alkyl ester content should lead to better barrier properties by introducing alkyl-ester bridges connecting adjacent crystallites. FTIR phase transition analyses and DSC experiments should provide information on the respective crystalline structures and phase miscibilities of the wax blends to finally draw conclusions on the susceptibility to different accelerating adjuvants.

4.4.1 Policosanol and rice bran wax as model wax constituents

Wax composition may vary greatly among species (Jetter *et al.*, 2008). Since one single species may comprise 50 different chemical compounds, a clear discrimination of each individual contribution to the barrier seems doubtful. Hence, establishing a general cuticular model wax contributing physical and chemical properties representing all cuticular waxes appeared pointless. However, as Staiger *et al.* (2019) have recently shown, mainly aliphatic constituents build up the barrier against penetrating compounds (Staiger *et al.*, 2019). Therefore, wax mixtures exclusively contributing VLCAs were considered in this study. It seemed reasonable to use candelilla wax as a basic model for diffusion studies, since it consists of 70% n-alkanes, which in many cases form a main constituent of crop specific cuticular waxes (Bianchi *et al.*, 1980; Szafranek and Synak, 2006; Wang *et al.*, 2011b; Shaheenuzzamn *et al.*, 2019). Other components found in candelilla wax, such as free fatty acids and n-alcohols, may also be present in crop cuticular waxes (Shaheenuzzamn *et al.*, 2019).

Policosanol was added to simulate an increasing alcohol content as found in many crops (Beattie and Marcell, 2002; Szafranek and Synak, 2006; Mao *et al.*, 2012; Shaheenuzzamn *et al.*, 2019). While it would have been advantageous to use pure substances (e.g., octacosanol)

instead of policosanol to define diffusion effects or phase transitions more precisely, the spin coating process used to produce the wax layers required such high amounts of wax, which were no longer within commercially available limits. GC analysis confirmed that policosanol consisted almost exclusively of octacosanol (> 90 %) and contained small proportions of other n-alcohols, which in total represented a quite realistic image of naturally occurring cuticular waxes found in many epicuticular wax fractions (Müller and Riederer, 2006).

Although alkyl esters tend to play a minor role as constituent in crop specific cuticular waxes, it cannot be excluded that even low alkyl ester contents, such as those found in the cuticular waxes of barley, maize or rice (Lee and Suh, 2015) may have an immense effect on the diffusion kinetics of adjuvants and AIs. In addition, crops exist that contain significant alkyl ester amounts in their cuticular waxes (e.g. *Camelina sativa*) (Razeq *et al.*, 2014). Moreover, there is no indication of the quantity required for organic compound diffusion modification yet and hence, crop protection science has tremendous interest in characterizing adjuvant uptake in cuticular waxes contributing significant proportions of very-long-chain alkyl esters. As for diffusion studies in candelilla/policosanol blends, it would have been certainly advantageous to use pure alkyl ester blends, but very long-chain alkyl esters with a chain length of up to 64 carbon atoms are not commercially available and the synthesis of corresponding components, as well as the yield and subsequent purification, turned out to be laborious (personal communication Pascal Seufert). Moreover, most cuticular waxes do not contribute single alkyl esters with one specific chain length, but instead offer chain length distributions ranging from C36 up to C70 (Gülz *et al.*, 1993; Shepherd *et al.*, 1995; Sümmchen *et al.*, 1995). GC analysis showed that rice bran wax consisted of nearly 88% long-chain alkyl esters with chain lengths between 42 and 62 carbon atoms, making it an excellent model wax compound.

4.4.2 FTIR and DSC phase behavior analysis

Previous studies already demonstrated the usefulness of the FTIR method for determining the phase behavior of cuticular and artificial waxes (Merk *et al.*, 1997; Patel *et al.*, 2001; Seufert, 2020). For example, Merk *et al.* (1997) were able to determine midpoints of the melting ranges of cuticular waxes both being extracted from isolated cuticles or impregnating isolated cuticles of *Hedera helix* and *Juglans regia* (Merk *et al.*, 1997). The proposed method is based on the evaluation of VLCA-specific CH_2 band positions. It is assumed that the melting process of a wax

mainly results from the transition from *all-trans* to *gauche* conformers, which eventually leads to a band shift of the CH_2 stretching vibrations to higher wavenumbers (Hastie and Roberts, 1994).

ATR-FTIR melting curves were recorded for candelilla/policosanol and candelilla/rice bran wax blends ranging from 0 and 100% admixture (Figure 40). The candelilla/policosanol blends showed band shifts towards higher temperatures with increasing policosanol content for both the asymmetric and symmetric CH_2 stretching vibrations. The asymmetric stretching vibration showed one defined band shift, indicating the phase transition from solid to liquid, and melting midpoints were determined using the logistic model (Patel *et al.*, 2001). The linear regression of the mid points of the melting ranges determined by logistic fits showed a high coefficient of determination (0.99) (Figure 41). Consequently, a linear dependency between n-alcohol content and increasing midpoint of melting ranges was observed.

In contrast to the candelilla/policosanol blends, the melting behavior of the candelilla/rice bran wax blends determined by ATR-FTIR was much more undefined and did not increase continuously with increasing rice bran wax content. Although a linear regression successfully showed the correlation between increasing phase transition temperature and rice bran wax content, the coefficient of determination of 0.69 was significantly lower than that of the linear correlation of candelilla/policosanol melting experiments. Alkyl esters, as typically found in cuticular waxes, carry mostly centrally located functional ester groups derived from the fusion of n-alcohols and free fatty acids of comparable chain lengths (Gülz *et al.*, 1993). It is therefore conceivable that the resulting "kink" within the molecule gives rise to metastable crystallite conformations as mixed with n-alkanes (mainly hentriacontane in candelilla wax) and may therefore lead to unidentifiable band shifts such as those found here (Figure 42).

In order to investigate not only solid-liquid phase transitions, but also to look at solid-solid phase transitions of the individual wax components, possibly revealing phase separation of individual VLCAs, DSC analyses of the respective wax mixtures were performed in addition to the FTIR experiments. Several attempts aimed to characterize cuticular (model) wax phase transition behavior by DSC (Reynhardt and Riederer, 1994; Reynhardt, 1997; Casado and Heredia, 1999; Carreto *et al.*, 2002; Perkins *et al.*, 2005; Dassanayake *et al.*, 2009; Fagerström *et al.*, 2013; Seufert, 2020).

Both Carreto *et al.* (2002) and Reynhardt and Riederer (1994) observed epicuticular wax extracts consisting mainly of long chain n-alcohols coexist as crystalline and fluid phases at

ambient temperatures (Reynhardt and Riederer, 1994; Carreto *et al.*, 2002). Thus, the expected solid phase immiscibility would tend to make a mosaic of phase domains even at very low temperatures.

For odd-numbered n-alkanes, and cuticular waxes in general, it is well established that crystallites are packed in an orthorhombic lattice at room temperature and undergo a transition to hexagonal state with rising temperature (Reynhardt and Riederer, 1991, 1994). Four transitions were found for candelilla/policosanol mixtures during the 3rd DSC heating and cooling cycles (Figure 44) and phase diagrams were prepared (Figure 50).

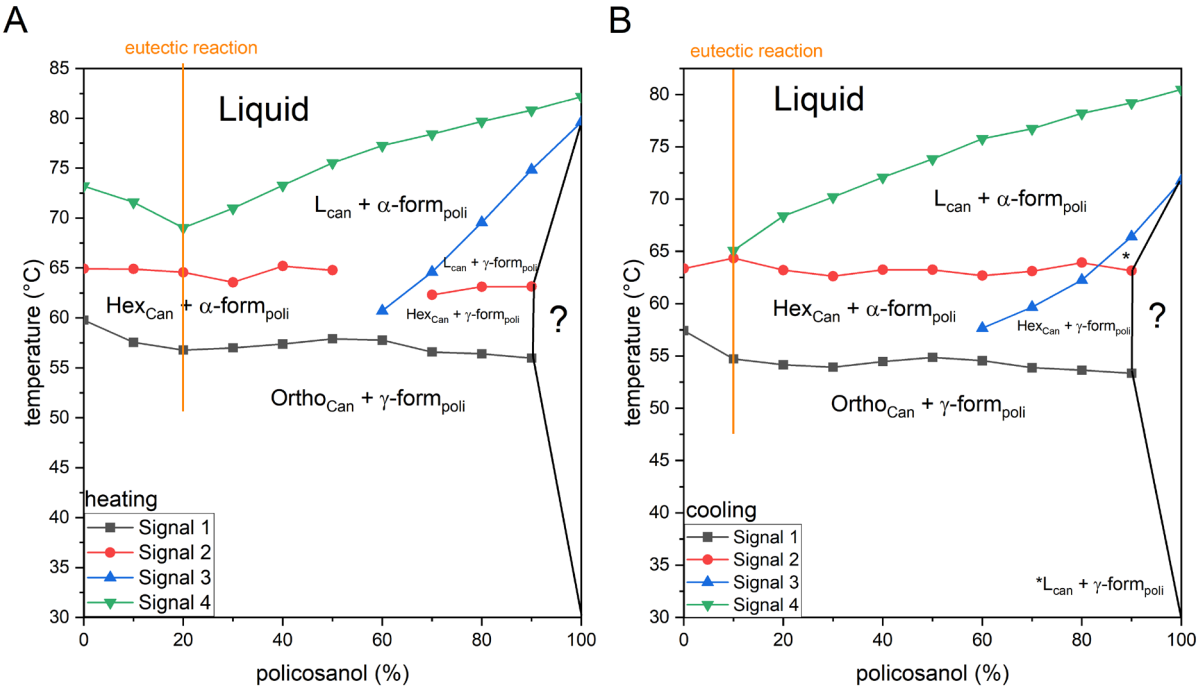

Figure 50. Phase diagrams obtained from DSC (A) 3rd heating cycle and (B) 3rd cooling cycle of candelilla/policosanol blends. Phase transitions and solid or liquid phases of respective wax constituents as well as eutectic reactions are shown.

The first signal (signal 1) was consistently recorded between 0 and 90% policosanol content. It largely appeared at the same temperature, regardless of respective policosanol concentrations, although the addition of up to 20% policosanol initiated a slight shift to lower temperatures (Figure 50).

According to previous results of Briard *et al.* (2003), the signal occurring at ~ 60 °C was interpreted as an initial solid-solid phase transition from orthorhombic to hexagonal state of candelilla wax dominating hentriacontane (Figure 21) (Briard *et al.*, 2003). However, phase transition temperatures reported by Briard *et al.* (2003) were slightly lower than those obtained here. This was not surprising since the observed C30 and C32 fatty acids in candelilla

wax both are capable of introducing hydrogen bonds (Bowman and Mason, 1951), consequently leading to higher melting points than that of solely by weak Van-Der-Waals-forces stabilized hentriacontane. A second signal (signal 2) was identified, which occurred between 0 % to 50 % and 70 % to 90 % policosanol (heating) and between 0 % to 90% policosanol (cooling). This signal consequently corresponded to the phase transition of the hentriacontane specific transition from hexagonal to liquid state (Craig *et al.*, 1994; Briard *et al.*, 2003). This signal also remained largely constant at the same temperature considering the experimental policosanol concentrations. According to Tanaka *et al.* (1959), the first policosanol specific peak (signal 3) represented a phase transition from the stable monoclinic γ-form, typical for even-numbered n-alcohols (Ventolà *et al.*, 2003), to a metastable rotator α-form (Tanaka *et al.*, 1959). Usually, this phase transition can only be detected during the cooling cycle (Figure 50B), but here it was seen during heating as well (Figure 50A). Watanabe (1963) observed same effects, when using n-alcohol samples contributing impurities of other n-alcohols with different chain lengths, representing polydisperse n-alcohol mixtures (Watanabe, 1963). Hence the polydisperse nature of policosanol, being dominated by octacosanol, but contributing significant proportions of C26ol and C30ol may explain this transition observed during heating. The second policosanol specific peak (signal 4) was interpreted as a phase transition from rotator α-form to liquid state (Tanaka *et al.*, 1959), indicating melting of the investigated wax mixtures. A comparison of the melting points determined by FTIR with the phase transition of the rotator α-phase transition showed good agreement (Figure 51).

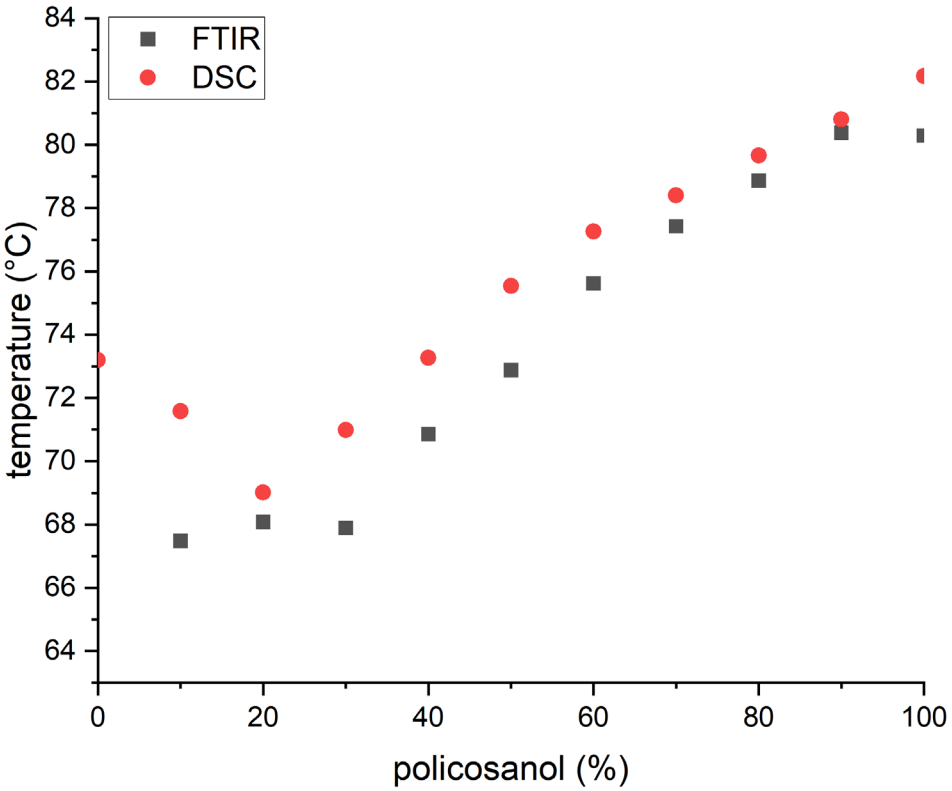

Figure 51. Midpoints of candelilla/policosanol blend melting ranges determined via FTIR and endotherm phase transitions (heating) of policosanol specific α-rotator to liquidus phase transitions of candelilla/policosanol mixtures recorded via DSC.

It can therefore be assumed that the melting curves recorded by FTIR mainly indicated the solid-to-liquid phase transition of the alcohol fraction, but not of the alkane fraction, which already transitioned to liquid state at lower temperatures. Surprisingly, signal 4 was already observed in pure candelilla wax during heating, probably being assigned to n-alcohols present in candelilla wax (Figure 50A). This signal was shifted to lower temperatures until 20 % policosanol, while being shifted to higher temperatures beyond 20 % policosanol content. The apparent plateau level at 20 % policosanol (Mazee, 1957), in concordance with overall constant n-alkane-specific transitions, strictly indicated the presence of an eutectic reaction (Mnyukh, 1960; Dorset, 2005). Due to the eutectic reaction, partial immiscibility of solid n-alkane and n-alcohol phases appeared likely, as was already observed for binary blends of pentadecane and undecanol (Rathgeber *et al.*, 2013). However, especially during cooling, co-existing hexagonal candelilla and γ-form or α-form of policosanol were observed, depending on respective wax compositions, revealing extraordinary complex crystallite formations and stabilization modes.

The DSC analysis of the candelilla/rice bran wax mixtures showed a completely different behavior both during heating and cooling (Figure 52).

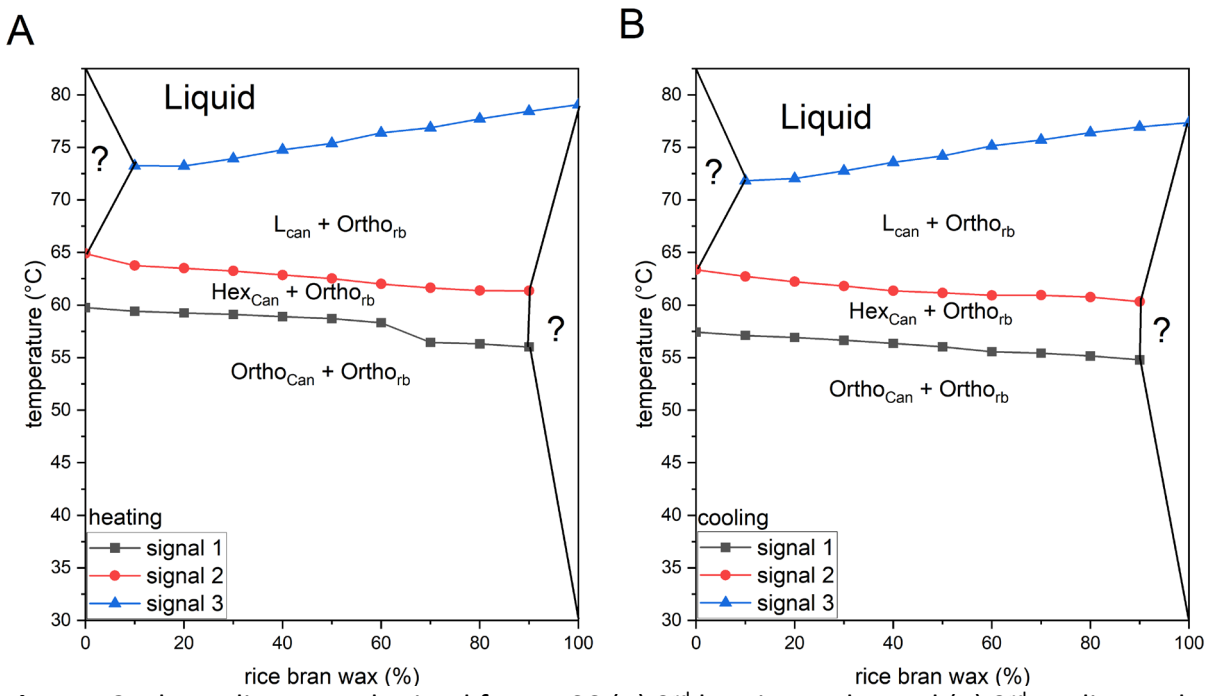

Figure 52. Phase diagrams obtained from DSC (A) 3rd heating cycles and (B) 3rd cooling cycles of candelilla/rice bran wax blends. Phase transitions and solid or liquid phases of respective wax constituents are shown.

Slightly decreasing transition temperatures of both hentriacontane specific phase transitions (signal 1 and 2) were apparent with increasing rice bran wax content (Figure 52). This can be explained by the fact that the endo- and exothermic peaks were less pronounced with increasing alkyl ester content and that the peaks also broadened (Figure 44C, D). Therefore, the peaks became more ill-defined and their centers corresponding to the transition temperatures were slightly shifted. Furthermore, the alkyl ester fraction may have acted as a solvent for free fatty acids of the candelilla wax, extracting melting point-increasing hydrogen bonds from out of the solid alkane phase. As a results, continuous reduction of the phase transition temperatures of the alkane phase became apparent. It was found that the only observable phase transition of the rice bran wax from orthorhombic to liquid state (Dassanayake *et al.*, 2009) was very broad due to the Gaussian chain length distribution of the alkyl ester fraction (C42 to C62) and was continuously shifted to higher temperatures with increasing rice bran wax content. However, there was no eutectic reaction detectable. It must be noted that a eutectic reaction might occur when considering candelilla/rice bran wax blends with rising alkyl ester content up to 10 %. DSC data considering candelilla/rice bran wax

blends contributing between 0 and 10 % rice bran wax is lacking. Consequently, no conclusion whether eutectic reactions occurred during heating or cooling could be drawn. However, due to the extraordinarily high chain length difference between hentriacontane (C31) and the alkyl-ester fraction (dominated by C56), total immiscibility of solid alkane and alkyl ester fraction appeared likely anyway. Mixed liquid phases of candelilla wax and rice bran wax above the respective alkyl ester transition temperature from orthorhombic to liquid state were apparent. The absolute melting temperatures were all above those determined by ATR-FTIR (Figure 53).

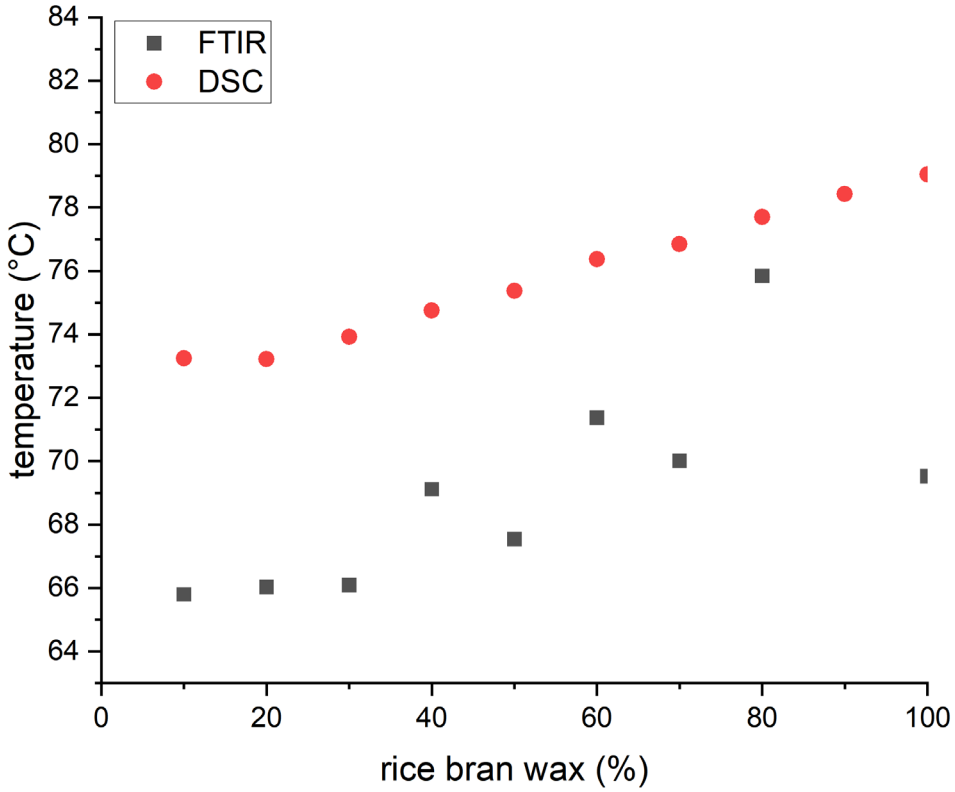

Figure 53. Midpoints of candelilla/rice bran wax blend melting ranges determined via FTIR and endotherm phase transitions of alky-ester specific orthorhombic to liquidus phase transitions of candelilla/rice bran wax mixtures recorded via DSC.

It is quite conceivable that the melting curves recorded by ATR-FTIR did not reflect the phase transition of the alkyl esters *per se*, but rather represented intermediate *all-trans* to *gauche* transitions of mixed alkane/alkyl-ester phases. These phases are presumed to occur due to the presence of alkyl-esters bridging two adjacent crystallites and thereby reinforcing the mechanical and structural stability of the wax blends as was earlier stated and discussed in chapter 2 (Riederer and Schreiber, 1995; Reynhardt, 1997; Bueno *et al.*, 2019). Thus,

predicting adjuvant diffusion kinetics based on the observed phase behavior with predictably complex crystalline structures using FTIR and DSC appeared doubtful.

4.4.3 Determination of adjuvant diffusion kinetics in candelilla wax blends

Using ATR-FTIR, diffusion curves of the accelerating adjuvants methyl oleate, TEHP, C12E2, C12E4, and C12E6 were recorded in candelilla/policosanol and candelilla/rice bran wax mixtures. Since the Fickian model (equation 10) inadequately described the experimentally determined diffusion curves due to initial lag phases, all diffusion curves deviated to varying degrees from the previously assumed Fickian diffusion (Schreiber and Riederer, 1996a). As already mentioned in chapter 2, the lag phase reflected initial plasticization necessary for exponential diffusion, leading to enhanced build-up of wax internal adjuvant concentration.

This study showed that the policosanol content inevitably led to higher melting points of respective wax blends (Figure 41; Figure 50A; Figure 51), which in principle results in higher mechanical stability and resistance to penetrating plasticizing adjuvants. DSC heating and cooling cycles led to the assumption of immiscible solid policosanol and candelilla wax phases either obtained from heating or cooling cycle (Figure 50). During methyl oleate diffusion, decreasing mobility (indicated by slower diffusion kinetics) and decreasing solubility (indicated by lower absolute absorption) were observed when adding 10 % policosanol (Figure 45A), probably inducing increased policosanol specific level of hydrogen-bonds. The same effect was observed for C12E6 diffusion until reaching 30 % policosanol content (Figure 47A), both suggesting enhancement of barrier-functions. However, both mobility and solubility of the investigated accelerator adjuvants were drastically increased in candelilla/policosanol mixtures beyond assumed eutectic reaction points. This was confirmed by the decreasing time required to reach half-maximal IR-absorptions or adjuvant concentrations with increasing policosanol content (Figure 45; Figure 46; Figure 48).

Although the diffusion kinetics of the investigated adjuvants each showed appropriately discussed trends depending on the respective policosanol concentrations, a high variance of the individual curves was demonstrated. It is unclear from where this variance could have originated. One possibility is the decreasing thickness of the wax layers generated by spin coating with increasing policosanol content (Figure 49A). Furthermore, neither FTIR nor DSC phase transition analysis were capable of determining ultrastructural arrangements of partially immiscible solid candelilla wax and policosanol phases. Based on several studies, a

lamellar arrangement of pure alkanes and alcohols of similar chain lengths mainly establishing crystalline zone A is likely (Hastie and Roberts, 1994; Riederer and Schreiber, 1995; Michaud *et al.*, 2000). However, the candelilla wax-specific proportions of free fatty acids and triterpenoids, as well as unidentified impurities, inevitably led to an undefinable influence on the wax structure. Since naturally occurring cuticular waxes often contribute up to 50 components (Jetter *et al.*, 2008), accurate prediction of diffusion kinetics of accelerating adjuvants appears doubtful and, just as here, only trends in diffusion kinetics can be determined.

As was observed for AEs, diffusion kinetics were delayed with increasing ethoxylation level, as was already stated by Coret and Chamel (1994) and was confirmed for candelilla and carnauba wax in chapter 2. A negative log-linear dependence of time points of half-maximal absorptions (x0) and increasing policosanol content was found for each of the investigated AEs (Figure 48A). However, the absolute time required to reach half-maximal absorptions in each wax composition raised with increasing ethoxylation level. Based on these results, it can be concluded that cuticular waxes are on the one hand more susceptible to more lipophilic AEs with smaller numbers of ethoxylate units and on the other hand more are more susceptible with increasing n-alcohol content, probably due to phase separation.

In contrast to the accelerated diffusion kinetics of the adjuvants in candelilla/policosanol mixtures, except for TEHP, delayed diffusion kinetics were detected in candelilla/rice bran wax mixtures with increasing rice bran wax content. This finding agrees well with the diffusion kinetic discrepancies of methyl oleate and AEs, found between alkyl-ester less candelilla wax and alkyl-ester dominated carnauba wax, the latter exhibiting significantly better barrier properties against adjuvant penetration due to its high alkyl ester content (Chapter 2).

The phase diagrams discussed previously provide conclusions about phase separation of the solid phases of candelilla wax and rice bran wax. Reynhardt and Riederer (1997) suggested, based on the heterogeneity of chain lengths in cuticular wax of *Hordeum vulgare*, that despite phase separation, perfect crystalline structures cannot form, with the defect distribution of chain ends favoring incorporation of single long-chain alkyl ester chains (Reynhardt, 1997). Accordingly, it seems quite reasonable that due to the Gaussian chain length distribution of alkyl esters in rice bran wax (Figure 39B), these are incorporated into neighboring crystallites of the solid alkane phase of candelilla wax during crystallization, with the centrally located ester groups being found in the amorphous phase between the two crystallites. Reynhardt

and Riederer (1997) simultaneously prepared X-ray powder diffractograms supporting the "bridging" of adjacent crystallites in the cuticular wax of *Hordeum vulgare* (Reynhardt, 1997). However, ultrastructural assessment of candelilla blends with altered VLCA content is lacking and thus precise evaluation and prediction of adjuvant diffusion kinetics will appear problematic in future studies. Investigating model wax blends on a molecular level using XRD and electron diffractometry will be of utmost importance to improve prediction of respective adjuvant diffusion kinetics and plasticization susceptibility.

5 Chapter 4: Effects of adjuvants and co-penetrating water on CNP diffusion

5.1 Introduction

5.1.1 Objectives and research questions

Cuticular waxes form the main barrier against the penetration of organic compounds (Riederer and Schönherr, 1985). It has already been shown that mainly the VLCAs are responsible for this barrier (Jetter and Riederer, 2016; Staiger *et al.*, 2019). Nevertheless, no discrimination of penetration processes in waxes whose chemical composition is dominated by different VLCAs has been made so far. In the last two chapters, the diffusion kinetics and the self-accelerating effect of different adjuvants in alkane-dominated candelilla wax, candelilla blends with altered VLCA content and alkyl ester-dominated carnauba wax were investigated, and conclusions were drawn about the respective modifications of the wax structure. Based on this, the aim of this study was to find out how adjuvant treatment affects organic model AI mobility and solubility and whether discrimination as a function of adjuvant effectiveness is possible in waxes dominated by different VLCA fractions. It has already been shown that the plasticizing adjuvants do not only increase AI penetration rates but can also enhance transpiration rates as an undesirable side effect. Maintaining the native transpiration rate is of utmost importance, especially when using adjuvants in arid regions, otherwise the vitality of the plant to be protected will be negatively affected (Riederer and Schönherr, 1990; Räsch *et al.*, 2018). Accordingly, the aim of this study was not only to characterize the diffusion kinetics of a model AI under the influence of different adjuvants, but furthermore to analyze co-penetrating water diffusion kinetics accommodated with CNP uptake into cuticular model waxes. Lipophilic adjuvants such as methyl oleate or TEHP were assumed to have only a minor effect on water diffusion, whereas increased water diffusion kinetics were predicted under the influence of monodisperse AEs due to their hydrophilic ethoxylate groups. Therefore, it was hypothesized that water molecules penetrating the wax would themselves induce "secondary" plasticization of the wax, eventually leading to enhanced uptake of AI models.
To study the diffusion kinetics of a model AI or water, eliminating potential influences of co-penetrating adjuvants was necessary. Therefore, diffusion kinetics were consistently analyzed

after the waxes had been treated with pure adjuvants for periods well beyond the attainment of equilibrium conditions (see Chapter 2).

This study, together with the results from chapter 2 should give insight into the relationship between adjuvant-induced modification of the model wax structure, model AI mobility and solubility and elucidating the role of co-penetrating water. Significant differences between the diffusion coefficients and partition coefficients were suspected, as well as the permeability coefficients of CNP between carnauba wax and candelilla wax depending on the respective adjuvant – water- wax interactions.

5.2 Material and methods

5.2.1 Chemicals

All chemicals used within this study are listed in Table 1. Candelilla wax and carnauba wax represented cuticular model waxes. CNP and D_2O were used as model diffusants. Methyl oleate, TEHP, C12E2, C12E4 and C12E6 represented adjuvants for model AI diffusion studies.

5.2.2 ATR-FTIR experimental setup and data collection for CNP and D_2O diffusion

Diffusion kinetics of CNP or D_2O in accelerator treated candelilla and carnauba wax were separately determined via ATR-FTIR. Wax layers were generated by spin-coating liquid wax onto ATR crystals. The wax films were incubated with pure liquid adjuvants over least 12 hours. Constant flows of D_2O or aqueous solutions of CNP (7.5 g l^{-1}) were applied on ATR crystals covered with adjuvant treated wax films. The diffusion towards the crystal-wax interface resulted in an increase of the respective molecular concentrations within the evanescent wave over time. As a result, there was an increase in IR-absorption induced either by the fused asymmetrical and symmetrical stretching vibrations of D_2O at 2500 cm^{-1} or by the stretching vibration of the nitrile functional group at 2230 cm^{-1}. Respective absorptions were integrated for each recorded spectrum and assigned to the respective measurement time.

An ATR crystal was first covered with an equally distributed thin wax layer. Afterwards, the with wax covered ATR crystal was attached to a water heated flow through Gateway™ ATR top plate (Specac Ltd, Orpington, United Kingdom). Flexible tubes from a thermostat (Thermo Scientific Haake DC30-K20, Karlsruhe, Germany) were connected to the water inlet and outlet ports of the top plate to establish water circulation, enabling measurements at a constant temperature of 25 °C. The thermostabilized flow through top plate sample inlet and outlet

ports were connected to flexible tubes, ensuring a circulating flow of D_2O or aqueous CNP solution. An intermediary attached peristaltic pump allowed a continuous solvent flow (5 ml min^{-1}) over the wax-coated ATR crystal. To attain a steady-state flow of aqueous CNP solution and to compensate potential diffusant loss in the donor medium, a thermostabilized liquid reservoir with a volume capacity of approximately 50 ml was constructed and implemented into the circuit. The large reservoir volume ensured that the CNP concentration in the donor medium did not significantly decrease during the experimental period. Subsequently, the top plate was put into a Gateway™ ATR-FTIR spectrometer accessory (Specac Ltd, Orpington, United Kingdom). FTIR absorption spectra recorded with a Fourier-transform infrared spectrometer (FTIR, Bruker Invenio R with liquid N2-cooled MCT-detector, Bruker, Ettlingen, Germany) within a wavenumber range of 500 to 4000 cm^{-1}. Resolution was set to 2 cm^{-1} with 16 scans for each averaged spectrum. The Gateway™ unit and the FTIR-spectrometer were purged with dry CO2 -free air (K-MT-LAB 3, Parker Hannifin, Kaarst, Germany). Background spectra of bare ATR crystals were used, instead of with wax coated ATR crystals. Subsequently after turning on the peristaltic pump to enable circulating flow of aqueous CNP solutions or D_2O, IR-absorption spectra were recorded every 20 seconds to 2 minutes over a time range of up to 16 hours. To control the FTIR-apparatus and to collect absorption spectra, the software OPUS 8.2 (Bruker, Ettlingen, Germany) was used.

5.2.3 Preparation of wax samples and determination of wax film thickness

Preparation of wax samples was performed according to 3.2.3 and determination of wax film thickness was performed according to 2.2.4.

5.2.4 Determination of diffusion coefficients by ATR-FTIR

The diffusion coefficients of CNP after adjuvant treatment were determined in candelilla wax and carnauba wax according to 2.2.5.

5.2.5 Data evaluation of ATR-FTIR absorption spectra

IR-Absorption spectra were imported in OriginPro 9 (OriginLab Corporation, Northampton, MA, USA) and only the relevant vibrations of CNP (C≡N stretching ~ 2230 cm-1) and D_2O (O-D stretching ~ 2500 cm^{-1}) were considered, respectively. Baseline fits were equally performed for each recorded spectrum, setting the same anchor points for each time point. To determine

CNP diffusion coefficients Levenberg-Marquardt linear-least-square regression analysis of integrated absorptions within a distinct time range was conducted with OriginPro 9 (OriginLab Corporation, Northampton, MA, USA), using equation (10) where D and A_{eq} were the only adjustable parameters. The coefficient of determination (r^2) was used to determine the accuracy of the model compared to the experimental data.

Water diffusion kinetics were not described by the Fickian diffusion model according to equation (10). Hence, instead of determining a constant diffusion coefficient to comprehensively analyze diffusion kinetics, half-maximal absorptions at respective time points x0 were calculated by fitting the logistic model to diffusion data.

5.2.6 Determination of CNP concentration, partitioning and permeability

The increasing IR-absorption of CNP (C≡N stretching ~ 2230 cm^{-1}) in candelilla and carnauba wax during diffusion was translated to respective CNP concentrations. Therefore, an external calibration was prepared using ATR-FTIR. Chloroform was used as solvent for CNP, because of its refractive index (= 1.445) being close to the model waxes assumed refractive index (= 1.5). Using chloroform as a solvent with a RI close to that of the investigated waxes led to negligible deviations of the penetration depth of the evanescent wave. Hence, the number of molecules detected should be comparable to the number of scanned molecules at final equilibrium absorptions obtained from diffusion experiments. The same ATR-FTIR setup and spectral conditions as for D_2O and CNP diffusion experiments were used. Temperature of cycling water was set to 25 °C. A clean ZnSe ATR crystal was covered with CNP solutions with increasing concentrations raising from 2.5 g l^{-1} to 40.0 g l^{-1}. The ATR top plate unit was sealed with an aluminum plate to eliminate solvent evaporation. The crystal was cleaned after each measurement using chloroform to ensure residual CNP was purged off. Linear regression of CNP specific integrated absorption (C≡N stretching ~ 2230 cm^{-1}) versus respective concentrations was performed using OriginPro 9 (OriginLab Corporation, Northampton, MA, USA). Using the slope of the regression line and y-intercept fixed at 0, concentrations at final equilibrium states of diffusion were determined. Wax-water partition coefficients K_{ww} relating CNP concentrations of CNP equilibrium absorptions within wax layers and concentrations of aqueous CNP donor solutions (7.5 g l^{-1}) were determined. Multiplication of D and K_{ww} revealed permeability coefficients p.

5.2.7 Statistics

Statistical analysis of CNP diffusion coefficients (Appendix 2 and Appendix 3), partition coefficients (Appendix 4 and Appendix 5) and permeability coefficients (Appendix 6 and Appendix 7) was performed using OriginPro 9 (OriginLab Corporation, Northampton, MA, USA). Some samples did not show normality according to Shapiro-Wilk test ($p < 0.05$). Lognormal transformation of diffusion coefficients, partition coefficients and permeability coefficients after methyl oleate treatment in candelilla wax almost entirely resulted in normality according to Shapiro-Wilk test ($p < 0.05$). However, lognormal transformation of permeability coefficients after C12E6 treatment in candelilla wax did not show normal distribution. In similarity to other permeability coefficients, normal distribution would most likely have been observed simply by using more samples ($n > 4$). Hence, CNP permeability coefficients determined in C12E6 incubated candelilla wax were treated as they showed normal distribution. 2-way-ANOVA test with Tukeys post-hoc test ($p < 0.05$) was used to detect statistically significant differences.

5.3 Results

All presented IR-absorption patterns recorded over time and model fits to respective integrated absorptions are examples of multiple experiments (n=4). Detailed breakdown of CNP diffusion coefficients, absolute absorptions and wax layer thicknesses is given in Appendix 8 and detailed listing of CNP equilibrium concentrations, wax water partition coefficients and permeability coefficients is given in Appendix 9.

5.3.1 CNP diffusion kinetics in wax after methyl oleate treatment

CNP diffusion kinetics in candelilla wax (Figure 54) and carnauba wax (Figure 55) were recorded after methyl oleate treatment via ATR-FTIR. As observed, the CNP specific IR-absorption resulting from the C≡N stretching vibration at 2230 cm^{-1} reached an equilibrium level in spin coated candelilla wax after approximately 500 s (Figure 54A).

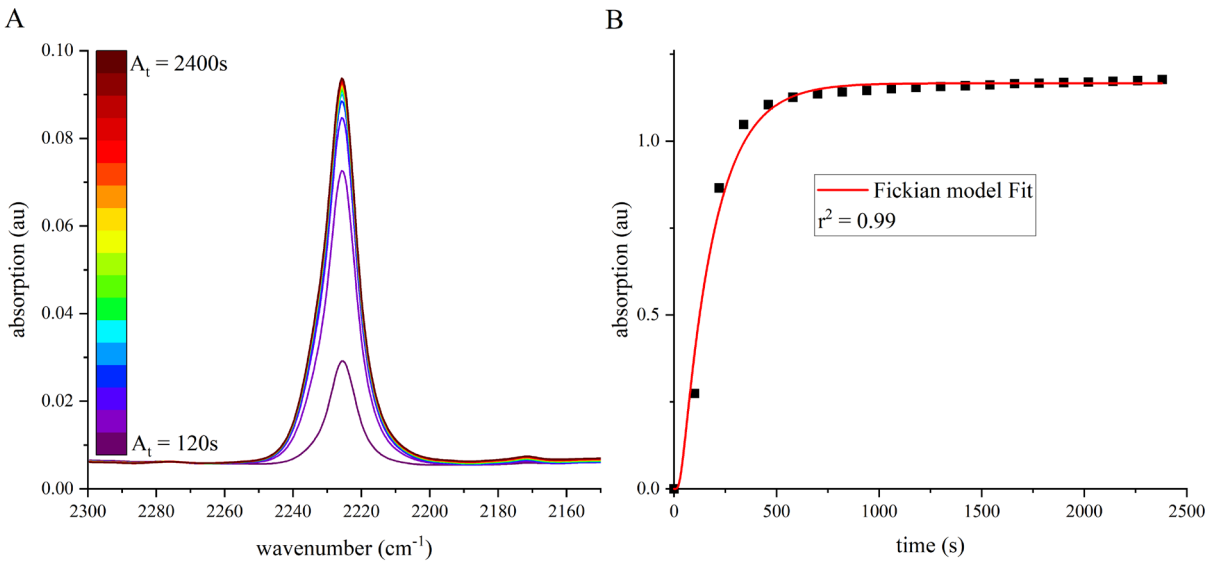

Figure 54. (A) Increasing absorption of 4-cyanophenol specific C≡N stretching vibration (~2230 cm^{-1}) during diffusion in candelilla wax pretreated with methyl oleate and (B) integrated absorption versus time fitted to equation (10).

By integrating the absorption band at each recorded measurement time point, the CNP diffusion kinetics were determined (Figure 54B). Fitting the experimentally determined increase of integrated absorption to equation (10) revealed Fickian diffusion kinetics.

Equilibrium conditions of CNP diffusion in carnauba wax were reached after approximately 4000 s (Figure 55A).

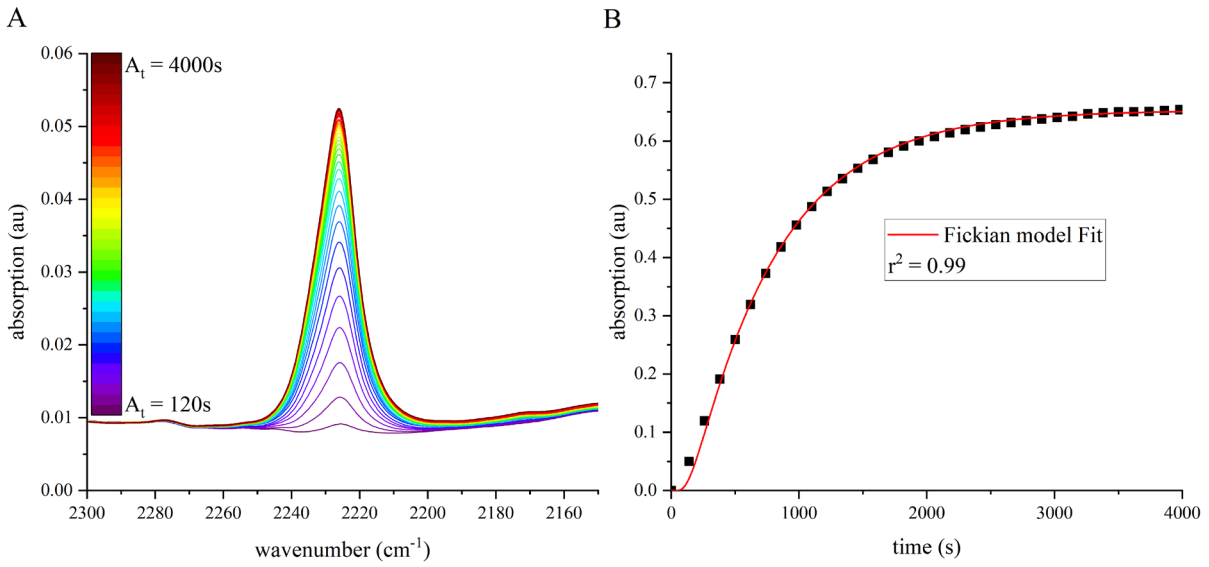

Figure 55. (A) Increasing absorption of 4-cyanophenol specific C≡N stretching vibration (~2230 cm^{-1}) during diffusion in carnauba wax pretreated with methyl oleate and (B) integrated absorption versus time fitted to equation (10).

Fickian diffusion kinetics were obtained for CNP diffusion in carnauba wax pretreated with methyl oleate (Figure 55B).

5.3.2 CNP diffusion kinetics in wax after TEHP treatment

CNP diffusion kinetics were also recorded after TEHP treatment of spin coated candelilla wax (Figure 56) and carnauba wax (Figure 57).

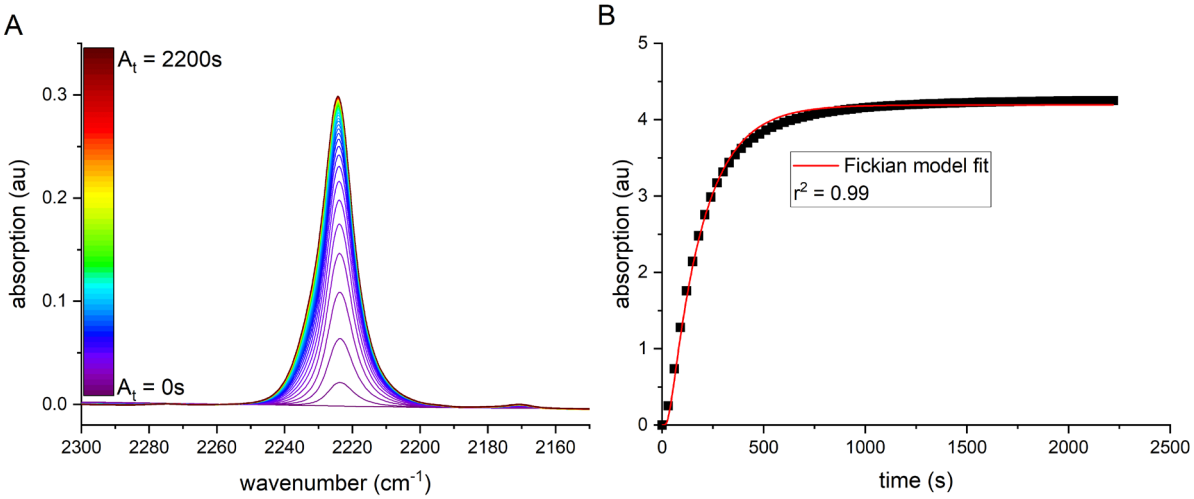

Figure 56. (A) Increasing absorption of 4-cyanophenol specific C≡N stretching vibration (~2230 cm-1) during diffusion in candelilla wax pretreated with TEHP and (B) integrated absorption versus time fitted to equation (10).

Equilibrium absorption in candelilla wax was reached after 1000s (Figure 56A) and diffusion kinetics obtained from integrated absorptions over time were perfectly described by the Fickian model (Figure 56B).

Diffusion kinetics of CNP in carnauba wax after TEHP treatment reached equilibrium conditions after approximately 300s (Figure 57A). Integrating obtained absorption spectra revealed Fickian diffusion kinetics (Figure 57B).

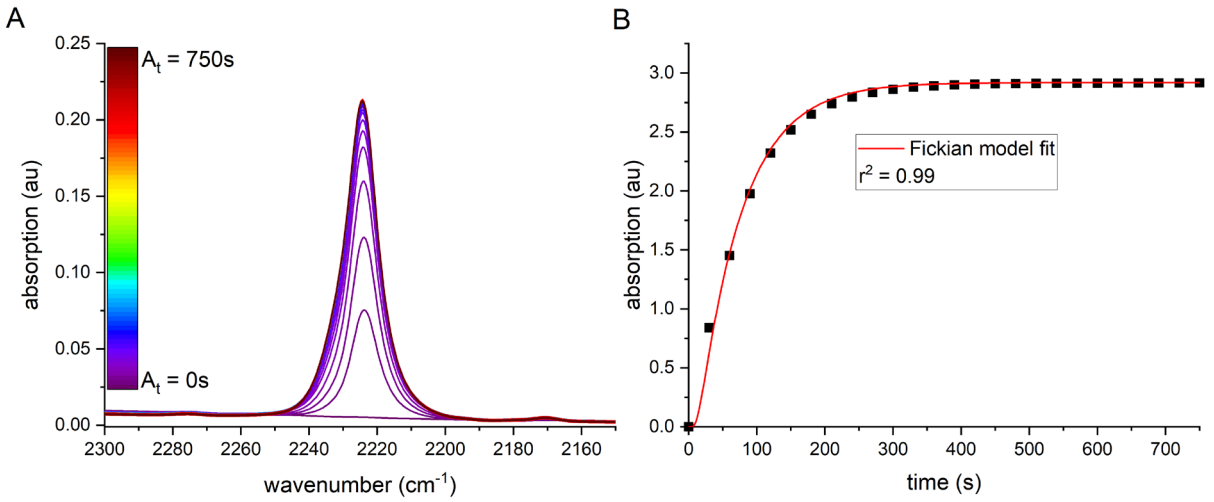

Figure 57. (A) Increasing absorption of 4-cyanophenol specific C≡N stretching vibration (~2230 cm-1) during diffusion in carnauba wax pretreated with TEHP and (B) integrated absorption versus time fitted to equation (10).

5.3.3 CNP diffusion kinetics in wax after alcohol ethoxylate treatment

Analogous to the diffusion analysis of CNP in candelilla and carnauba wax after treatment with methyl oleate or TEHP, the diffusion kinetics were determined after treatment with the monodisperse AEs C12E2, C12E4, and C12E6 (Figure 58; Figure 59).

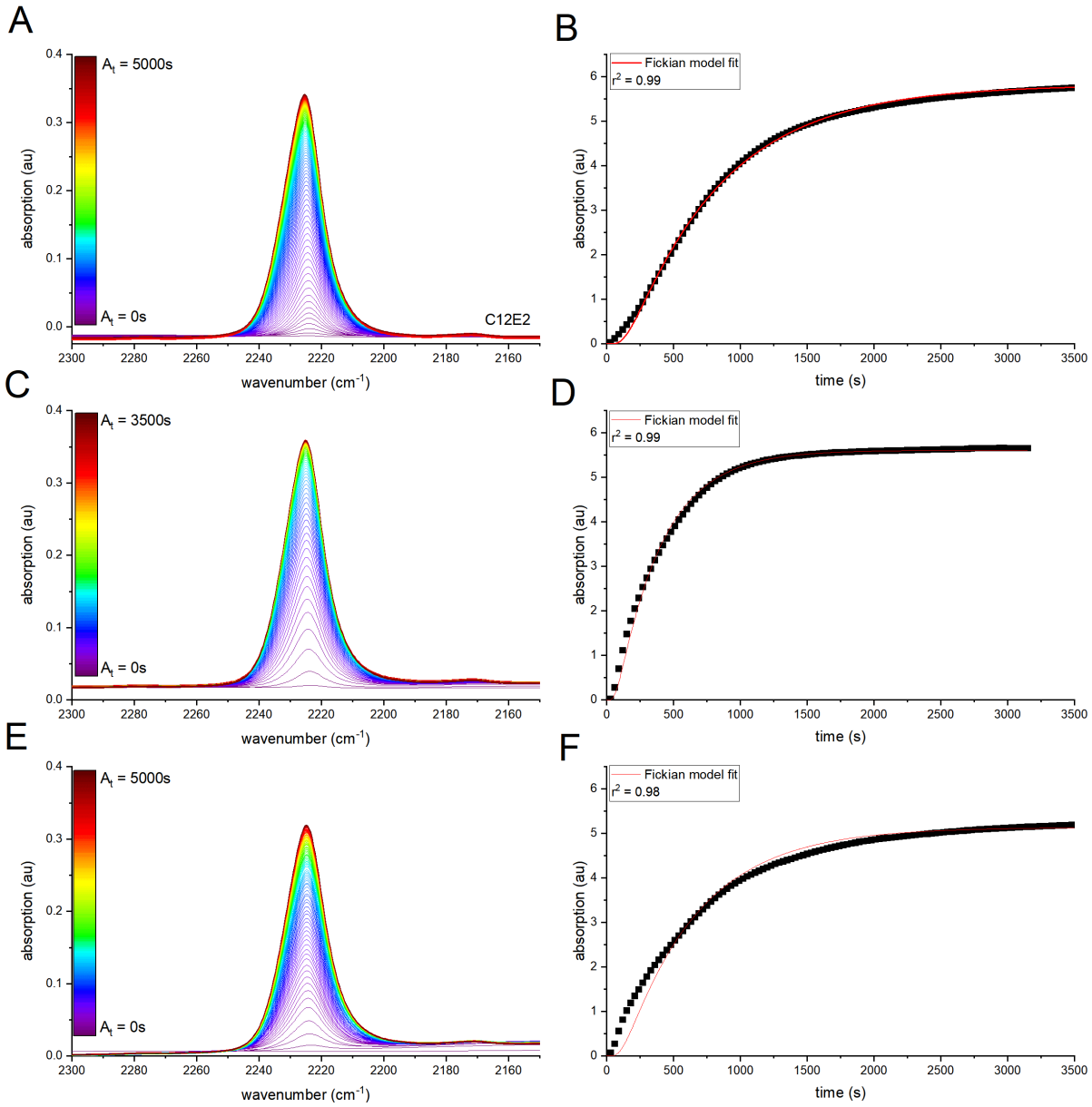

Figure 58. (A) Increasing absorption of 4-cyanophenol specific C≡N stretching vibration (~2230 cm^{-1}) during diffusion in candelilla wax pretreated with (A) C12E2, (C) C12E4 and (E) C12E6 and integrated absorptions versus experimental time scales fitted to equation (10) for (B) C12E2, (D) C12E4 and (F) C12E6.

Raising absorption of CNP specific C≡N stretching vibration was observed for all the tested AEs (Figure 58A, C, E). Respective diffusion kinetics of CNP in candelilla wax were successfully described by Fickian diffusion (Figure 58B, D, F).

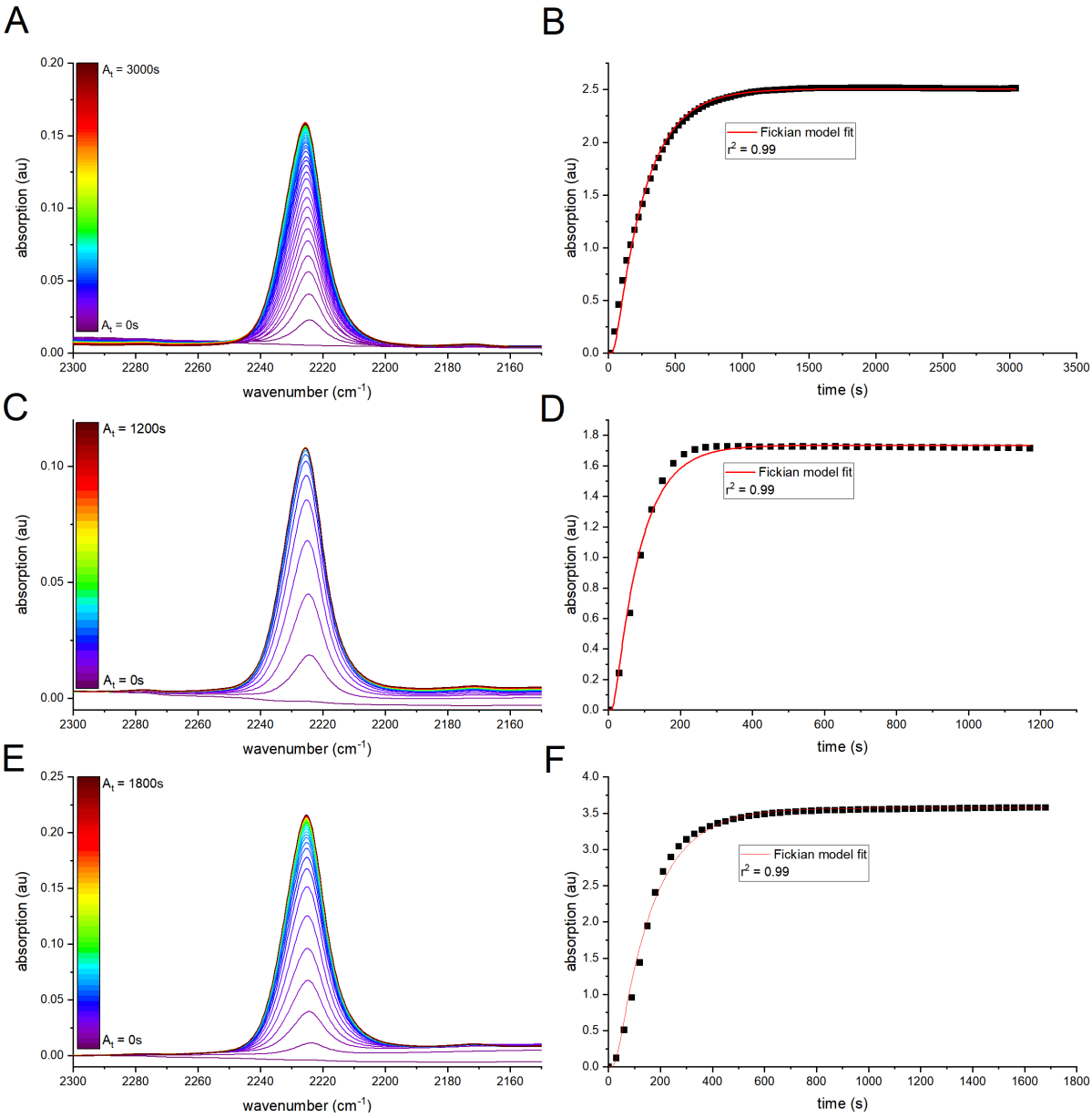

Figure 59. (A) Increasing absorption of 4-cyanophenol specific C≡N stretching vibration (~2230 cm-1) during diffusion in carnauba wax pretreated with (A) C12E2, (C) C12E4 and (E) C12E6 and integrated absorptions versus experimental time scales fitted to equation (10) for (B) C12E2, (D) C12E4 and (F) C12E6.

As for diffusion in candelilla wax, increasing absorptions of CNP specific C≡N stretching vibration were observed for the tested AEs in carnauba wax (Figure 59A, C, E). Integrating absorptions revealed Fickian diffusion in each case (Figure 59B, D, F).

5.3.4 Comparison of CNP diffusion coefficients after adjuvant treatment

In section 5.3.1 to 5.3.3, Fickian diffusion kinetics of CNP after adjuvant treatment of candelilla and carnauba wax layers were demonstrated. Accordingly, a comparative analysis of the determined diffusion coefficients from respective model fits is presented (Figure 60).

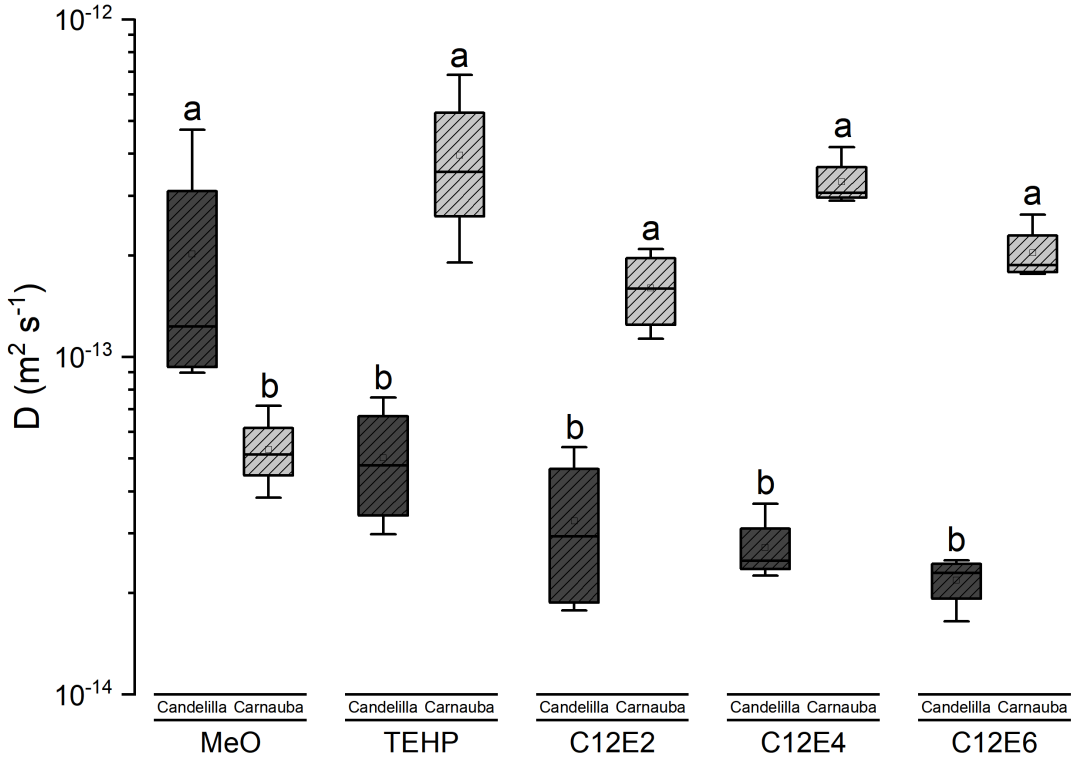

Figure 60. Logarithmic scale of CNP diffusion coefficients (*D*) after adjuvant treatment in candelilla and carnauba wax. Boxes represent 25th and 75th percentile, squares represent means, horizontal lines represent the medians. Whiskers represent 10th and 90th percentile. Letters indicate significant differences (2-way-ANOVA test with Tukeys post-hoc test, $p < 0.05$, n= 4).

All CNP diffusion coefficients ranged between 10^{-14} to 10^{-13} m^2 s^{-1}, irrespective to the applied adjuvants in both investigated waxes. However, significant differences of CNP diffusion coefficients in either candelilla or carnauba wax were observed after respective adjuvant treatments. CNP diffusion coefficients were significantly higher in candelilla wax than in carnauba wax after methyl oleate treatment. In contrast, concerning TEHP and the investigated surfactants, inversed phenomena were observed for CNP diffusion coefficients, all being higher in carnauba wax than in candelilla wax. No significant differences were found

comparing CNP diffusion coefficients after TEHP, C12E2, C12E4 and C12E6 treatment either in candelilla or carnauba wax.

5.3.5 CNP concentration and partitioning in waxes after adjuvant treatment.

According to Lambert-Beer, integrated absorptions measured by ATR-FTIR linearly correlate with respective molecular concentrations within the evanescent wave. Accordingly, equilibrium absorptions (A_{eq}) of CNP in candelilla and carnauba wax resulting from diffusion experiments were translated to equilibrium concentrations (C_{eq}). To infer the respective CNP concentration in the wax from the absorption, defined CNP solutions were prepared in chloroform and their respective absorptions of the C≡N stretching vibration were determined by ATR-FTIR (Figure 61A).

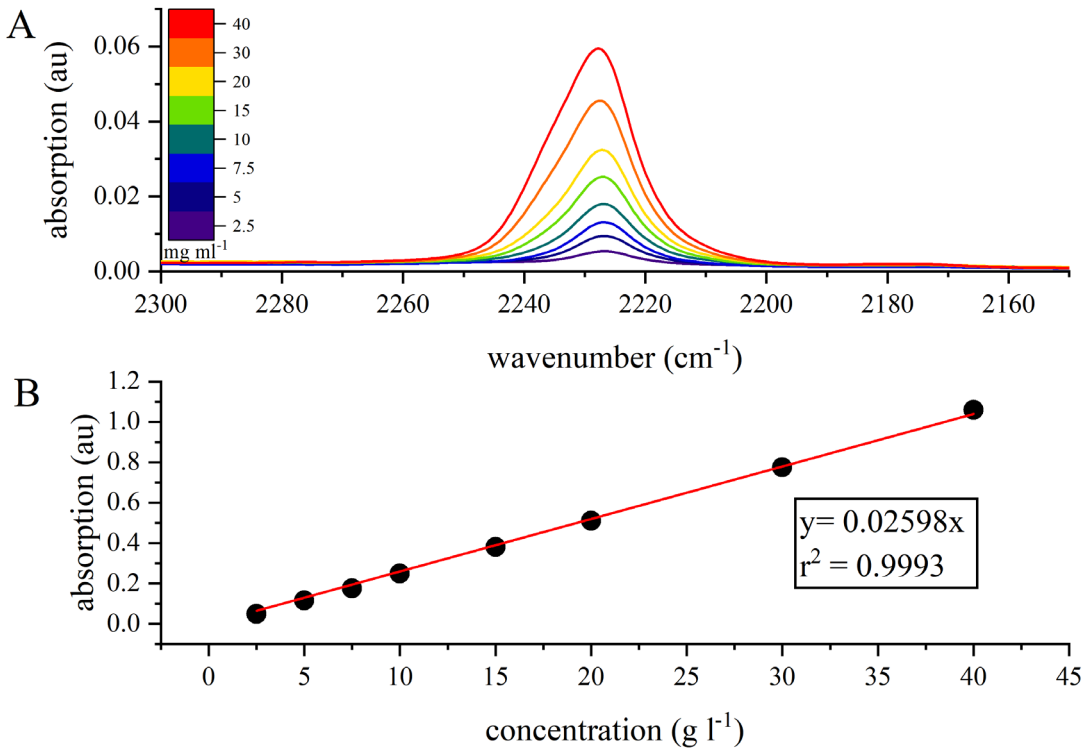

Figure 61. (A) Absorption bands of C≡N stretching vibration corresponding to CNP in chloroform solution, recorded via ATR-FTIR. (B) External calibration of integrated absorption vs. CNP concentration.

External calibration of integrated IR-absorptions vs. respective concentrations was performed (Figure 61B). Linear regression analysis relating integrated CNP specific absorption to respective concentrations gave excellent correlations (r^2 = 0.9993). Using the slope of the regression line, the equilibrium absorptions (A_{eq}) from diffusion experiments were translated

to equilibrium concentrations (C_{eq}) (Appendix 9) and according to equation (5), wax-water partition coefficients were calculated from the quotient of the CNP C_{eq} in the wax and the initial CNP concentration of the donor solution (assumed to be constant). Therefore, besides diffusion coefficients (5.3.4), wax-water partition coefficients (K_{ww}) were calculated as well (Figure 62).

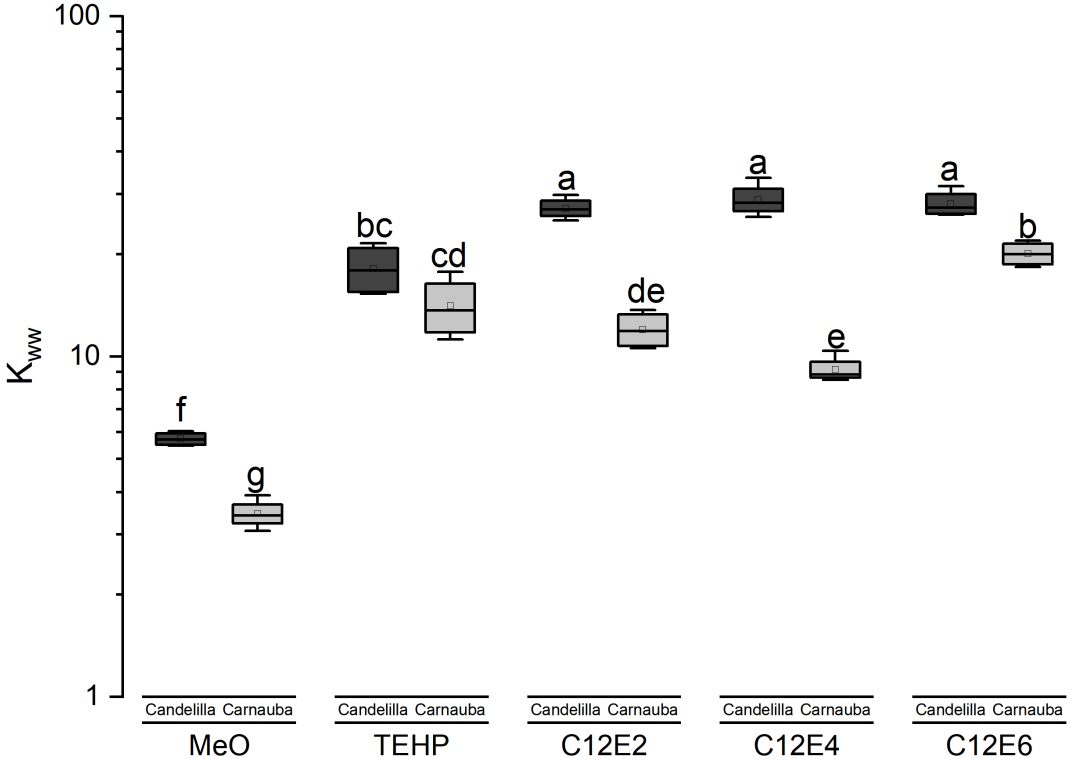

Figure 62. Logarithmic scale of wax-water partition coefficients *(K_{ww})* of CNP after adjuvant treatment in candelilla and carnauba wax. Boxes represent 25th and 75th percentile, squares represent means, horizontal lines represent the medians Whiskers represent 10th and 90th percentile. Letters indicate significant differences (2-way-ANOVA test with Tukeys post-hoc test, $p < 0.05$, n= 4).

2-way-ANOVA with Tukeys post-hoc test revealed significant differences between either investigated waxes or adjuvants. Hence, CNP partition coefficients were significantly higher in candelilla wax than in carnauba wax except after TEHP treatment, where only a non-significant trend for higher K_{ww} in candelilla wax was observed. However, K_{ww} were significantly lower in methyl oleate treated waxes than in TEHP or surfactant treated waxes. The highest discrepancies were found within the group of AEs, and especially for CNP K_{ww} after C12E2 and C12E4 treatment. However, the wax/water partition coefficients were highest in candelilla wax after surfactant treatment, suggesting a huge impact on solubility.

According to equation (4), the product of diffusion coefficient and partition coefficient relates the permeability coefficient *p*, acting as a material-specific property and therefore relating both mobility and solubility of a model compound within cuticular model waxes. Permeability coefficients of CNP were determined after adjuvant treatment (Figure 63).

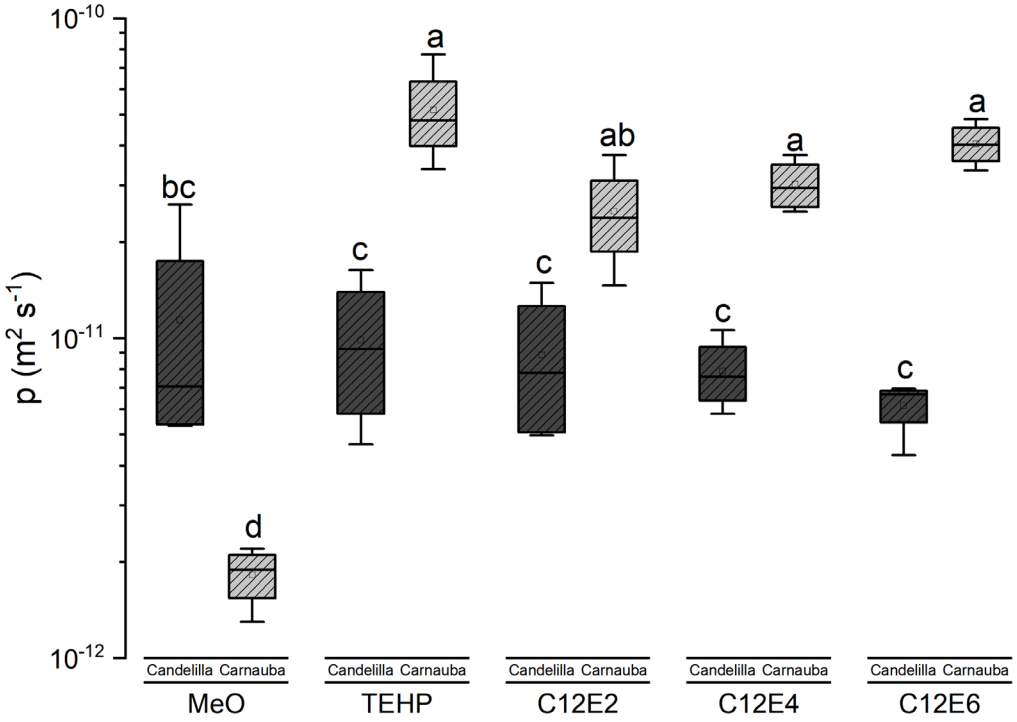

Figure 63. Logarithmic scale of permeability coefficients (*p*) of CNP after adjuvant treatment. Boxes represent 25th and 75th percentile, squares represent means, horizontal lines represent the medians Whiskers represent 10th and 90th percentile. Letters indicate significant differences (2-way-ANOVA test with Tukeys post-hoc test, $p < 0.05$, n= 4).

Significant differences between the permeability coefficients of CNP in dependance of adjuvant treatment were only found in carnauba wax, but not in candelilla wax. After methyl oleate treatment, *p* was higher for candelilla wax than for carnauba wax. This finding was not surprising, since both diffusion coefficients and partition coefficients were higher in candelilla wax. Moreover, after methyl oleate treatment in carnauba wax, permeability was significantly lowest observed in this study. The CNP permeation coefficients after TEHP treatment were higher in carnauba wax than in candelilla wax. However, since only the diffusion coefficient (Figure 60) but not the partition coefficient (Figure 62) was significantly higher in carnauba wax, the mobility dependence of CNP permeation became apparent.

After AE treatment, all CNP permeability coefficients were higher in carnauba wax than in candelilla wax. Even though partition coefficients were always significantly higher in candelilla

wax (Figure 62), rate-determining parameters were the significantly higher diffusion coefficients in carnauba wax (Figure 60).

5.3.6 Water diffusion kinetics in candelilla and carnauba wax after adjuvant treatment

Water diffusion kinetics were separately recorded in candelilla and carnauba wax after treatment with methyl oleate, TEHP, C12E2, C12E4 or C12E6. To distinguish between potentially absorbed atmospheric water (H_2O) and applied liquid water, D_2O was used as diffusant, representing comparable physical properties, but offering discriminable IR-spectra which are consistently shifted towards lower wavenumbers (Figure 64).

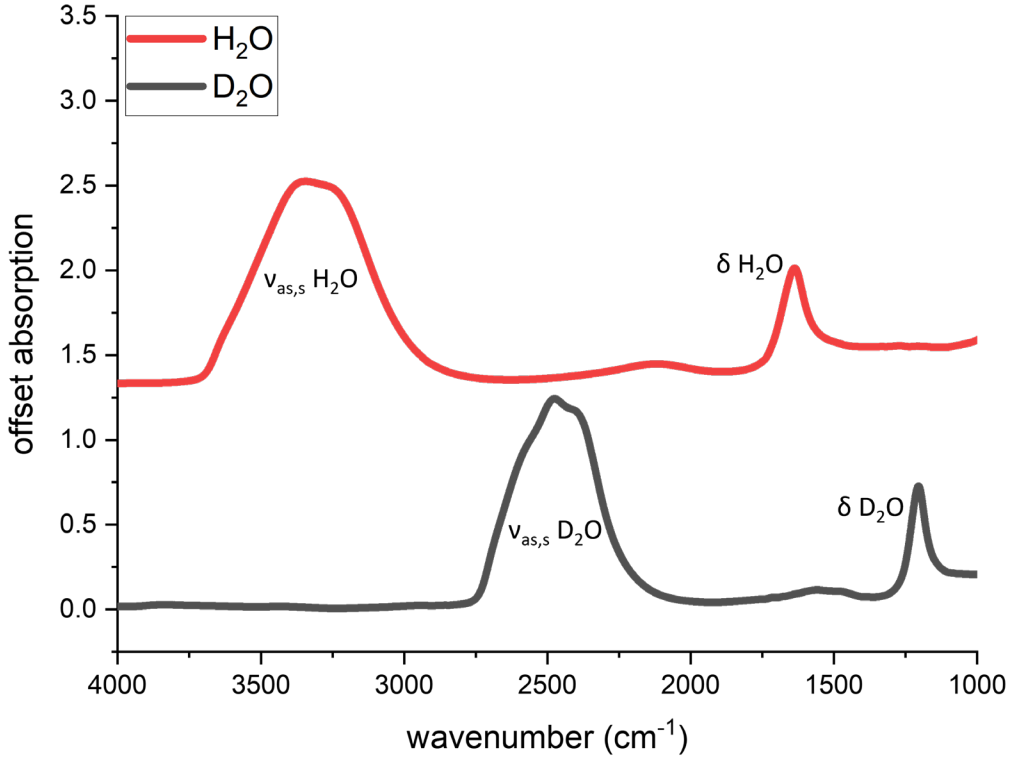

Figure 64. IR-absorption spectra of H_2O and D_2O. Asymmetrical and symmetrical stretching ($\nu_{as,\ s}$) and bending vibrations (δ) of D_2O are shifted to lower wavenumbers compared to the corresponding vibrations of H_2O.

The fused symmetrical and asymmetrical D_2O stretching vibration bands (at approximately 2500 cm^{-1}) instead of respective H_2O stretching vibration bands (at approximately 3400 cm^{-1}) were used to determine water diffusion kinetics. Hence, integrating the absorption bands of D_2O stretching vibrations in candelilla and carnauba wax over time reflected water diffusion kinetics (Figure 65).

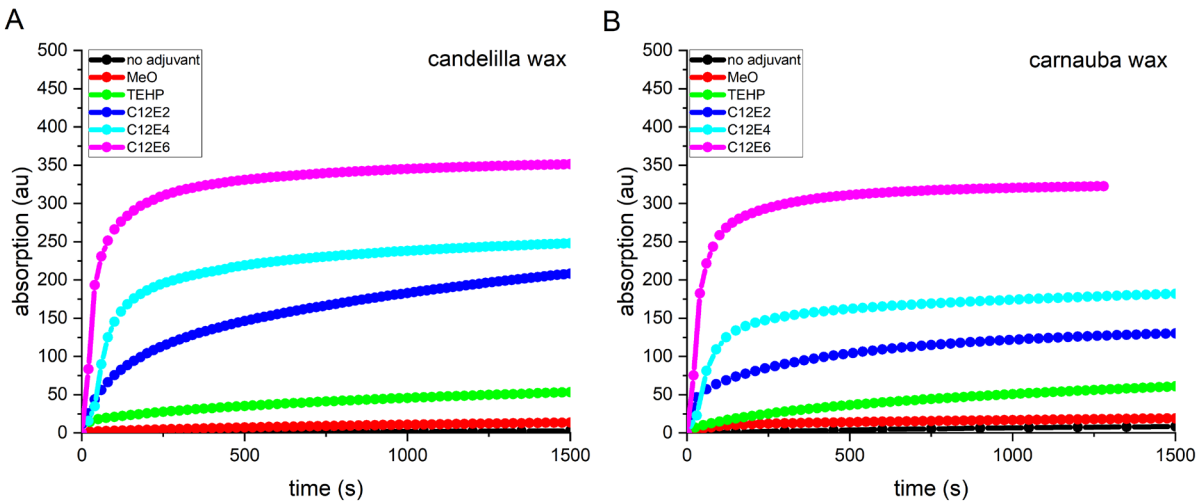

Figure 65. D_2O diffusion kinetics in adjuvant treated (A) candelilla and (B) carnauba wax, indicated by integrated D_2O stretching vibration bands over time, recorded via ATR.

D_2O showed slow diffusion kinetics and low absorptions of 2.7 au in candelilla wax and 8.4 au in carnauba wax over a time range up to 1500s. Hence, water solubility was approximately three times higher in carnauba wax. After methyl oleate treatment, water diffusion kinetics were slightly enhanced, reaching 13.5 and 19.0 au after 1500 s, respectively. TEHP application increased D_2O diffusion in candelilla and carnauba wax, reaching 53.2 au and 60.8 au after 1500s. Within the group of AEs, absorption plateaus were reached fastest after C12E6 treatment and slowest with C12E2 treatment both in candelilla and carnauba wax. Final absorption levels were highest after AE treatment. Effects relating absolute water specific IR-absorption with and without prior adjuvant treatment are given in Table 4.

Table 4. Integrated water specific IR-absorption of D_2O stretching vibrations at 1500s of diffusion and adjuvant effect.

adjuvant	absorption at 1500 s		effect[a]	
	candelilla	carnauba	candelilla	carnauba
none	2.71	8.42	n.d.	n.d.
methyl oleate	13.50	19.00	5	2.3
TEHP	53.20	60.80	19.7	7.2
C12E2	208.21	130.20	77.1	15.5
C12E4	247.80	181.88	91.8	21.7
C12E6	351.28	322.36	130.1	38.4

[a]Data is given as quotient of absorption at 1500s after adjuvant treatment and with no adjuvant treatment

C12E6 revealed highest effect on water solubility both in candelilla and carnauba wax followed in the order: C12E4 > C12E2 > TEHP > MeO. Due to initially lower water absorption in candelilla wax, effects were overall higher in candelilla than in carnauba wax. Water diffusion kinetics did not match the Fickian diffusion model. Hence, water diffusion kinetics after AE treatment were investigated by fitting to the logistic model, elucidating time points of half-maximal absorptions (x0), regardless to absolute absorptions (Figure 66).

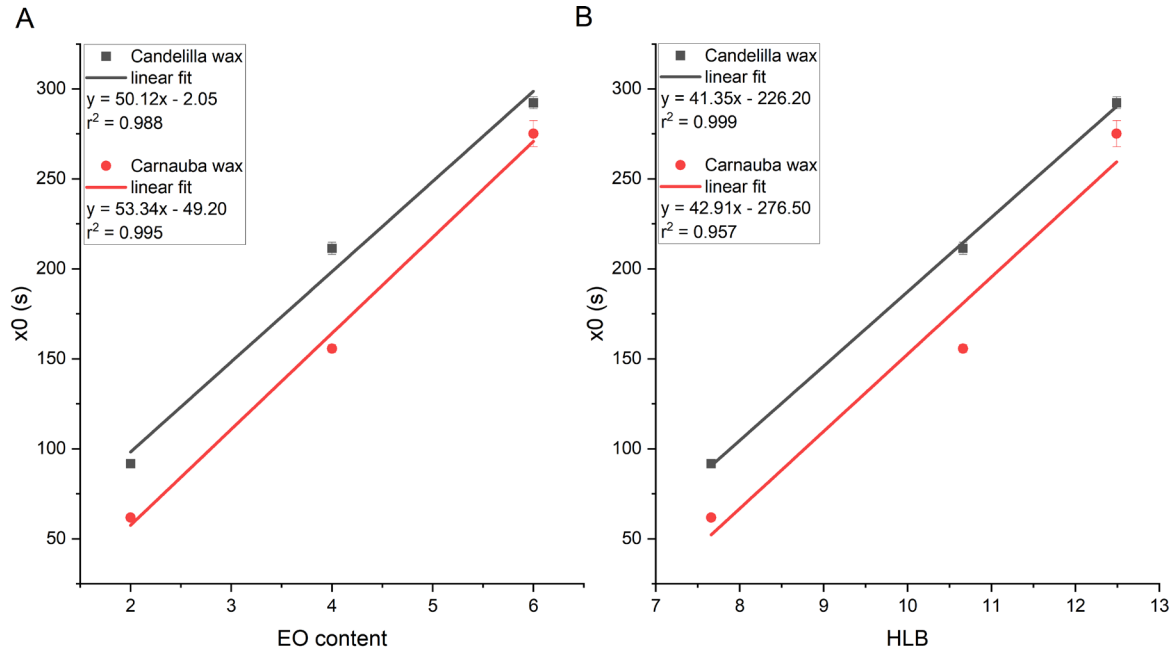

Figure 66. Half-maximal absorptions of water specific D_2O stretching vibrations after C12E2, C12E4 and C12E6 treatment (x0) according to a logistic model plotted versus (A) EO content or (B) AE HLB and linear fits. Error bars represent standard errors of logistic fits to the recorded diffusion kinetics.

Half-maximal absorptions linearly correlated with the number of EO units and respective HLB values. Slopes of regression lines derived from linear fits of half-maximal D_2O absorptions in candelilla wax and carnauba wax were parallel aligned. However, the intercepts differed with respect to the investigated waxes. Hence, the slope of the regression line defined a constant, describing AE ability to enhance water sorption as a function of the degree of ethoxylation or the HLB values, respectively, whereas the intercepts were assigned to wax specific properties.

5.4 Discussion

The aim of this study was to investigate the diffusion kinetics of the AI model CNP and water in candelilla wax and carnauba wax, representing VLCA-dominated cuticular model waxes well after the equilibrium accelerator adjuvant concentration was reached (Chapter 2). Before CNP

application, spin-coated wax layers were treated with pure adjuvants instead of using low-concentrated aqueous formulations. Thus, an "evaporative" system was established mimicking the field situation after fine spray droplets dried on the leaf surface (Ramsey *et al.*, 2005). In the field, the adjuvant uptake into the plant occurs from highly concentrated formulation residues (Schreiber, 1995; Schreiber *et al.*, 1996b), whereby desorption from isolated cuticles into the underlaying plant issue was previously shown to be negligible for lipophilic accelerators (Santier and Chamel, 1996). However, due to the experimental setup, the relative humidity present in the laboratory could not be eliminated, which led to atmospheric water taken up into the waxes by the application of, among others, hygroscopic adjuvants (Ramsey *et al.*, 2005). Although water diffusion analysis in parallel with CNP diffusion analysis would have been possible within a single ATR-FTIR experiment *per se*, diffusion kinetics possibly distorted by atmospheric water uptake were not considered during CNP uptake and instead separate diffusion measurements of liquid water were performed with D_2O instead of H_2O, thus exhibiting distinguishable IR spectra (Figure 64).

The effective modification of the penetration-limiting wax barrier is crucial to accomplish sufficient AI uptake under ecological and economical constraints (Green, 2000). This modification is mostly depicted as softening or plasticization (Schönherr and Baur, 1994). Accelerator adjuvants mixed with the AI are used in pesticide formulations, which penetrate the cuticular waxes and lead to a modification of the wax structure and, consequently, to an improved uptake of the AI into the plant (Penner, 2000). In Chapter 2, accelerator diffusion accommodated with wax plasticization events, indicated by decreasing orthorhombic crystallinity and wax molecule density were observed for methyl oleate, TEHP, and the surfactants C12E2, C12E4 and C12E6. Hence, within this study, striking differences in adjuvant affected CNP mobilities were assumed both in candelilla and carnauba wax.

It is well known that the AI uptake stops after the evaporation of water and a short evaporation time may be undesirable (Ramsey *et al.*, 2005; Wang and Liu, 2007). As described in the literature, some adjuvants, especially surfactants, exhibit humectant properties facilitating the uptake of hydrophilic AIs and water (Stock and Holloway, 1993). Hence, AI penetration is improved at high humidity as a result of both increased cuticle hydration state (Stock *et al.*, 1992; Kirkwood, 1999) and delayed droplet drying (Holly, 1953; Prasad *et al.*, 1967; Cook *et al.*, 1977; Ramsey *et al.*, 2005). As a result, adjuvants may prevent the AI from crystallization, keeping it in a state available to the plant (Hess *et al.*, 1981; Macisaac *et al.*,

1991; Baur *et al.*, 1997b; Asmus *et al.*, 2016). Furthermore, when an AI is taken up from a spray droplet, it is very likely that water enters the plant through the cuticle not only via the hydrophilic pathway but also via the lipophilic pathway studied here (Schreiber, 2005; Schönherr, 2006). However, the direct effect of co-penetrating water on the sorption kinetics of an organic AI as affected by the presence of accelerators has not been reported to date. To investigate the effect of co-penetrating water on the CNP uptake, CNP was applied to the adjuvant-treated wax layers dissolved in water rather than as a solid, and the applied solution was continuously fluctuated using a flow-through system to eliminate local concentration differences. This imitated a non-evaporating system during CNP diffusion as it is found under high humidity conditions in the field.

5.4.1 Methyl oleate effect on CNP and water uptake

CNP diffusion kinetics in methyl oleate treated wax layers were shown to perfectly follow the Fickian model, thus indicating the diffusion process solely being driven by a concentration gradient (Figure 54; Figure 55). The diffusion coefficients were orders of magnitude higher than those observed for CNP in unplasticized paraffin wax (chapter one) and for organic compounds of similar size and lipophilicity in reconstituted cuticular waxes (Schreiber, 2006). This is in accordance with previous results showing methyl oleate and other oil derivatives drastically enhancing the uptake of lipophilic AIs in isolated cuticles contributing barrier-forming cuticular waxes (Riederer and Schönherr, 1985; Gauvrit and Cabanne, 1993; Santier and Chamel, 1996; Nalewaja, 2002). The CNP diffusion coefficients recorded after methyl oleate treatment were found to strongly depend on the preceding decrease of orthorhombic crystallinity and were therefore higher in candelilla wax (1.22×10^{-13} m^2 s^{-1}) than in carnauba wax (5.13×10^{-14} m^2 s^{-1}) (Figure 60; Appendix 8). The results shown here suggest that the assumed alkyl ester bridges between crystallites are only marginally reduced by methyl oleate in carnauba wax, resulting in lower CNP mobility than in the alkyl ester-less candelilla wax.
Šimáňová *et al.* (2005) previously showed the AI mobility linearly correlates with the internal n-alkyl ester adjuvant concentration (Šimáňová *et al.*, 2005). In this study, a correlation of methyl oleate concentration in both investigated waxes and respective CNP diffusion coefficients confirmed this hypothesis as the methyl oleate equilibrium concentration in candelilla and carnauba wax differed by a similar factor (= 3.3, compare Figure 25B and Figure 26B) as the diffusion coefficients of CNP (= 2.4, compare Appendix 9).

It was also found that CNP partition coefficients were higher in candelilla wax (5.71) than in carnauba wax (3.42) (Figure 62), suggesting higher solubility in the former. Since both mobility and solubility were higher in candelilla wax, significantly higher permeability coefficients in candelilla wax (7.06 x 10^{-13} m^2 s^{-1}) than in carnauba wax (1.89 x 10^{-13} m^2 s^{-1}) (Figure 63) were apparent.

A model was established, specifically addressing the assumed plasticization affecting CNP permeability (Figure 67).

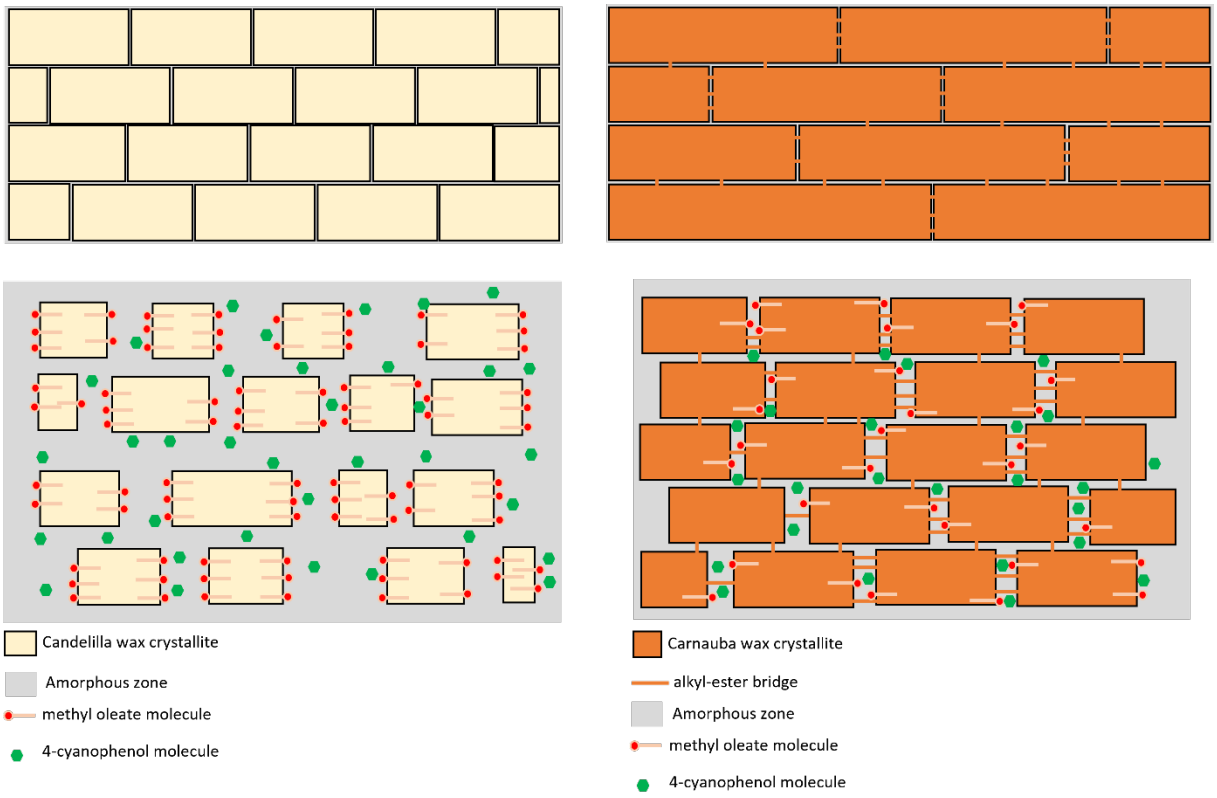

Figure 67. Illustration of candelilla and carnauba wax structure (top) according to (Riederer and Schreiber, 1995). Candelilla wax crystallites are shorter than those in carnauba wax, resulting from different average chain lengths and c-axis of the VLCAs (alkane-dominates vs. alkyl ester dominated) (Dorset, 1995). Carnauba wax crystallites are connected via intermolecularly aligned alkyl-ester bridges (Reynhardt, 1997; Bueno *et al.*, 2019). Methyl oleate penetration induces decreasing molecular density and decreasing orthorhombic crystallinity in candelilla wax and methyl oleate molecules are incorporated in crystalline zone A with methyl ester groups protruding into amorphous zone B and D (bottom left). Mobility and solubility of penetrating CNP are drastically enhanced. Methyl oleate penetration in carnauba wax is restricted due to interlamellar bridged crystallites. The ability of methyl oleate to penetrate carnauba wax is restricted due to interlamellar bridged crystallites and thus, methyl oleate is not capable of entirely disentangling alkyl ester bridges (bottom right). Consequently, CNP mobility and solubility are less enhanced in carnauba than in candelilla wax.

During penetration, methyl oleate polyethylene chains may be incorporated within crystalline zone A, their methyl ester groups protruding into amorphous zones B and D. It may be assumed that due to the double-bond in methyl oleate, motional freedom is restricted and as a result, incorporating methyl oleate in crystalline zone A leads to imperfectly lamellar orientated crystallite conformations. Hence, increasing the wax specific crystallite surface defect distribution consequently enhances CNP mobility. Analogous to the assumption of methyl oleate molecules being integrated into the semicrystalline wax structure, a previous study by Zhang *et al.* (2016) showed similar behavior for AEs, whose hydrocarbon chains may potentially be integrated within the crystalline zone, whereas ethoxylate units protrude into the amorphous zone (Zhang *et al.*, 2016).

In contrast to the methyl ester function of methyl oleate located within the amorphous zone, the more polar ethoxylate units of AEs were shown to possess humectant properties (Ramsey *et al.*, 2005). Thus, they may increase the wax hydration state by facilitating water uptake. Moreover, one study previously reported surfactant/water uptake leading to an overall more fluidic and softer cuticular wax (Fagerström *et al.*, 2014). Within this study, however, methyl oleate was shown to not significantly enhance water uptake (Figure 65). This is striking, since previously reported results showed significantly increased transpiration rates across isolated cuticles of *Prunus laurocerasus* and *Garcinia xanthochymus* (Staiger, 2022). The significant effect could have been due to the plasticization of the amorphous cutin matrix, whereas the waxes used here, despite their reduced orthorhombic crystallinity, did not exhibit increased capacity for hydrophilic water molecules after methyl oleate treatment. Accordingly, the herein observed lacking ability of methyl oleate to enhance water uptake in wax does refute the creation of a more fluidic environment for CNP diffusion, as it was observed after AE treatment (Figure 62), thoroughly explaining the strikingly lower CNP solubility.

In conclusion, methyl oleate is indeed suitable for accelerating the uptake of lipophilic AIs into cuticular waxes, but with the limitation that this mainly applies to plants with cuticular waxes contributing low or no alkyl ester moieties. Only the insignificant increase in water diffusion argues for the general use of methyl oleate since increasing the transpiration rate reflects an undesirable side effect (Räsch *et al.*, 2018). Maintaining the native transpiration rate is of utmost importance, especially when using adjuvants in arid regions, otherwise the vitality of the plant to be protected will be negatively affected.

5.4.2 TEHP effect on CNP and water uptake

CNP diffusion kinetics were recorded after TEHP treatment, using ATR-FTIR. Meaningful diffusion coefficients were calculated from the Fickian diffusion kinetics again suggesting diffusional resistance was largely reduced by prior plasticization (Figure 56; Figure 57). As was observed for CNP diffusion after methyl oleate treatment, diffusion coefficients also differed about one order of magnitude in candelilla (5.14×10^{-14} m^2 s^{-1}) and carnauba wax (35.31×10^{-14} m^2 s^{-1}[j]), respectively (Figure 60, Appendix 8). In contrast to the observation of CNP diffusion after methyl oleate treatment, the diffusion coefficients were higher in carnauba wax than in candelilla wax after TEHP treatment. This was surprising since final TEHP concentrations were shown to be higher in candelilla wax than in carnauba wax (Figure 29; Figure 30). Hence, a direct correlation of internal TEHP concentration on respective CNP mobilities (Figure 60; Appendix 8) as was found for internal methyl oleate (5.4.1) and alkyl-ester concentration (accelerator) (Šimáňová *et al.*, 2005) was rejected considering the two chemically distinct waxes.

CNP partition coefficients were slightly higher in candelilla wax (17.88) than in carnauba wax (13.66) but showing no significant difference (Figure 62; Appendix 9). This was not surprising since TEHP induced plasticization was more intense in candelilla wax than in carnauba wax leading to higher sorption capacity within the amorphous phase (chapter 2; Figure 31; Figure 32). However, in contrast to methyl oleate treatment (5.4.1), CNP partition coefficients were drastically higher in candelilla and carnauba wax after TEHP treatment (Figure 62). As was mentioned before, absolute adjuvant concentrations in the wax could not be determined via ATR-FTIR. It remained an open question whether a higher TEHP concentration compared with the methyl oleate concentration was responsible for the increased CNP solubility. To explain the higher CNP solubility from a chemical and structural perspective, the following model was designed (Figure 68).

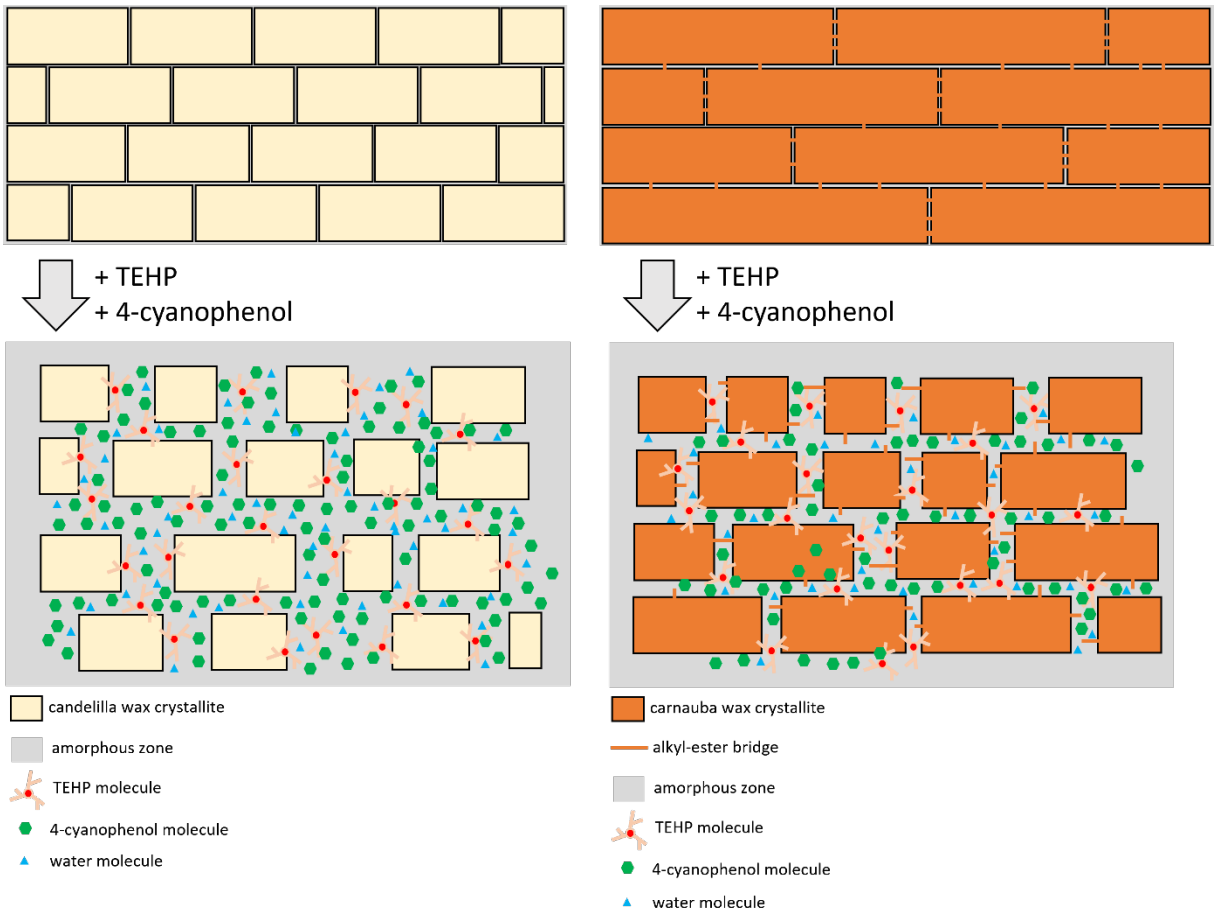

Figure 68. Illustration of candelilla and carnauba wax structure (top) according to (Riederer and Schreiber, 1995). Candelilla wax crystallites are shorter than those in carnauba wax, resulting from different average chain length and c-axis of the VLCAs (alkane-dominates vs. alkyl ester dominated) (Dorset, 1995). Carnauba wax crystallites are connected via intermolecularly aligned alkyl-ester bridges (Reynhardt, 1997; Bueno *et al.*, 2019). TEHP penetration induces decreasing molecular density and decreasing orthorhombic crystallinity in candelilla wax (bottom left) and due to the central intramolecular charge, TEHP molecules are rather incorporated in polar amorphous zones B and D. The ethylene groups of TEHP exhibit high mobility due to the single bond connecting them to the central oxygen atoms and, therefore, are probably rarely integrated into the rigid crystalline zone A. Incorporating TEHP molecules within the amorphous zone leads to rather pushing apart the crystallites interconnected by alkyl esters, thereby disentangling alkyl esters from their anchors in carnauba wax (bottom right). Furthermore, TEHP enhancing water uptake consequently leads to rising osmotic pressure inevitably causing crystallite shifting thereby increasing the amorphous zone, which is referred to as “secondary platicization”. Hence, (1) TEHP induced plasticization in combination with (2) increased water uptake may lead to high mobility and solubility of penetrating CNP in both waxes.

First, as already described in chapter 2, it is assumed that the polar phosphate group of TEHP is situated within the amorphous zones B and D. Due to the isometric conformation of the attached hydrocarbon chains, minor integration of these into crystalline zone A is presumable (Riederer and Schreiber, 1995). As a result, adjacent crystallites are pushed apart due to

increasing TEHP content within the amorphous phase, inevitably leading to higher CNP solubility within the increasing amorphous phase in candelilla wax.

The presumed ability of TEHP disentangling alkyl ester bridges connecting two or more adjacent crystallites leads to higher CNP solubility compared to carnauba wax after methyl oleate treatment not being able to break intercrystallite connections.

Second, although TEHP is a very lipophilic molecule (logP = 8.9), it was demonstrated here that water uptake into the wax was dramatically increased after TEHP treatment (Figure 65). To explain this phenomenon, the situation must be analyzed on a molecular level (Figure 69).

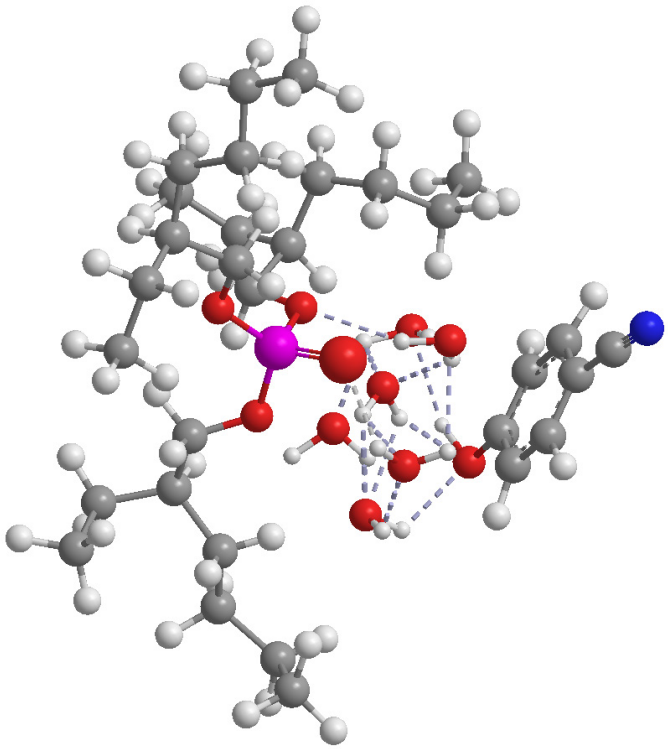

Figure 69. Illustration of a TEHP molecule and a CNP molecule, both being h-bonded to surrounding water molecules, which are connected among themselves. Due to single bonds of TEHP between oxygen atoms (red) and carbon atoms (grey), metastable TEHP conformers may build pockets with water situated inside, thus inevitable forming hydrogen-bonds between phosphate-specific oxygen atoms and water specific hydrogen atoms (white). Due to CNP conformational state, para-situated OH-group is located towards surrounding water molecules inevitable forming hydrogen-bonds. Purple balls represent phosphorus atoms, while blue balls represent nitrogen atoms. Dashed lines represent hydrogen bonds. Model was calculated with Chem3d 20.1 software using MM2-minimization and dynamics analysis (Ponder and Richards, 1987).

By means of modeling, it could be seen that TEHP may be capable of forming hydrogen bonds between its phosphate group contributing oxygen atoms and adjacent hydrogen atoms of water molecules. Furthermore, it was shown that the hydroxyl group of CNP also forms

intermolecular hydrogen bonds with neighboring water molecules. Consequently, the uptake of TEHP into the wax leads to an increased water uptake, which on the one hand causes an increased internal pressure in the wax, i.e. leads to a break-up of the intermolecular structures, and at the same time facilitates increasing CNP uptake.

Prima facie, it is striking that the CNP permeability coefficient in carnauba wax was highest after TEHP treatment (47.93 x 10^{-13} m^2 s^{-1}) (Figure 63). At second glance, this may be explained by the strong interaction and plasticization potential of TEHP on carnauba wax, primarily leading to high CNP mobility.

In conclusion, TEHP was found to be best suited to accelerate CNP uptake in two different model waxes. The wax composition played a minor role, which was reflected by the high diffusion and partition coefficients in both candelilla and carnauba wax. The results show that TEHP not only accelerated the uptake of CNP, but also had a dramatic effect on water sorption, which in turn most likely exerted an accelerating effect on CNP by swelling the wax.

5.4.3 Monodisperse alcohol ethoxylate effect on CNP and water uptake

CNP diffusion kinetics were recorded after wax treatment with either C12E2, C12E4 or C12E6. Resulting diffusion coefficients were significantly higher in carnauba wax (C12E2 = 24.95 x 10^{-14} m^2 s^{-1}; C12E4 = 30.69 x 10^{-14} m^2 s^{-1}; C12E6 = 18.71 x 10^{-14} m^2 s^{-1}) than in candelilla wax (C12E2 = 2.94 x 10^{-14} m^2 s^{-1}; C12E4 = 2.49 x 10^{-14} m^2 s^{-1}; C12E6 = 2.29 x 10^{-14} m^2 s^{-1}) (Figure 60; Appendix 8) ranging in the same orders of magnitude as CNP diffusion coefficients after methyl oleate or TEHP treatment. However, the comparable results should not be falsely attributed to the fact that all accelerators act in the same way in the two waxes studied. An inversely related effect was found between diffusion coefficient (mobility) and partition coefficient (solubility) of CNP in candelilla and carnauba wax (Figure 60; Figure 62).

The CNP diffusion coefficients were all higher in carnauba wax, whereas the partition coefficients derived from ratios of CNP equilibrium absorptions (A_{eq}) in the wax and absorptions of CNP in aqueous donor solutions were all higher in candelilla wax. This was not surprising as candelilla wax orthorhombic crystallinity was more affected than carnauba wax orthorhombic crystallinity, providing higher sorption capacity within the amorphous phase of the former. However, assuming CNP saturation in candelilla and carnauba wax is achieved within similar time courses, but absolute solubilities (represented by final absorption A_{eq}) are higher in candelilla wax, then mobilities are inversely proportional decreased (Figure 70).

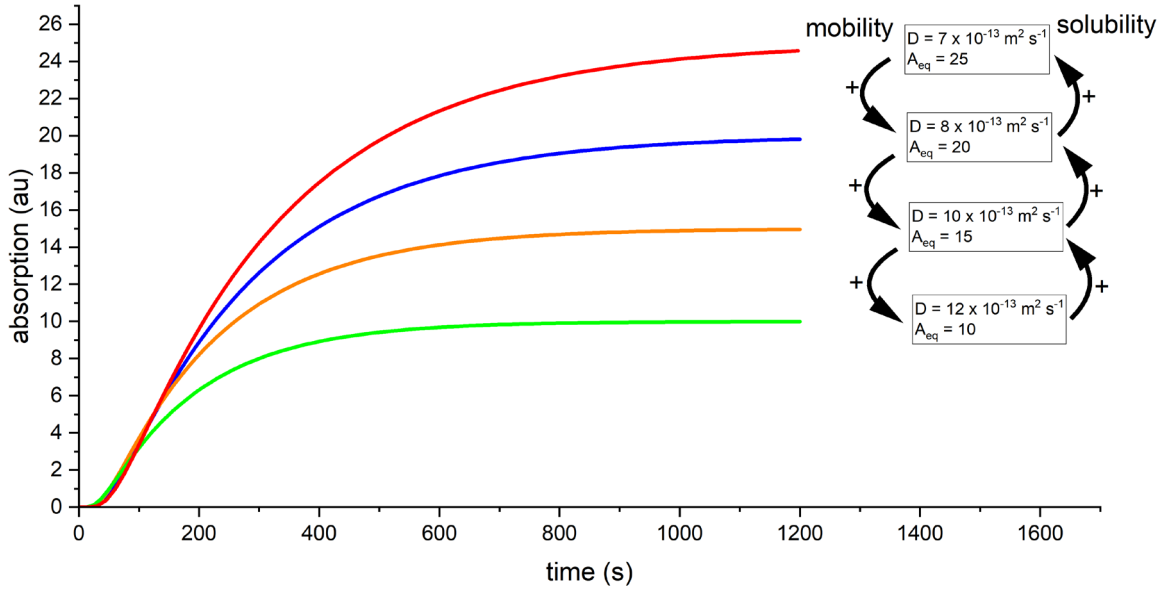

Figure 70. Simulated curves of equation (10) showing inverted proportionality of A_{eq} and D due to approximately same time course to achieve equilibrium conditions. The simulated red curve represents Fickian diffusion of an organic compound recorded via ATR-FTIR. Highest A_{eq} inevitable leads to lowest diffusion coefficient D and vice versa.

As was observed, diffusion coefficients and partition coefficients were not significantly different within the group of investigated AEs except for C12E6 (Figure 60; Figure 62). However, the overall similarity despite different ethoxylation levels of the AEs might be explained by antagonistic plasticization and water sorption effects. (1) AEs with low HLB values (C12E2 < C12E4 < C12E6) promote stronger wax plasticization (Schönherr, 1993a, b), due to their higher lipophilicity, consequently leading to enhanced uptake of lipophilic AIs such as CNP (logP = 1.6) (Stock *et al.*, 1993; Riederer *et al.*, 1995; Burghardt and Riederer, 1996; Burghardt *et al.*, 1998). (2) On the other hand, as was stated by Stevens and Bukovac (1987) and was confirmed here, water permeation linearly correlates with the ethoxylation level and with the HLB value (Stevens and Bukovac, 1987a) (Figure 66). Thus, increasing EO content (C12E2 < C12E4 < C12E6) contributes to larger water adhesion, consequently leading to swelling or breakup of the wax structure and increasing the aqueous phase within the waxes due to the increase of osmotic pressure. This in turn favors the uptake of hydrogen-bonded CNP. A model was developed to explain the observed findings (Figure 71).

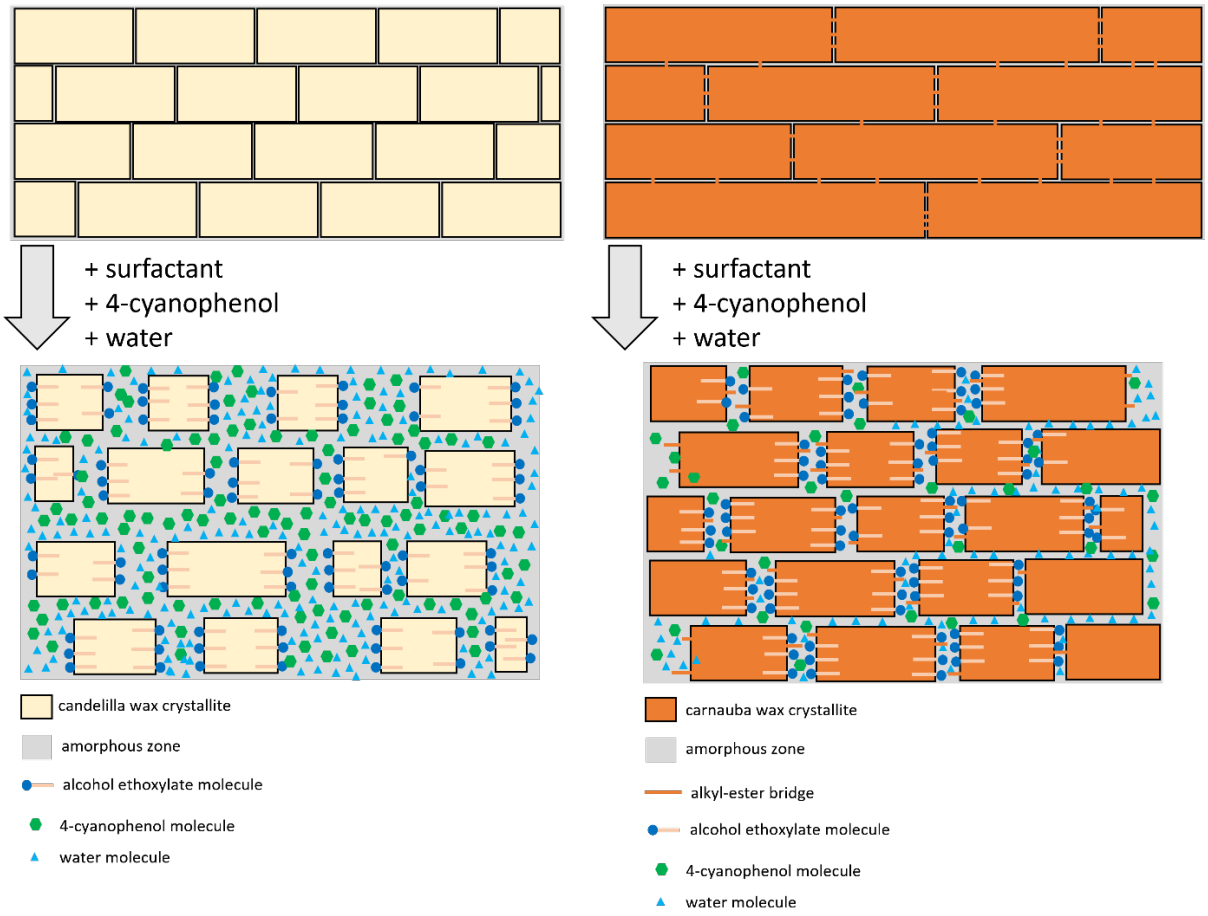

Figure 71. Illustration of candelilla and carnauba wax structure (top) according to (Riederer and Schreiber, 1995). Candelilla wax crystallites are shorter than those in carnauba wax, resulting from different average chain length and c-axis of the VLCAs (alkane-dominates vs. alkyl ester dominated) (Dorset, 1995). Carnauba wax crystallites are connected via intermolecularly aligned alkyl-ester bridges (Reynhardt, 1997; Bueno *et al.*, 2019). Hydrocarbon chains of AE molecules are incorporated in crystalline zone A, whereas polar ethoxy groups are protruding into amorphous zones B and D. AE penetration induces decreasing molecular density and decreasing orthorhombic crystallinity in candelilla wax (bottom left) leading to increased mobility and solubility of penetrating CNP. AE penetration in carnauba wax is restricted due to interlamellar bridged crystallites, but AE specific humectant properties lead to significant water ingress thus leading to swelling and disentangling of interlamellar alkyl ester bridged connecting two or more crystallites (bottom right). Water ingress in combination with setting up hydrogen bonds to CNP specific hydroxyl functional group, model AI mobility and solubility are enhanced.

From a chemical perspective, AEs are more related to methyl oleate than to TEHP, with respect to their aliphatic constitution. As many authors stated before, incorporation of the lipophilic hydrocarbon chain of AEs contributing 12 carbon atoms into the crystalline Zone A is presumable (Fagerström *et al.*, 2014; Zhang *et al.*, 2016; Pambou *et al.*, 2018).

Drastic water uptake into both investigated waxes was confirmed (Figure 65), depending on respective AE ethoxylation levels. Fagerström *et al.* (2014) suggested, surfactants may lead to

severe water absorption into boundaries of wax crystallites. Permeating water molecules may thereby enter the crevices (or grain borders) between individual crystallites, separating them and leading to a continuous less ordered wax/water/surfactant network (Fagerström *et al.*, 2014). Hence, it is assumed that water uptake causes "secondary plasticization" by wax swelling and with respect to carnauba wax, by disentangling of alkyl esters from their anchors located in adjacent crystallites. Considering the formation of hydrogen bonds between water molecules and between AEs and water molecules and CNP (Figure 72) (Kido Soule *et al.*, 2006), it is obvious that surfactant induced water ingress inevitably leads to drastically increasing CNP solubilities (Figure 62) within the amorphous phase, consequently leading to higher partition coefficients after AE treatment than after methyl oleate or TEHP treatment.

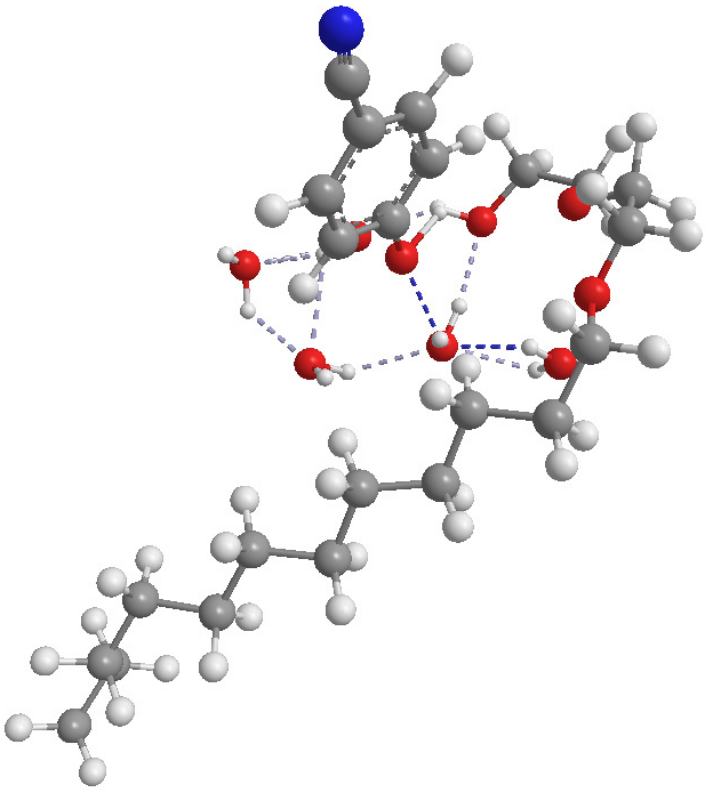

Figure 72. Illustration of an exemplary C12E2 molecule and a CNP molecule both being connected to water molecules via intermolecular hydrogen bindings. Oxygen atoms (red) of hydrophilic ethoxylate functions of C12E2 form hydrogen bonds with hydrogen atoms (white) of water molecules. Due to the CNP conformation, para-situated OH-group is located towards surrounding water molecules inevitable forming hydrogen-bonds. Grey atoms represent carbons atoms and blue balls represent nitrogen atoms. Dashed lines represent hydrogen bonds. Model was calculated with Chem3d 20.1 software using MM2-minimization and dynamics analysis (Ponder and Richards, 1987).

The permeability coefficients of CNP were all higher in carnauba wax than in candelilla wax, and due to overall higher diffusion coefficients, mobility-driven permeation is suggested.

It can be concluded that mainly the influence of water penetration in carnauba wax must be responsible for higher CNP permeability. This is hardly surprising, since Fagerström *et al.* (2014) already postulated that especially waxes with polar fractions, such as carnauba wax with a high n-alcohol content, inevitably have a stronger effect on water absorption, than those absent of polar compounds (Fagerström *et al.*, 2014). As a result, carnauba wax mainly contributing polar compounds such as n-alcohols and long-chain alkyl esters, showed a trend of increasing CNP permeability coefficients with increasing AE-specific EO content, whereas CNP permeability coefficients in candelilla wax, mainly contributing apolar n-alkanes, were largely unaffected by an increase in EO content (Figure 63).

In conclusion, AEs are suitable for enhancing CNP uptake irrespective to the chemical wax composition. Regarding the field situation, it can be assumed that the diffusion of lipophilic AIs is accelerated not only by the AE-induced plasticizer effect (Burghardt *et al.*, 1998), but also by the enhanced uptake of water molecules from the spray formulation, leading to a “secondary plasticization” of the barrier-forming wax structure.

6 Summarizing discussion and outlook

Crop protection science has always aimed to improve the effective application of pesticides to reach high biological activity in the plant. Elucidating the uptake parameters of systemic pesticides across the cuticular barrier is of utmost importance from an ecological and economic point of view. In the past decades, diffusion properties of systemic pesticides have mostly been examined across isolated cuticles (Chamel *et al.*, 1992; Schönherr, 1993b; Kirsch *et al.*, 1997; Buchholz, 2006; Schreiber and Schönherr, 2009; Gutenberger *et al.*, 2013; Staiger *et al.*, 2019). Furthermore, diffusion coefficients of organic compounds and accelerating adjuvants in reconstituted cuticular waxes, which have been shown to mainly provide barrier-forming properties of the cuticle (Riederer and Schönherr, 1985), were exclusively derived from desorption kinetics (Schreiber and Schönherr, 1993; Schreiber *et al.*, 1996b; Kirsch *et al.*, 1997; Burghardt *et al.*, 1998; Schreiber, 2006). However, the mentioned studies investigated diffusion kinetics without considering the individual chemical wax compositions and structural properties and could therefore not provide information on the relationships between compound penetration and the wax modifications potentially associated with it. A recent study showed that explicitly the very-long chain aliphatic (VLCA) moiety of cuticular waxes is responsible for building up an effective barrier against organic compound penetration (Staiger *et al.*, 2019). Therefore, it is assumed that the VLCA composition of cuticular waxes determines the respective crystallinity properties which are thought to mainly define the barrier function (Buchholz, 2006). Deciphering the barrier contributions of individual VLCA fractions such as n-alkanes, n-alcohols, or long-chain alkyl esters in cuticular waxes is therefore of utmost importance for understanding and predicting the diffusion of organic compounds.

To diminish the exceptionally good wax barrier against penetrating active ingredients (AIs), accelerating adjuvants offering wax-modifying plasticizing properties are commonly used in aqueous pesticide formulations (Schönherr *et al.*, 1991; Penner, 2000; Schönherr *et al.*, 2001). Plasticization effects were mostly depicted as wax disruption (Hazen, 2000; Perkins *et al.*, 2005), softening (Schönherr and Baur, 1994; Fagerström *et al.*, 2014), increase of fluidity (Schreiber *et al.*, 1996b; Schreiber *et al.*, 1997) or modification of crystallinity properties (Zhang *et al.*, 2016; Webster *et al.*, 2018). However, none of the mentioned studies has been able to decipher plasticization activity by elucidating a direct correlation between adjuvant diffusion kinetics and wax modification events.

Accordingly, this thesis pursued the establishment of a reliable method being capable of (1) determining real-time diffusion kinetics of (model) AIs and (2) accelerating adjuvants in cuticular model waxes. Furthermore, (3) information from wax modification events recorded simultaneously during adjuvant diffusion should be characterized. (4) The (model) AI diffusion kinetics should be recorded after adjuvant treatment of cuticular model waxes with respect to co-penetrating water, as it is present in aqueous pesticide formulations to obtain deeper knowledge about adjuvant and water effects on AI permeability.

Establishment of ATR-FTIR for diffusion analysis in cuticular waxes

Herein, an ATR-FTIR system based on early works of Fieldson and Barbari (1993) was successfully established, providing the above-mentioned properties. One basic requirement of the proposed system was the generation of uniformly distributed wax layers on ATR crystals to determine accurate diffusion kinetics. Several authors already demonstrated the reliable production of thin, uniformly distributed polymer layers on ATR crystals by the spin coating technique, subsequently used for diffusion kinetics analysis of water and organic molecules via ATR-FTIR (Van Alsten and Lustig, 1992; Fieldson and Barbari, 1993; Sutandar *et al.*, 1994; Fieldson and Barbari, 1995; Yi *et al.*, 2002; Murphy *et al.*, 2003; Flavin *et al.*, 2006; Vasconcelos *et al.*, 2010). Analogously, in this work, the method was shown to be eminently suitable for quickly and effectively generating multiple layers of cuticular model waxes with thicknesses lower than 10 µm. However, an essential drawback of this method raised due to the relatively high amount of required wax for each individual coating. Hence, the amount of wax required for each coating procedure far exceeded the amount of cuticular waxes that could be obtained from the extraction of isolated cuticles (Riederer and Schneider, 1989). Consequently, instead of using reconstituted cuticular waxes, a polydisperse paraffin wax, exclusively consisting of barrier-forming alkanes with an average chain length of 30.32 carbon atoms, typical for cuticular waxes (Holloway, 1994), and furthermore being commercially available in huge quantities at low costs for the operator, was chosen to set base for developing the proposed method.

This study showed the initially recorded diffusion kinetics of the organic model AIs heptyl parabene (HPB) and 4-cyanophenol (CNP) by ATR-FTIR in paraffin wax exhibited a behavior according to the Fickian diffusion model as was generally assumed for diffusion kinetics in reconstituted cuticular waxes by several authors before (Schreiber and Schönherr, 1993;

Schreiber and Riederer, 1996a; Riederer and Schreiber, 2001). Valid diffusion coefficients of 1.73 x 10^{-15} m^2 s^{-1} and 1.48 x 10^{-15} m^2 s^{-1} were derived for HPB and CNP from initial diffusion kinetics, respectively, which, as will be shown later in the discussion, were significantly lower than CNP diffusion coefficients after waxes had been treated with barrier-modifying adjuvants. Raising respective measuring temperatures from 25 °C to 40 °C led to increasing diffusion coefficients. According to the Arrhenius formalism, the natural logarithms of respective diffusion coefficients were plotted versus the inversed absolute temperatures. Hence, ln-linear dependencies between diffusion coefficients and temperature were found within this study, which is in line with the already demonstrated relationship between temperature and the diffusion of organic molecules across isolated cuticles (Baur and Schönherr, 1995; Baur *et al.*, 1997a). Derived activation energies of 66.2 kJ mol^{-1} for HPB and 56.4 kJ mol^{-1} for CNP were found to be within the expected range of activation energies of comparable organic molecules in isolated cuticles. Thus, the cuticular barrier against organic compounds established by aliphatic-dominated waxes could be confirmed here.

During late-time diffusion, however, linearly increasing, instead of asymptotically proceeding diffusion kinetics were observed, showing abnormal behavior compared to the proposed Fickian diffusion model. Although the behavior shown is by no means typical of CNP diffusion in synthetic polymers or human skin, as several studies have already confirmed (Pellett *et al.*, 1997b, a; Romonchuk and Bunge, 2006), a similar finding was reported by McAuley *et al.* (2010) for CNP diffusion in silicone membranes (McAuley *et al.*, 2010). They observed emerging small discrete solvent pools between ATR crystals and annealed polymer membranes due to co-penetrating solvent molecules (water) of CNP donor solutions by spectroscopic imaging. Accumulating water trapped between the ATR crystal and the silicone layer, acting as a solvent for diffusing CNP molecules itself, consequently led to an emerging continuous concentration gradient between the solvent pool and the donor solution beyond reaching the CNP equilibrium concentration in the silicone membrane. Based on the increasing IR-absorption of the donor solution-specific O-H stretching vibration beyond the assumed equilibrium concentration, similar effects were suspected of the system shown here. Conclusively, the fundamental findings showed the ATR-FTIR based tool in combination with the spin coating technique was able to successfully determinate high-resolution model AI diffusion kinetics in paraffin wax.

Selection of cuticular model waxes

Although paraffin wax was exceptionally well suited for basic studies, “real” cuticular waxes contribute to larger variabilities of aliphatic constituents (Jetter *et al.*, 2008), which inevitably causes implications on their crystalline arrangements and barrier properties (Buchholz, 2006). Moreover, chain length distributions of aliphatic cuticular wax fractions are mostly limited to a smaller range (Jetter *et al.*, 2008) than that observed in paraffin wax. Accordingly, the proposed ATR-FTIR based method was further used to determine the diffusion kinetics of first adjuvants and later model AIs and water after adjuvant treatment in plant waxes closer to natural cuticular waxes.

The selection of the model waxes was based on the following criteria: (1) A broad spectrum of VLCAs, contributing various functional groups should be covered to reveal the role of individual aliphatic components to the waxy barrier. (2) To apply spin-coating for generating equally distributed wax layers, model waxes had to be commercially available in high quantities. (3) Potential solvents or foreign substances originating from the refining process of commercially available plant waxes should be avoided as far as possible.

After extensive search and corresponding analyses, candelilla wax mainly consisting of C31, but also contributing minor amounts of free fatty acids and n-alcohols of similar chain-lengths, as well as carnauba wax, being dominated by very-long chain alkyl esters and n-alcohols were chosen. Both waxes represented ideal model waxes covering a broad variety of barrier-forming VLCA constituents (Riederer and Schreiber, 1995; Jetter *et al.*, 2008). Furthermore, investigating adjuvant diffusion properties in cuticular model waxes with altered VLCA composition was provided by the admixture of n-alcohols (policosanol) and long-chain alkyl esters (rice bran wax) to candelilla wax. In the next section, striking differences in the diffusion kinetics of adjuvants and corresponding plasticization events will be discussed, demonstrating that VLCAs do not equally contribute to barrier functions, but their individual physical and chemical compositions determining the barrier.

Accelerator adjuvant diffusion and wax plasticization

To gain deeper knowledge on respective MoAs, diffusion kinetics of the pure liquid accelerator adjuvants methyl oleate from the group of oil derivatives (Nalewaja, 2002), the organophosphate ester TEHP (Muehlebach *et al.*, 2011) and the monodisperse alcohol ethoxylates C12E2, C12E4 and C12E6 (Burghardt *et al.*, 1998) in candelilla and carnauba wax

were simultaneously recorded with wax modification events via ATR-FTIR. It was previously shown that the orthorhombic crystalline arrangement of aliphatic molecules constitutes the stable form in cuticular waxes, whereas the hexagonal rotator phase represents the metastable configuration (Reynhardt and Riederer, 1991, 1994). Hence, within this study the apparent decrease of orthorhombic crystallinity, occurring simultaneously during adjuvant diffusion, was interpreted as wax plasticization. In line with this, Webster *et al.* (2018) already showed a wax disrupting effect of methyl oleate in tristearin, serving as a cuticular model wax. They showed that especially the stable α-crystallite level decreased with increasing adjuvant alkyl ester concentration while the metastable β-crystallite level increased (Webster *et al.*, 2018). Moreover, Zhang *et al.* (2016) showed a reduction of crystallinity in carnauba wax induced by the nonionic surfactant polysorbate 60 using XRD. The decrease in wax-specific absorption during diffusion of the adjuvant was interpreted as affecting the dense packing mode and structural alignment of the studied waxes.

The methyl oleate diffusion coefficient observed in this study was strikingly higher in alkane-dominated candelilla wax (5.3 x 10^{-14} m^2 s^{-1}) than in alkyl-ester dominated carnauba wax (2.0 x 10^{-15} m^2 s^{-1}), indicating higher mobility in the former. Furthermore, a drastically stronger decrease of wax specific IR-absorption and orthorhombic crystallinity was observed in candelilla wax than in carnauba wax, both simultaneously determined during methyl oleate diffusion via ATR-FTIR and suggesting better barrier against methyl oleate induced wax modification in the latter. In addition, this study demonstrated a much higher methyl oleate equilibrium absorption, or equilibrium concentration, i.e. maximum solubility in candelilla wax than in carnauba wax, which is again indicative of the significantly better barrier of the latter. The diffusion kinetics of TEHP in candelilla wax recorded here also followed Fickian diffusion resulting in a diffusion coefficient of 5.3 x 10^{-14} m^2 s^{-1}, which was slightly higher than for methyl oleate diffusion in candelilla wax. The TEHP diffusion kinetics in carnauba wax, however, entirely deviated from the Fickian model and adopted a sigmoidal course accompanied by a significant initial lag phase, again indicating significant diffusional resistance in carnauba wax. Nevertheless, compared to the methyl oleate induced decrease of orthorhombic crystallinity in carnauba wax, the TEHP induced decrease of orthorhombic crystallinity was significantly higher, which on the one hand allowed the assumption of carnauba wax exhibiting higher resistance to TEHP than candelilla wax, but on the other hand showing carnauba wax being more susceptible against TEHP than against methyl oleate induced plasticization.

Furthermore, candelilla wax again exhibited a significantly higher capacity for TEHP than did carnauba wax.

The diffusion kinetics of alcohol ethoxylates observed here also deviated from the proposed Fickian model with increasing degree of ethoxylation, transforming them to sigmoidal diffusion patterns both in candelilla and carnauba wax. Diffusion rates were retained with decreasing lipophilicity / increasing ethoxylation in the order C12E2 > C12E4 > C12E6 in all studied waxes. Moreover, equilibrium concentrations were overall higher in candelilla wax, than in carnauba wax, suggesting higher sorptive capacity for alcohol ethoxylates in candelilla wax than in carnauba wax, as was also observed for the other adjuvants. However, comparing final concentrations by relating AE-specific IR-absorptions is limited. Due to the different dipole moments defined by the number of ethoxylate units (Günzler and Gremlich, 2012), alcohol ethoxylates are assumed to have higher absorption-to-concentration ratios with rising EO content. Therefore, a secondary measurement, e.g., an external calibration, is required first to draw conclusions on AE equilibrium concentrations, derived from respective AE equilibrium absorptions. Even though no information on absolute concentration relations were delivered within this study, previous results reported lipophilic AEs being more readily absorbed into cuticular waxes than hydrophilic variants (Riederer *et al.*, 1995; Burghardt *et al.*, 1998; Burghardt *et al.*, 2006). This allowed the conclusion of increasing AE amounts absorbed into both candelilla and carnauba wax in the order C12E2 > C12E4 > C12E6.

A significantly stronger effect on the reduction of orthorhombic crystallinity was shown in candelilla wax than in carnauba wax. The crystallinity reduction became more pronounced with increasing lipophilicity (and maybe concentration) of respective AEs (C12E2 > C12E4 > C12E6). Accordingly, the different degrees of susceptibility to adjuvant-induced plasticization agree with the results of methyl oleate and TEHP diffusion, which also induced a higher effect on decreasing orthorhombic crystallinity in candelilla wax than in carnauba wax.

Taken the findings together, carnauba wax appeared to promote better barrier properties and plasticization resistance compared to candelilla wax. Hence, the results suggest very-long chain alkyl-esters, as present in carnauba wax, somehow enhancing the structural stability of cuticular waxes on a molecular level compared to those waxes lacking alkyl-esters.

Accordingly, the presence of alkyl esters within cuticular waxes is assumed to enhance structural and mechanical integrity and ultimately leading to higher plasticization resistance to accelerating adjuvants. The results obtained here led to the conclusion of very-long chain

alkyl esters being incorporated into the lamellar arrangement of adjacent crystallites along their longitudinal axes. This is in line with previously reported results, suggesting analogous structural reinforcement either in polydisperse paraffin wax contributing fractions of significantly different chain-length populations or in cuticular wax of *Hordeum vulgare* contributing both n-alkane and very-long chain alkyl ester populations with significantly different average chain-lengths (Reynhardt, 1997; Dorset, 2005). To understand the role of structure-reinforcing alkyl esters in natural systems, Bueno *et al.* (2019) investigated the cuticular wax of the desert plant *Phoenix dactylifera*. The presence of an alkyl ester population alongside other VLCAs with significantly shorter average chain lengths resulted in low water permeability of the isolated cuticle. This is of enormous importance for the plant, especially under drought conditions, as the occurrence of thermally induced structural defects is prevented by crystallite bridging alkyl ester rods (Bueno *et al.*, 2019).

In agreement with the assumption of very-long chain alkyl esters strengthening structural integrities within cuticular waxes, methyl oleate and alcohol ethoxylates diffusion kinetics were delayed when adding significant amounts of long-chain alkyl esters, contributing chain-length up to 62 carbon atoms. Contrastingly, respective diffusion kinetics were accelerated in candelilla wax blends contributing raising amounts of n-alcohols with comparable chain-length as the candelilla wax specific n-alkane fraction. This may be explained by DSC data recorded here, suggesting partial phase separation which eventually led to decreased mechanical stability and enhanced susceptibility against adjuvant-induced plasticization.

In conclusion, enhancing the structural integrity of candelilla wax by introducing reinforcing crystallite bridging rods appeared likely, as was observed for the strengthened mechanical stability of alkyl-ester dominated carnauba wax. However, this trend was not observed considering TEHP diffusion. Hence, in contrast to methyl oleate and probably also alcohol ethoxylates, TEHP was found to be able to disentangle the postulated alkyl ester bridges from their anchors, allowing the assumption of strikingly different MoAs between the investigated adjuvants.

Several explanations of potential intermolecular wax interactions and plasticization modes were given in this study explaining the discrepancies between respective adjuvant plasticization activities:

According to the model of Riederer and Schreiber (1995), polar wax constituents are situated in the amorphous phase, rather than within lamellar crystalline regions. Therefore, the results

obtained here suggest the aliphatic C18-chain of methyl oleate being integrated into the lamellar arranged crystallites in cuticular waxes, while the more polar methyl ester group is thought to protrude into the amorphous zone. This is in line with a previous study of Zhang *et al.* (2016), hypothesizing the polyethylene chains of aliphatic monodisperse AEs being integrated into lamellar crystalline regions, whereas the polar ethoxylate units are postulated to be integrated within the amorphous phase (Zhang *et al.*, 2016).

Along with this hypothesis, the results presented here show that monodisperse alcohol ethoxylates acting in the same way as methyl oleate does, thoroughly explaining their commonly lower plasticizing activity in carnauba wax than in candelilla wax. Nevertheless, the mobilities of the investigated AEs, as well as their effect on orthorhombic crystallinity were significantly more pronounced than that of methyl oleate in carnauba wax. Hence, the results obtained here suggest the short methyl ester group of methyl oleate hardly possessing any long-chain ester disentangling effect, whereas the long-chain ethoxylate groups of the alcohol ethoxylates are somehow capable of leveraging long-chain alkyl ester bridges out of their anchors, situated within adjacent crystallites.

By far the highest influence on orthorhombic crystallinity and wax molecular density in carnauba wax was observed during TEHP diffusion, suggesting a drastically different MoA compared to methyl oleate and alcohol ethoxylates. The results presented here allowed the assumption of the centrally located polar phosphate group within TEHP being accumulated in the amorphous phase. As a result, the hydrocarbon chains of TEHP are not integrated into the crystalline phase due to their isometric arrangement and high mobility, and therefore inevitably push adjacent crystallites apart. To confirm this hypothesis, crystallographic studies using XRD and electron diffractometry are mandatory to investigate the structural wax properties after TEHP treatment in future studies.

CNP diffusion and water-induced secondary plasticization after adjuvant treatment

It is well known that AI permeability in the cuticular barrier is drastically increased with the help of plasticizing adjuvants (Riederer *et al.*, 1995; Santier and Chamel, 1996; Schreiber *et al.*, 1996b; Burghardt *et al.*, 1998; Arand *et al.*, 2018). Concerning adjuvant affected AI diffusion kinetics, mobilities were exclusively determined in cuticular waxes which were premixed with adjuvants in the liquid state (Burghardt *et al.*, 1998; Šimáňová *et al.*, 2005; Burghardt *et al.*,

2006). This inevitably influenced respective crystallization modes of the waxes, which probably do naturally not occur in this way. Accordingly, information on the effect of AI mobility and solubility considering the natural penetration and plasticization process of adjuvants from an external spray formulation is lacking. Furthermore, to date there is no clear evidence on how far the accumulation of co-penetrating water from a potential spray solution in the wax affects the mobility and solubility of model AIs. Hence, within this study, diffusion kinetics of the AI modelling CNP and water were exclusively recorded after external application of the accelerating adjuvants methyl oleate, TEHP, C12E2, C12E4 and C12E6 onto thin layers of spin coated candelilla and carnauba wax.

After spray droplet evaporation, adjuvant residues typically remain on the leaf surface (Gaskin and Holloway, 1992). Thus, plasticization does mainly occur from highly concentrated adjuvant pools rather than from the aqueous spray formulation. Surfactants possessing humectant properties (Asmus *et al.*, 2016) are usually co-formulated to ensure the AI being kept in a gel-like state after droplet evaporation, preventing it from crystallization and rendering it unavailable to the plant (Cook *et al.*, 1977; Stevens and Bukovac, 1987b; Gaskin and Holloway, 1992). Also oil adjuvants may keep the AI in a state available to the plant after water has fully evaporated (Hess and Falk, 1990) and consequently, due to their extraordinary low vapor pressures at moderate temperature (Hinckley *et al.*, 1990), this is obviously also true for organophosphate esters. However, diffusion of AIs from aqueous spray droplets already occurs when the water has not yet completely evaporated. Therefore, the effect of the adjuvant on the co-penetration of water and the associated effect on AI permeation remains to be deciphered.

Within this study, the permeability determining parameters of mobility (diffusion coefficient) and solubility (partition coefficient) of CNP as well as the solubility of co-penetrating water from the donor solutions were precisely determined via ATR-FTIR.

The cuticular path for diffusing molecules is separated in (1) the hydrophilic route, favoring transport of small hydrophilic polar solutes and (2) the lipophilic pathway, taken by non-electrolyte apolar solutes of bigger sizes (Müller and Riederer, 2006). Indeed, water is thought to mainly penetrate the cuticle via the hydrophilic route (Popp *et al.*, 2005), which is assumed not to be highly affected by plasticizing adjuvants (Shi *et al.*, 2005a). However, due to its non-electrolyte state, water was also repeatedly estimated to take the lipophilic pathway (Schreiber, 2005; Schönherr, 2006), which is mainly modified by plasticizing adjuvants. The

diffusion experiments performed here showed water uptake was only slightly enhanced by prior methyl oleate treatment both in candelilla and carnauba wax, whereas it was drastically increased after TEHP and AE treatment. The discrepancies of adjuvant-induced water uptake may be explained by the adjuvant specific physical properties and assumed impacts on the lipophilic pathway.

The hydrocarbon chains of monodisperse AEs (here C12) are assumed to be integrated within lamellar arranged crystallites along their longitudinal axis, whereas their polar ethoxylate groups (here E2, E4 and E6) may protrude the amorphous zone. This is in line with findings by Zhang *et al.* (2016) who proposed comparable integration of ethoxylated polysorbates within cuticular waxes (Zhang *et al.*, 2016). Accordingly, due to their humectant properties established by hygroscopic ethoxylate units (Ramsey *et al.*, 2005), increasing the waxes hydration state by either absorbing atmospheric water or water of the spray droplet into the amorphous phase, led to severe swelling or softening of the wax, which is referred to as "secondary plasticization". This assumption is in accordance with previously reported results, showing combined surfactant/water uptake leading to an overall more fluidic and softer cuticular wax (Fagerström *et al.*, 2014). In fact, the results obtained here allow the assumption of methyl oleate polyethylene chains also being integrated within lamellar arranged crystallites. However, due to their short and less polar methyl ester groups potentially protruding into the amorphous zone, the lacking ability of adhering water molecules consequently led to minor water uptake from a donor solution and less pronounced wax swelling, as was observed here.

In this study, a drastically increased water uptake was not only induced by AEs but also by the organophosphate ester TEHP. Considering herein generated simulations, TEHP molecules potentially adhere water molecules by building up hydrogen bonds between the centrally located polar phosphate group and adjacent water molecules. Thus, the significantly increased water uptake by TEHP could also have led to strong swelling and secondary plasticization of the wax.

Now, that water uptake influenced by adjuvants has been extensively discussed, the differences in CNP diffusion coefficients and partition coefficients at the molecular level can also be explained. Under the assumption that attracted water molecules may have acted as hydrogen bond donors to CNP molecules themselves, which was already demonstrated before

(Kido Soule *et al.*, 2006), a stringent correlation of water induced wax swelling with increased CNP mobility and solubility became apparent.

CNP diffusion coefficients were higher in carnauba wax than in candelilla wax, both after treatment with TEHP (35.31 x 10^{-14} m^2 s^{-1} vs. 5.14 x 10^{-14} m^2 s^{-1}) or monodisperse alcohol ethoxylates (C12E2: 24.95 x 10^{-14} m^2 s^{-1} vs. 2.94 x 10^{-14} m^2 s^{-1}; C12E4: 30.69 x 10^{-14} m^2 s^{-1} vs. 2.49 x 10^{-14} m^2 s^{-1}; C12E6: 18.71 x 10^{-14} m^2 s^{-1} vs. 2.29 x 10^{-14} m^2 s^{-1}), respectively. This can be explained by the different polarity of the respective wax components. While candelilla wax mainly contributed apolar constituents such as hentriacontane, carnauba wax contributed more polar aliphatic molecules like n-alcohols and long chain alkyl ester. Therefore, the water absorbed into the wax by the adjuvants could possibly interact more strongly with the polar functional groups of the carnauba wax, allowing higher mobility of the attached CNP molecules. However, CNP diffusion coefficients were significantly higher in methyl oleate treated candelilla wax (12.23 x 10^{-14} m^2 s^{-1}) than in methyl oleate treated carnauba wax (5.13 x 10^{-14} m^2 s^{-1}). This finding may be explained with the higher internal methyl oleate concentration at equilibrium state in the former, being in line with the results reported by Šimáňová *et al.* (2005), showing the mobility of lipophilic AIs linearly correlates with the internal alkyl ester adjuvant concentration in cuticular waxes (Šimáňová *et al.*, 2005). Hence, due to the previously discussed lacking ability of methyl oleate to induce effective water uptake, the higher CNP mobility is attributed solely to the higher internal methyl oleate concentration and adjuvant-induced plasticization susceptibility of candelilla wax, but not on water-induced secondary plasticization.

Concerning the herein determined CNP partition coefficients, striking differences between both investigated waxes were found either after methyl oleate treatment (candelilla: 5.71; carnauba: 3.42) or after TEHP (candelilla: 17.88; carnauba: 13.66) and AE treatment (candelilla: C12E2 = 27.04, C12E4 = 28.31, C12E6 = 27.40; carnauba: C12E2 = 11.88, C12E4 = 8.85, C12E6 = 20.02). Hence, the results suggest adjuvant-induced co-penetration of water acting as a secondary plasticizer, leading to (1) significantly enhanced CNP mobility in carnauba wax after TEHP and AE treatment and (2) drastically higher CNP partitioning in both waxes after TEHP and alcohol ethoxylate treatment, compared to methyl oleate treatment.

This work demonstrated that the novel ATR-FTIR based tool in combination with the spin coating technique is exceptionally well suited for the precise determination of high-resolution adjuvant-, water- and model AI diffusion kinetics in cuticular model waxes. Significant

differences of adjuvant induced wax modification in terms of reduction of orthorhombic crystallinity and molecular wax density were observed. It was shown that the AI permeability was enhanced by an accelerating oil adjuvant, an organophosphate ester, and three monodisperse AEs. The observed differences in AI mobilities and solubilities depended on (1) the adjuvant structural and physical properties, (2) the individual chemical composition and mechanical integrity of aliphatic-dominated waxes and (3) the level of attracted water, potentially acting as a secondary plasticizer. The assumption that especially co-penetrating water from the model AI donor solution, respectively from the formulation spray drop, was responsible for the drastic mobility and solubility differences, should consequently give impulses to analyze especially the water induced secondary plasticization contribution to adjuvant-wax-AI interactions. Considering the high societal demands for safety and ecological compatibility, the proposed ATR-FTIR should find future application in crop protection science to specifically ensure rapid and effective development of new pesticide formulations.

7 References

Arand K, Asmus E, Popp C, Schneider D, Riederer M. 2018. The Mode of Action of Adjuvants—Relevance of Physicochemical Properties for Effects on the Foliar Application, Cuticular Permeability, and Greenhouse Performance of Pinoxaden. Journal of Agricultural and Food Chemistry **66**, 5770-5777.

Asmus E, Popp C, Friedmann A, Arand K, Riederer M. 2016. Water sorption isotherms of surfactants: a tool to evaluate humectancy. Journal of Agricultural and Food Chemistry **64**, 5310-5316.

Bargel H, Koch K, Cerman Z, Neinhuis C. 2006. Evans Review No. 3: Structure–function relationships of the plant cuticle and cuticular waxes—a smart material? Functional Plant Biology **33**, 893-910.

Barthlott W, Neinhuis C, Cutler D, Ditsch F, Meusel I, Theisen I, Wilhelmi H. 1998. Classification and terminology of plant epicuticular waxes. Botanical Journal of the Linnean Society **126**, 237-260.

Basson I, Reynhardt E. 1988. An investigation of the structures and molecular dynamics of natural waxes. II. Carnauba wax. Journal of Physics D: Applied Physics **21**, 1429.

Bauer H, Schönherr J. 1992. Determination of mobilities of organic compounds in plant cuticles and correlation with molar volumes. Pesticide Science **35**, 1-11.

Baur P. 1999. Surfactant effects on cuticular penetration of neutral polar compounds: dependence on humidity and temperature. Journal of Agricultural and Food Chemistry **47**, 753-761.

Baur P, Buchholz A, Schönherr J. 1997a. Diffusion in plant cuticles as affected by temperature and size of organic solutes: similarity and diversity among species. Plant, Cell & Environment **20**, 982-994.

Baur P, Marzouk H, Schönherr J. 1999. Estimation of path lengths for diffusion of organic compounds through leaf cuticles. Plant, Cell & Environment **22**, 291-299.

Baur P, Marzouk H, Schönherr J, Grayson BT. 1997b. Partition coefficients of active ingredients between plant cuticle and adjuvants as related to rates of foliar uptake. Journal of Agricultural and Food Chemistry **45**, 3659-3665.

Baur P, Schönherr J. 1995. Temperature dependence of the diffusion of organic compounds across plant cuticles. Chemosphere **30**, 1331-1340.

Beattie G, Marcell L. 2002. Effect of alterations in cuticular wax biosynthesis on the physicochemical properties and topography of maize leaf surfaces. Plant, Cell & Environment **25**, 1-16.

Becker M, Kerstiens G, Schönherr J. 1986. Water permeability of plant cuticles: permeance, diffusion and partition coefficients. Trees **1**, 54-60.

Bianchi G, Lupotto E, Borghi B, Corbellini M. 1980. Cuticular wax of wheat. Planta **148**, 328-331.

Bird DA. 2008. The role of ABC transporters in cuticular lipid secretion. Plant Science **174**, 563-569.

Bohannan DR, Jordan TN. 1995. Effects of ultra-low volume application on herbicide efficacy using oil diluents as carriers. Weed Technology **9**, 682-688.

Bowman R, Mason R. 1951. 611. Synthetic long-chain aliphatic compounds. Part V. N-nonatricosanoic and n-hexapentacosanoic acids. Journal of the Chemical Society (Resumed), 2748-2751.

Briard A-J, Bouroukba M, Petitjean D, Hubert N, Dirand M. 2003. Experimental enthalpy increments from the solid phases to the liquid phase of homologous n-alkane series (C18 to C38 and C41, C44, C46, C50, C54, and C60). Journal of Chemical & Engineering Data **48**, 497-513.

Bruce JA, Penner D, Kells JJ. 1993. Absorption and activity of nicosulfuron and primisulfuron in quackgrass (Elytrigia repens) as affected by adjuvants. Weed Science **41**, 218-224.

Buchholz A. 2006. Characterization of the diffusion of non-electrolytes across plant cuticles: properties of the lipophilic pathway. Journal of Experimental Botany **57**, 2501-2513.

Buchholz A, Schönherr J. 2000. Thermodynamic analysis of diffusion of non-electrolytes across plant cuticles in the presence and absence of the plasticiser tributyl phosphate. Planta **212**, 103-111.

Bueno A, Alfarhan A, Arand K, Burghardt M, Deininger A-C, Hedrich R, Leide J, Seufert P, Staiger S, Riederer M. 2019. Effects of temperature on the cuticular transpiration barrier of two desert plants with water-spender and water-saver strategies. Journal of Experimental Botany **70**, 1613-1625.

Burghardt M, Friedmann A, Schreiber L, Riederer M. 2006. Modelling the effects of alcohol ethoxylates on diffusion of pesticides in the cuticular wax of Chenopodium album leaves. Pest Management Science **62**, 137-147.

Burghardt M, Riederer M. 1996. Sorption of monodisperse and polydisperse nonionic surfactants in isolated plant cuticles and reconstituted cuticular wax. Journal of Experimental Botany **47**, 51-51.

Burghardt M, Riederer M. 2008. Cuticular transpiration. Annual Plant Reviews, Biology of the Plant Cuticle. Blackwell publishing **23**, 292.

Burghardt M, Schreiber L, Riederer M. 1998. Enhancement of the diffusion of active ingredients in barley leaf cuticular wax by monodisperse alcohol ethoxylates. Journal of Agricultural and Food Chemistry **46**, 1593-1602.

Büscher K. 1960. Messung der Dichte, des spezifischen Volumens und des kubischen Ausdehnungskoeffizienten plastischer Massen mit Hilfe des Haake-Konsistometers. Erdöl Kohle **13**, 102-106.

Carreto L, Almeida AR, Fernandes AC, Vaz WL. 2002. Thermotropic mesomorphism of a model system for the plant epicuticular wax layer. Biophysical Journal **82**, 530-540.

Casado CG, Heredia A. 1999. Structure and dynamics of reconstituted cuticular waxes of grape berry cuticle (Vitis vinifera L.). Oxford University Press.

Chai M, Isa M. 2013. The oleic acid composition effect on the carboxymethyl cellulose based biopolymer electrolyte.

Chamel A, Gambonnet B, Coret J. 1992. Effects of two ethoxylated nonylphenols on sorption and penetration of [14C] isoproturon through isolated plant cuticles. Plant physiology and biochemistry (Paris) **30**, 713-721.

Cook GT, Babiker AG, Duncan HJ. 1977. Penetration of bean leaves by aminotriazole as influenced by adjuvants and humidity. Pesticide Science **8**, 137-146.

Coret J, Chamel A. 1994. Effect of some ethoxylated alkylphenols and ethoxylated alcohols on the transfer of [14C] chlorotoluron across isolated plant cuticles. Weed Research **34**, 445-451.

Coret J, Chamel A. 1995. Effects and possible mode of action of some nonionic surfactants on the diffusion of [14C] glyphosate and [14C] Chlorotoluron acorss isoltated plant cuticles. Pesticide Science **43**, 163-166.

Coret JM, Chamel AR. 1993. Influence of some nonionic surfactants on water sorption by isolated tomato fruit cuticles in relation to cuticular penetration of glyphosate. Pesticide Science **38**, 27-32.

Coward JL. 2010. FTIR spectroscopy of synthesized racemic nonacosan-10-ol: a model compound for plant epicuticular waxes. Journal of Biological Physics **36**, 405-425.

Craig SR, Hastie GP, Roberts KJ, Sherwood JN. 1994. Investigation into the structures of some normal alkanes within the homologous series C13H28 to C60H122 using high-resolution synchrotron X-ray powder diffraction. Journal of Materials Chemistry **4**, 977-981.

Cronfeld P, Lader K, Baur P. 2001. Classification of adjuvants and adjuvant blends by effects on cuticular penetration. *Pesticide Formulations and Application Systems: Twentieth Volume*: ASTM International.

Cussler E, Hughes SE, Ward III WJ, Aris R. 1988. Barrier membranes. Journal of Membrane Science **38**, 161-174.

Cussler EL. 2009. *Diffusion: mass transfer in fluid systems*: Cambridge university press.

Darbre PD, Harvey PW. 2008. Paraben esters: review of recent studies of endocrine toxicity, absorption, esterase and human exposure, and discussion of potential human health risks. Journal of Applied Toxicology **28**, 561-578.

Dassanayake LSK, Kodali DR, Ueno S, Sato K. 2009. Physical properties of rice bran wax in bulk and organogels. Journal of the American Oil Chemists' Society **86**, 1163.

Dhoot G, Auras R, Rubino M, Dolan K, Soto-Valdez H. 2009. Determination of eugenol diffusion through LLDPE using FTIR-ATR flow cell and HPLC techniques. Polymer **50**, 1470-1482.

Diarte C, de Souza AX, Staiger S, Deininger A-C, Bueno A, Burghardt M, Graell J, Riederer M, Lara I, Leide J. 2021. Compositional, structural and functional cuticle analysis of Prunus laurocerasus L. sheds light on cuticular barrier plasticity. Plant Physiology and Biochemistry **158**, 434-445.

Dias M, Hadgraft J, Raghavan S, Tetteh J. 2004. The effect of solvent on permeant diffusion through membranes studied using ATR-FTIR and chemometric data analysis. Journal of Pharmaceutical Sciences **93**, 186-196.

Dias M, Raghavan S, Hadgraft J. 2001. ATR-FTIR spectroscopic investigations on the effect of solvents on the permeation of benzoic acid and salicylic acid through silicone membranes. International Journal of Pharmaceutics **216**, 51-59.

Döppers L-M, Breen C, Sammon C. 2004. Diffusion of water and acetone into poly (vinyl alcohol)–clay nanocomposites using ATR-FTIR. Vibrational Spectroscopy **35**, 27-32.

Dorset DL. 1995. The crystal structure of waxes. Acta Crystallographica Section B: Structural Science **51**, 1021-1028.

Dorset DL. 2005. *Crystallography of the polymethylene chain: an inquiry into the structure of waxes*: Oxford University Press on Demand.

Elabd YA, Baschetti MG, Barbari TA. 2003. Time-resolved Fourier transform infrared/attenuated total reflection spectroscopy for the measurement of molecular diffusion in polymers. Journal of Polymer Science Part B: Polymer Physics **41**, 2794-2807.

Ensikat HJ, Boese M, Mader W, Barthlott W, Koch K. 2006. Crystallinity of plant epicuticular waxes: electron and X-ray diffraction studies. Chemistry and Physics of Lipids **144**, 45-59.

España L, Heredia-Guerrero JA, Segado P, Benítez JJ, Heredia A, Domínguez E. 2014. Biomechanical properties of the tomato (Solanum lycopersicum) fruit cuticle during development are modulated by changes in the relative amounts of its components. New Phytologist **202**, 790-802.

Fagerström A, Kocherbitov V, Westbye P, Bergström K, Arnebrant T, Engblom J. 2014. Surfactant softening of plant leaf cuticle model wax–A Differential Scanning Calorimetry (DSC) and Quartz Crystal Microbalance with Dissipation (QCM-D) study. Journal of Colloid and Interface Science **426**, 22-30.

Fagerström A, Kocherbitov V, Westbye P, Bergström K, Mamontova V, Engblom J. 2013. Characterization of a plant leaf cuticle model wax, phase behaviour of model wax–water systems. Thermochimica Acta **571**, 42-52.

Falk R. 1994. Influence of formulation and adjuvants on the foliar location and physical form of the active ingredient. *Interactions between adjuvants, agrochemicals and target organisms*: Springer, 53-82.

Fernández V, Khayet M, Montero-Prado P, Heredia-Guerrero JA, Liakopoulos G, Karabourniotis G, Del Rio V, Domínguez E, Tacchini I, Nerín C. 2011. New insights into the properties of pubescent surfaces: peach fruit as a model. Plant Physiology **156**, 2098-2108.

Fich EA, Segerson NA, Rose JK. 2016. The plant polyester cutin: biosynthesis, structure, and biological roles. Annual Review of Plant Biology **67**, 207-233.

Fieldson G, Barbari T. 1993. The use of FTi. r.-atr spectroscopy to characterize penetrant diffusion in polymers. Polymer **34**, 1146-1153.

Fieldson GT, Barbari TA. 1995. Analysis of diffusion in polymers using evanescent field spectroscopy. AIChE Journal **41**, 795-804.

Flavin K, Hughes H, Dobbyn V, Kirwan P, Murphy K, Steiner H, Mizaikoff B, Mcloughlin P. 2006. A comparison of polymeric materials as pre-concentrating media for use with ATR/FTIR sensing. International Journal of Environmental Analytical Chemistry **86**, 401-415.

Fox R. 1958. The relationship of wax crystal structure to the water vapor transmission rate of wax films. Tappi **41**, 283-289.

Foy CL, Smith LW. 1969. The role of surfactants in modifying the activity of herbicidal sprays. *Advances in Chemistry*, Vol. 86: ACS Publications, 55-69.

Gaskin RE, Holloway PJ. 1992. Some physicochemical factors influencing foliar uptake enhancement of glyphosatemono (isopropylammonium) by polyoxyethylene surfactants. Pesticide Science **34**, 195-206.

Gauvrit C, Cabanne F. 1993. Oils for weed control: uses and mode of action. Pesticide Science **37**, 147-153.

Gouni-Berthold I, Berthold HK. 2002. Policosanol: clinical pharmacology and therapeutic significance of a new lipid-lowering agent. American Heart Journal **143**, 356-365.

Grant C, Twigg P, Bell G, Lu JR. 2008. AFM relative stiffness measurement of the plasticising effect of a non-ionic surfactant on plant leaf wax. Journal of Colloid and Interface Science **321**, 360-364.

Green J. 2000. Adjuvant outlook for pesticides. Pesticide Outlook **11**, 196-199.

Griffin WC. 1954. Calculation of HLB values of non-ionic surfactants. Journal of the Society of Cosmetic Chemists **5**, 249-256.

Gülz P-G, Markstädter C, Riederer M. 1993. Isomeric alkyl esters in Quercus robur leaf cuticular wax. Phytochemistry **35**, 79-81.

Günzler H, Gremlich H-U. 2012. *IR-Spektroskopie: Eine Einführung*: John Wiley & Sons.

Guo W, Chen J, Sun S, Zhou Q. 2016. In situ monitoring the molecular diffusion process in graphene oxide membranes by ATR-FTIR spectroscopy. The Journal of Physical Chemistry C **120**, 7451-7456.

Guo Y, Li JJ, Busta L, Jetter R. 2018. Coverage and composition of cuticular waxes on the fronds of the temperate ferns Pteridium aquilinum, Cryptogramma crispa, Polypodium glycyrrhiza, Polystichum munitum and Gymnocarpium dryopteris. Annals of Botany **122**, 555-568.

Gutenberger A, Zeisler VV, Berghaus R, Auweter H, Schreiber L. 2013. Effects of poly-and monodisperse surfactants on 14C-epoxiconazole diffusion in isolated cuticles of Prunus laurocerasus. Pest Management Science **69**, 512-519.

Hamilton RJ. 1993. Structure and general properties of mineral and vegetable oils used as spray adjuvants. Pesticide Science **37**, 141-146.

Hastie G, Roberts K. 1994. Investigation of inter-and intra-molecular packing in the solid state for crystals of normal alkanes and homologous mixtures using FT-IR spectroscopy. Journal of Materials Science **29**, 1915-1919.

Hazen JL. 2000. Adjuvants—terminology, classification, and chemistry. Weed Technology **14**, 773-784.

Heredia-Guerrero JA, Benítez JJ, Domínguez E, Bayer IS, Cingolani R, Athanassiou A, Heredia A. 2014. Infrared and Raman spectroscopic features of plant cuticles: a review. Frontiers in Plant Science **5**, 305.

Heredia-Guerrero JA, Benítez JJ, Domínguez E, Bayer IS, Cingolani R, Athanassiou A, Heredia A. 2016. Infrared spectroscopy as a tool to study plant cuticles. Spectroscopy Europe **28**, 10-13.

Heredia A. 2003. Biophysical and biochemical characteristics of cutin, a plant barrier biopolymer. Biochimica et Biophysica Acta (BBA)-General Subjects **1620**, 1-7.

Hess F, Bayer D, Falk R. 1981. Herbicide dispersal patterns: HI. As a function of formulation. Weed Science **29**, 224-229.

Hess FD. 1999. Surfactants and additives. *Proceedings of the California Weed Science Society*, Vol. 51, 156-172.

Hess FD, Falk RH. 1990. Herbicide deposition on leaf surfaces. Weed Science **38**, 280-288.

Hess FD, Foy CL. 2000. Interaction of surfactants with plant cuticles. Weed Technology **14**, 807-813.

Hinckley DA, Bidleman TF, Foreman WT, Tuschall JR. 1990. Determination of vapor pressures for nonpolar and semipolar organic compounds from gas chromatograhic retention data. Journal of Chemical and Engineering Data **35**, 232-237.

Hoffmann R. 1964. Distribution of electronic levels in alkanes. The Journal of Chemical Physics **40**, 2047-2048.

Holloway PJ. 1994. Plant cuticles: physicochemical characteristics and biosynthesis. *Air pollutants and the leaf cuticle*: Springer, 1-13.

Holly K. 1953. The penetration of chlorinated phenoxyacetic acids into leaves. The penetration of chlorinated phenoxyacetic acids into leaves.

Holmes MG, Keiller DR. 2002. Effects of pubescence and waxes on the reflectance of leaves in the ultraviolet and photosynthetic wavebands: a comparison of a range of species. Plant, Cell & Environment **25**, 85-93.

Hsin-Fei M. 2013. *Polymer electronics*: CRC Press.

Huang H, Burghardt M, Schuster A-C, Leide J, Lara I, Riederer M. 2017. Chemical composition and water permeability of fruit and leaf cuticles of Olea europaea L. Journal of Agricultural and Food Chemistry **65**, 8790-8797.

Jeffree C. 1986. The cuticle, epicuticular waxes and trichomes of plants, with reference to their structure, functions and evolution. Insects on the Plant Surface, 23-64.

Jeffree C. 1996. Structure and ontogeny of plant cuticles. Plant cuticles: an integrated functional approach, 33-82.

Jetter R, Kunst L, Samuels AL. 2008. Composition of plant cuticular waxes. Biology of the Plant Cuticle **23**, 145-181.

Jetter R, Riederer M. 2016. Localization of the transpiration barrier in the epi-and intracuticular waxes of eight plant species: water transport resistances are associated with fatty acyl rather than alicyclic components. Plant Physiology **170**, 921-934.

Johnson EJ, Dorot O, Liu J, Chefetz B, Xing B. 2007. Spectroscopic characterization of aliphatic moieties in four plant cuticles. Communications in Soil Science and Plant Analysis **38**, 2461-2478.

Johnson JF. 1954. Phase transformations in commercial paraffin waxes. Industrial & Engineering Chemistry **46**, 1046-1048.

Kappen L. 1981. Ecological significance of resistance to high temperature. *Physiological Plant Ecology*: Springer, 439-474.

Kido Soule MC, Hore DK, Jaramillo-Fellin DM, Richmond GL. 2006. Differing Adsorption Behavior of Environmentally Important Cyanophenol Isomers at the Air− Water Interface. The Journal of Physical Chemistry B **110**, 16575-16583.

Kirkwood RC. 1993. Use and mode of action of adjuvants for herbicides: a review of some current work. Pesticide Science **38**, 93-102.

Kirkwood RC. 1994. Surfactant—pesticide—plant interactions. Biochemical Society Transactions **22**, 611-616.

Kirkwood RC. 1999. Recent developments in our understanding of the plant cuticle as a barrier to the foliar uptake of pesticides. Pesticide Science **55**, 69-77.

Kirsch T, Kaffarnik F, Riederer M, Schreiber L. 1997. Cuticular permeability of the three tree species Prunus laurocerasus L., Ginkgo biloba L. and Juglans regia L.: comparative investigation

of the transport properties of intact leaves, isolated cuticles and reconstituted cuticular waxes. Journal of Experimental Botany **48**, 1035-1045.

Kodali DR. 2009. The utilization of rice bran wax to stabilize long chain ω-3 polyunsaturated fatty acid esters. Lipid Technology **21**, 254-256.

Kolattukudy P. 1985. Enzymatic penetration of the plant cuticle by fungal pathogens. Annual Review of Phytopathology **23**, 223-250.

Krauss P, Markstädter C, Riederer M. 1997. Attenuation of UV radiation by plant cuticles from woody species. Plant, Cell & Environment **20**, 1079-1085.

Krenek MR, King DN. 1987. The relative phytotoxicity of selected hydrocarbon and oxygenated solvents and oils. *Pesticide Formulations and Application Systems: Sixth Volume*: ASTM International.

Kunst L, Samuels A, Jetter R. 2005. The plant cuticle: formation and structure of epidermal surfaces. Plant Lipids—Biology, Utilisation and Manipulation, D. Murphy, ed (Oxford, UK: Blackwell), 270-302.

Lai C, Kunst L, Jetter R. 2007. Composition of alkyl esters in the cuticular wax on inflorescence stems of Arabidopsis thaliana cer mutants. The Plant Journal **50**, 189-196.

Lee SB, Suh MC. 2015. Advances in the understanding of cuticular waxes in Arabidopsis thaliana and crop species. Plant Cell Reports **34**, 557-572.

Leide J, Nierop KG, Deininger A-C, Staiger S, Riederer M, de Leeuw JW. 2020. Leaf cuticle analyses: Implications for the existence of cutan/non-ester cutin and its biosynthetic origin. Annals of Botany **126**, 141-162.

Liu N, Zhao L, Tang L, Stobbs J, Parkin I, Kunst L, Karunakaran C. 2020. Mid-infrared spectroscopy is a fast screening method for selecting Arabidopsis genotypes with altered leaf cuticular wax. Plant, Cell & Environment **43**, 662-674.

Lohar G, Shinde S, Fulari V. 2014. Structural, morphological, optical and photoluminescent properties of spray-deposited ZnSe thin film. Journal of Semiconductors **35**, 1-5.

Lommerse JP, Price SL, Taylor R. 1997. Hydrogen bonding of carbonyl, ether, and ester oxygen atoms with alkanol hydroxyl groups. Journal of Computational Chemistry **18**, 757-774.

López-Casado G, Matas AJ, Domínguez E, Cuartero J, Heredia A. 2007. Biomechanics of isolated tomato (Solanum lycopersicum L.) fruit cuticles: the role of the cutin matrix and polysaccharides. Journal of Experimental Botany **58**, 3875-3883.

Lourens J, Reynhardt E. 1979. NMR investigation of Fischer-Tropsch waxes. Journal of Physics D: Applied Physics **12**, 1963.

Macisaac SA, Paul RN, Devine MD. 1991. A scanning electron microscope study of glyphosate deposits in relation to foliar uptake. Pesticide Science **31**, 53-64.

Manthey F, Nalewaja J, Szelezniak E, Chow P, Grant C, Hinshalwood A, Simundsson E. 1989. Esterified seed oils with herbicides. Adjuvants and Agrochemicals **2**.

Mao B, Cheng Z, Lei C, Xu F, Gao S, Ren Y, Wang J, Zhang X, Wang J, Wu F. 2012. Wax crystal-sparse leaf2, a rice homologue of WAX2/GL1, is involved in synthesis of leaf cuticular wax. Planta **235**, 39-52.

Marinangeli CP, Kassis AN, Jain D, Ebine N, Cunnane SC, Jones PJ. 2007. Comparison of composition and absorption of sugarcane policosanols. British Journal of Nutrition **97**, 381-388.

Martin JT, Juniper BE. 1970. *The cuticles of plants*.

Mazee W. 1957. Thermal analysis of normal alkanes. Analytica Chimica Acta **17**, 97-106.

McAuley W, Lad M, Mader K, Santos P, Tetteh J, Kazarian S, Hadgraft J, Lane M. 2010. ATR-FTIR spectroscopy and spectroscopic imaging of solvent and permeant diffusion across model membranes. European Journal of Pharmaceutics and Biopharmaceutics **74**, 413-419.

McAuley WJ, Mader KT, Tetteh J, Lane ME, Hadgraft J. 2009. Simultaneous monitoring of drug and solvent diffusion across a model membrane using ATR-FTIR spectroscopy. European Journal of Pharmaceutical Sciences **38**, 378-383.

McCarley KD, Bunge AL. 2003. Absorption into silicone rubber membranes from powders and aqueous solutions. International Journal of Pharmaceutics **250**, 169-180.

McMullan PM. 2000. Utility adjuvants. Weed Technology **14**, 792-797.

Merk S, Blume A, Riederer M. 1997. Phase behaviour and crystallinity of plant cuticular waxes studied by Fourier transform infrared spectroscopy. Planta **204**, 44-53.

Michaud F, Ventolà L, Calvet MT, Cuevas-Diarte MA, Solans X, Font-Bardía M. 2000. The γ-form of n-eicosanol. Acta Crystallographica Section C: Crystal Structure Communications **56**, 219-221.

Miller P, Westra P. 1998. Herbicide surfactants and adjuvants. Crop series. Production; no. 0.559.

Mnyukh YV. 1960. The structure of normal paraffins and of their solid solutions. Journal of Structural Chemistry **1**, 346-365.

Moser K, Kriwet K, Froehlich C, Naik A, Kalia YN, Guy RH. 2001. Permeation enhancement of a highly lipophilic drug using supersaturated systems. Journal of Pharmaceutical Sciences **90**, 607-616.

Muehlebach M, Cederbaum F, Cornes D, Friedmann AA, Glock J, Hall G, Indolese AF, Kloer DP, Le Goupil G, Maetzke T. 2011. Aryldiones incorporating a [1, 4, 5] oxadiazepane ring. Part 2: chemistry and biology of the cereal herbicide pinoxaden. Pest Management Science **67**, 1499-1521.

Müller C, Riederer M. 2006. *Biology of the plant cuticle*.

Murphy B, Kirwan P, McLoughlin P. 2003. Study of the impact of penetrant characteristics upon diffusion into Teflon membranes to further assess the performance of an ATR/FTIR sensor. Analytical and Bioanalytical Chemistry **377**, 195-202.

Nalewaja JD. 2002. Oils as and with herbicides. *Spray Oils Beyond 2000: Sustainable Pest and Disease Management: Proceedings of a Conference Held from 25 to 29 October 1999 in Sydney, New South Wales, Australia*: University of Western Sydney, 290.

Pambou E, Hu X, Li Z, Campana M, Hughes A, Li P, Webster JR, Bell G, Lu JR. 2018. Structural features of reconstituted cuticular wax films upon interaction with nonionic surfactant C12E6. Langmuir **34**, 3395-3404.

Patel S, Nelson DR, Gibbs AG. 2001. Chemical and physical analyses of wax ester properties. Journal of Insect Science **1**, 1-7.

Pellett MA, Watkinson AC, Hadgraft J, Brain KR. 1997a. Comparison of permeability data from traditional diffusion cells and ATR-FTIR spectroscopy Part I. Synthetic membrances. International Journal of Pharmaceutics **154**, 205-215.

Pellett MA, Watkinson AC, Hadgraft J, Brain KR. 1997b. Comparison of permeability data from traditional diffusion cells and ATR-FTIR spectroscopy. Part II. Determination of diffusional pathlengths in synthetic membranes and human stratum corneum. International Journal of Pharmaceutics **154**, 217-227.

Penner D. 2000. Activator adjuvants. Weed Technology **14**, 785-791.

Pereira AM, Lopes M, Timmer J, Keurentjes J. 2005. Solvent sorption measurements in polymeric membranes with ATR-IR spectroscopy. Journal of Membrane Science **260**, 174-180.

Perkins MC, Roberts CJ, Briggs D, Davies MC, Friedmann A, Hart C, Bell G. 2005. Macro and microthermal analysis of plant wax/surfactant interactions: plasticizing effects of two alcohol ethoxylated surfactants on an isolated cuticular wax and leaf model. Applied Surface Science **243**, 158-165.

Piringer OG, Baner AL. 2008. *Plastic packaging: interactions with food and pharmaceuticals*: John Wiley & Sons.

Ponder JW, Richards FM. 1987. An efficient newton-like method for molecular mechanics energy minimization of large molecules. Journal of Computational Chemistry **8**, 1016-1024.

Popp C, Burghardt M, Friedmann A, Riederer M. 2005. Characterization of hydrophilic and lipophilic pathways of Hedera helix L. cuticular membranes: permeation of water and uncharged organic compounds. Journal of Experimental Botany **56**, 2797-2806.

Prasad R, Foy C, Crafts A. 1967. Effects of relative humidity on absorption and translocation of foliarly applied dalapon. Weeds **15**, 149-156.

Ramsey R, Stephenson G, Hall J. 2005. A review of the effects of humidity, humectants, and surfactant composition on the absorption and efficacy of highly water-soluble herbicides. Pesticide Biochemistry and Physiology **82**, 162-175.

Räsch A, Hunsche M, Mail M, Burkhardt J, Noga G, Pariyar S. 2018. Agricultural adjuvants may impair leaf transpiration and photosynthetic activity. Plant Physiology and Biochemistry **132**, 229-237.

Rathgeber C, Schmit H, Hiebler S. 2013. Mixtures of alkanes, fatty acids and alcohols as novel phase change materials: preparation and characterization with DSC and T-history. *2nd International Conference on Sustainable Energy Storage in Buildings, Dublin*.

Razeq FM, Kosma DK, Rowland O, Molina I. 2014. Extracellular lipids of Camelina sativa: characterization of chloroform-extractable waxes from aerial and subterranean surfaces. Phytochemistry **106**, 188-196.

Reynhardt E. 1997. The role of hydrogen bonding in the cuticular wax of Hordeum vulgare L. European Biophysics Journal **26**, 195-201.

Reynhardt E, Riederer M. 1991. Structure and molecular dynamics of the cuticular wax from leaves of Citrus aurantium L. Journal of Physics D: Applied Physics **24**, 478.

Reynhardt E, Riederer M. 1994. Structures and molecular dynamics of plant waxes. European Biophysics Journal **23**, 59-70.

Ribeiro da Luz B. 2006. Attenuated total reflectance spectroscopy of plant leaves: a tool for ecological and botanical studies. New Phytologist **172**, 305-318.

Riederer M. 1990. Estimating partitioning and transport of organic chemicals in the foliage/atmosphere system: discussion of a fugacity-based model. Environmental Science & Technology **24**, 829-837.

Riederer M, Burghardt M, Mayer S, Obermeier H, Schoenherr J. 1995. Sorption of monodisperse alcohol ethoxylates and their effects on the mobility of 2, 4-D in isolated plant cuticles. Journal of Agricultural and Food Chemistry **43**, 1067-1075.

Riederer M, Müller C. 2008. *Annual Plant Reviews, Biology of the Plant Cuticle*: John Wiley & Sons.

Riederer M, Schneider G. 1989. Comparative study of the composition of waxes extracted from isolated leaf cuticles and from whole leaves of Citrus: Evidence for selective extraction. Physiologia Plantarum **77**, 373-384.

Riederer M, Schönherr J. 1985. Accumulation and transport of (2, 4-dichlorophenoxy) acetic acid in plant cuticles: II. Permeability of the cuticular membrane. Ecotoxicology and Environmental Safety **9**, 196-208.

Riederer M, Schönherr J. 1990. Effects of surfactants on water permeability of isolated plant cuticles and on the composition of their cuticular waxes. Pesticide Science **29**, 85-94.

Riederer M, Schreiber L. 1995. Waxes: the transport barriers of plant cuticles. In: Hamilton RJ, ed. *Waxes: chemistry, molecular biology and functions*, Vol. 6. Dundee: The Oily Press LTD., 131-155.

Riederer M, Schreiber L. 2001. Protecting against water loss: analysis of the barrier properties of plant cuticles. Journal of Experimental Botany **52**, 2023-2032.

Romonchuk WJ, Bunge AL. 2006. Permeation of 4-cyanophenol and methyl paraben from powder and saturated aqueous solution through silicone rubber membranes and human skin. Journal of Pharmaceutical Sciences **95**, 2526-2533.

Russeau W, Mitchell J, Tetteh J, Lane ME, Hadgraft J. 2009. Investigation of the permeation of model formulations and a commercial ibuprofen formulation in Carbosil® and human skin using ATR-FTIR and multivariate spectral analysis. International Journal of Pharmaceutics **374**, 17-25.

Sammon C, Mura C, Yarwood J, Everall N, Swart R, Hodge D. 1998. FTIR− ATR studies of the structure and dynamics of water molecules in polymeric matrixes. A comparison of PET and PVC. The Journal of Physical Chemistry B **102**, 3402-3411.

Sangster J. 1997. *Octanol-water partition coefficients: fundamentals and physical chemistry*: John Wiley & Sons.

Santier S, Chamel A. 1996. Penetration of triolein and methyl oleate through isolated plant cuticles and their effect on penetration of [14C] quizalofop-ethyl and [14C] fenoxaprop-ethyl. Weed Research **36**, 167-174.

Santos MC, Bendiksen B, Elabd YA. 2017. Diffusion of liquid water in free-standing polymer films using pressure-contact time-resolved fourier transform infrared attenuated total reflectance spectroscopy. Industrial & Engineering Chemistry Research **56**, 3464-3476.

Saunders R, Lonnecker W. 1967. Physiological aspects of using nonphytotoxic oils with herbicides. *Proceedings North Central Control Conference*, Vol. 21, 62-73.

Schick MJ. 1987. *Nonionic surfactants: physical chemistry*: CRC Press.

Schönherr J. 1976. Water permeability of isolated cuticular membranes: the effect of cuticular waxes on diffusion of water. Planta **131**, 159-164.

Schönherr J. 1993a. Effects of alcohols, glycols and monodisperse ethoxylated alcohols on mobility of 2, 4-D in isolated plant cuticles. Pesticide Science **39**, 213-223.

Schönherr J. 1993b. Effects of monodisperse alcohol ethoxylates on mobility of 2, 4-D in isolated plant cuticles. Pesticide Science **38**, 155-164.

Schönherr J. 2006. Characterization of aqueous pores in plant cuticles and permeation of ionic solutes. Journal of Experimental Botany **57**, 2471-2491.

Schönherr J, Baur P. 1994. Modelling penetration of plant cuticles by crop protection agents and effects of adjuvants on their rates of penetration. Pesticide Science **42**, 185-208.

Schönherr J, Baur P. 1996. Effects of temperature, surfactants and other adjuvants on rates of uptake of organic compounds. Plant Cuticles, 135-155.

Schönherr J, Riederer M. 1988. Desorption of chemicals from plant cuticles: evidence for asymmetry. Archives of Environmental Contamination and Toxicology **17**, 13-19.

Schönherr J, Riederer M, Schreiber L, Bauer H. 1991. Foliar uptake of pesticides and its activation by adjuvants: Theories and methods for optimization. Pesticide chemistry. VCH Verlag Chemie Weilheim, D.

Schönherr J, Schreiber L, Buchholz A. 2001. Effects of temperature and concentration of the accelerators ethoxylated alcohols, diethyl suberate and tributyl phosphate on the mobility of [14C] 2, 4-dichlorophenoxy butyric acid in plant cuticles. Pest Management Science: formerly Pesticide Science **57**, 17-24.

Schreiber L. 1995. A mechanistic approach towards surfactant/wax interactions: effects of octaethyleneglycolmonododecylether on sorption and diffusion of organic chemicals in reconstituted cuticular wax of barley leaves. Pesticide Science **45**, 1-11.

Schreiber L. 2005. Polar paths of diffusion across plant cuticles: new evidence for an old hypothesis. Annals of Botany **95**, 1069-1073.

Schreiber L. 2006. Review of sorption and diffusion of lipophilic molecules in cuticular waxes and the effects of accelerators on solute mobilities. Journal of Experimental Botany **57**, 2515-2523.

Schreiber L, Kirsch T, Riederer M. 1996a. Transport properties of cuticular waxes of Fagus sylvatica L. and Picea abies (L.) Karst.: estimation of size selectivity and tortuosity from diffusion coefficients of aliphatic molecules. Planta **198**, 104-109.

Schreiber L, Riederer M. 1996a. Determination of diffusion coefficients of octadecanoic acid in isolated cuticular waxes and their relationship to cuticular water permeabilities. Plant, Cell & Environment **19**, 1075-1082.

Schreiber L, Riederer M. 1996b. Ecophysiology of cuticular transpiration: comparative investigation of cuticular water permeability of plant species from different habitats. Oecologia **107**, 426-432.

Schreiber L, Riederer M, Schorn K. 1996b. Mobilities of organic compounds in reconstituted cuticular wax of barley leaves: effects of monodisperse alcohol ethoxylates on diffusion of pentachlorophenol and tetracosanoic acid. Pesticide Science **48**, 117-124.

Schreiber L, Schönherr J. 1992. Analysis of foliar uptake of pesticides in barley leaves: role of epicuticular waxes and compartmentation. Pesticide Science **36**, 213-221.

Schreiber L, Schönherr J. 1993. Mobilities of organic compounds in reconstituted cuticular wax of barley leaves: determination of diffusion coefficients. Pesticide Science **38**, 353-361.

Schreiber L, Schönherr J. 2009. *Water and solute permeability of plant cuticles*: Springer Berlin, Heidelberg.

Schreiber L, Schorn K, Heimburg T. 1997. 2H NMR study of cuticular wax isolated from Hordeum vulgare L. leaves: identification of amorphous and crystalline wax phases. European Biophysics Journal **26**, 371-380.

Schuster A-C, Burghardt M, Alfarhan A, Bueno A, Hedrich R, Leide J, Thomas J, Riederer M. 2016. Effectiveness of cuticular transpiration barriers in a desert plant at controlling water loss at high temperatures. AoB Plants **8**, plw027.

Serrano M, Coluccia F, Torres M, L'Haridon F, Métraux J-P. 2014. The cuticle and plant defense to pathogens. Frontiers in Plant Science **5**, 274.

Seufert P. 2020. Chemical and physical structure of the barrier against water transpiration of leaves: Contribution of different wax compounds, Universität Würzburg.

Shaheenuzzamn M, Liu T, Shi S, Wu H, Wang Z. 2019. Research advances on cuticular waxes biosynthesis in crops: A review. International Journal of Agriculture And Biology **21**, 911-921.

Shahzad I, Wittchen S, Cepus V. 2019. In Situ Migration Analysis and Diffusion Coefficient Determination of Bio-Based Plasticizer From NBR Using FTIR-ATR and Estimation of Migrated Plasticizer Contents by TGA Analysis. Macromolecular Symposia **384**, 1800158.

Shepherd T, Robertson G, Griffiths D. 1995. Compositional analysis of intact alkyl esters in leaf epicuticular wax of swede by capillary gas chromatography and electron-impact mass spectrometry. Phytochemical Analysis **6**, 65-73.

Shepherd T, Wynne Griffiths D. 2006. The effects of stress on plant cuticular waxes. New Phytologist **171**, 469-499.

Shi T, Schönherr J, Schreiber L. 2005a. Accelerators increase permeability of cuticles for the lipophilic solutes metribuzin and iprovalicarb but not for hydrophilic methyl glucose. Journal of Agricultural and Food Chemistry **53**, 2609-2615.

Shi T, Simanova E, Schönherr J, Schreiber L. 2005b. Effects of accelerators on mobility of 14C-2, 4-dichlorophenoxy butyric acid in plant cuticles depends on type and concentration of accelerator. Journal of Agricultural and Food Chemistry **53**, 2207-2212.

Šimáňová E, Shi T, Schönherr J, Schreiber L. 2005. Sorption in reconstituted waxes of homologous series of alcohol ethoxylates and n-alkyl esters and their effects on the mobility of 2, 4-dichlorophenoxybutyric acid. Pest Management Science: formerly Pesticide Science **61**, 383-389.

Sitte P, Rennier R. 1963. Untersuchungen an cuticularen Zellwandschichten. Planta **60**, 19-40.

Smirnova A, Leide J, Riederer M. 2013. Deficiency in a very-long-chain fatty acid β-ketoacyl-coenzyme a synthase of tomato impairs microgametogenesis and causes floral organ fusion. Plant Physiology **161**, 196-209.

Staiger S. 2022. Chemical and physical nature of the barrier against active ingredient penetration into leaves: effects of adjuvants on the cuticular diffusion barrier, Universität Würzburg.

Staiger S, Seufert P, Arand K, Burghardt M, Popp C, Riederer M. 2019. The permeation barrier of plant cuticles: uptake of active ingredients is limited by very long-chain aliphatic rather than cyclic wax compounds. Pest Management Science **75**, 3405-3412.

Stannett V, Ranade G, Koros W. 1982. Characterization of water vapor transport in glassy polyacrylonitrile by combined permeation and sorption techniques. Journal of Membrane Science **10**, 219-233.

Stevens PJ, Bukovac MJ. 1987a. Studies on octylphenoxy surfactants. Part 1: effects of oxyethylene content on properties of potential relevance to foliar absorption. Pesticide Science **20**, 19-35.

Stevens PJ, Bukovac MJ. 1987b. Studies on octylphenoxy surfactants. Part 2: Effects on foliar uptake and translocation. Pesticide Science **20**, 37-52.

Stock D, Edgerton BM, Gaskin RE, Holloway PJ. 1992. Surfactant-enhanced foliar uptake of some organic compounds: Interactions with two model polyoxyethylene aliphatic alcohols. Pesticide Science **34**, 233-242.

Stock D, Holloway PJ. 1993. Possible mechanisms for surfactant-induced foliar uptake of agrochemicals. Pesticide Science **38**, 165-177.

Stock D, Holloway PJ, Grayson BT, Whitehouse P. 1993. Development of a predictive uptake model to rationalise selection of polyoxyethylene surfactant adjuvants for foliage-applied agrochemicals. Pesticide Science **37**, 233-245.

Stoytcheva M. 2011. *Pesticides: Formulations, effects, fate*: BoD–Books on Demand.

Sümmchen P, Markstädter C, Wienhaus O. 1995. Esters of Picea abies needle cuticular wax. Phytochemistry **40**, 599-600.

Sutandar P, Ahn DJ, Franses EI. 1994. FTIR ATR analysis for microstructure and water uptake in poly (methyl methacrylate) spin cast and Langmuir-Blodgett thin films. Macromolecules **27**, 7316-7328.

Szafranek BM, Synak EE. 2006. Cuticular waxes from potato (Solanum tuberosum) leaves. Phytochemistry **67**, 80-90.

Tada A, Ishizuki K, Yamazaki T, Sugimoto N, Akiyama H. 2014. Method for the determination of natural ester-type gum bases used as food additives via direct analysis of their constituent wax esters using high-temperature GC/MS. Food Science & Nutrition **2**, 417-425.

Tanaka H, Machida Y. 2008. 10 The cuticle and cellular interactions. Annual Plant Reviews, Biology of the Plant Cuticle **23**, 312.

Tanaka K, Seto T, Watanabe A, Hayashida T. 1959. Phase Transformation of n-Higher Alcohols.(II). Bulletin of the Institute for Chemical Research, Kyoto University **37**, 281-293.

Tsubaki S, Sugimura K, Teramoto Y, Yonemori K, Azuma J-i. 2013. Cuticular membrane of Fuyu persimmon fruit is strengthened by triterpenoid nano-fillers. PLoS One **8**.

Tu M, Hurd C, Randall JM. 2001. Weed control methods handbook: tools & techniques for use in natural areas.

Tu M, Randall J. 2003. Adjuvants. TU, M. et al. Weed control methods handbook the nature conservancy. Davis: TNC, 1-24.

Tukey Jr H. 1970. The leaching of substances from plants. Annual Review of Plant Physiology **21**, 305-324.

Van Alsten JG, Lustig SR. 1992. Polymer mutual diffusion measurements using infrared ATR spectroscopy. Macromolecules **25**, 5069-5073.

Van Esch G, Organization WH. 2000. *Flame retardants: tris (2-butoxyethyl) phosphate, tris (2-ethylhexyl) phosphate, tetrakis (hydroxymethyl) phosphonium salts*: World Health Organization.

Vasconcelos KL, Bhasin A, Little DN. 2010. Measurement of water diffusion in asphalt binders using Fourier transform infrared–attenuated total reflectance. Transportation Research Record **2179**, 29-38.

Ventolà L, Calvet T, Cuevas-Diarte M, Solans X, Mondieig D, Négrier P, van Miltenburg J. 2003. Solid state equilibrium in the n-alkanols family: the stability of binary mixed samples. Physical Chemistry Chemical Physics **5**, 947-952.

Vieth WR. 1991. *Diffusion in and through polymers: principles and applications*. New York: Hanser.

Vogg G, Fischer S, Leide J, Emmanuel E, Jetter R, Levy AA, Riederer M. 2004. Tomato fruit cuticular waxes and their effects on transpiration barrier properties: functional characterization of a mutant deficient in a very-long-chain fatty acid β-ketoacyl-CoA synthase. Journal of Experimental Botany **55**, 1401-1410.

Wang C, Liu Z. 2007. Foliar uptake of pesticides—present status and future challenge. Pesticide Biochemistry and Physiology **87**, 1-8.

Wang M, Wu P, Sengupta SS, Chadhary BI, Cogen JM, Li B. 2011a. Investigation of water diffusion in low-density polyethylene by attenuated total reflectance fourier transform infrared spectroscopy and two-dimensional correlation analysis. Industrial & Engineering Chemistry Research **50**, 6447-6454.

Wang Z, Guhling O, Yao R, Li F, Yeats TH, Rose JK, Jetter R. 2011b. Two oxidosqualene cyclases responsible for biosynthesis of tomato fruit cuticular triterpenoids. Plant Physiology **155**, 540-552.

Watanabe A. 1963. The synthesis and the physical properties of normal higher primary alcohols. V. Thermal and X-ray studies of the polymorphism of alcohols of odd carbon numbers from undecanol to heptatriacontanol. Bulletin of the Chemical Society of Japan **36**, 336-340.

Webster GR, Bisset NB, Cahill DM, Jones P, Killick A, Hawley A, Boyd BJ. 2018. Tristearin as a Model Cuticle for High-Throughput Screening of Agricultural Adjuvant Systems. ACS Omega **3**, 16672-16680.

Wolska KI, Grudniak AM, Fiecek B, Kraczkiewicz-Dowjat A, Kurek A. 2010. Antibacterial activity of oleanolic and ursolic acids and their derivatives. Central European Journal of Biology **5**, 543-553.

Yeats TH, Rose JK. 2013. The formation and function of plant cuticles. Plant Physiology **163**, 5-20.

Yi X, Nerbonne K, Pellegrino J. 2002. Diffusion measurements using FT-IR ATR spectroscopy: Lubricant diffusion in polypropylene. Applied Spectroscopy **56**, 509-514.

Zaki O, Abbes B, Safa L. 2009. Non-Fickian diffusion of amyl acetate in polypropylene packaging: Experiments and modelling. Polymer Testing **28**, 315-323.

Zeisler-Diehl V, Müller Y, Schreiber L. 2018. Epicuticular wax on leaf cuticles does not establish the transpiration barrier, which is essentially formed by intracuticular wax. Journal of Plant Physiology **227**, 66-74.

Zeisler V, Schreiber L. 2016. Epicuticular wax on cherry laurel (Prunus laurocerasus) leaves does not constitute the cuticular transpiration barrier. Planta **243**, 65-81.

Zerbi G, Gallino G, Del Fanti N, Baini L. 1989. Structural depth profiling in polyethylene films by multiple internal reflection infra-red spectroscopy. Polymer **30**, 2324-2327.

Zhang Y, Adams MJ, Zhang Z, Vidoni O, Leuenberger BH, Achkar J. 2016. Plasticisation of carnauba wax with generally recognised as safe (GRAS) additives. Polymer **86**, 208-219.

8 Appendix

Appendix 1. Fitting parameters of logistic model to ATR-FTIR specific phase transition curves of candelilla/policosanol and candelilla/rice bran wax blends.

wax composition	A1	A2	x0	p-value	r^2
0 % policosanol	2915.82921	2921.89518	64.88103	148.14223	0.99834
10% policosanol	2915.85379	2922.14428	67.4802	36.73469	0.99723
20% policosanol	2915.7874	2921.87617	68.07475	36.18343	0.99648
30% policosanol	2915.75041	2921.9325	67.89112	30.6558	0.99638
40% policosanol	2916.06103	2922.57905	70.85349	26.1377	0.99494
50% policosanol	2916.2312	2922.88953	72.88103	26.49829	0.99261
60% policosanol	2916.51919	2922.79918	75.6178	30.17985	0.98794
70% policosanol	2916.29252	2921.85229	77.42321	39.95086	0.98236
80% policosanol	2916.22983	2921.78202	78.86693	66.15519	0.9819
90% policosanol	2916.24151	2921.68596	80.38242	134.95593	0.98393
100% policosanol	2916.16362	2921.21454	80.29194	108.39115	0.9963
0 % rice bran	2915.82921	2921.89518	64.88103	148.14223	0.99834
10% rice bran	2915.87671	2921.91352	65.80055	50.54901	0.99634
20% rice bran	2915.8913	2921.96373	66.03037	45.23908	0.99844
30% rice bran	2916.01152	2922.05182	66.09058	37.40265	0.99832
40% rice bran	2915.92108	2921.99665	69.11359	27.26573	0.99875
50% rice bran	2915.95081	2921.92144	67.54204	33.74433	0.99864
60% rice bran	2916.07429	2922.13068	71.36815	27.44234	0.99636
70% rice bran	2916.02961	2921.85616	70.01047	32.53135	0.99677
80% rice bran	2916.34892	2922.21131	75.84333	44.76754	0.99011
100% rice bran	2915.97176	2921.62239	69.52366	120.41476	0.99693

Appendix 2. Two-way ANOVA ($p < 0.05$) of (log) diffusion coefficient analysis of CNP in adjuvant treated candelilla and carnauba wax.

	DF	Sum of Squares	Mean Square	F Value	P Value
wax	1	4.04258	4.04258	133.06868	1.49E-12
adjuvant	4	0.46453	0.11613	3.82268	0.01257
Interaction	4	3.26242	0.8156	26.84703	1.56E-09
Model	9	7.76952	0.86328	28.41639	2.63E-12
Error	30	0.91139	0.03038		
Corrected Total	39	8.68092			

Appendix 3. Tukeys post-hoc test analysis ($p < 0.05$) of (log) CNP diffusion coefficients in candelilla and carnauba wax after adjuvant treatment.

wax	adjuvant	wax	adjuvant	MeanDiff	q Value	Sig	LCL	UCL
Candelilla	TEHP	Candelilla	MeO	-0.52304	6.00165	1	-0.94346	-0.10262
Candelilla	C12E2	Candelilla	MeO	-0.72918	8.36706	1	-1.1496	-0.30876
Candelilla	C12E2	Candelilla	TEHP	-0.20614	2.36541	0	-0.62656	0.21428
Candelilla	C12E4	Candelilla	MeO	-0.76916	8.82582	1	-1.18958	-0.34874
Candelilla	C12E4	Candelilla	TEHP	-0.24612	2.82417	0	-0.66654	0.1743
Candelilla	C12E4	Candelilla	C12E2	-0.03998	0.45876	0	-0.4604	0.38044
Candelilla	C12E6	Candelilla	MeO	-0.86315	9.90434	1	-1.28357	-0.44273
Candelilla	C12E6	Candelilla	TEHP	-0.34011	3.90269	0	-0.76053	0.0803
Candelilla	C12E6	Candelilla	C12E2	-0.13397	1.53728	0	-0.55439	0.28645
Candelilla	C12E6	Candelilla	C12E4	-0.09399	1.07852	0	-0.51441	0.32643
Carnauba	MeO	Candelilla	MeO	-0.48179	5.52831	1	-0.9022	-0.06137
Carnauba	MeO	Candelilla	TEHP	0.04125	0.47333	0	-0.37917	0.46167
Carnauba	MeO	Candelilla	C12E2	0.24739	2.83875	0	-0.17303	0.66781
Carnauba	MeO	Candelilla	C12E4	0.28737	3.29751	0	-0.13305	0.70779
Carnauba	MeO	Candelilla	C12E6	0.38137	4.37603	0	-0.03905	0.80178
Carnauba	TEHP	Candelilla	MeO	0.35602	4.08523	0	-0.0644	0.77644
Carnauba	TEHP	Candelilla	TEHP	0.87906	10.08688	1	0.45864	1.29948
Carnauba	TEHP	Candelilla	C12E2	1.0852	12.45229	1	0.66478	1.50562
Carnauba	TEHP	Candelilla	C12E4	1.12518	12.91105	1	0.70476	1.5456
Carnauba	TEHP	Candelilla	C12E6	1.21917	13.98957	1	0.79876	1.63959
Carnauba	TEHP	Carnauba	MeO	0.83781	9.61354	1	0.41739	1.25823
Carnauba	C12E2	Candelilla	MeO	-0.00404	0.04632	0	-0.42446	0.41638
Carnauba	C12E2	Candelilla	TEHP	0.519	5.95533	1	0.09858	0.93942
Carnauba	C12E2	Candelilla	C12E2	0.72514	8.32074	1	0.30472	1.14556
Carnauba	C12E2	Candelilla	C12E4	0.76512	8.7795	1	0.3447	1.18554
Carnauba	C12E2	Candelilla	C12E6	0.85911	9.85802	1	0.4387	1.27953
Carnauba	C12E2	Carnauba	MeO	0.47775	5.48199	1	0.05733	0.89817
Carnauba	C12E2	Carnauba	TEHP	-0.36006	4.13155	0	-0.78048	0.06036
Carnauba	C12E4	Candelilla	MeO	0.31791	3.64786	0	-0.10251	0.73833
Carnauba	C12E4	Candelilla	TEHP	0.84094	9.64951	1	0.42052	1.26136
Carnauba	C12E4	Candelilla	C12E2	1.04709	12.01492	1	0.62667	1.46751
Carnauba	C12E4	Candelilla	C12E4	1.08707	12.47368	1	0.66665	1.50749
Carnauba	C12E4	Candelilla	C12E6	1.18106	13.5522	1	0.76064	1.60148
Carnauba	C12E4	Carnauba	MeO	0.79969	9.17617	1	0.37927	1.22011
Carnauba	C12E4	Carnauba	TEHP	-0.03812	0.43737	0	-0.45854	0.3823
Carnauba	C12E4	Carnauba	C12E2	0.32194	3.69418	0	-0.09848	0.74236
Carnauba	C12E6	Candelilla	MeO	0.10643	1.22126	0	-0.31399	0.52685
Carnauba	C12E6	Candelilla	TEHP	0.62947	7.22291	1	0.20905	1.04989
Carnauba	C12E6	Candelilla	C12E2	0.83561	9.58832	1	0.41519	1.25603
Carnauba	C12E6	Candelilla	C12E4	0.87559	10.04708	1	0.45517	1.29601
Carnauba	C12E6	Candelilla	C12E6	0.96958	11.1256	1	0.54916	1.39
Carnauba	C12E6	Carnauba	MeO	0.58822	6.74957	1	0.1678	1.00864
Carnauba	C12E6	Carnauba	TEHP	-0.24959	2.86397	0	-0.67001	0.17083
Carnauba	C12E6	Carnauba	C12E2	0.11047	1.26758	0	-0.30995	0.53089
Carnauba	C12E6	Carnauba	C12E4	-0.21148	2.4266	0	-0.63189	0.20894

Appendix 4. Two-way ANOVA ($p < 0.05$) of (log) partition coefficient analysis of CNP in adjuvant treated candelilla and carnauba wax.

	DF	Sum of Squares	Mean Square	F Value	P Value
wax	1	0.71424	0.71424	270.80738	1.46E-16
adjuvant	4	2.55459	0.63865	242.1468	2.28E-22
Interaction	4	0.20501	0.05125	19.43246	5.55E-08
Model	9	3.47384	0.38598	146.34716	2.78E-22
Error	30	0.07912	0.00264		
Corrected Total	39	3.55296			

Appendix 5. Tukeys post-hoc test analysis ($p < 0.05$) of (log) CNP partition coefficients in candelilla and carnauba wax after adjuvant treatment.

wax	adjuvant	wax	adjuvant	MeanDiff	q Value	Sig	LCL	UCL
Candelilla	TEHP	Candelilla	MeO	-0.00794	0.0902	0	-0.4327	0.41681
Candelilla	C12E2	Candelilla	MeO	-0.05421	0.61565	0	-0.47896	0.37055
Candelilla	C12E2	Candelilla	TEHP	-0.04626	0.52545	0	-0.47102	0.37849
Candelilla	C12E4	Candelilla	MeO	-0.06779	0.76994	0	-0.49255	0.35696
Candelilla	C12E4	Candelilla	TEHP	-0.05985	0.67974	0	-0.4846	0.36491
Candelilla	C12E4	Candelilla	C12E2	-0.01358	0.15429	0	-0.43834	0.41117
Candelilla	C12E6	Candelilla	MeO	-0.17275	1.96203	0	-0.59751	0.252
Candelilla	C12E6	Candelilla	TEHP	-0.16481	1.87183	0	-0.58956	0.25994
Candelilla	C12E6	Candelilla	C12E2	-0.11855	1.34638	0	-0.5433	0.30621
Candelilla	C12E6	Candelilla	C12E4	-0.10496	1.19209	0	-0.52971	0.31979
Carnauba	MeO	Candelilla	MeO	-0.70244	7.97795	1	-1.12719	-0.27768
Carnauba	MeO	Candelilla	TEHP	-0.6945	7.88774	1	-1.11925	-0.26974
Carnauba	MeO	Candelilla	C12E2	-0.64823	7.3623	1	-1.07299	-0.22348
Carnauba	MeO	Candelilla	C12E4	-0.63465	7.20801	1	-1.0594	-0.20989
Carnauba	MeO	Candelilla	C12E6	-0.52969	6.01592	1	-0.95444	-0.10493
Carnauba	TEHP	Candelilla	MeO	0.73983	8.40259	1	0.31507	1.16458
Carnauba	TEHP	Candelilla	TEHP	0.74777	8.49279	1	0.32301	1.17252
Carnauba	TEHP	Candelilla	C12E2	0.79403	9.01824	1	0.36928	1.21879
Carnauba	TEHP	Candelilla	C12E4	0.80762	9.17253	1	0.38286	1.23237
Carnauba	TEHP	Candelilla	C12E6	0.91258	10.36462	1	0.48782	1.33733
Carnauba	TEHP	Carnauba	MeO	1.44226	16.38054	1	1.01751	1.86702
Carnauba	C12E2	Candelilla	MeO	0.41793	4.74661	0	-0.00683	0.84268
Carnauba	C12E2	Candelilla	TEHP	0.42587	4.83681	1	0.00111	0.85062
Carnauba	C12E2	Candelilla	C12E2	0.47213	5.36226	1	0.04738	0.89689
Carnauba	C12E2	Candelilla	C12E4	0.48572	5.51654	1	0.06096	0.91047
Carnauba	C12E2	Candelilla	C12E6	0.59068	6.70864	1	0.16592	1.01543
Carnauba	C12E2	Carnauba	MeO	1.12036	12.72455	1	0.69561	1.54512
Carnauba	C12E2	Carnauba	TEHP	-0.3219	3.65598	0	-0.74665	0.10285
Carnauba	C12E4	Candelilla	MeO	0.52133	5.92105	1	0.09658	0.94609
Carnauba	C12E4	Candelilla	TEHP	0.52928	6.01126	1	0.10452	0.95403
Carnauba	C12E4	Candelilla	C12E2	0.57554	6.5367	1	0.15079	1.00029
Carnauba	C12E4	Candelilla	C12E4	0.58912	6.69099	1	0.16437	1.01388
Carnauba	C12E4	Candelilla	C12E6	0.69409	7.88308	1	0.26933	1.11884
Carnauba	C12E4	Carnauba	MeO	1.22377	13.899	1	0.79902	1.64853
Carnauba	C12E4	Carnauba	TEHP	-0.21849	2.48154	0	-0.64325	0.20626

Carnauba	C12E4	Carnauba	C12E2	0.10341	1.17445	0	-0.32135	0.52816
Carnauba	C12E6	Candelilla	MeO	0.65004	7.38285	1	0.22529	1.07479
Carnauba	C12E6	Candelilla	TEHP	0.65798	7.47305	1	0.23323	1.08274
Carnauba	C12E6	Candelilla	C12E2	0.70425	7.9985	1	0.27949	1.129
Carnauba	C12E6	Candelilla	C12E4	0.71783	8.15278	1	0.29308	1.14259
Carnauba	C12E6	Candelilla	C12E6	0.82279	9.34488	1	0.39804	1.24755
Carnauba	C12E6	Carnauba	MeO	1.35248	15.36079	1	0.92772	1.77723
Carnauba	C12E6	Carnauba	TEHP	-0.08979	1.01975	0	-0.51454	0.33497
Carnauba	C12E6	Carnauba	C12E2	0.23211	2.63624	0	-0.19264	0.65687
Carnauba	C12E6	Carnauba	C12E4	0.12871	1.46179	0	-0.29605	0.55346

Appendix 6. Two-way ANOVA ($p < 0.05$) of (log) permeability coefficient analysis of CNP in adjuvant treated candelilla and carnauba wax.

	DF	**Sum of Squares**	**Mean Square**	**F Value**	**P Value**
wax	1	1.489	1.489	48.01784	1.07E-07
adjuvant	4	2.48856	0.62214	20.06291	3.96E-08
Interaction	4	3.11008	0.77752	25.07367	3.40E-09
Model	9	7.08764	0.78752	25.39602	1.13E-11
Error	30	0.93028	0.03101		
Corrected Total	39	8.01792			

Appendix 7. Tukeys post-hoc test analysis ($p < 0.05$) of (log) CNP permeability coefficients in candelilla and carnauba wax after adjuvant treatment.

wax	**adjuvant**	**wax**	**adjuvant**	**MeanDiff**	**q Value**	**Sig**	**LCL**	**UCL**
Candelilla	TEHP	Candelilla	MeO	-0.00794	0.0902	0	-0.4327	0.41681
Candelilla	C12E2	Candelilla	MeO	-0.05421	0.61565	0	-0.47896	0.37055
Candelilla	C12E2	Candelilla	TEHP	-0.04626	0.52545	0	-0.47102	0.37849
Candelilla	C12E4	Candelilla	MeO	-0.06779	0.76994	0	-0.49255	0.35696
Candelilla	C12E4	Candelilla	TEHP	-0.05985	0.67974	0	-0.4846	0.36491
Candelilla	C12E4	Candelilla	C12E2	-0.01358	0.15429	0	-0.43834	0.41117
Candelilla	C12E6	Candelilla	MeO	-0.17275	1.96203	0	-0.59751	0.252
Candelilla	C12E6	Candelilla	TEHP	-0.16481	1.87183	0	-0.58956	0.25994
Candelilla	C12E6	Candelilla	C12E2	-0.11855	1.34638	0	-0.5433	0.30621
Candelilla	C12E6	Candelilla	C12E4	-0.10496	1.19209	0	-0.52971	0.31979
Carnauba	MeO	Candelilla	MeO	-0.70244	7.97795	1	-1.12719	-0.27768
Carnauba	MeO	Candelilla	TEHP	-0.6945	7.88774	1	-1.11925	-0.26974
Carnauba	MeO	Candelilla	C12E2	-0.64823	7.3623	1	-1.07299	-0.22348
Carnauba	MeO	Candelilla	C12E4	-0.63465	7.20801	1	-1.0594	-0.20989
Carnauba	MeO	Candelilla	C12E6	-0.52969	6.01592	1	-0.95444	-0.10493
Carnauba	TEHP	Candelilla	MeO	0.73983	8.40259	1	0.31507	1.16458
Carnauba	TEHP	Candelilla	TEHP	0.74777	8.49279	1	0.32301	1.17252
Carnauba	TEHP	Candelilla	C12E2	0.79403	9.01824	1	0.36928	1.21879
Carnauba	TEHP	Candelilla	C12E4	0.80762	9.17253	1	0.38286	1.23237
Carnauba	TEHP	Candelilla	C12E6	0.91258	10.36462	1	0.48782	1.33733
Carnauba	TEHP	Carnauba	MeO	1.44226	16.38054	1	1.01751	1.86702
Carnauba	C12E2	Candelilla	MeO	0.41793	4.74661	0	-0.00683	0.84268
Carnauba	C12E2	Candelilla	TEHP	0.42587	4.83681	1	0.00111	0.85062
Carnauba	C12E2	Candelilla	C12E2	0.47213	5.36226	1	0.04738	0.89689

Carnauba	C12E2	Candelilla	C12E4	0.48572	5.51654	1	0.06096	0.91047
Carnauba	C12E2	Candelilla	C12E6	0.59068	6.70864	1	0.16592	1.01543
Carnauba	C12E2	Carnauba	MeO	1.12036	12.72455	1	0.69561	1.54512
Carnauba	C12E2	Carnauba	TEHP	-0.3219	3.65598	0	-0.74665	0.10285
Carnauba	C12E4	Candelilla	MeO	0.52133	5.92105	1	0.09658	0.94609
Carnauba	C12E4	Candelilla	TEHP	0.52928	6.01126	1	0.10452	0.95403
Carnauba	C12E4	Candelilla	C12E2	0.57554	6.5367	1	0.15079	1.00029
Carnauba	C12E4	Candelilla	C12E4	0.58912	6.69099	1	0.16437	1.01388
Carnauba	C12E4	Candelilla	C12E6	0.69409	7.88308	1	0.26933	1.11884
Carnauba	C12E4	Carnauba	MeO	1.22377	13.899	1	0.79902	1.64853
Carnauba	C12E4	Carnauba	TEHP	-0.21849	2.48154	0	-0.64325	0.20626
Carnauba	C12E4	Carnauba	C12E2	0.10341	1.17445	0	-0.32135	0.52816
Carnauba	C12E6	Candelilla	MeO	0.65004	7.38285	1	0.22529	1.07479
Carnauba	C12E6	Candelilla	TEHP	0.65798	7.47305	1	0.23323	1.08274
Carnauba	C12E6	Candelilla	C12E2	0.70425	7.9985	1	0.27949	1.129
Carnauba	C12E6	Candelilla	C12E4	0.71783	8.15278	1	0.29308	1.14259
Carnauba	C12E6	Candelilla	C12E6	0.82279	9.34488	1	0.39804	1.24755
Carnauba	C12E6	Carnauba	MeO	1.35248	15.36079	1	0.92772	1.77723
Carnauba	C12E6	Carnauba	TEHP	-0.08979	1.01975	0	-0.51454	0.33497
Carnauba	C12E6	Carnauba	C12E2	0.23211	2.63624	0	-0.19264	0.65687
Carnauba	C12E6	Carnauba	C12E4	0.12871	1.46179	0	-0.29605	0.55346

Appendix 8. Parameters of 4-cyanophenol diffusion in candelilla and carnauba wax after adjuvant treatment.

		Candelilla wax				Carnauba wax			
Adjuvant	**measure no.**	**D x 10^{14} (m^2 s^{-1})**	**A_{eq} (au)**	**L x 10^6 (m)**	**r^2**	**D x 10^{14} (m^2 s^{-1})**	**A_{eq} (au)**	**L x 10^6 (m)**	**r^2**
Methyl oleate	1	9.73	1.17	6.17	0.989	5.17	0.68	6.50	0.998
	2	8.98	1.05	5.86	0.996	3.83	0.65	8.02	0.998
	3	14.9	1.14	5.55	0.994	5.10	0.76	7.87	0.995
	4	47.1	1.08	6.17	0.997	7.16	0.60	7.10	0.995
	Median	**12.23**	**1.11**	**6.02**	**n.a.**	**5.13**	**0.67**	**7.50**	**n.a.**
	25^{th} – 75^{th} quartile	9.35 – 30.99	1.07 – 1.16	5.71 – 6.17	n.a.	4.46 – 6.17	0.63 – 0.72	6.80 – 7.95	n.a.
TEHP	1	4.54	2.98	6.01	0.998	19.05	3.46	7.76	0.994
	2	7.59	4.19	5.55	0.996	68.59	2.19	7.72	0.999
	3	5.75	3.92	5.57	0.996	33.21	2.92	7.25	0.996
	4	2.98	3.05	5.40	0.982	37.42	2.40	7.56	0.999
	Median	**5.14[a]**	**3.49**	**5.56**	**n.a.**	**35.31**	**2.66**	**7.64**	**n.a.**
	25^{th} – 75^{th} quartile	3.76 – 6.67	3.02 – 4.06	5.48 – 5.79	n.a.	26.13 – 53.00	2.30 – 3.19	7.41 – 7.74	n.a.
C12E2	1	5.41	5.36	5.55	0.986	11.34	2.51	8.02	0.996

	2	1.74	5.82	5.55	0.999	20.89	2.12	8.18	0.973
	3	1.98	4.89	5.40	0.996	29.01	1.67	8.17	0.992
	4	3.90	5.18	5.86	0.978	41.85	1.74	8.80	0.992
	Median	**2.94**	**5.27**	**5.55**	**n.a.**	**24.95**	**1.93**	**8.18**	**n.a.**
	25^{th} – 75^{th} quartile	1.86 – 4.66	5.04 – 5.59	5.48 – 5.71	n.a.	16.12 – 35.43	1.71 – 2.32	8.10 – 8.50	n.a.
C12E4	1	2.45	6.52	5.86	0.987	31.12	2.03	9.26	0.998
	2	3.68	5.61	5.55	0.996	30.25	1.71	8.33	0.995
	3	2.26	5.00	5.71	0.983	29.01	1.67	8.17	0.992
	4	2.52	5.4	6.02	0.996	41.85	1.74	8.80	0.992
	Median	**2.49**	**5.51**	**5.79**	**n.a.**	**30.69**	**1.73**	**8.57**	**n.a.**
	25^{th} – 75^{th} quartile	2.36 – 3.10	5.20 – 6.07	5.63 – 5.94	n.a.	29.63 – 36.49	1.69 – 1.89	8.25 – 9.03	n.a.
C12E6	1	2.20	6.16	5.40	0.950	17.71	3.69	9.40	0.998
	2	2.38	5.54	5.40	0.981	26.41	3.57	9.57	0.995
	3	2.50	5.14	5.86	0.982	19.42	4.27	9.10	0.997
	4	1.65	5.09	5.40	0.963	18.00	4.10	8.02	0.993
	Median	**2.29**	**5.40**	**6.02**	**n.a.**	**18.71**	**3.90**	**9.25**	**n.a.**
	25^{th} – 75^{th} quartile	1.93 – 2.44	5.40 – 5.63	5.71 – 6.17	n.a.	17.86 – 22.912	3.63 – 4.19	8.56 – 9.49	n.a.

Appendix 9. Concentrations, wax/water partition coefficients (K_{ww}) and permeability coefficients (p) of 4-cyanophenol in candelilla and carnauba wax after adjuvant treatment.

		Candelilla wax			**Carnauba wax**		
adjuvant	**measure no.**	**C_{eq} (g l^{-1})**	**K_{ww}**	**p x 10^{13} (m^2 s^{-1})**	**C_{eq} (g l^{-1})**	**K_{ww}**	**p x 10^{13} (m^2 s^{-1})**
MeO	1	40.50	5.47	5.32	25.12	3.44	1.78
	2	44.90	6.04	5.42	25.99	3.40	1.30
	3	43.92	5.86	8.71	29.40	3.92	2.00
	4	41.69	5.55	26.16	23.06	3.01	2.20
	Median	**42.81[a]**	**5.71**	**7.06**	**25.56**	**3.42**	**1.89**
	25^{th} – 75^{th} quartile	41.10 – 44.41	5.51 – 5.95	5.37 – 17.4	24.09 – 27.70	3.24 – 3.68	1.54 – 2.10
TEHP	1	114.70	15.29	6.94	133.18	17.76	33.83
	2	161.28	21.50	16.32	84.30	11.24	77.09
	3	150.89	20.12	11.57	112.39	14.99	49.77
	4	117.40	15.65	4.66	92.38	12.32	46.09

	Median	**134.15**	**17.88**	**9.26**	**102.39**	**13.66**	**47.93**
	25^{th} – 75^{th} quartile	116.05 – 156.89	15.48 – 20.82	5.80 – 13.95	88.34 – 122.79	11.79 – 16.37	39.96 – 63.43
C12E2	1	206.31	27.51	14.88	96.61	12.88	14.61
	2	224.01	29.87	5.20	81.60	10.88	22.73
	3	188.22	25.10	4.97	64.28	8.57	24.86
	4	199.38	26.58	10.37	66.97	8.93	37.37
	Median	**202.85**	**27.04**	**7.79**	**74.29**	**11.88**	**23.80**
	25^{th} – 75^{th} quartile	193.80 – 215.16	25.85 – 28.68	5.09 – 12.63	65.63 – 89.11	10.73 - 13.29	18.67 – 31.12
C12E4	1	250.96	33.46	8.20	78.14	10.42	32.42
	2	215.94	28.80	10.60	65.82	8.78	26.55
	3	192.46	25.66	5.80	64.28	8.57	24.86
	4	207.85	27.71	6.98	66.97	8.93	37.37
	Median	**211.90**	**28.31**	**7.59**	**66.40**	**8.85**	**29.49**
	25^{th} – 75^{th} quartile	200.16 – 233.45	26.76 – 31.13	6.39 – 9.40	65.05 – 72.56	8.67 – 9.65	25.71 – 34.90
C12E6	1	237.11	31.61	6.96	142.03	18.94	33.54
	2	213.24	28.43	6.77	137.41	18.32	48.39
	3	197.84	26.38	6.59	164.36	21.91	42.56
	4	195.92	26.12	4.31	157.81	21.04	37.88
	Median	**205.54**	**27.40**	**6.68**	**149.92**	**20.02**	**40.22**
	25^{th} – 75^{th} quartile	196.88 – 225.18	26.25 – 30.03	5.45 – 6.87	139.72 - 161.09	18.62 – 21.44	35.71 – 45.48

Acknowledgements

Publication list

Kunz M; Staiger S; Burghardt M; Popp C; George N; Roberts K; Riederer M; (2022). Diffusion Kinetics of Active Ingredients and Adjuvants in Wax Films: An Attenuated Total Reflection-Infrared Spectroscopy Study of a Leaf Surface Model. *Agricultural Science and Technology* (doi: 10.1021/acsagscitech.2c00054)

Kunz M; Staiger S; Burghardt M; Popp C; Riederer M; Methyl oleate diffusion and accelerated sorption kinetics of 4-cyanophenol in selected plant waxes determined by Attenuated Total Reflection Infrared Spectroscopy (ATR-FTIR), *in preparation*

Curriculum vitae

Affidavit

I hereby confirm that my thesis entitled „Diffusion kinetics of organic compounds and water in plant cuticular model wax under the influence of diffusing barrier-modifying adjuvants" is the result of my own work. I did not receive any help or support from commercial consultants. All sources and / or materials applied are listed and specified in the thesis.

Furthermore, I confirm that this thesis has not yet been submitted as part of another examination process neither in identical nor in similar form.

Würzburg,

Place, Date Signature

Eidesstattliche Erklärung

Hiermit erkläre ich an Eides statt, die Dissertation „Diffusionskinetiken organischer Verbindungen und Wasser in pflanzlichem kutikulärem Modellwachs unter dem Einfluss von diffundierenden, barriere-modifizierenden Adjuvantien" eigenständig, d.h. insbesondere selbständig und ohne Hilfe eines kommerziellen Promotionsberaters, angefertigt und keine anderen als die von mir angegebenen Quellen und Hilfsmittel verwendet zu haben.

Ich erkläre außerdem, dass die Dissertation weder in gleicher noch in ähnlicher Form bereits in einem anderen Prüfungsverfahren vorgelegen hat.

Würzburg,

Ort, Datum Unterschrift